ANTHROPOGENIC IMPACTS ON THE PROPERTIES AND THE DISTRIBUTION OF THE TERRESTRIAL BIOGENIC SILICA POOL

Antropogene effecten op de eigenschappen en de distributie van het terrestrische biogeen siliciumopslag

Dissertation for the degree of doctor in Biology at the University of Antwerp to be defended by

Dácil Unzué-Belmonte

Promotors:
Eric Struyf
Patrick Meire

Research Group
Ecosystem Management
University of Antwerp

Para ti mamá:

porque todo lo que soy y seré…

es gracias a ti.

やった!!

Acknowledgements*/farewell?*

My grandfather only left Spain once in his life. He came to Antwerp to attend a photography course. I am so happy we shared this destiny/coincidence contributing to our future that I will always be thankful to this city. But of course I couldn't have come without the proposal SOGLO, the funding of Belspo and the selection by Patrick and Eric. Thank you.

This work wouldn't have been possible without many of you who have helped me academically. Thanks to all jury members for reading this book and improving the content with your comments. Thanks to all the other Si-geeks all around the world (mainly in Belgium, Germany and Sweden) for your collaboration and contributions to my work and Si-support. We might look like Si-crazy people, but *we're in this together*! Thanks to Nick Schenkels, aka 'the magician', for his work carried out with the modeling and his willingness to explain the code to me. Thank you all!

Special thanks to Eric for being an excellent supervisor and helping me 'keep the *faith'* in silica during all this time. I'm now convinced that silicon is the most important element in the world! Thanks for your patience and tactfulness bringing the bad news when things did not go how they should have. I have always felt fortunate because you replied my emails in one week at most... o_O. And I'm really sorry, my Godfather, that our silica group/mafia ends here.

Thanks to all ECOBE members. You all made me believe that making this *planet of the sun* a bit better is possible. Special thanks to Floor and Lúcia, my former silica fellows, for allowing me to learn from you and for always answering with kindness to this clumsy Si-ignorant girl. Thanks to my favorite Belgian people: Lindsay, Annelies and Anne, for all the conversations by the Skalar and during breaks/lunches/dinners/drinks. Also, thanks to my *beloved* English speaking bunch of people: Lúcia (you are mentioned twice! o_O), for understanding all my critics and complaints

best XD; Alex (my Eras in ECOBE will remain as 'before and after you left'); and Rebecca (our international from Brussels -what a country!-For our English redoubt!). Girls, thank you for always being there for me!

Thanks to all members of the SOGLO team from whom I have learnt the *soil's song* (and also a few differences between Walloons and Flemish). Especial thanks to Yolanda and Marie-Liesse as you are now more than colleagues, you have become friends. Thank you for the LLN parties and the dirty jokes, even if it was always difficult to come to Anvers… But it's ok, eh?

Thanks to everyone who has ever switched to English in my presence. Thank you, really. I hope the *karmacode* returns something good to you!

I would like to thank other non-academically related people who have helped me and kept my feet on solid ground during these four years:

To my new not *too many friends* I have met in this country: The few Spanish people, especially Rosa and Chris and the supporting Spanish women's group for making me feel closer to home. Thanks to the drums and music lovers, teacher Ricardo, Adilia and Egle for the coffees and chats trying to fix the world. I would like to say a big big thanks to all the geek/freak antisocial boardgamers that became like my second family; for all the games played, laughs shared and side plans involving beers, bbq's or more games (XD). I specially want to thank the other captains: Iván, Takao and Jork, I won't forget how we learnt to *enjoy the silence* to be able to think (!). I will miss to beat you! (ha!).

Thank you all for understanding me, keeping my mental health ok-ish, making me feel a bit less alone here, and filling many of the coold evenings and weekends of this rainy place.

I want to thank Burak for putting up with me for quite some time and making me try to be a better person. Humanity is underrated! I know I will have a friend in you forever. Heard/see you on the *radio/video*!! Also, thanks to Tippex, for all hide and seek games and for always allowing me to pet him… whenever he wanted… XD

Although we didn't meet often, I would like to thank my friends from home: to my brother's group of friends who have made me feel still connected and *refill*-ed *my soul* every time we have met. Thanks to the funniest 'bílogos' for making me feel *still young* (well…). Thanks to 'los masterianos' for always giving positive conservationist energy. Also, thanks to my favorite crazy girls: Jo, Raquel and Lau, because our friendship *always* continues where we left it no matter which country we live in.

A huge thank to my family, especially to my mum and my brother (+Anita! superhappis!). You know that *without you I am nothing*. Thank you for your company and listening about silica, co-authors, Belgians, writing, Skalar, modeling and Turkish with a smile on your faces. Your support is the greatest thing I do have.

Lastly, thanks to everyone who has had supporting words during these hysteric last months at *the end of the road*.

I don't know where my next journey will take me. If I leave, be sure that I will leave a *million little pieces* of my heart in this country.

Thank you.

"Good morning, and in case I don't see ya, good afternoon, good evening, and good night!"

"*One day, in retrospect, the years of struggle will strike you as the most beautiful.*"

— Sigmund Freud

Summary

The terrestrial Si-cycle has received increased attention in the past two decades. Multiple studies show several processes involved: interactions among primary lithology and weathering, biotic Si uptake, formation of secondary pedogenic phases and environmental controls such as precipitation, temperature and hydrology. Plants take up dissolved Si (DSi) from soil water, forming protective structures called phytoliths, often referred to as biogenic silica (BSi). The presence of phytoliths confers some benefits for the plant like resistance against herbivores or stress alleviation (Epstein, 1994). The solubility of BSi in soils is higher than other pedogenic Si phases which results in an active plant-soil Si turnover that controls the terrestrial Si-filter (Struyf and Conley, 2009). The importance of characterize and quantify the BSi pool in soils is thus important in order to better understand the terrestrial Si cycle.

Global change is defined as a set of several ongoing processes (i.e. climate change, land use change, population increase) (Steffen et al., 2004)(Steffen et al., 2004) that have a direct impact on humans (human health), food provision and on the natural functioning of the Earth's system (biodiversity, water and element cycles). In the terrestrial system scarce knowledge is available about the possible consequences of global change on BSi pools' distribution and properties and the consequent implications for the ecosystem Si-filter.

In this thesis the most relevant effects of global change on the terrestrial BSi pool were studied: the effect of fire, the decrease in abundance of large grazers and the combined effects of land use change and erosion. It was found that burned BSi is more soluble than fresh or unburned BSi; the effect of conversion from forest to cropland decreases the BSi pool in the short-term and erosion increases BSi accumulation and possible storage at bottom-slope positions, but the two effects combined results in a stronger BSi depletion and a larger accumulation; the presence

of large grazers on the African savannah controls the Si transport from grasses to the river, that eventually reaches the big lakes.

Moreover, the work carried out studying the effects of the global change challenged the method used to characterize and quantified BSi in soils. A refinement of the methodology used was consequently developed which consists on a better performance of the modeling and a novel calculation of an interval of confidence for each parameter estimated. The script developed is available from: https://github.com/nschenkels/AlkExSi/tree/v1.0.0.

Samenvatting

De terrestrische Si-cyclus heeft in de afgelopen twee decennia meer aandacht gekregen. Verscheidene studies tonen dat hierin meerdere processen een rol spelen: interacties tussen primaire lithologie en verwering, biotische Si opname, vorming van secundaire pedogenetische fasen en omgevingsvariabelen zoals neerslag, temperatuur en hydrologie. Planten nemen opgelost Si (DSi) uit het water op en vormen hiermee beschermende structuren ofwel 'fytolieten', ook wel biogeen silicium genoemd (BSi). De aanwezigheid van fytolieten biedt een aantal voordelen voor de plant zoals resistentie tegen herbivorie of stressvermindering (Epstein, 1994). De oplosbaarheid van BSi in bodems is hoger dan andere pedogene Si-fasen. Hierdoor ontstaat een actieve plant-bodem turnover die de terrestrische Si-filter aanstuurt (Struyf and Conley, 2009). Het karakteriseren en kwantificeren van de BSi-opslag in de bodems is dus belangrijk om een beter inzicht te krijgen in de terrestrische Si cyclus.

Wereldwijde veranderingen (zoals klimaatverandering, landgebruiksverandering, demografische groei) (Steffen et al., 2004)(Steffen et al., 2004) hebben een directe impact op de mens (gezondheid), voedselvoorziening, en op het natuurlijk functioneren van het ecosysteem (biodiversiteit, water en stoffencycli). Voor het terrestrische systeem is maar weinig kennis beschikbaar over de mogelijke gevolgen van wereldwijde veranderingen op de verdeling en kenmerken van BSi stocks en de hieruit volgende effecten op de natuurlijke Si-filter.

In dit doctoraat worden de meest relevante effecten van wereldwijde veranderingen op de terrestrische BSi-opslag bestudeerd: het effect van brand, de densiteitsafname van grote grazers en het gecombineerde effect van landgebruiksverandering en erosie. Het onderzoek toont aan dat verbrand BSi gemakkelijker oplosbaar is dan vers of ongebrand BSi; het effect van omzetting van bos naar akker verlaagt de BSi-stock op korte termijn en erosie vergroot de BSi-accumulatie en de mogelijke opslag aan

de voet van de helling, maar de twee effecten samen resulteren in een sterkere BSi-uitputting en een grotere accumulatie; de aanwezigheid van grote grazers op de Afrikaanse savanne stuurt het Si transport van graslanden naar de rivier, die uiteindelijk uitmonden in de grote meren.

Daarnaast leidde dit onderzoek naar effecten van wereldwijde veranderingen tot een verbetering van de bestaande methode om BSi in bodems te kenmerken en kwantificeren. Deze methode werd verfijnd met een nieuwe berekening van het betrouwbaarheidsinterval van iedere parameter, wat resulteerde in een betere performantie van het model. Het ontwikkelde script kan gedownload worden via https://github.com/ nschenkels/ AlkExSi/tree/v1.0.0.

Index

Chapter 1

Introduction

1

Introduction

The global biogeochemical silicon cycle

Silicon (Si), the 14th element in the periodic table, was discovered in 1823 by Jonz Jakob Brazilius (Weeks, 1932). Si is a tetravalent metalloid with high affinity for oxygen which occurs in the Earth's mantle. In fact, Si is the second most abundant element in the Earth's crust (Wedepohl, 1995). Humans have used silicate rocks and minerals as construction materials, ceramics, and more recently for electronics. In aquatic ecosystems, the biological importance of the Si cycle has been known for a long time: Si plays a crucial role for diatoms, which represent a large part of riverine, coastal and ocean primary production. In a biogeochemical context, Si is always associated with oxygen (SiO_2), and referred to as 'silica'.

A first description of the global biogeochemical Si cycle was made by Wollast and Mackenzie (1984). There are two large compartments in the cycle: the ocean and the terrestrial system, connected by the water continuum. Si from the terrestrial system mostly flows to the ocean through rivers in its dissolved form (DSi, H_4SiO_4). Only at a geological time-scale Si returns to the terrestrial system through volcanic and tectonic processes. Silica derived from the dissolution of the bedrock is the primary source of all silicon in soils. Chemical and biological soil processes subsequently control transformations of Si into both solid and dissolved phases (**Figure 1.1**).

The ocean Si sub-cycle has been widely studied. In the ocean Si is absorbed mainly by phytoplankton. Diatoms are unicellular algae with exoskeletons called frustules that consist of hydrated silicon dioxide (SiO_2nH_2O), biogenic silica (BSi). In order to build the frustules, diatoms need to absorb DSi from the water column. Diatoms constitute an important component of the ocean food web and are the single most important aquatic organisms for the sequestration of carbon dioxide (CO_2). The primary production associated to diatoms varies between 20 to 40% of the total ocean production (Nelson et al., 1995; Tréguer et al., 1995). In other words, diatoms are crucially needed in order to maintain the ocean food web. In the oceans and coastal zones, DSi concentrations are frequently near or at limitation. BSi from dead diatoms is therefore fast recycled in the water column, creating an extremely active Si turnover that maintains most of the ocean primary production. Only an estimated 3% of the BSi produced by diatoms is lost and trapped within the sediment (Ragueneau et al., 2006; Tréguer and De La Rocha, 2013), along with a substantial amount of carbon.

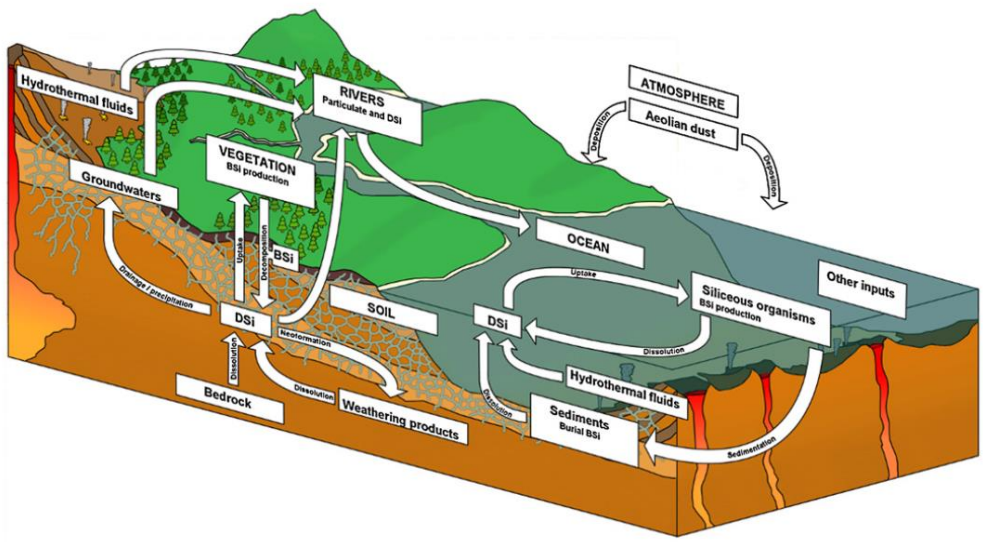

Figure 1.1. Processes and compartments involved in the global Si cycle. Adapted from Opfergelt et al., (2012).

While the ocean biological Si cycle is thus highly efficient in recycling its own Si, still an annual replenishment of about 6Tmole of Si is necessary to sustain the ocean diatom Si cycle (Treguer & De La Rocha 2013). This input

mainly originates from riverine input. The Si input is not only necessary to sustain diatom production. It has also a crucial role in determining the proportion between the abundances of other algae and diatoms (Ittekkot et al., 2000) in estuaries and the coastal zone. The presence of Si benefits diatom growth. On the contrary, when relatively low Si concentration exists, other algae and flagellate phytoplankton proliferate, often leading to coastal eutrophication processes (Humborg et al., 1997; Yool and Tyrrell, 2003).

The important connection between the ocean and terrestrial systems thus mainly relies on lentic systems where aquatic vegetation and diatoms grow, potentially affecting Si transport processes. Si is transported in the dissolved form or as a part of particles in suspension (Jeandel and Oelkers, 2015). However, while the ocean Si sub-cycle is quite well studied, the terrestrial and lentic biological Si cycle has only started to attract attention during the last 2 decades (e.g. Alexandre et al., 1997; Conley, 2002; Meunier et al., 1999; Sommer et al., 2006; Struyf and Conley, 2012). In fact, the most recent insights show that a large part of the output of Si into the rivers and eventually the oceans, is actually controlled by biological processes in terrestrial vegetation, and the cycling of this plant biogenic Si in ecosystem soils.

The terrestrial Si sub-cycle

In the soil system silica is present in multiple forms. Silicate minerals derived from the bedrock are the ultimate source of all silica cycling in terrestrial soils. Soil silicate weathering, including both physical and chemical processes, transforms primary Si minerals into secondary minerals, which includes phyllosilicates, micro crystalline phases, poorly ordered Si compounds and amorphous Si (Chadwick et al., 1987; Drees et al., 1989; Iler, 1955). The released DSi can have multiple fates: new secondary clay minerals and hydroxy-aluminosilicates (HAS) can be formed and DSi can be absorbed onto oxides. These processes depend on specific conditions like pH, water content, cation exchange capacity and the presence of organic compounds.

The final DSi concentration also depends on the weathering state which depends in turn on the parent material, topography, temperature (Berger et al., 1994; Hartmann et al., 2009), precipitation (Dove and Icenhower, 1997; Fraysse et al., 2006a), age and biota (Cornelis and Delvaux, 2016). Young or low-weathered soils normally contain a large abundance of primary Si-minerals and are scarce in secondary clay minerals and Si-oxides. On the contrary, long-term weathering processes results in highly developed soils depleted in primary minerals with a large abundance of secondary clay Si-minerals and Si-oxides (Kendrick and Graham, 2004; Schaetzl and Anderson, 2005). An overview of Si phases present in soils can be seen in **Figure 1.2**.

A variety of biogenic solid Si fractions are also present in soils. Microorganisms like testate amoeba (Aoki et al., 2007), diatoms (Patrick, 1977; Round et al., 1990), sponges (Clarke, 2003), as well as plants (Lucas, 2001; Meunier et al., 1999) take up DSi through organic processes (**Figure 1.2**). A crucial process here is the uptake of DSi by plants. Plants absorb DSi and incorporate it within the plant tissues, creating amorphous silicate structures called phytoliths that provide structural support (Piperno, 2006), resistance against herbivores (increasing leave's hardness) and stress resistance (Adrees et al., 2015; Epstein, 1994; Marschner, 1995), e.g. the Si co-precipitation with Al reducing free Al^{3+} toxicity for plants that in turn promotes plant growth (Major et al., 2010; Meyer and Keeping, 2001). Thus, although not an essential element to most plants, Si is crucial for plant fitness, leading some authors to suggest that Si should be considered as an essential nutrient (Currie and Perry, 2007; Epstein, 1994; Savant et al., 1997).

The Si content of plants is determined by two main factors: the species and the DSi content in the soil. Phytoliths abundance (Cornelis et al., 2010a; Jones and Handreck, 1967), shapes (Piperno, 2006) and properties (Fraysse et al., 2009) are species dependent (**Figure 1.3**). For example, conifers have less soluble prismatic shape phytoliths while phanerogams have different shape phytoliths (conical, stars…) (Piperno, 2006) and higher solubilities (Cornelis et al., 2010a). The plant Si content is also directly correlated with the DSi content in the soil, although the Si uptake is often considered to be passive

(Mitani and Ma, 2005). This has been recently questioned by authors that found no correlation between DSi content in the soil and Si accumulation in plant tissues (Keeping, 2017).

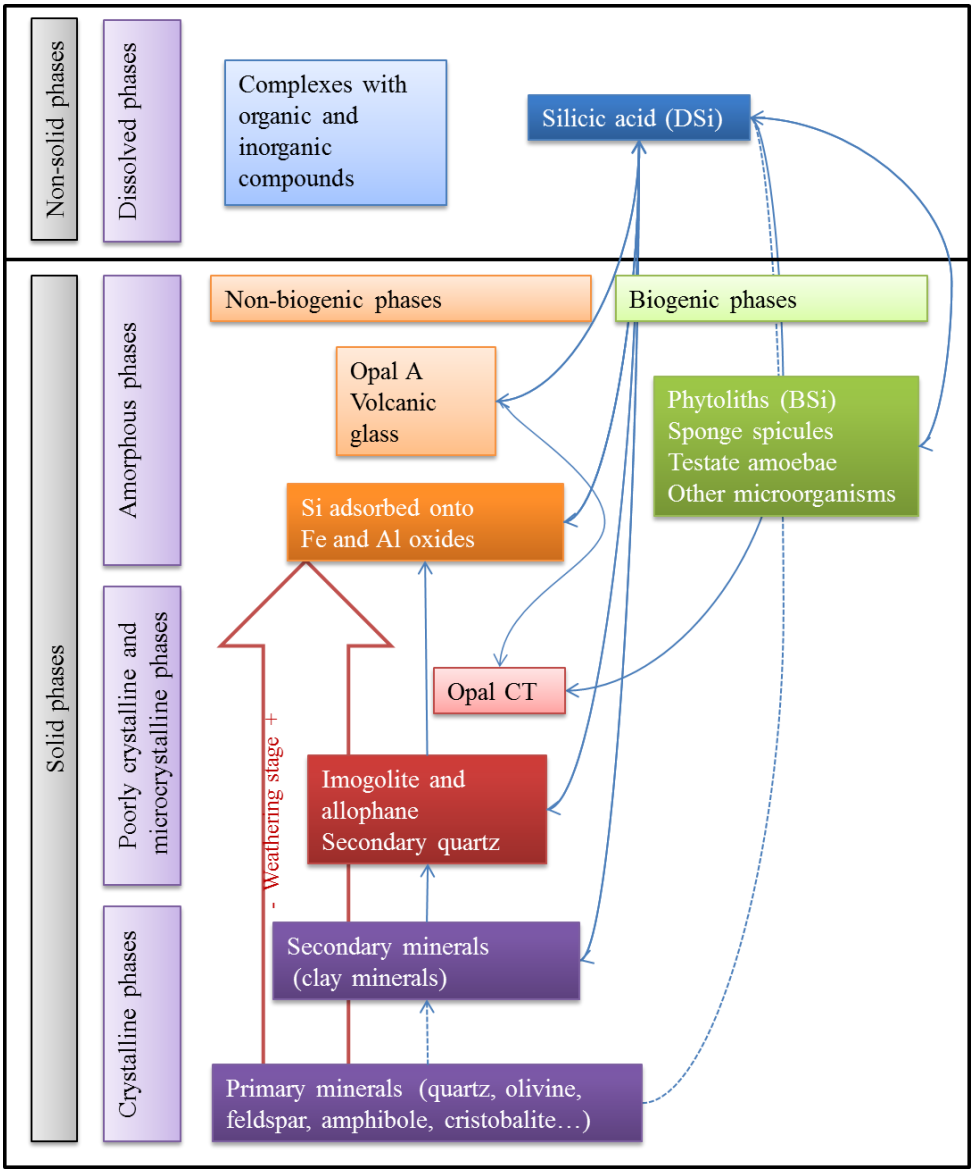

Figure 1.2. Overview of phases in soils containing Si. Red arrow shows the relative abundance of different phases as the weathering degree advances. Blue arrows show possible transformations between phases. Adapted from Sauer et al., (2006).

Moreover, there are multiple grass species that actively take up Si through a specialized Si uptake system consisting of aquaporin channels with high affinity for Si in their roots cells (Liang et al., 2006; Ma et al., 2006). These

species are often called Si-accumulators (Hodson et al., 2005; Takahashi et al., 1990). The Si fixation by plants is strongly significant for the global Si cycle, being estimated to be in the same order of magnitude as the annual Si fixation by diatoms (Loucaides et al., 2008). Yet, despite equally strong cycling going on in plant related biological Si processes compared to diatoms, this sub-cycle only relatively recently started to attract scientific attention.

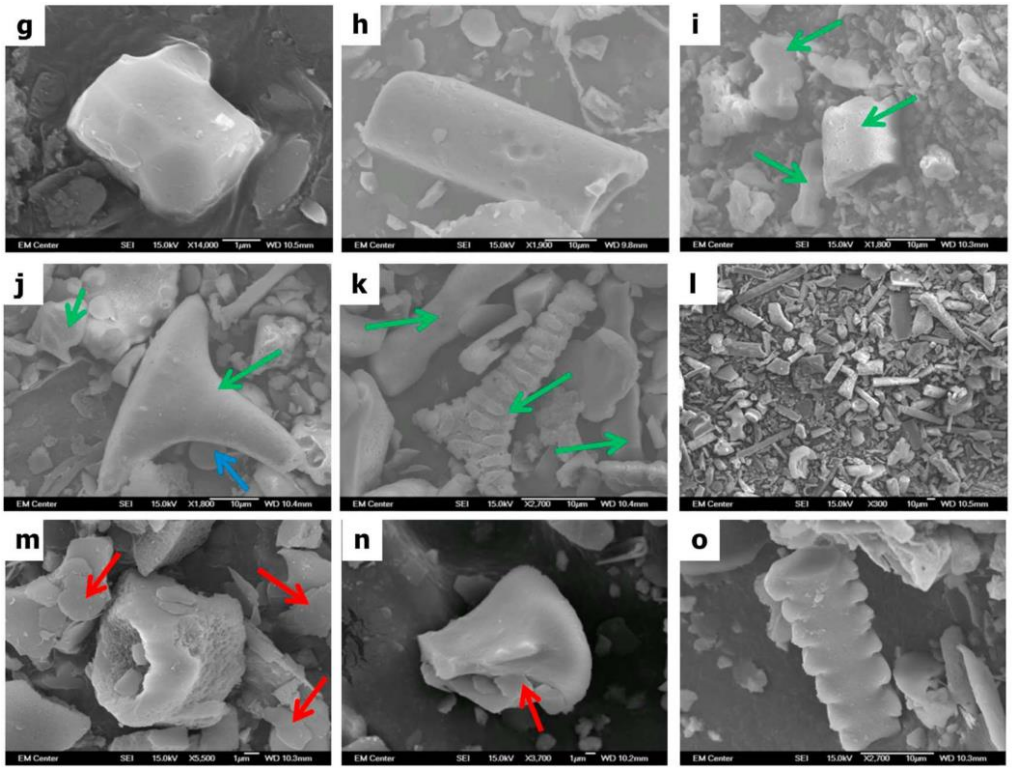

Figure 1.3. Scanning electron microscopy (SEM) pictures of phytoliths (Vandevenne et al., 2015).

Plants have a strong impact on the functioning of the terrestrial Si cycle (Alexandre et al., 1997; Carey and Fulweiler, 2012; Frings et al., 2014a; Kelly et al., 1998; Lucas, 2001). Plants promote the dissolution of silicate minerals through the exudation of organic compounds (Carey and Fulweiler, 2012). In topsoil, the effect of Si uptake by vegetation contributes to the stabilization of secondary silicates (Derry et al., 2005; Lucas et al., 1993), showing how plants can also control inorganic processes to some extent. Moreover, plants control water dynamics and affect the chemistry of the soil solution (Lucas,

2001). White et al., (2012) described how the mineral weathering controls Si processes in deeper horizons, but biogenic cycling governs Si processes in top soils. When plants die, plant BSi is incorporated into the soil where it can be dissolved again, contributing to the availability of DSi and creating a biological Si cycle in soils based on the turnover (deposition/re-dissolution) of phytoliths. The phytoliths content in soils was estimated to be between 0.01 wt% to 50 wt% (Alexandre et al., 1997; Clarke, 2003; Jones and Beavers, 1964). Among the multiple Si compounds in soils, BSi has been proven to be the most soluble (Blecker et al., 2006; Cornelis et al., 2010a; Fraysse et al., 2006a; Ronchi et al., 2015). The higher solubility of phytoliths contributes to an active Si turnover between plants and soil. Alexandre et al., (1997) estimated that the vast 92% of the total BSi is continuously being recycled, while only 8% of the total BSi is permanently stored in soils. The sum of all soil and biological processes affecting Si cycling in terrestrial ecosystems has been termed the ecosystem Si-filter (Struyf and Conley, 2012). The mechanisms controlling BSi dissolution in soils however are still under study, as we still don't know all processes involved that could affect BSi distribution, solubility and export.

Solubility of silicate minerals is known to be affected by factors like temperature (Chou and Wollast, 1985; Kodama and Ross, 1991), plant exudates (Carey and Fulweiler, 2012) or soil moisture, but it is not clear if the solubility of phytoliths would be affected in the same way or to the same extent. It is known that high Al content within phytoliths (Bartoli and Wilding, 1980), high abundance of organic acids (Piperno, 2006), low pH (Fraysse et al., 2006a) and low content of Ca^{2+} in the system (Nguyen et al., 2013) decreases the solubility of phytoliths. On the contrary, low solid to solute ratios or high soil moisture content increased dissolution of phytoliths under controlled conditions (Fraysse et al., 2009). Finally, it has been shown that after the passage of phytoliths through the digestive system of herbivores and consequent deposition, the solubility of phytoliths increases (Vandevenne et al., 2013). The role of large herbivores on the Si cycle might be more relevant than we nowadays acknowledge.

The integration of all processes affecting translocation and solubility of Si-phases and DSi export, determine the final DSi concentration in the system and the probability for the Si to be exported to the lentic compartment. Derry et al., (2005) showed that 69 to 90% of the DSi reaching the river had previously passed though the soil-plant cycle. Given the importance of the BSi recycling in soils for the global Si cycle, it is essential to study the processes affecting the distribution and solubility of phytoliths. In the frame of the global change is especially interesting to study the effects on the BSi distribution and recycling as a consequence of rapid environmental changes.

Global change and the terrestrial biological Si cycle

Global change is defined as a set of several ongoing processes including climate change (increase in temperature and changes in precipitation patterns, see **Figure 1.4**), changes in land use-land cover (LULC, conversion of land uses), increases in contamination and pollution (at atmospheric, water and soil levels) and the increase of world population (increasing exponentially) (Steffen et al., 2004). These changes have a direct impact on humans (human health (McMichael et al., 2005)), food provision, (IPCC, 2014), and on the natural functioning of the Earth's system (biodiversity, water (IPCC, 2014) and element cycles (Steffen et al., 2004)). However, the effect of global change can differ strongly between different regions. For instance, the rise in temperature in dried subtropical and Mediterranean regions will increase the fire risk more heavily than in humid or boreal regions. Although a relatively high number of effects of global change are currently being studied, the synergy between different driver's effects is difficult to tackle. This might be the next step towards a full understanding of global change.

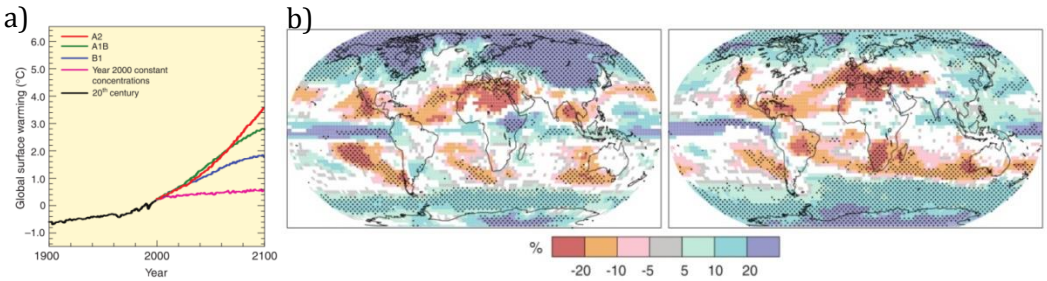

Figure 1.4. a) Expected increase in global surface temperature according to the IPCC's scenarios. b) Relative changes in precipitation patterns expected for the period 2000-2099 for December to February (left) and June to August (right), (IPCC, 2014).

Most of the studies carried out in relation to the global Si cycle were done in temperate ecosystems, and tropical and subtropical ecosystems are strongly underrepresented. Some of the effects of the global change are expected to be extremely severe in tropical and subtropical regions: i.e. temperature rise and droughts (IPCC, 2014), which together result in higher fire risk, changes in water regimes that will depend on the specific system (humid or dry tropical and subtropical systems) and economic practices in these countries (exploitation and conservation) (IPCC, 2014). Moreover, given the fact that a generalized increase in temperatures will occur in the whole globe it is especially interesting to study the warmest and driest systems in Earth: actual temperate regions might have tropical and subtropical conditions in the future.

The global Si cycle is prone to be affected by alterations of the water and element cycles due to e.g. land use and climate change. For example, diatom growth is affected by temperature (Eppley, 1972; Montagnes and Franklin, 2001), while in lentic systems the functioning and flow rates are modified due to dam construction and changes in nutrient inputs, hydrological cycles (Ittekkot et al., 2000) and sediment translocation. This potentially affects the Si input into the ocean as well as other biogeochemical cycles (Al, Ca) in the oceans, disrupting as a result the ocean Si cycle (Bienfang et al., 1982; Tréguer and De La Rocha, 2013). The terrestrial Si sub-cycle however has generally received only sparse attention at this respect.

Precipitation volume and in turn soil moisture, increase dissolution of silica compounds and probably DSi export. Higher soil pore water content increase solid to solution ratio, dissolving larger amounts of solid Si phases (Georgiadis et al., 2015) and possibly phytoliths (Fraysse et al., 2009). Higher temperatures are known to increase weathering rates of silicate minerals (Drees et al., 1989; Rimstidt and Barnes, 1980) and Si-minerals solubility though the increase of soil temperature (Neal et al., 2005), which consequently increases the release of DSi into the soil solution. However, we do not know if the solubility of phytoliths would be affected to the same extent with the increase in soil temperature. Moreover, the increase in temperature in dry regions will boost the fire's occurrence and intensity. Some authors showed that amorphous silica mineralized when pyrolized at temperatures higher than 500°C (Guo and Chen, 2014). We however have no knowledge of the effects on phytolith solubility after burning at lower temperatures.

Another crucial aspect of global change is land use change. Agriculture in particular removes large amounts of biogenic Si from soil systems through the harvest of the crops (Guntzer et al., 2012a; Meunier et al., 1999) as phytoliths do not return to the soil. This has been linked to a long-term Si depletion in temperate croplands (Vandevenne et al., 2015b). Moreover it has been determined that the depletion of the phytolith pool in several croplands in France, could possibly happen in 12-15 years since deforestation (Keller et al., 2012). It has been shown that the conversion from forest to cropland causes a rapid increase of DSi fluxes in the short-term from the cropland to the river in temperate systems (Conley et al., 2008) but followed by a decrease in DSi fluxes in a longer-term (Struyf et al., 2010b), also described by Legesse et al., (2003) in a comparison between croplands and woodlands in Ethiopia. In **Figure 1.5**, a schema showing the changes in DSi fluxes according to the land use or ecosystem develop stage is represented.

Deforestation contributes to enduring erosion processes which in turn depletes soil Si stocks through the direct export of soil material. Clymans et al., (2015) showed how the increase of Si mobilization in croplands is not a

consequence of tillage technique or crop type but of soil loss due to the increase of erosion. The increase of erosion rates derived from agriculture is known to increase the DSi export up to 40% after a rainfall event (Smis et al., 2011). Deposition at lower positions of other elements like carbon (C) and nitrogen have been already described in sloped terrains affected by land use change (Gregorich et al., 1998; Navas et al., 2012; Quinton et al., 2010). Ibrahim and Lal, (2014) showed an accumulation of C and amorphous Si, as well as ready-soluble Si at bottom-slopes in temperate forests. Possibly land use change enhances as well the deposition of BSi at bottom positions in a topo-sequence, but this remains unknown. Studies combining the aggregation of effects, for instance deforestation and erosion, are still needed.

The agricultural practice of fertilizing adds exogenous Si into the system (Bélanger et al., 1995; Liang et al., 2006) that in turn affects the terrestrial Si cycling. Indeed the addition of Si contributes to benefit crop resistance (Fauteux et al., 2005) and was shown to increase wheat growth by 4.1–9.3%, and rice growth up to 17% in field experiments (Ma and Takahashi, 2002). Moreover, Si application increased yield production in rice fields as well (Guntzer et al., 2012a). Yet, the different properties between Si-sources, whether an inorganic or organic fertilizer is applied to soils, may influence the plant preferences in Si uptake, the Si recycling by crops and thus locally the overall terrestrial Si cycle functioning.

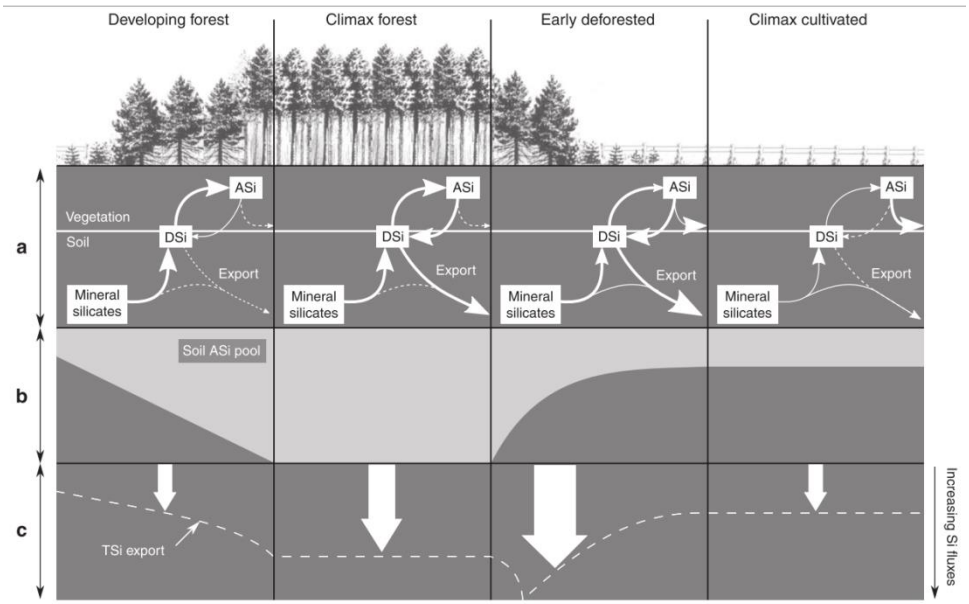

Figure 1.5. Differences in terrestrial Si cycling according to the land use/ecosystem stage (Struyf et al., 2010).

Quantifying biogenic silica in soils

Given the large importance of bio-terrestrial Si cycling in the ocean-terrestrial Si connection, good methods to quantify BSi in soils are necessary. Below is a short introduction to the evolution of the methodology to analyze BSi in soils and sediments.

A chemical extraction in Na_2CO_3 has being used in marine ecology to extract and quantify diatom content (DeMaster, 1981) in the water column. The method assumes that all diatoms dissolve during the first half hour and only minerals subsequently dissolve. The intercept of the linear mineral dissolution line is then calculated and is considered to be the BSi content (**Eq. 1** and **Figure 1.6**), assuming constant mineral dissolution during the whole extraction, and all non-linearly reacting Si to be biogenic.

This results in following equation:

$$\mathrm{Si}_t = Si_i \times b + BSi \qquad \textbf{(1)}$$

where Si_t is the DSi present at any given time in the extraction, Si_i the initial amount of Si from mineral phases, *b* is the dissolution rate of the mineral phase and BSi the total content of BSi in the sample.

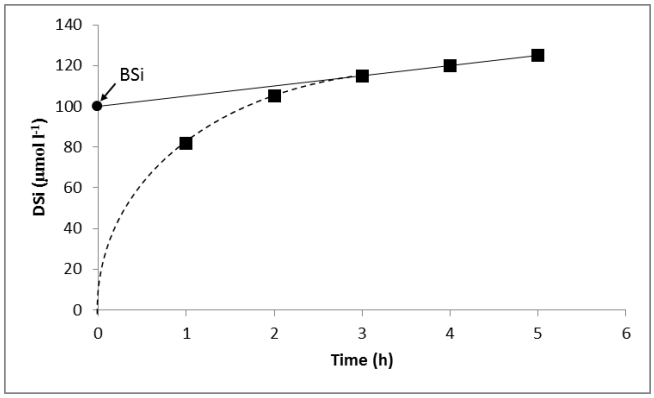

Figure 1.6. Hypothetical dissolution behavior of a sample extracted in Na_2CO_3. The linear phase after the 3rd extraction hour corresponds to the dissolution of the remaining minerals in the sample. The intercept of the linear dissolution of minerals then accounts for the BSi content in the sample.

However, analyzing some more complex marine sediments, it was discovered that some clay minerals also have high non-linear solubility in alkaline solvents. Thus, some clays might be dissolved in the first half hour, resulting in an overestimation of the amount of BSi. Until some years ago, an extraction in 0.1 M Na_2CO_3 was still the most common method used to estimate BSi content. As clays and oxides are particularly present in soils, some new approximation had to be developed.

Already in 2002, Koning et al. (2002) suggested a new method, that consisted in extracting samples in 0.5 M NaOH measuring Si and Al dissolved concentrations continuously during the extraction (**Figure 1.7**). Modeling the two curves together and relating the two concentrations, a Si/Al ratio can be assigned to the different fractions dissolving (**Eq. 2**).

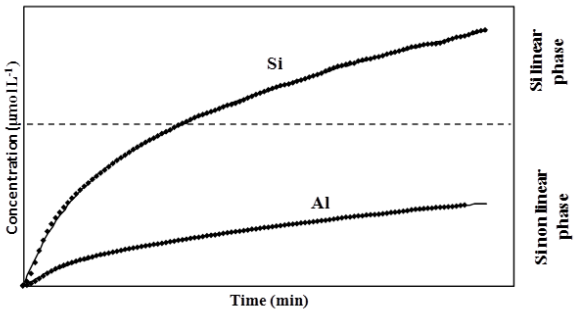

Figure 1.7. Dissolution curves of Si and Al during the continuous extraction. The linear and the non-linear phase of the Si are noted. In Barão et al. (2015).

This results in following equations:

$$Si_t = \left(\sum_{i=1}^{n} AlkExSi_i \times \left(1 - e^{-k_i \times t}\right)\right) + b \times t$$

$$Al_t = \left(\sum_{i=1}^{n} \frac{AlkExSi_i}{Si/Al_i} \times \left(1 - e^{-k_i \times t}\right)\right) + \frac{b \times t}{Si/Al_{min}} \quad \textbf{(2)}$$

where Si_t and Al_t are the concentrations of Si and Al respectively, at any given time. The equations consist of two parts: the mineral fraction which has a linear dissolution behavior (DeMaster, 1981; Koning et al., 2002) and the fractions exhibiting non-linear dissolving behavior. For the mineral fraction, the model renders a linear dissolution rate (b) and the Si/Al ratio (Si/Al_{min}) of that linear fraction. Non-linearly dissolving fractions are characterized by: the total amount of Si (alkaline extractable Si (AlkExSi), mg g^{-1} dry weight of initial sample mass), the Si/Al ratio (concentration of Si over concentration of Al) of that fraction and its dissolution rate (k, min^{-1}). Assuming the same Si and Al release rate from the same compound and relating the Si and Al concentration equations through the Si/Al ratio, with the three parameters estimated (AlkExSi, k and Si/Al ratio) the different fractions dissolving non-linearly are distinguished. The same model is fitted with one, two or three first order equations (summation to n in the formula) and the solution showing least error (F test) from the three fits is kept. For the non-linear fractions, the Si/Al ratio of the fraction is used to determine its origin. Silicate

clay minerals normally have Si/Al ratios ranging from 1 to 5 (Koning et al., 2002). Diatoms contain much more Si than Al, showing ratios above 5. Using this method, the inorganic fraction can be discriminated, avoiding the overestimation of BSi (diatom) content.

Recently, the previous method was adapted for soils by Barão et al. (2014), in order to better quantify the soil BSi pool. A new problem arose when applying the method in the terrestrial system. In soils, the inorganic fractions and minerals containing Si are more abundant and variable than in water environments. Besides clay minerals, hydroxy-aluminosilicates (HAS) and Si adsorbed onto oxides can be particularly abundant in some types of soils, for instance highly weathered soils (Delvaux et al., 1989; Kendrick and Graham, 2004; McFadden and Hendricks, 1985; Opfergelt et al., 2009). Some Si adsorbed onto oxides showed high solubility in alkaline solvents. Si adsorbed onto oxides is always lower than the adsorbed Al: when coupling the dissolution curves of Si and Al the resulting fraction will show a Si/Al ratio below 1. Secondary clay minerals in soils normally show Si/Al ratios between 1 and 5, because the proportion of the two elements within the clay. Finally, phytoliths, like diatoms, show a high Si content resulting in Si/Al ratios above 5. The authors described thus three different fractions or pools: BSi (phytolith pool) (Si/Al>5), secondary clay minerals (1>Si/Al<5) and HAS, hydrous- and hydrated clays or Si adsorbed onto oxides (Si/Al<1).

Other additional methods exist to extract and quantify BSi in soils (Saccone et al., 2006; Sauer et al., 2006). The physical extraction of phytoliths (Parr et al., 2001; Piperno, 2006) and subsequent quantification is a reliable method that isolates phytoliths for measuring the Si concentration afterwards. The method consists on successive digestions and a total of 12 methodological steps. As some phytoliths can be stored in soils (up to 8% (Alexandre et al., 1997), this method is also used in paleo-ecological studies where characteristics (size, shape, etc.) of phytoliths are used to described past vegetation (Blinnikov, 2005) thanks to the species-dependent phytoliths characteristics (Piperno, 2006). This method, although accurate in the

estimation, is extremely time-consuming and expensive (Saccone et al., 2006; Zhao and Pearsall, 1998) for BSi quantification.

In this thesis, I applied the Barão et al. (2014) method to address multiple ongoing global change effects on soil and terrestrial ecosystem biogenic Si stocks.

Objectives

Despite the advances made in acquisition of knowledge concerning the functioning of the terrestrial Si cycle in the last decades it is clear that there is a still a long path to fully apprehend how soil-BSi behaves under changing environmental circumstances. Among several global change drivers this thesis addresses the most relevant yet non-quantified effects of global change drivers related to the terrestrial system, that possibly affect soil BSi abundance and distribution: fire risk (climate change), land use change, erosion and the possible extinction of large herbivores. The implementation of an improved methodological approach for the application of the continuous alkaline extraction became essential after the work carried out in this thesis. The last chapter therefore consists of a mathematical refinement of the methodology to model Si and Al dissolution curves to better constrain our results. An overview of the topics studied is presented in **Figure 1.8**.

Challenge one: Does fire affect the solubility of BSi?

Given the importance of the expected future changes regarding fire occurrence and intensity particularly in dry climates, in **Chapter 2**, I studied the effect of ecosystem fires on the solubility of BSi. Will the structural changes that phytoliths experienced after burning influence their solubility? Up to date, there were no studies regarding this respect. Is the method able to determine correctly the BSi content from burned biomass?

Challenge two: How land use change affects soil BSi pool in tropical regions?

In **Chapter 3**, I studied the changes in abundance and distribution of BSi in tropical soils affected by deforestation and erosion, and the possible synergic

effect of the two drivers acting together. The study was carried out in a subtropical soil from a basaltic origin. No earlier studies have adopted the Barão et al. (2014) method in tropical soils where the presence of high amount of secondary weathering products, like oxides, make this study a challenge for the application of the method.

Challenge three: How the type of fertilizer and soil type influence the BSi soil pool and the plant uptake?

In **Chapter 4**, I conducted a cooperative study to test the effects of inorganic and organic fertilizers on the Si recycling by plants in tropical/subtropical soils. In order to investigate this, two types of soils (moderate and highly weathered soil) were fertilized with an inorganic and organic (biochar) Si source. A crop was grown on those systems afterwards and Si cycle functioning was studied. Does the Si-recycling by plants depend on soil weathering state and/or type of Si (inorganic or organic) added? And moreover, is the method used able to distinguish the BSi pool from the other Si pools in soils?

Challenge four: How relevant is the influence of hippopotamus on the Si transfer to the river?

In **Chapter 5**, I studied to which extent the Si cycling in the African savannah can be determined by the African hippo. A study in the Mara River is carried out in order to investigate the influence of hippo depositions on the Si input in the river and possible consequences for the Si cycle. What will be the consequence for the Si cycle on the Mara River if hippos disappear or are extremely reduced? The Barão et al. (2014) method was significantly challenged: strong volcanic interference is present in the Mara river basin, potentially strongly increasing reactive mineral interference in the analysis.

Challenge five: Applying the knowledge acquired to refine the method to determine BSi in soils (Barão et al., 2014).

Based on all the experience gained in the previous chapters, I initiated cooperation with the Maths department to standardize the curve analysis

protocol, and quantify the uncertainty that is associated with the mathematical determination of BSi based on the curve analyses. A refinement for the methodological analysis is performed in Chapter 6, and the script produced can be used for the rapid analysis of all soil and sediment samples for BSi in the future. Specific recommendations are made, and potential remaining pitfalls and challenges identified.

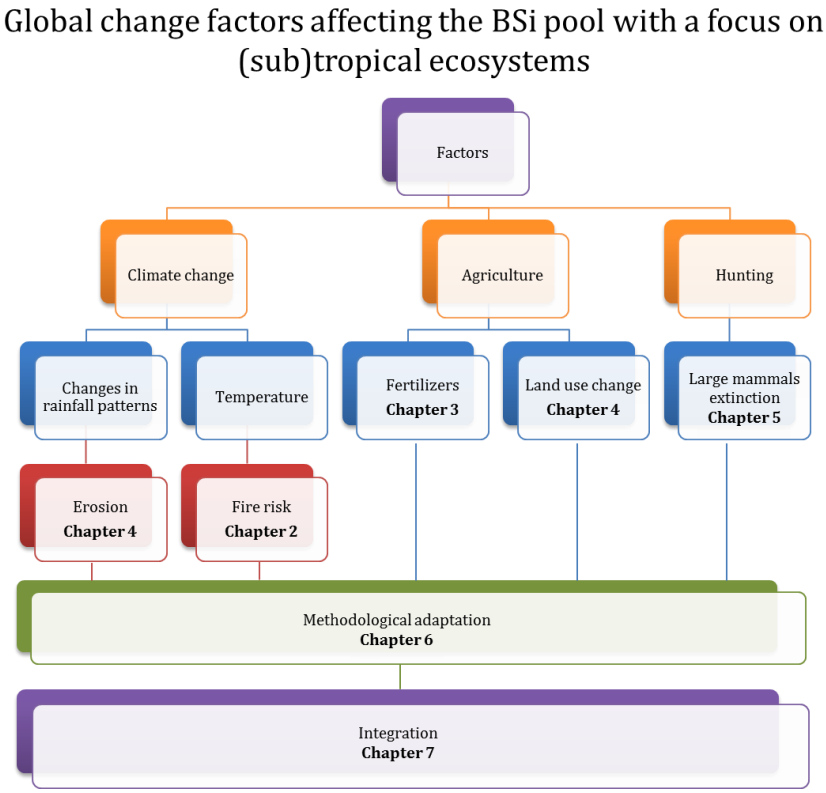

Figure 1.8. Diagram including factors studied in this thesis with the respectively Chapter which they are included in.

Chapter 2

Fire enhances solubility of biogenic silica

This chapter is based on:

Unzué-Belmonte, D., Struyf, E., Clymans, W., Tischer, A., Potthast, K., Bremer, M., Meire, P. and Schaller, J., 2016. *Sciencie of the Total Environment* 572, 1289-1296.

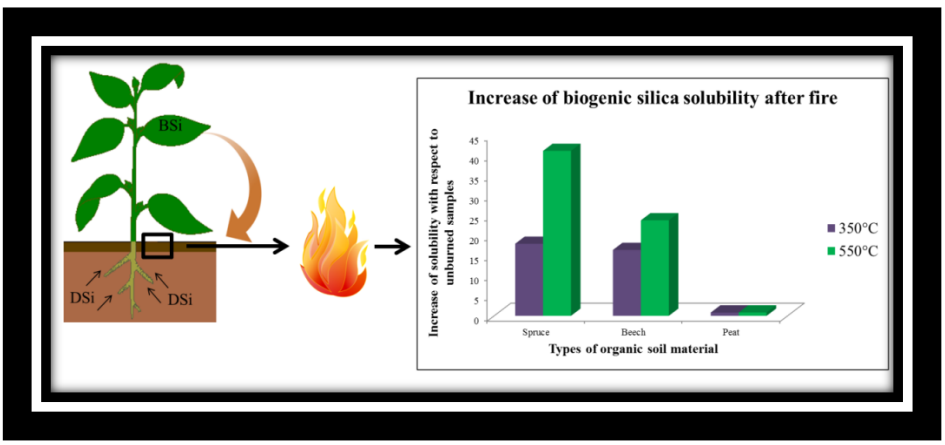

2

Fire enhances solubility of biogenic silica

2.1. Introduction

Natural fires can have severe effects on ecosystems, including the alteration of ecosystem productivity, biodiversity and functioning, reflected by changes in soil biogeochemistry, plant communities and animal populations (Bowman et al., 2011). For example, in the topsoil of post-fire ecosystems, the presence of ashes causes changes in nutrient content, cation exchange capacity, water repellency and sorption capacity for nutrients (Pereira et al., 2012).

The impact of natural fires on ecosystems depends on weather conditions, as they regulate the duration and the severity of the fire. According to the IPCC Report (Intergovernmental Panel on Climate Change, Kovats et al., 2014, IPCC 5th Report), longer drought periods in temperate regions will increase the number and intensity of natural fires. Besides natural fires, humans commonly use controlled application of fires, i.e. prescribed fires, as a tool in ecosystem management. Temperatures in natural fires usually range between 200°C and 300°C (Rundel, 1983), but can reach up to 500 to 700°C in heavy fires (Dunn and DeBano, 1977). The fire properties, i.e. duration and severity, will be reflected in the characteristics of the produced ashes. As the

recovery of the ecosystem depends on the fire properties, most studies have focused on the description of ashes' characteristics (Bodí et al., 2011, Pereira et al., 2011). The resulting classification reflects the content of unburned matter, the content of macro- and micro nutrients, the pH or the reactivity of the ashes (Haglund et al., 2008).

The biogeochemical effects of fire on major elements such as C, N and P have been broadly studied across various climate regions (Bodí et al., 2014). Briefly, while fires emit C into the atmosphere, they also create black carbon with a longer residence time in soil than non-burned C (Schmidt et al., 2011). Black carbon is thus considered to act as a long-term C sink (Bodí et al., 2014). Fires can cause substantial losses of N (estimated at 22-25%) from the soil (Gómez-Rey et al., 2013), as well as increasing P availability up to 10-fold with a potential increase of P-export to rivers (Schaller et al., 2015).

However, little attention has been paid to fire effects on biogeochemical Si cycling (Struyf and Conley, 2012). Plants take up dissolved Si (DSi) from soil water, forming protective structures called phytoliths, often referred to as biogenic silica (BSi). The concentration of Si in plants is often higher than those of other trace elements like Mg or Fe, resulting in high concentration of Si also in the plant litter (e.g., Eleuterius and Lanning, 1987). Weathering, biogenic and pedogenic processes result in a large variety of Si fractions in soils, i.e. DSi, primary and secondary silicate minerals, BSi and amorphous silica precipitates (Sauer et al., 2006, Cornelis et al., 2011a), all with different solubility (Van Cappellen, 2003). The solubility of each fraction determines its contribution to plant-available silica, with the biogenic silica as one of the most soluble forms (Van Cappellen, 2003; Fraysse et al., 2010). The different silica pools and their availability in soils have recently received a surge of scientific attention (Barão et al., 2014; Cornelis et al., 2014a; Georgiadis et al., 2014; Opfergelt and Delmelle, 2012) as they effectively control the output of Si to groundwater and rivers, a concept known as the ecosystem Si filter (Meunier et al., 1999; Struyf and Conley, 2012). Hence, it is necessary to investigate how fire could affect the solubility and composition of BSi in top soils.

Anthropogenic interventions in the landscape can alter the functioning of the ecosystem Si filter (Carey and Fulweiler, 2011; Struyf et al., 2010c). Deforestation and agricultural practices, i.e. harvest of crops and grazing by cattle, strongly affect soil Si pools (Guntzer et al., 2012b; Vandevenne et al., 2012) and BSi solubility (Vandevenne et al., 2013), affecting the Si export to rivers. Still, we do not fully apprehend the diversity and magnitude of processes that alter the Si sink/source function of soils. A better understanding of the abiotic variables that control Si storage and dissolution in soils is essential to better understand terrestrial Si cycling and the important interconnections to the C cycle in particular.

Fire could be a crucial study topic in this regard. We aim to examine the effect of fire on mobilization of Si from organic soil material (European Soils Bureau Network, 2005) and how different fire temperatures affect the solubility. The few data available indicate that highest Si availability in ashes is obtained at mid-temperatures (black carbon product) (Pereira et al., 2012), while at higher temperatures, Si crystallization of amorphous Si is observed, potentially lowering Si availability (Xiao et al., 2014). We hypothesized that fire affects soil Si solubility as a trade-off function between organic matter losses and degree of crystallization. To evaluate our hypothesis, three representative temperate ecosystems with different properties were selected (Berg and McClaugherty, 2008): beech forest, spruce forest and peatland, and their organic soil material was exposed to two burning treatments. Characterization of the Si fractions of burned and non-burned samples was investigated by performing an alkaline extraction, while batch experiments in rain water were carried out to mimic natural dissolution rates.

2.2. Material and methods

Experimental setup

Samples

Organic soil material samples (uppermost 2 cm) consisting of dead and partially decomposed needles (spruce) or leaves (beech), were collected from

two forest systems grown in Dystric Cambisols in Tharandt (Dresden, Germany): Norway spruce (Picea abies) and European beech (Fagus sylvatica). Tharandt forest is located in the suboceanic/subcontinental climate. The mean annual temperature is 7.8°C and the mean annual precipitation is 823 mm (Grünwald and Bernhofer, 2007). The total organic layer thickness at the sites was 8±3 cm for the spruce and 4±2 cm for the beech. No ferns or mosses, which could supply organic matter were observed. In addition, a commercial peat (Sphagnum sp.) with low (<5%) mineral and nutrient content, was selected. Coniferous forests, deciduous forests and peat bogs are representative ecosystems for temperate climates (Berg and McClaugherty, 2008). After the removal of roots and branches, organic soil material (OSM) was crushed and passed through a 2 mm sieve. Subsequently, OSM was dried at 40°C until constant weight before burning.

Samples had an initial carbon content of 470 mg g^{-1}, 350 mg g^{-1} and 480 mg g^{-1} for spruce, beech and peat OSM respectively. The initial nitrogen content was 20 mg g^{-1} for spruce OSM, 18 mg g^{-1} for beech OSM and 11 mg g^{-1} for peat OSM. Carbon and nitrogen content were measured with Elementar vario El III (Hanau, Germany) in accordance with DIN-ISO-10694, 1995. The initial phosphorus content (measured according to Bray and Kurtz, (1945)) was 0.83 mg g^{-1} for spruce OSM , 5.1 mg g^{-1} for beech OSM and 0.27 mg g^{-1} for peat OSM.

Fire treatment

Two different fire treatments were applied in order to obtain black carbon (350°C) (Nguyen et al., 2010) and white ashes (550°C, DIN-EN-12879, 2001). The heating was conducted in a muffle furnace until a constant weight was obtained. Black carbon produced in the first treatment is the most common product after a fire (Rundel, 1983). White ash is typically produced in a severe fire when all organic matter is expected to be consumed (Giovannini et al., 1988). For the control treatment, no heating was applied. For every ecosystem, net mass loss was calculated after the treatments.

Analysis of the samples

X-ray diffraction analysis

X-ray diffraction was done for ash samples to characterize the crystalline silica present in the samples. The analysis was performed using the Diffractometer FPM (FreibergerPräzesionsmechanik, Freiberg, Germany) RD7 (CuK_α radiation; Ni monochromator; angle range of 2 – 80° 2θ, step scan 8.0 s, step sizes 0.02°). 10 – 20 % zinc oxide was added to the ash as internal standard. Rietveldt refinement was performed using BGNM program (Schaller et al., 2015).

Alkaline extractable Si

A total of 27 samples, three replicates per fire treatment and ecosystem, were analyzed in a continuous flow analyzer (Skalar, Breda, the Netherlands), using a continuous analysis technique recently refined for terrestrial environments by Barão et al. (2014). Samples were gently crushed prior to analysis. The extraction is performed in 180 mL of 0.5 M NaOH, at 85 °C for half an hour. Dissolved Si and dissolved aluminum (Al) are measured continuously during the extraction, obtaining two dissolution curves which are fitted with first order equations **(1)**.

$$Si_t = \left(\sum_{i=1}^{n} AlkExSi_i \times (1 - e^{-k_i \times t})\right) + b \times t$$

$$Al_t = \left(\sum_{i=1}^{n} \frac{AlkExSi_i}{Si/Al_i} \times (1 - e^{-k_i \times t})\right) + \frac{b \times t}{Si/Al_{min}} \quad \textbf{(1)}$$

The method distinguishes between the mineral fractions which have a linear dissolution behavior (DeMaster, 1981; Koning et al., 2002) and the fractions exhibiting non-linear dissolving behavior. The curve model (with one, two or three non-linearly reactive fractions) exhibiting the lowest error was kept. For the mineral fraction, the model renders a linear dissolution rate (b) and the Si/Al ratio (Si/Al_{min}). Non-linearly reactive fractions are characterized by: the total amount of Si (alkaline extractable Si (AlkExSi),

mg g^{-1} dry weight of initial sample mass), the Si/Al ratio (Si/Al) of that fraction and its reactivity (how fast it dissolves, k). The Si/Al ratio of the fraction is used to determine the origin of the non-linear fraction. Barão et al. (2014) distinguished the following fractions: ratio >5 was considered as indicative of a biogenic fraction, as the proportion of Al in phytoliths is low (Bartoli, 1985; Piperno, 2006). A fraction with a Si/Al ratio between 1 and 5 was considered as representative of the mineral fractions and Si/Al ratios <1 can indicate multiple pedogenic Si fractions, including absorbed Si. The total AlkExSi was re-calculated for each reactive fraction relative to the initial mass of the sample before the burning treatments.

Dissolution experiment

A dissolution experiment in rain water was set up to mimic natural reactivity of Si after burning. The amount of material incubated in 35 mL plastic tubes was scaled to obtain identical initial soil masses (prior to burning) per incubation experiment to mimic a natural scenario. This implies that the added amounts were: for spruce 0.1 g, 0.034 g and 0.01 g of initial organic material, black carbon and ash respectively; for beech 0.1 g, 0.046 g and 0.03 g of initial organic material, black carbon and ash, respectively; and for peat 0.1 g, 0.03 g and 0.007 g of initial organic material, black carbon and ash, respectively. Five replicates per ecosystem-treatment combination were incubated. Each tube was filled with 10 mL air-captured rain water (pH: 6.64, conductivity 34.5 µS cm^{-1} and DSi: 0.05 mg Si L^{-1}). The dissolution experiment was carried out in a dark incubator at 20°C and samples were collected at 9 time intervals (5 and 30 minutes, and 1, 2, 5, 10, 15, 18 and 24 hours). At each time step, the solution was filtered at 0.45 µm and analyzed for DSi using ICP-AES. Total amount of DSi (mg L^{-1}) after 24 hours for every ecosystem-treatment was normalized by initial mass incubated (mg g^{-1}). Afterwards, percentages were calculated based on the AlkExSi content obtained in the alkaline extraction, as the DSi extracted in rain water is expected to be part of the most reactive Si extracted in the continuous extraction. Additionally, the percentage related to the total Si (AlkExSi + crystalline Si) was also calculated.

2.3. Results

Mass loss results

Mass loss after burning at 350°C (black carbon) reached 64 ± 3% (mean±SD) for spruce forest, 54 ± 4% for beech forest and 70 ± 3% for peat samples. For the ash treatment (550°C) the attained loss percentages were 89 ± 0.4% for spruce, 70 ± 1.4% for beech and 93 ± 0.5% for peat samples, published in more detail in Schaller et al. (2015).

Crystalline silica in ashes

There were clear differences in crystalline silica quality and quantity for the ashes of the different soil organic material types. The percentages of mineral fraction in the ashes were 12% for spruce forest, 59-63% for beech forest and 40% for peat. This implies, according to the mass loss results, that the original soil organic material contained 1.3% of crystalline Si in spruce forest soil, 18% in beech forest and 2.6% in peat, published in more detail in Schaller et al. (2015).

Continuous extraction

The AlkExSi normalized to the non-burned mass was relatively constant over all treatments for spruce (25.1 ± 2.1 mg g^{-1}) and beech (15.4 ± 0.9 mg g^{-1}), but was not constant for the peat samples (1.2 ± 0.5 mg g^{-1}, see Total AlkExSi from **Table 2.1**). The non-burned peat samples showed an extremely low BSi content and an increase in AlkExSi with increased burning temperatures.

In the spruce forest samples, almost all AlkExSi consisted of one fraction (25.2 ± 1.91 mg g^{-1}) with a high Si/Al ratio (60 ± 22) and a reactivity of 0.77 ± 0.03 min^{-1}. A second additional fraction (small in amount) appeared only in four of the samples, of which the two black carbon samples had a lower Si/Al ratio. Among the treatments, the larger fraction did not show a difference in Si/Al ratios but a slight decrease in reactivity after the first burning treatment (350°C resulting in black carbon) (77.6 ± 18.7 and 0.65 ± 0.09 min^{-1}, Si/Al ratio and reactivity respectively for the black carbon treatment). After the

second burning treatment (550°C resulting in ash), there was a decrease in Si/Al ratio as well as in reactivity (30.1 ± 2.41 and 0.52 ± 0.11 min^{-1}, Si/Al ratio and reactivity respectively for the ash treatment).

The beech forest non-burned material, black carbon and ashes consistently showed a large fraction with a high Si/Al ratio (>10) and high reactivity (1.02 ± 0.20 min^{-1}), and a second fraction with high Si/Al ratio (>20) and low reactivity (0.25 ± 0.11 min^{-1}). The large fraction made up about 70 % of the total AlkExSi. The same fractions were obtained for the black carbon and the ash samples. In the black carbon, there was a slight decrease of the Si/Al ratio, both in the large (12.9 ± 0.7, Si/Al ratio value for the second replicate was not considered in the calculation) and in the smaller fraction (17.0 ± 11.4). The reactivity slightly decreased in the large fraction (0.77 ± 0.28 min^{-1}) and the small fraction (0.13 ± 0.07 min^{-1}). Ashes from the beech samples showed no decrease in the Si/Al ratio of the large fraction (20.1 ± 8.25), and a slight decrease in the reactivity (0.72 ± 0.11 min^{-1}). However, the small fraction showed a strong decrease in Si/Al ratio (2.9 ± 1.67) and also in reactivity (0.12 ± 0.02 min^{-1}).

The peat fractionation was much more heterogeneous. The fractionation for two of the control samples consisted of one single fraction (0.73 ± 0.14 mg g^{-1}) with a high Si/Al ratio (>50) and a reactivity of 0.27 ± 0.09 min^{-1}. The last replicate showed one fraction (1.0 mg g^{-1}) with a Si/Al ratio of 1.15 and a reactivity of 0.99 min^{-1}. The peat samples had an extremely low BSi content (<1 mg g^{-1} of the original mass). The black carbon samples consisted, in two cases, of a larger fraction (0.85 ± 0.01 mg g^{-1}) with a high Si/Al ratio (>70) and a reactivity of 0.19 ± 0.06 min^{-1} and a small fraction (0.17 ± 0.10 mg g^{-1}) with a Si/Al ratio <1 and a reactivity of 0.37 ± 0.2 min^{-1}. The third black carbon sample consisted of two similar fractions (0.48 and 0.65 mg g^{-1}) both with high Si/Al ratio (>30) and a reactivity of 0.10 and 0.36 min^{-1}, respectively. The ashes consisted in two of the replicates of three fractions with high (>100), intermediate (from 1 to 4) and low (<1) Si/Al ratios.

Table 2.1. Results from the continuous extraction for the different treatments ("Treat." control, black carbon and ashes, C, BC and A respectively). From left to right: Total AlkExSi obtained and fractions obtained ordered by reactivity. The amount of AlkExSi (AlkExSi, mg g^{-1} of sample, relative to the unburned mass), the reactivity (k, min^{-1}) and the Si/Al ratio (Si/Al) are shown for each fraction (see **Eq. 1**). Missing values indicate the absence of additional fractions according to the curve model.

OSM Type	Treat.	Total AlkExSi	$AlkExSi_1$	k_1	Si/Al_1	$AlkExSi_2$	k_2	Si/Al_2	$AlkExSi_3$	k_3	Si/Al_3
	C	25.3	25.3	0.81	31.5						
	C	24.2	23.7	0.73	85.8	0.52	0.17	>100			
	C	25.0	25.0	0.76	63.1						
	BC	21.4	19.5	0.78	99.9	1.93	0.20	6.52			
Spruce	BC	25.5	22.2	0.57	78.7	0.76	0.03	11.5	2.55	0.03	4.11
	BC	24.8	24.8	0.59	54.1						
	A	25.1	25.1	0.49	33.4						
	A	29.2	25.5	0.68	27.9	1.79	0.10	44.2	1.87	0.10	29.4
	A	26.2	26.2	0.41	28.8						
	C	15.5	12.1	0.79	23.7	3.33	0.13	39.8			
	C	15.4	12.3	1.00	11.2	3.03	0.22	26.1			
	C	14.4	9.74	1.27	14.7	4.69	0.40	20.0			
	BC	15.3	12.4	0.37	13.6	2.92	0.04	4.83			
Beech	BC	14.4	9.06	1.04	>100	5.33	0.20	13.9			
	BC	15.6	10.3	0.89	12.2	5.27	0.14	32.3	0.11	0.17	0.14
	A	16.1	11.1	0.57	16.0	5.02	0.13	1.77			
	A	17.0	12.0	0.80	12.7	4.97	0.13	1.66			
	A	14.4	8.16	0.80	31.6	6.27	0.10	5.22			
	C	0.87	0.87	0.17	52.7						
	C	0.60	0.59	0.36	>100						
	C	1.04	1.04	0.99	1.15						
	BC	1.12	0.86	0.12	>100	0.26	0.57	0.32			
Peat	BC	1.13	0.65	0.35	37.7	0.48	0.10	>100			
	BC	0.91	0.84	0.25	75.0	0.07	0.17	0.16			
	A	2.15	0.35	0.88	>100	1.47	0.05	1.72	0.33	0.40	0.35
	A	1.74	0.13	2.91	>100	1.06	0.05	1.79	0.56	0.50	0.48
	A	1.44	0.66	1.25	>100	0.78	0.07	3.98			

The last replicate lacked the presence of the low Si/Al ratio fraction. The amount of AlkExSi obtained for the fraction with a high Si/Al ratio was 0.38 ± 0.22 mg g^{-1} and the reactivity of 1.68 ± 0.88 min^{-1}. For the intermediate Si/Al ratio fraction, the AlkExSi content was 1.10 ± 0.29 mg g^{-1} and a low reactivity of 0.06 ± 0.01 min^{-1}. The last fraction (Si/Al ratio <1) was 0.44 ± 0.11 mg g^{-1} and its reactivity was 0.45 ± 0.05 min^{-1}.

Dissolution experiment

All incubations showed a rapid release of dissolved Si following a typical logarithmic dissolution pattern. DSi was log-transformed ($Ln(DSi) = \alpha Ln(t) \pm b$), in order to normalize its distribution. Log-transformed DSi plotted against dissolution time for each ecosystem and treatment is shown in **Figure 2.1**. Low dissolution rates were obtained after 24 h (**Table 2.2**).

The dissolution experiment in rain water showed clear differences between organic soil material types and treatments. The DSi concentration obtained after 24 hours as well as the dissolution rates at different time steps are shown in **Table 2.2**. Control incubations showed the lowest final concentration (all < 0.70 mg L^{-1}), followed by the black carbon (from 0.52 up to 6.4 mg L^{-1}) and finally the ashes which reached the highest final concentrations (from 0.93 to 29 mg L^{-1}). There were large differences between the OSM types for ashes and black carbon: dissolved concentrations were lowest for the peat samples, intermediate for the beech and highest for the spruce (see **Table 2.2**).

The total amount of Si dissolved after 24 hours related to the initial biomass sample for spruce and beech samples is shown in **Table 2.2**. The total DSi extracted for the spruce samples increased from 0.06 ± 0.01 mg g-1 to 1.07 ± 0.3 mg g-1 and to 2.76 ± 0.23 mg g-1, for the control, black carbon and ashes treatment, respectively. For beech samples the DSi concentration attained was 0.04 ± 0.004 mg g-1, 0.65 ± 0.24 mg g-1 and 0.98 ± 0.14 mg g-1 (control, black carbon and ashes, respectively). The DSi obtained for the peat samples was 0.05 ± 0.01 mg g-1, 0.05 ± 0.01 mg g-1 and 0.09 ± 0.02 mg g-1 (control, black carbon and ashes, respectively). The percentages of DSi after

24 hours related to AlkExSi (obtained in the continuous extraction) as well as the percentages related to the total Si (AlkExSi + CrystallineSi) for spruce, beech and peat samples are shown in **Table 2.2**.

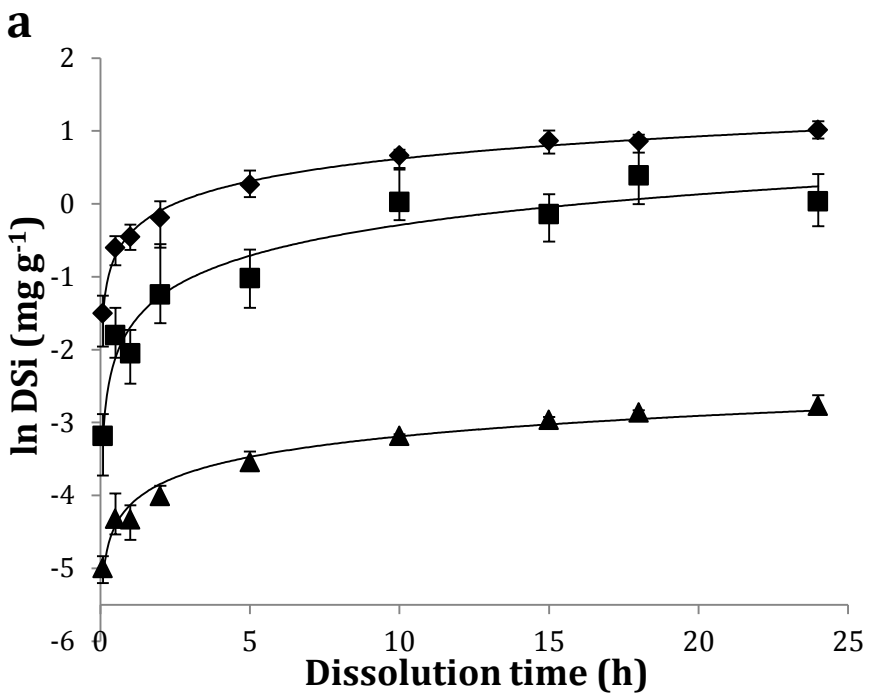

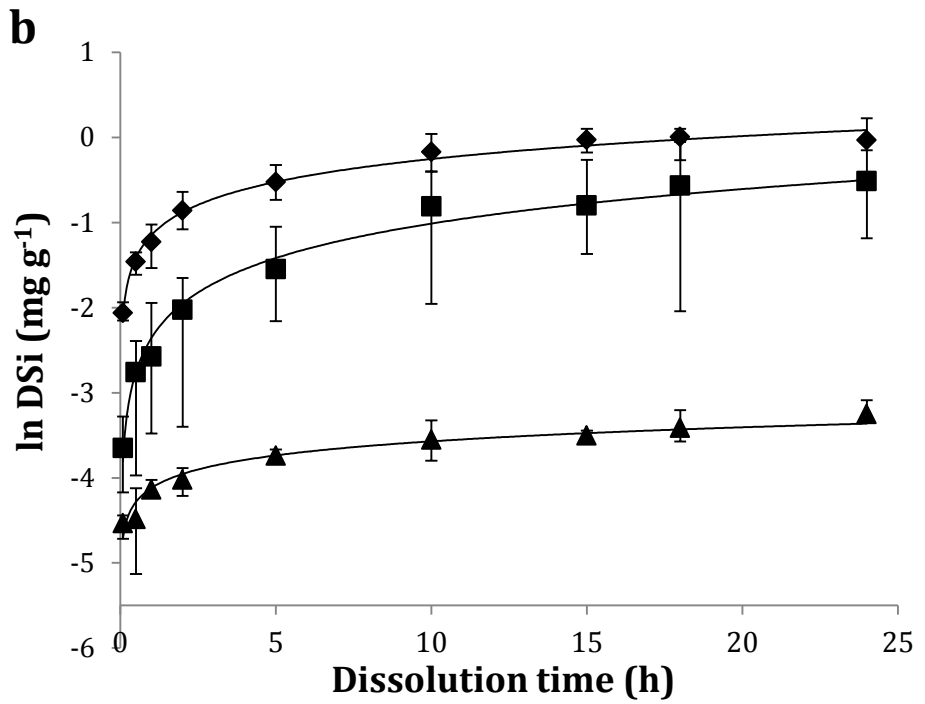
b
1
0
-1
-2
-3
-4
-5
-6
ln DSi (mg g-1)
0
5
10
15
20
25
Dissolution time (h)

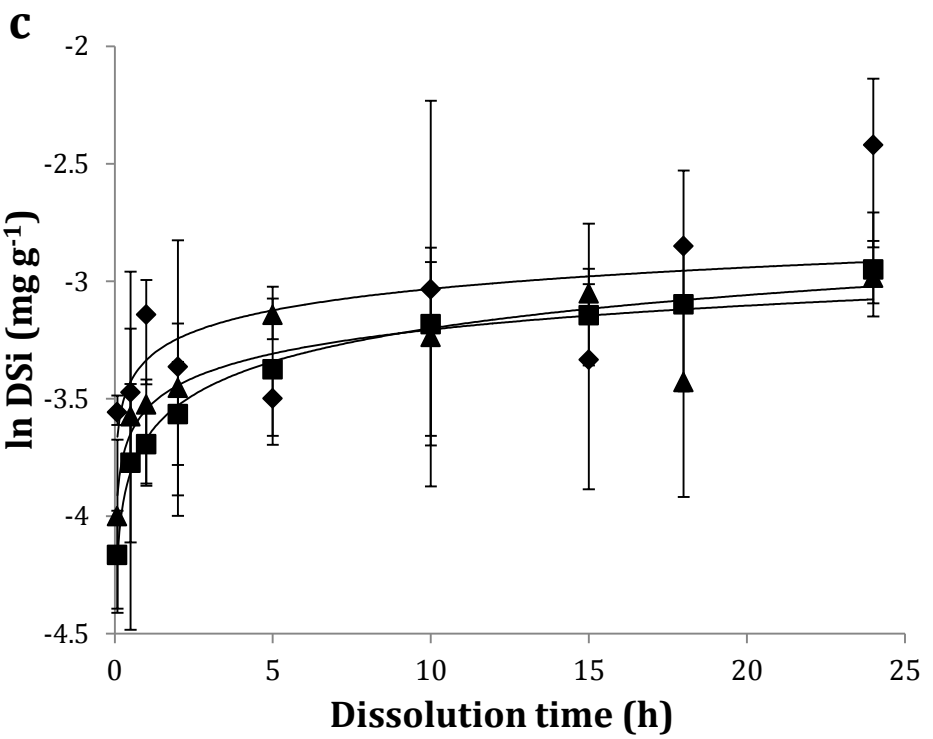
c
-2
-2.5
-3
-3.5
-4
-4.5
ln DSi (mg g-1)
0
5
10
15
20
25
Dissolution time (h)

Figure 2.1. Dissolved Si (ln DSi, mg dissolved per g incubated organic soil material) released during dissolution experiments (5 replicates per experiment) in natural rain water at different timesteps (Dissolution time, h). a: Spruce forest, b: beech forest and c: peat. Each dataset represent a treatment: Control (triangle), black carbon (square) and ash (diamond).

2.4. Discussion

Our dissolution experiment clearly demonstrates that the solubility of biogenic Si in the organic soil material from spruce and beech forests (containing over 1% of BSi by soil weight) increased after burning. The severity of burning (Keeley, 2009), is an important aspect for the observed dissolution rates: the highest degree of burning treatment (ashes) showed a higher dissolution rate in water compared to the other treatments for the forest organic soil material. On the other hand, the solubility of Si in peat samples poor in BSi (containing below 0.1% of BSi of soil weight) did not show any observable changes following fire treatments.

Composition of BSi in organic layer

The untreated samples of the spruce and beech forests showed that all alkaline reactive Si was dominantly biogenic. The organic soil material is mostly composed of dead vegetation, and phytoliths are thus expected to make up the major part of the BSi. The total AlkExSi

Table 2.2. Dissolution rates (mg g^{-1} h^{-1}) at different time steps. Total DSi extracted after 24 hours in mg L^{-1} and mg g^{-1} of sample. Total AlkExSi (mg g^{-1}) obtained on the continuous extraction.

OSM Type	Treatment	Dissolution rates 1/2 – 2h	2 – 10h	10 – 24h	DSi mg L^{-1}	DSi mg g^{-1}	AlkExSi mg g^{-1}	% AlkExSi	% Total Si
Spruce	Control	0.01	2.91E-03	1.52E-03	0.63 (0.06)*	0.06 (0.01)*	24.86	0.25§	0.17°
	Black carbon	0.43	0.28	1.66E-03	10.82 (2.98)*	1.07 (0.3)*	23.91	4.49§	2.93°
	Ash	3.02	1.28	0.56	28.72 (3.07)*	2.76 (0.23)*	26.83	10.28§	6.96°
Beech	Control	3.78E-03	1.37E-03	7.06E-04	0.39 (0.03)*	0.04 (0.00)*	15.08	0.26§	0.02°
	Black carbon	0.15	0.10	0.02	6.35 (2.30)*	0.65 (0.24)*	15.12	4.27§	0.33°
	Ash	0.51	0.17	0.03	9.90 (1.33)*	0.98 (0.14)*	15.84	6.19§	0.50°
Peat	Control	0.01	1.10E-03	6.55E-04	0.45 (0.13)*	0.05 (0.01)*	0.83	6.13§	0.19°
	Black carbon	0.02	0.01	3.28E-03	0.52 (0.04)*	0.05 (0.01)*	1.05	5.00§	0.19°
	Ash	0.05	0.03	0.05	0.93 (0.25)*	0.09 (0.02)*	1.78	5.16§	0.33°

* mean (SD), § (% from the total AlkExSi (on the continuous extraction) that was extracted in rain water after 24 hours), ° (% from the Total Si (AlkExSi + CrystallineSi) that was extracted after 24 hours in rain water).

content (related to initial biomass) was constant over the burning treatments. The OSM from spruce forest showed a higher content of BSi than the OSM from the beech forest, suggesting a higher BSi content from evergreen litter compared to deciduous tree species. These results are in line with part of the findings of Cornelis et al. (2011b), who found a BSi concentration in the humus layer of 1.2% for European beech (*Fagus sylvatica*), and a slightly higher concentration (1.5%) for a Douglas fir (*Pseudotsuga menziesii*). However, in the same study, black pine (*Pinus nigra*) had 0.5% of BSi in biomass. Transpiration and phylogenetic age of a species have been recently shown to also influence Si content of plants, and a difference between coniferous and deciduous species should therefore not be generalized (Cornelis et al., 2010b; Hodson et al., 2005; Trembath-Reichert et al., 2015). Moreover, there exists large variability of phytoliths, related to their morphology and silica content, and even the reactivity, which varies within and between species (Bartoli, 1985; Piperno, 2006).

Spruce control samples contained a single biogenic fraction, while beech control samples had two biogenic fractions, a large one (~80% of BSi) with a higher reactivity and a smaller fraction (~20% of BSi) with lower reactivity (in NaOH). This coincides with findings by Fraysse et al. (2010), who described two plant BSi pools for both deciduous and evergreen trees: a concentrated pool of phytoliths that is not embedded in any organic matrix (largest pool, most reactive) and individual molecules or small polymers of H_4SiO_4 embedded in an organic matrix or bounded within the cell walls (small fraction, less reactive). Hilli et al. (2010) showed low decomposition rates of lignin-rich coniferous needles. In our continuous extraction, beech samples clearly showed the reactivity and pool differentiation described by Fraysse et al. (2010), as well as a few of the samples for the spruce that showed existence of BSi with low reactivity.

The low-reactive BSi fraction in the beech samples showed a strong decrease in Si/Al ratio in the ash treatment compared to the other treatments. Such a strong pattern was not observed for any of the other BSi fractions, although there was an apparent but less sudden drop of Si/Al in ash

from the spruce treatment. The low Si/Al ratios encountered for the low-reactive BSi fractions correspond, according to our model, to clay minerals, which have a crystalline structure. Observations of decreasing Si/Al ratio agree with the studies by Xiao et al. (2014) and Guo and Chen (2014), which showed that amorphous Si crystalizes when temperature is >500°C, potentially resulting in a lower Si/Al ratio in our observations. A strong Al adsorption onto biochars derived from rice straw was observed >400°C in Qian and Chen (2013). According to the authors, the processes of dehydration, polymerization and subsequent cracking of the organic compounds lead to an exposure of the silica which is restructured together with other released elements (i.e. Al) in crystalline forms. The increase of Si surfaces areas after the combustion of the organic matter and the fact that mineral Si content was much higher in the beech than in the spruce organic layer could explain the higher crystallization observed in the beech samples. According to our results the total BSi crystallized in the beech ashes only mounted to 5 mg g^{-1}, which will contribute minimally to crystalline silica estimates from the X-ray diffraction analysis.

Si release from BSi in organic layer

Dissolution rates as well as concentrations attained during the dissolution experiment were very low for all untreated samples. This resulted in a minor fraction of incubated Si released after 24 hours (<0.3%). These results correspond with the observations of Vandevenne et al. (2013) and Schaller and Struyf (2013), who found a low release of BSi from grass litter. Fraysse et al. (2010) reported similar dissolution rates in a batch experiment for pine litter, finding 0.01 mg g^{-1} h^{-1} during the first minutes (0.25 h) and 0.002 mg g^{-1} h^{-1} from 2 to 7 h. Organic matter bonds are known to be hydrophobic (Almendros et al., 1992; Bodí et al., 2011; Knicker, 2007), which partly explains the low dissolution rates for the control treatment in the batch experiment. A remarkable increase of the percentage of dissolved BSi was observed for the black carbon and the ash sample of the spruce forests, with more than 10% of BSi dissolved in the ash samples. Much higher DSi concentrations were attained, despite equal incubation amounts of BSi. Water

repellency is known to disappear around 350-400°C (Bodí et al., 2011). This might explain the increase in dissolution capacity in all burning treatments across the forest organic soil material types. The combustion of organic matter leads to an increase of reactive surface area of Si compounds which might be the explanation behind the increase of solubility.

Interestingly, while the percentage of dissolved BSi was similar for non-burned organic soil material from both forests, the beech samples showed a much smaller increase in dissolution capacity in the ash samples. This might depend on a trade-off between the organic matter (OM) removal (increasing solubility) and the stronger crystallization (lower Si/Al ratios) of the BSi observed for the silica-OM-complexed fraction of the beech ash (decreasing solubility). This could imply that the dissolution potential of BSi after burning increases in the absence of any mineral material that can trigger crystallization.

The fact that the same amount of original mass was incubated meant that the amount of ashes incubated was less than the amount of organic soil material for the non-burned treatment, resulting in different solid-to-solution ratios. Since only very low equilibrium concentrations were attained for the untreated OSM samples, the attained concentrations in the containers did not demonstrate any artifact of different solid-to-solution ratios. Related to the amounts of BSi incubated, solid-to-solution ratios were equal among the treatments. In addition, the intention of this experiment was to mimic natural conditions. We considered that the same amount of water would come into contact with a more compact and denser OSM in the case of non-burned systems in contrast to significantly reduced amount of material after burning. Different studies have investigated the amount of nutrients in ashes after a fire (Bodí et al., 2014; Pereira et al., 2011), but usually these samples are collected only after a natural fire and relating the amount of nutrients to the initial mass prior burning was not possible.

These results parallel the results of Vandevenne et al. (2013). In that study, it was observed that passage of BSi through herbivore guts increased

dissolution in water, while reactivity in NaOH decreased. These authors related this observation to the fact that after passage through the herbivore, the organic matrix of BSi was completely removed, increasing the dissolution capacity of the BSi. A similar effect is likely for burning, which removes most of the organic C from the biomass matrix. This implies that any process removing the organic matrix from litter could strongly increase Si release. Other similar processes could be microbial decomposition of litter, although sound evidence is lacking (Fraysse et al., 2009) and potentially mycorrhizal activity (Quirk et al., 2014). In Vandevenne et al. (2013), the apparent decrease of reactivity of the BSi in NaOH was ascribed to release of most of the reactive BSi into the grazer's urine. A similar release is not possible in the burning treatments. We have no immediate explanation for the apparent decrease in solubility in NaOH, besides increased crystallization of the BSi.

Composition and Si release from low-BSi samples

The commercial peat sample had a Si/Al ratio >5 and extremely low BSi concentrations, below 0.1%. Here we treat the samples as representative of a sample with almost no-BSi content compared to the mineral fraction (2.6%, see section 3.2). Low *Sphagnum* peat concentrations of BSi have earlier been found in Kokfelt et al. (2009) and Bennett et al. (1991), although other studies found high BSi concentrations in peatlands in the Arctic region, mainly due to the abundance of diatoms in the samples (Alfredsson et al., 2015; Struyf et al., 2010a). *Sphagnum* peat accumulates very low amounts of Si, resulting in low Si-availability. This could be explained by the fact that the stratification in the peat results in an increase of pH with depth that dissolves all BSi, creating a desilicated underlayer of clays (Bennet et al., 1991). During the burning treatment, we observe a relatively large (although small in absolute number) increase in AlkExSi, especially in the ash treatment. The increase in AlkExSi after burning was related to the appearance of low Si/Al fractions that became non-linearly reactive in the extraction after burning. This indicates an apparent change in dissolution characteristics of the mineral fraction due to the burning treatment or the appearance of new fractions. Mineral Si and Al absorbed by organic complexes could be released

after organic matter combustion, which is in line with Steenari et al. (1999) who found acid soluble Si associated with Al in peat ashes when samples were burned at 550°C.

Despite the results of the continuous extraction, the solubility in rain water was not affected by fire. The same amount of Si was dissolved for all the treatments. The peat samples indicate that mineral Si fractions do not become more reactive in the burning treatment. The released Al^{3+}, evident from the presence of AlkExSi fractions with low Si/Al ratios after burning, may become attached to the BSi decreasing its solubility (Nguyen et al., 2014; Qian and Chen, 2013). The resulting dissolution capacity would be the result of two effects counteracting at the same time: an increase of solubility due to the disappearance of organic matter in the tiny phytolith pool and a decrease of solubility due to the Al^{3+} complexing with the phytoliths. Also the resulting pH (not measured) could affect the solubility of the phytoliths present. Phytoliths' solubility increases at higher pH (Fraysse et al., 2006a).

Implications

We are among the first to investigate the effect of fire on the storage and solubility of Si from the organic layer. Although our results are limited to spruce, beech and low BSi-peat ecosystems, they demonstrated some clear patterns. The solubility of BSi increases sharply after burning. An apparent crystallization also occurs when silica is complexed with organic matter. Crystallization of BSi during the burning can limit the increase in solubility and it might be more pronounced when a source of Al is available. While the large Si-content variability among species does not allow generalizing the difference in terms of evergreen vs. deciduous trees, it suggests there are species specific Si dynamics that deserve further detailed studies (Cornelis et al., 2010; Hodson et al., 2005; Trembath-Reichert et al., 2015). However, ecosystems low in BSi will not show drastic alteration in the Si cycle due to fire.

From a biogeochemical cycle perspective, our observations have strong implications. Fire is widely used as a management tool for ecosystems. A study from Melzer et al. (2009) suggested increased storage of BSi after prescribed fires in savannah grasslands. The strong and effective internal cycling of Si by the Si-rich savannah grasses may cause this apparent difference with our experimental study on ash properties, which suggests higher dissolution (and thus export-capacity). The burned soils could provide a strong and immediate Si source to the grasses. Pereira et al. (2012) showed higher Si availability to plants after burning. Our results clearly suggest that BSi will be more susceptible to dissolution after burning. *In situ* ecosystem characteristics will determine the fate of the dissolved Si. The balance between leaching and DSi uptake by vegetation will determine whether DSi remains in the ecosystem or is exported to the aquatic system. If we consider that a large part of the BSi can be dissolved after 24 hours, considerable losses of BSi from ecosystems can occur after burning and subsequent precipitation. On the other hand, in ecosystems with low general Si availability, fire could increase the availability of a limited nutrient for plants.

Deforestation is known to be determinant in the Si export from watersheds. A rapid increase of DSi export after deforestation was shown by some authors (Carey and Fulweiler, 2011; Conley et al., 2008), as water can more easily access BSi and the re-uptake of DSi by vegetation is low. Burning was described to have a similar effect, increasing DSi export after a wildfire (Engle et al., 2008). If forests are replaced by croplands, the depletion in BSi in soils after sustained harvesting, can result in low Si fluxes from deforested watersheds in the long-term (Struyf et al., 2010b; Vandevenne et al., 2012). Thus, burning can potentially reduce the time interval between the state of an increased Si release immediately after a fire, and a later BSi-depleted state.

Fires and precipitation are predicted to increase in temperate regions with climate change (Kovats et al., 2014), with potentially even stronger increases in e.g. warmer and drier climates, for which our data are not representative. However, it is clear that if after a fire there is a subsequent rain event, this could cause high increases in DSi export and strong disturbances of

ecosystem Si fluxes. The magnitude of these changes will be determined by the ecosystem hydrology and precipitation. Furthermore, the organic soil material type, the lithology and the presence of minerals in the soil, as well as burning severity, will play an important role in the ecosystem Si balance. Our data fit into the emerging view that the terrestrial silica cycle can be out of steady state (Carey and Fulweiler, 2012; Frings et al., 2014a). Further studies about Si biogeochemistry will help to better understand the effects of fire on terrestrial Si fluxes and the total Si exported from soils to the adjacent aquatic environment.

Chapter 3

Land use change affects biogenic silica pool distribution in a subtropical soil toposequence

This chapter is based on:

Unzué-Belmonte, D., Ameijeiras-Mariño, Y., Opfergelt, S., Cornelis, J.-T., Barão, L., Minella, J., Meire, P. and Struyf, E., 2017. *Solid Earth* 8, 737-750.

3

Land use change affects biogenic silica pool distribution in a subtropical soil toposequence

3.1. Introduction

The terrestrial Si-cycle has received increased attention in the past two decades. Multiple studies show its complexity, with a strong interaction among primary lithology and weathering, biotic Si uptake, the formation of secondary pedogenic phases and environmental controls such as precipitation, temperature and hydrology (Struyf and Conley, 2012). Lithology controls the primary source of Si through the weathering of silicate minerals of the bedrock (Drever, 1994). This process provides Si to the soil solution in the form of monosilicic acid (H_4SiO_4), also referred to as dissolved silicon (DSi). This DSi is taken up by plants and, is resupplied to the soil in the form of relatively soluble (compared to crystalline silicates) biogenic silicates (BSi) upon plant die-off, usually in the form of phytoliths (plant silica bodies) (Piperno, 2006). Biogenic silica is one of the most soluble forms of Si in soils (e.g. Van Cappellen, 2003), although some pedogenic compounds have similar reactivities (Sauer et al., 2006; Sommer et al., 2006; Vandevenne et al., 2015a). During soil formation, the DSi released to the soil solution through the dissolution of lithogenic and biogenic silicates contributes to the neoformation of pedogenic silicates, i.e. secondary phyllosilicates (Sommer et al., 2006). The biogenic control on the DSi availability in soil increases with

weathering degree. Soil mineralogy, strongly governed by geological and climatic conditions, therefore plays a key role in the DSi transfer from soil to plants (Cornelis and Delvaux, 2016). The complex interactions described above, that act to control the Si cycle in terrestrial ecosystems, are often referred to as the 'ecosystem Si-filter' (Struyf and Conley, 2012), and ultimately determine an important part of the Si fluxes towards rivers.

Land use change is a particularly interesting global change driver to address in this context. Dissolution of soil BSi increases immediately after deforestation (Conley et al., 2008), increasing DSi fluxes out of the soil and the ecosystem. However, in the long-term, Struyf et al. (2010) showed a decrease of overall DSi fluxes from cultivated land. The conversion from forest to croplands decreases the soil biogenic Si stock, the most important contributor to the easily available Si pool for plants. The decrease in soil biogenic Si stock has been related to two important factors. The first factor is the harvesting of crops (Guntzer et al., 2012b; Meunier et al., 1999; Vandevenne et al., 2012). Harvest prevents the return of plant phytoliths to the soil, depleting the phytolith pool. The resulting decrease of DSi availability also reduces the formation of non-biogenic secondary Si fractions (Barão et al., 2014). A thorough analysis separating both biogenic and non-biogenic fractions is crucial in this regard, since traditional extraction procedures to quantify biogenic Si may also dissolve non-biogenic Si fractions. The second factor affecting BSi losses is erosion. In cultivated catchments, preferential BSi mobilization is associated with erosion during strong rainfall events (Clymans et al., 2015b). During such events, biogenic Si can represent up to 40% of the easy-soluble Si inputs to rivers (Smis et al., 2011). Clymans et al., (2015) found that Si mobilization did not depend on tillage technique or crop type but solely on soil loss rate due to erosion.

While it is now accepted that cultivation can cause significant changes in soil Si pools and Si fluxes in temperate climates (Keller et al., 2012), the effect of cultivation on (sub)tropical soil Si pools or on soils of volcanic origin is poorly known. Only specific ecosystems, such as rice fields, have been studied (Guntzer et al., 2012b) in this regard. Yet, the increasing demand for

firewood, timber, pasture and food crops is causing an increase in land conversion to croplands, implying ongoing rapid land degradation in tropical and subtropical forests (Von Braun, 2007; Hall et al., 1993). The aim of our study was to investigate the interactive effects of land use change and terrain slope (as a proxy for erosion) on the distribution of the BSi pool in a subtropical soil system derived from a basaltic parent material. For this purpose, we studied terrestrial Si pools in a natural forest and cultivated land, in gently and steeply sloped locations, applying a recently developed alkaline extraction technique that permits the biogenic and non-biogenic phases to be distinguished.

3.2. Methods

Study area

The study area is situated near Arvorezinha, in the south of Brazil (28°55''54.88" S, 52°6''33.65" W) (**Figure 3.1**). Four sites with identical climatic conditions (warm temperate, fully humid with warm summer, Cfb, (Kottek et al., 2006) were selected. Annual mean temperature is between 14 and 18°C and annual mean precipitation between 1700 and 1800 mm (Minella et al., 2014)).

The four sampling sites also have the same parent material (rhyodacite). The mineralogy was similar in all sites with sanidine and quartz as the main minerals (Ameijeiras-Mariño, 2017). Soil type corresponded to an Acrisol in three of the sites and a Leptosol (IUSS Working Group WRB, 2015) in the fourth (steep slope of the cropland), with pH values between 4.7 and 5.9. They represent two land uses, a well conserved forest and a cropland, and two slope steepnesses (a steep and a gentle slope), resulting in four different factor combinations (see **Figure 3.2**).

The forest site consists of a semi-deciduous forest with *Araucaria angustifolia*, *Luehea divaricata*, *Nectandra grandiflora* and *Campomanesia guaviroba* as the dominant species. Within the same forest area, two adjacent sites with different slopes were chosen, a gentle slope (maximum 10°) and a

steeper slope (maximum 18°). On the gentle slope, some scattered small patches of Yerba mate crop (*Ilex paraguarensis*) were recently planted (<3 years ago), occupying less than 10 % of the study site. All studied sampling locations were separated at least 5 meters from these mate patches.

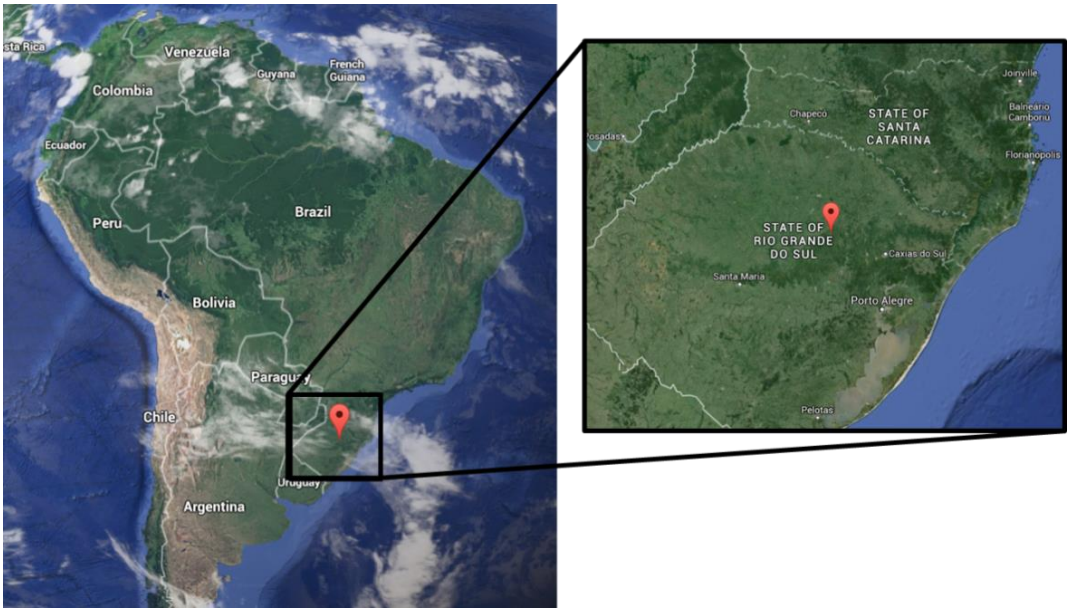

Figure 3.1. Location of study site.

The cropland sites were located in two geographically separated areas, 1.4 km apart. Deforestation occurred around 50 years ago and they have since experienced the same historical agricultural practices. Intensive soil tillage occurred from the time of deforestation to 2003, since when a cover cropping and a minimum tillage practice was introduced (Minella et al., 2014). The actual soil tillage is traditional, based on topsoil mixing and making ridges and furrows. Crops in the gently sloping cropland (maximum 7°) rotate between soybean (*Glycine max*) in summer and black oat (*Avena sativa*) in winter. Some cattle occasionally graze during the vegetative stage, and after the oat is harvested the biomass is left to produce mulch (cover) to soybean seeding based on the no-till system. The cropland of the steep slope (maximum 18°) rotates between tobacco (*Nicotiana sp.*) or maize (*Zea mays*) in summer and fallow or black oat in winter. The winter crop on this slope is also left behind to produce cover for the next crop.

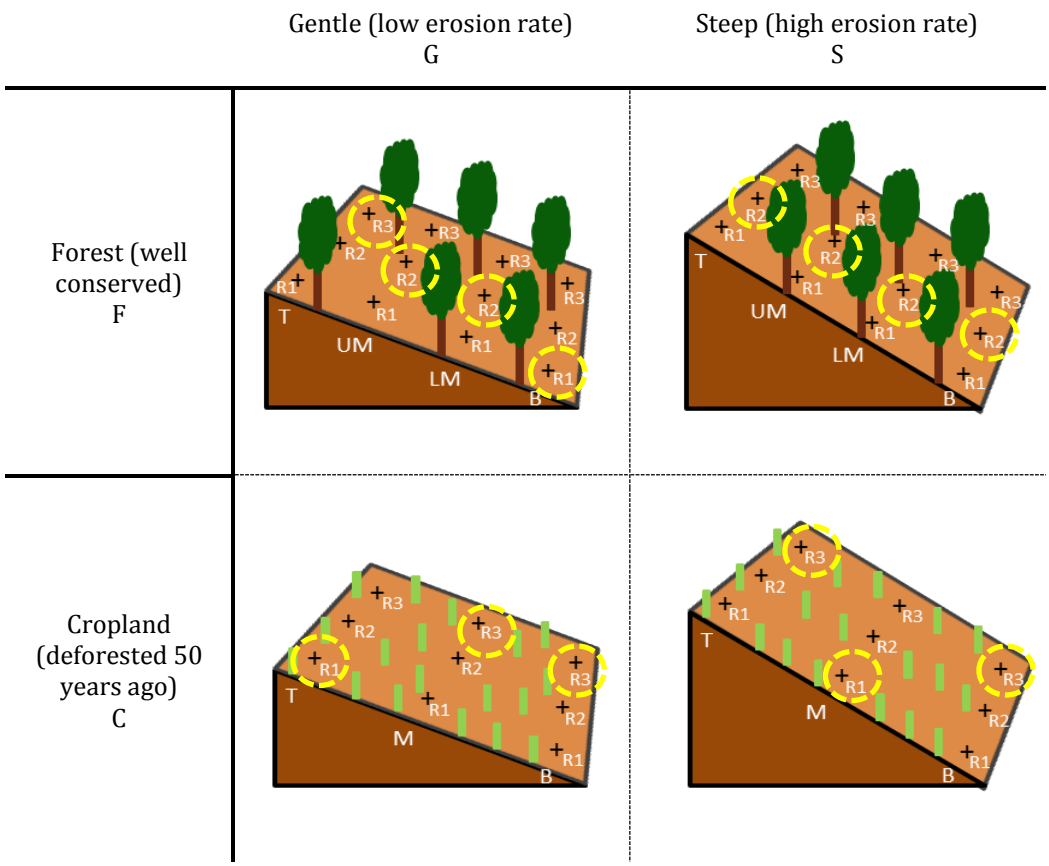

Figure 3.2. Diagram of the studied sites and the acronyms used in the text ordered by ecosystem (F=Forest, C=Cropland), slope (G=Gentle, S=Steep), position (T=Top, UM=Upper middle, LM=Lower middle, M=middle, B=Bottom) and replicate (R1=Replicate 1, R2=Replicate 2, R3=Replicate 3). Plus signs represent sampling points and yellow circles the selected pits.

Soil sampling

Bulk soil samples (n=297) were collected during the summer of 2014. In the forest sites, 4 positions along the slope (from top to bottom) were selected. In the croplands, due to time constraints during the field campaign, only 3 positions along the slope (from top to bottom) were selected. Three replicate soil pits were dug per position and soil samples were collected every 10 cm (from top to 50 cm deep) and every 20 cm (from 50 to 110 deep) (**Figure 3.2**). Deeper depths were sampled every 50 cm until 200 cm deep or until the saprolite was reached. At each depth, 10 cm of soil (around 2 kg) was collected. At larger sample intervals, the 10 cm sample was collected in

the middle of the depth interval. Soil samples were mixed, dried (~40°C), gently crushed and sieved (2 mm) prior to analysis.

Kopecky ring samples were also collected at each sampled depth. Samples were weighted before and after drying at 105°C in order to calculate bulk densities.

Analyses

One pit per position was selected as a representative pit due to the impossibility of carrying out the novel alkaline extraction analyses on such a high number of samples (297), resulting in a total of 81 samples. The selection avoided pits containing large inclusions (visually) or pits shallower than the other two replicas. The acronyms and selected pits are shown in **Figure 3.2**.

Physicochemical analyses

A portion of the bulk samples was crushed and a sub-sample was heated at 105°C and 1000°C to obtain the dry weight and the loss on ignition. The total element content was obtained through borate fusion (Chao and Sanzolone, 1992) of another sub-sample of the crushed sample; 100 mg were fluxed at 1000°C for 5 min in a graphite crucible with 0.4 g Li-tetraborate and 1.6 g Li-metaborate, then cooled and dissolved in 100 ml of 2M HNO_3 under magnetic agitation at 90–100°C. Elemental contents were determined by Inductively Coupled Plasma-Atomic Emission Spectrometry (ICP-AES); the total reserve of bases (TRB=[Ca]+[Mg]+[K]+[Na]) was calculated afterwards. TRB is commonly used as a weathering index as it estimates the content of weatherable minerals (Herbillon, 1986).

Particle size distribution was executed with a Beckman Coulter device (LSTM-13320) to quantify the sand (2mm-50µm), silt (50µm-2µm) and clay (<2µm) fractions.

The mineralogy of sand and silt fractions was determined by powder X-ray diffraction (XRD, Cu Ka, D8). Clay fraction mineralogy was assessed by XRD

after K^+ and Mg^{2+} saturation, ethylene glycol solvation and thermal treatments at 300 and 550°C (Robert and Tessier, 1974).

Alkaline continuous extraction

All samples from selected pits (n=81) together with some additional depths from other pits, were analyzed for biogenic and non-biogenic Si content, resulting in a total of 145 bulk soil samples (84 on the forest sites and 61 on the croplands). Samples were analyzed in a continuous flow analyzer (Skalar, Breda, the Netherlands), using a continuous alkaline extraction recently adapted for soils by Barão et al. (2014). The extraction in 180 mL of 0.5 M NaOH, at 85 °C runs for half an hour. Dissolved Si and dissolved aluminum (Al) are measured continuously (with the spectrophotometric molybdate blue method and the lumogallion fluorescence method, respectively), obtaining two dissolution curves which are fitted with first order **Eq. (1)**.

$$\mathrm{Si}_t\ (mg\ g^{-1}) = \left(\sum_{i=1}^{n} \mathrm{AlkExSi}_i \times \left(1 - \mathrm{e}^{-\mathrm{k}_i \times t}\right)\right) + \mathrm{b} \times t \qquad \textbf{(1)}$$

$$\mathrm{Al}_t\ (mg\ g^{-1}) = \left(\sum_{i=1}^{n} \frac{\mathrm{AlkExSi}_i}{\mathrm{Si/Al}_i} \times \left(1 - \mathrm{e}^{-\mathrm{k}_i \times t}\right)\right) + \frac{\mathrm{b} \times t}{\mathrm{Si/Al_{min}}}$$

where Si_t and Al_t are the concentrations of Si and Al respectively, at any given time. The equations consist of two parts: the mineral fraction which has a linear dissolution behavior (DeMaster, 1981; Koning et al., 2002) and the fractions exhibiting non-linear dissolving behavior. For the mineral fraction, the model renders a linear dissolution rate (b) and the Si/Al ratio (Si/Al_{min}) of that linear fraction. Non-linearly dissolving fractions are characterized by: the total amount of Si (alkaline extractable Si (AlkExSi), mg g^{-1} dry weight of initial sample mass), the Si/Al ratio (concentration of Si over concentration of Al) of that fraction and its dissolution rate (k, min^{-1}). Assuming the same Si and Al release rate from the same compound and relating the Si and Al concentration equations through the Si/Al ratio, with the three parameters

estimated (AlkExSi, k and Si/Al ratio) the different fractions dissolving non-linearly are distinguished. The same model is fitted with one, two or three first order equations (summation to n in the formula) and the solution showing least error (F test) from the three fits is kept. For the non-linear fractions, the Si/Al ratio of the fraction is used to determine its origin. Barão et al. (2014) recognised the following fractions: fractions showing Si/Al ratio >5 was considered as indicative of a biogenic fraction, as the concentration of Al in phytoliths is low (Bartoli, 1985; Piperno, 2006). A fraction showing a Si/Al ratio <5 was considered as representative of non-biogenic or pedogenic Si fractions (clay minerals, oxides and organo-Al complexes). We opted to discard fractions that represent less than 0.1 mg Si g^{-1}, as they are smaller than or equal to the detection limit of the method (Barão et al., 2015). Fractions with k<0.1 were also discarded, as they represent near linearly dissolving fractions.

Post-data treatments.

AlkExSi pools or stocks every 10 cm depth (kg Si m^{-2}) for selected pits were calculated according to **Eq. (2)**.

$$AlkExSi\ stock\ (kg\ Si\ m^{-2}) = \frac{[AlkExSi] \times BD \times h}{100} \qquad \textbf{(2)}$$

where [AlkExSi] is the concentration (mg g^{-1}) obtained in the alkaline continuous extraction, BD is the bulk density (g cm^{-3}) of that sample, h is the thickness of the depth interval of the sample (cm) and 100 is a conversion factor from mg cm^{-2} to kg m^{-2}. This calculation takes into account the bulk density of each sample, correcting the amount of AlkExSi per gram of dried soil according to the water content at that specific soil depth. It also calculates the amount of AlkExSi in relation to the thickness of the interval collected (10 cm). For larger intervals, where only 10 cm was collected at mid-interval depth, values of the non-sampled depths were linearly interpolated between two known values. The result is given in kg per square meter, in our case, at 10 cm deep intervals.

In order to estimate the total biogenic and non-biogenic AlkExSi pools per pit, the sum of all 10 cm-depth biogenic and non-biogenic AlkExSi pools of each pit was made.

Once having the biogenic and the non-biogenic AlkExSi pools per pit, averages between the 3 (for the croplands) or 4 (for the forests) selected pits were made, in order to assign average biogenic and non-biogenic AlkExSi pool values to the slope and to be able to compare AlkExSi pools between different sites. Then, comparisons between the different study sites were made. In order to compare the biogenic and non-biogenic AlkExSi pools from the forests with the croplands, two different methods were considered, taking into consideration that the number of positions along the slope in the forest sites is higher than in the cropland sites (4 and 3 respectively): Average 1 using all available measurements for the forest (the 4 positions along the slope) and cropland sites, and Average 2, using a pre-calculated average between upper and lower middle positions measurements in the forest sites.

To study the accumulation of biogenic and non-biogenic AlkExSi pools at the bottom of the slope we have calculated the Accumulation (AC) using the pool in the bottom compared to the summed pools along the slope for the forests (**Eq. (3)**) and the croplands (**Eq. (4)**). The closer the AC value is to 100%, the higher the accumulation results.

$$AC_{Forest} = \frac{AlkExSi_{bottom}}{AlkExSi_{top}+AlkExSi_{upper\ middle}+AlkExSi_{lower\ middle}+AlkExSi_{bottom}} \times 100 \quad \textbf{(3)}$$

$$AC_{Cropland} = \frac{AlkExSi_{St-bottom}}{AlkExSi_{top}+AlkExSi_{middle}+AlkExSi_{bottom}} \times 100 \quad \textbf{(4)}$$

Statistical differences between biogenic AlkExSi pool averages for top pits, middle slope pits, bottom pits and differences between biogenic AlkExSi pool averages from the top pit and the bottom pit within the same slope were tested pair by pair for significance at the 5% level confidence using a Student t-test assuming unequal variances.

3.3. Results

Soil physico-chemical characteristics

Results from total element content, particle size, bulk density and TRB values for selected pits are shown in **Tables S3.2-S3.4**. The XRD mineralogical analysis of the bedrock (rhyodacitic volcanic rocks) reveals that sanidine (feldspar group) is the most abundant mineral (45-55%), followed by very fine grained quartz (~38%) embedded in a matrix of hematite, goethite and clays (~8%) (Ameijeiras-Mariño, 2017). Bulk densities of selected pits ranged from 0.7 to 1.54 mg cm^{-3}.

AlkExSi concentrations

AlkExSi values (mg g-1 dried soil) with the corresponding k values and Si/Al ratio per fraction are presented in **Table S3.1.** In order to distinguish fractions according to the Si/Al ratio, the thresholds applied by Barão et al. (2014) were used: fractions showing Si/Al ratios above 5 were considered to be biogenic and fractions showing Si/Al ratios below 5 were considered to be non-biogenic fractions.

Figure 3.3 shows the concentrations of biogenic (Si/Al > 5) and non-biogenic AlkExSi fractions (Si/Al < 5) within the soil profiles of selected pits. Overall, the highest concentrations of biogenic AlkExSi appear in the top of the profiles or near the surface and decrease with depth. Biogenic AlkExSi is also more abundant at the bottom positions of the slopes. On the other hand, non-biogenic AlkExSi fractions are generally absent in the top soil layers and increase in concentration with depth.

AlkExSi pools

The biogenic and non-biogenic AlkExSi pools of selected pits at 10 cm intervals are presented in **Table S3.5**.

Figure 3.4 shows the biogenic and non-biogenic AlkExSi pools as a soil profile cut from the top to the bottom of the slope, for the four study sites.

The averages of biogenic and non-biogenic AlkExSi pools per position, land use and slope are shown in **Table 3.1**. As mentioned, another averaged AlkExSi pools were calculated when comparing forest to cropland ('Average 2' in **Table 3.1**). The pre-calculated average between the upper middle and lower middle position was used in the calculation for 'Average 2' (**Table 3.1**) (i.e. values used for the gentle slope 'Average 2' calculation were: 16.7 (top), 16.1 (middle) and 6.79 (bottom) kg m^{-2}). While the gentle and the steep slope of the forest showed near equal biogenic AlkExSi pools (+10% for the steep slope), non-biogenic AlkExSi pool might be higher on the steep slope (+81% for the steep slope).

In the cropland, results were slightly different. Both AlkExSi pools were higher on the gently sloped cropland (+35% for the biogenic AlkExSi pool and +85% for the non-biogenic AlkExSi pool).

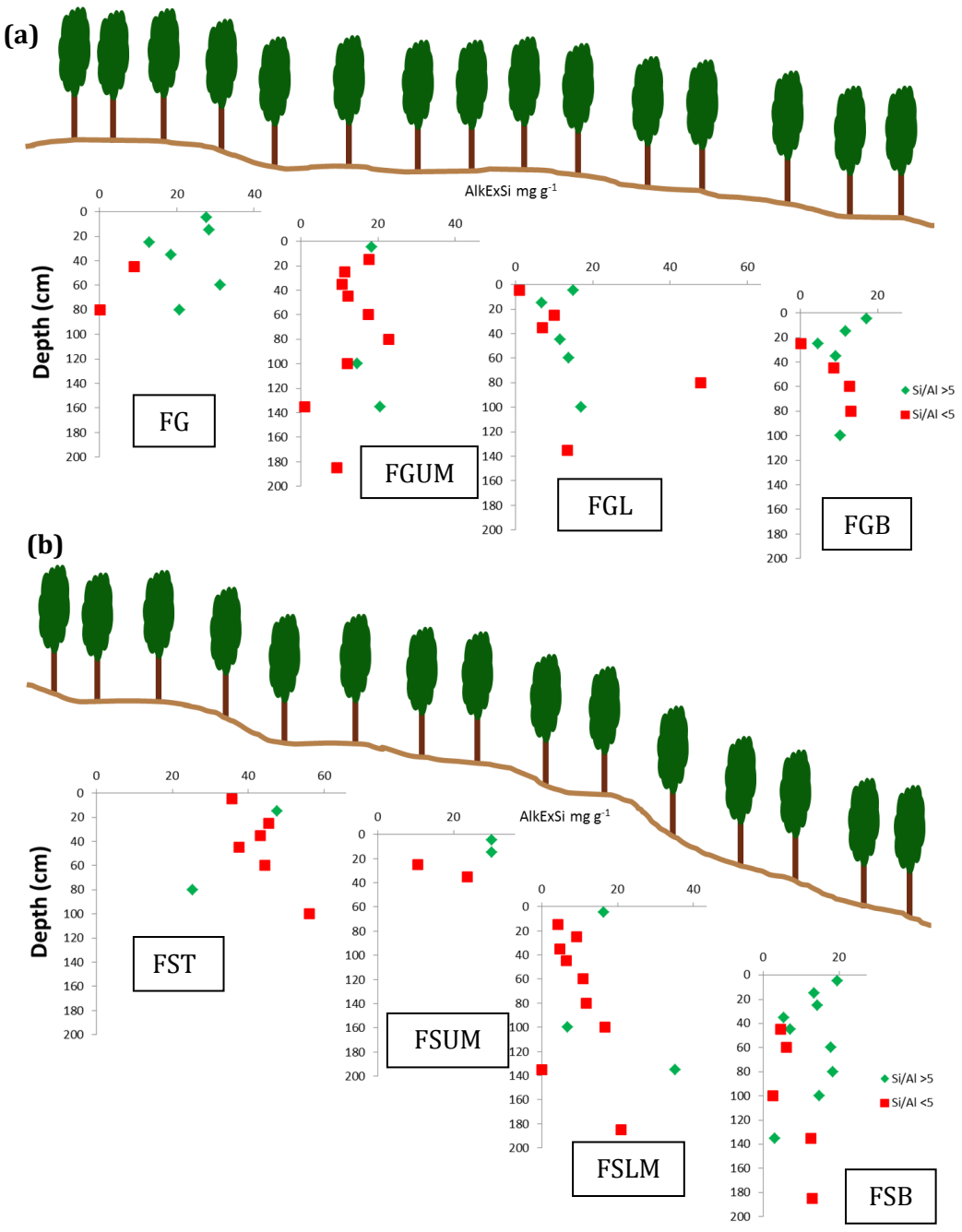
(a)
AlkExSi mg g-1
Depth (cm)
FG
FGUM
FGL
FGB
Si/Al >5
Si/Al <5
(b)
AlkExSi mg g-1
Depth (cm)
FST
FSUM
FSLM
FSB
Si/Al >5
Si/Al <5

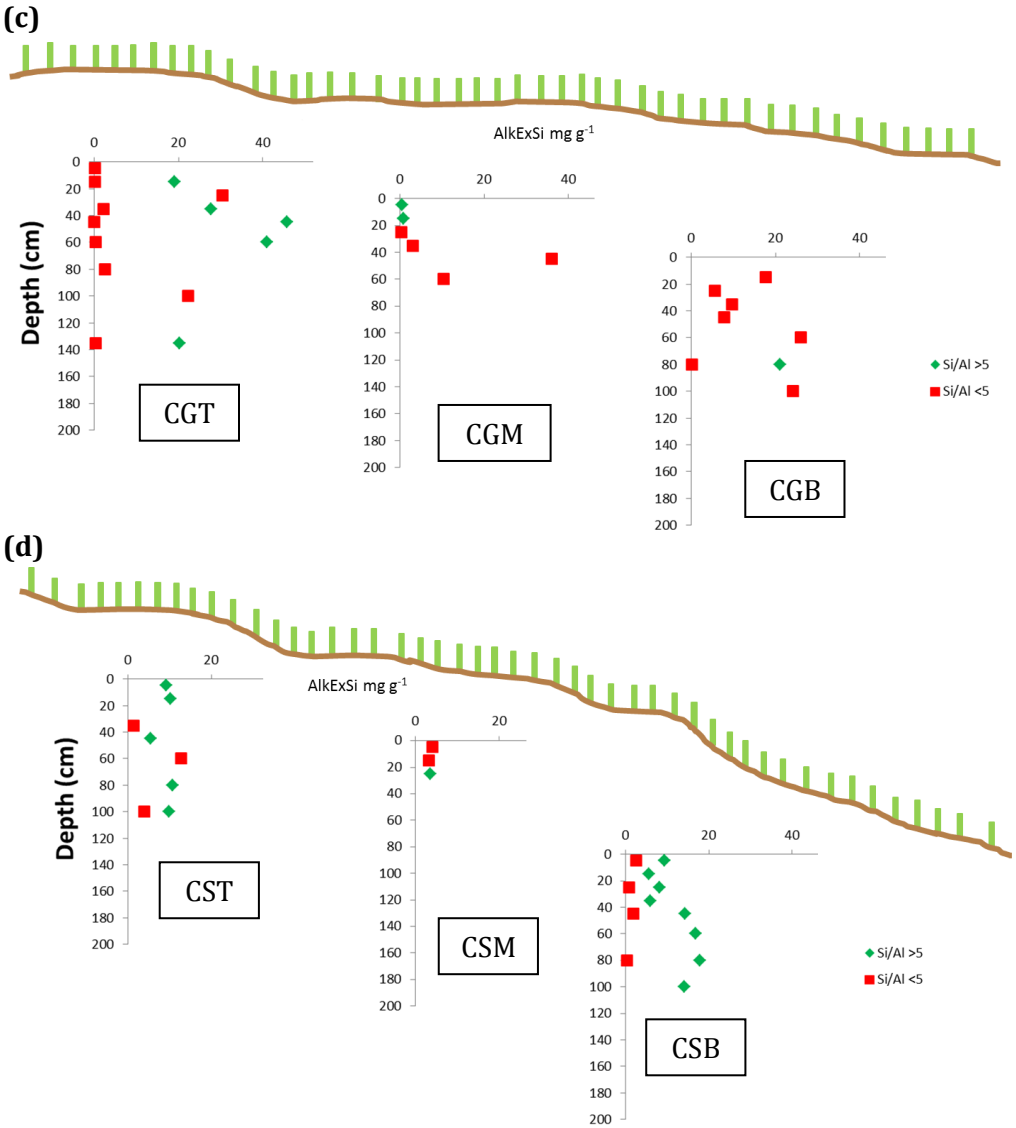

Figure 3.3. Biogenic and non-biogenic AlkExSi concentrations (mg g^{-1} dried soil) from selected pits of the sites studied: a) Gentle slope of the forest, b) Steep slope of the forest, c) Gentle slope of the cropland and d) Steep slope of the cropland. Graphs from left to right: Top, upper middle, lower middle (or middle) and bottom pit.

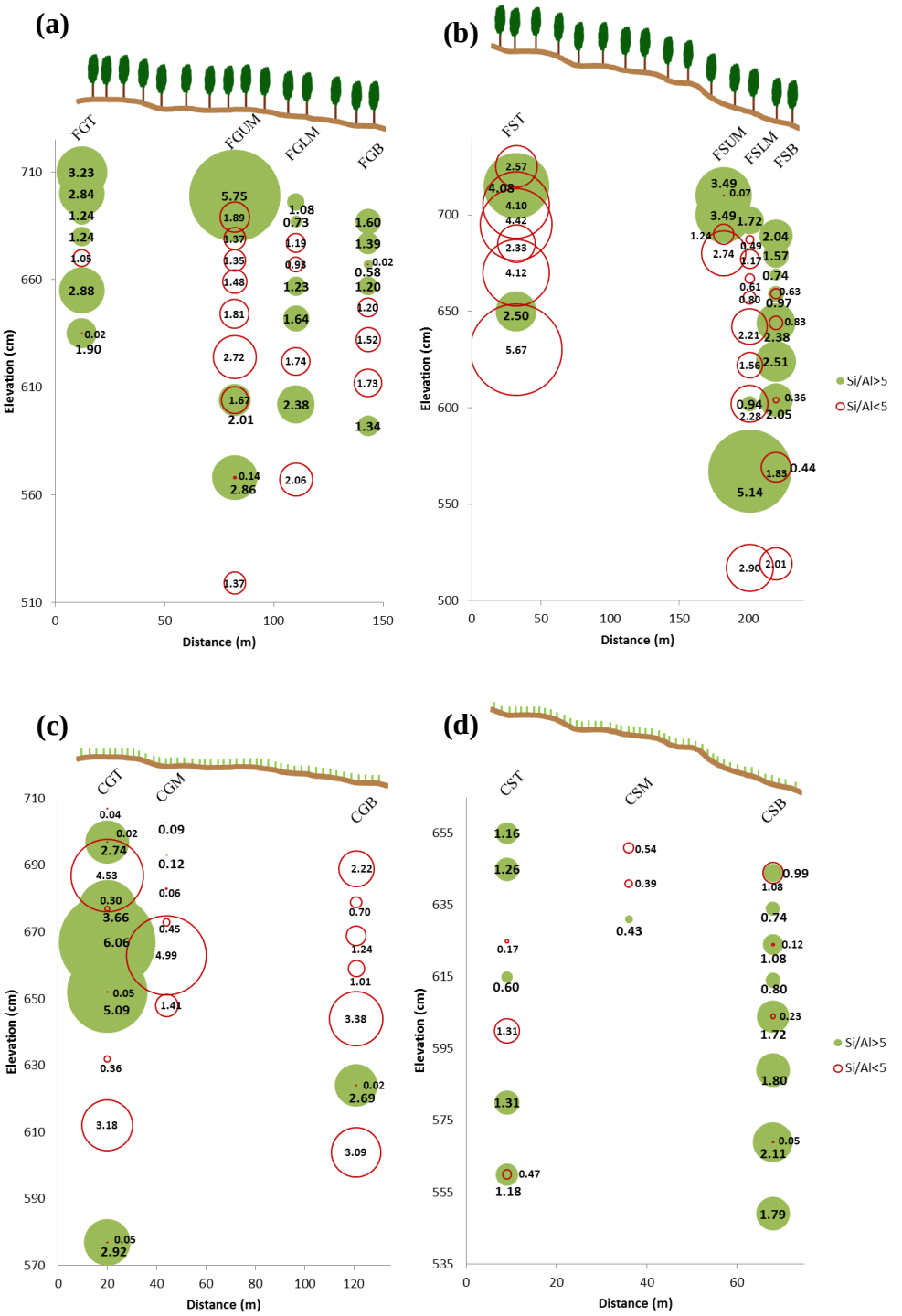

Figure 3.4. Biogenic and non-biogenic AlkExSi pools (kg m-2) in the studied sites: a) Gentle slope of the forest (FG), b) steep slope of the forest (FS), c) gentle slope of the cropland (CG) and d) steep slope of the cropland (CS). Green bubbles represent biogenic AlkExSi pools. Red empty bubbles represent non-biogenic AlkExSi pools. Labels show values of the pools (kg m-2). Note that the x scales are different.

When comparing gently sloped forest and cropland (using 'Average 2' for forests), there was only a small difference for biogenic AlkExSi pool (-12% for the cropland), but non-biogenic AlkExSi might be higher in the cropland (+57% for the cropland).

On the steep slopes, it was clear that both AlkExSi pools were much lower in the cropland compared to the forest (-53% for the biogenic AlkExSi pool and -90% for the non-biogenic AlkExSi pool).

The sum of the AlkExSi pools of selected pits per land use and slope, are shown in the **Table 3.1** ('Total (Sum)'). The accumulation of the biogenic and non-biogenic AlkExSi pools at the bottom position of each slope is also shown in **Table 3.1**. Both steep slopes clearly showed higher accumulation of both pools at the lowest position than the gentle slopes with the exception of the non-biogenic AlkExSi pool in the steep slope of the cropland.

Pairs showing significant differences are represented with the same letter in **Table 3.1**.

3.4. Discussion

One of the most striking observations in our study is the interaction between slope and land use effect. On the steep slope, there is a decrease of AlkExSi pools from forest to cropland. In contrast, the gentle slopes had similar biogenic AlkExSi pools. It is also clear that there is redistribution of biogenic AlkExSi towards the bottom positions of the slope on steeply sloped croplands and forests.

Redistribution of AlkExSi concentrations in depth and along the toposequence

In general, the distribution of biogenic AlkExSi shows the same pattern within each pit: the concentration decreases with depth and highest concentrations are found at the bottom of the slope (with the exception of the gentle slope of the cropland). This agrees with earlier observations on the

distribution of BSi along a toposequence in several soil catenas from temperate areas (Saccone et al., 2007). The distribution of non-biogenic AlkExSi shows a complementary pattern. Non-biogenic AlkExSi fractions are rarely present at the top of the profiles but higher concentrations are found in deeper layers. Similar patterns were reported in a study carried out in arkosic sediment soils in California (Kendrick and Graham, 2004) and for temperate Luvisols in Belgium and Sweden (Barão et al., 2014; Vandevenne et al., 2015a). Upon leaching of DSi after BSi dissolution, the DSi infiltrates and reacts to form e.g. secondary clays. It can also be adsorbed onto oxides. The rate of adsorption of DSi by oxides is determined by water infiltration rate, pH, water residence time and weathering intensity (Cornelis et al., 2011a; Jones and Handreck, 1963). A large amount of oxides in soil (see 'Mineralogy' in **Table S3.4**), high DSi supply, strong water infiltration rates and high pH may result in larger concentrations of Si absorbed by oxides. Our studied sites satisfy these conditions with the exception of the pH (4.7-5.9). Uehara and Gillman (1981) suggested that weathered soil systems can result in a desilicated soil enriched in Fe and Al oxides, with pH close to neutral values. Similar processes might occur in our soils, although they are not desilicated, but do show a high weathering intensity.

Biogenic Si concentrations from Vandevenne et al. (2015a) in temperate Luvisols were one order of magnitude lower than in our study. The high silica content of the rhyodacite bedrock in our study sites, together with high weathering rates characteristic of tropical and subtropical soils (Drever, 1994), supply a large amount of DSi to the soil. In addition, weathering stimulated by plants is particularly strong in the tropics (Blecker et al., 2006; Kelly et al., 1998);turnover rates of nutrients are also higher in tropical and subtropical ecosystems than in temperate regions (Alexandre et al., 1997; Derry et al., 2005), due to high water availability and temperature. Meunier et al. (2010) showed that the DSi supply from the dissolution of basalts was 1.8 times higher than the DSi produced from the dissolution of the litter in a Leptosol of La Réunion Island (Indian Ocean).

Table 3.1. Biogenic and non-biogenic AlkExSi pools (kg Si m-2), of the selected pits, for the two ecosystems (forest, cropland), for the different slopes (gentle, steep), along different positions along the slope (top, upper middle, lower middle and bottom). Total (sum), Average 1 (Averaged pool between all selected pits) and Average 2 (for the forest sites: Averaged pool between top, pre-calculated average between the upper middle and the lower middle pit (i.e. for the biogenic AlkExSi pool of FG: 16.1 kg Si m-2) and bottom pits) of biogenic and non-biogenic AlkExSi pools per site. Accumulation of the biogenic and non-biogenic AlkExSi pools (see Eq. (3) and (4)). Averages by row showing the same letter are statistically different ($p<0.05$). *Difference between the top and the bottom pit averages from that slope is statistically significant ($p<0.05$). †Statistical comparison between middle position between forest sites and cropland sites were calculated taking the two middle pits (Upper and Lower middle) for the forests.

	Forest				Cropland			
	Gentle		Steep		Gentle		Steep	
	Biogenic	Non-biogenic	Biogenic	Non-biogenic	Biogenic	Non-biogenic	Biogenic	Non-biogenic
Top	17.6^{a}	1.32	9.06	31.0	30.7^{b}	15.0	7.50^{ab}	3.25
Upper middle	19.3†^{ab}	22.1	6.98†^{cd}	3.98	0.21^{ad}	8.50	0.43^{bc}	0.93
Lower middle	12.9	10.3	25.8	25.7				
Bottom	6.79^{ab}	7.63	24.8^{ac}	20.3	5.38^{cd}	16.0	15.8^{bd}	0.80
Total (Sum)	56.6	41.3	66.6	81.0	36.3	39.5	23.8	4.97
Average 1	14.2 ± 5	10.3 ± 7.6	16.6 ± 8.7	20.3 ± 10	12.1 ± 13	13.2 ± 3.3	7.92 ± 6.3	1.66 ± 1
Average 2	13.5 ± 5	8.4 ± 6.1	16.7 ± 6	22.1 ± 6.7				
Accumulation	12%*	18%	37%	25%	15%*	41%	67%*	16%

Effects of erosion and land use change on the biogenic AlkExSi pool along the toposequence

For cropland, it is well documented that the harvest of crops exports large amounts of BSi from the system. This generates BSi depleted systems in the long-term (e.g. Vandevenne et al. 2015b). Results from Clymans et al. (2011) in long-term croplands from Sweden showed a BSi pool reduction of 10% compared to a forested system.

Guntzer et al. (2012) showed the importance of crop rotation in the turnover and accumulation of phytoliths in soil. The accumulation of phytoliths is also influenced by the geochemical stability of phytoliths (Song et al., 2012). However, the crops rotating in both fields are different and have different Si-demands. Maize and black oat are known to have high Si content, while tobacco and soy do not (Currie and Perry, 2007; Piperno, 2006). The

turnover between maize/tobacco and fallow/black oat on the steep slope might be an explanation for the smaller biogenic AlkExSi pool at this site. Moreover, the higher erosion rate increases the biogenic AlkExSi deposition at the bottom of the steeply sloped cropland. In fact, the TRB in this slope was higher than at any of the other sites (the lower the TRB, the more weathered the soil is, or vice versa - the higher the TRB, the closer the soil is to the composition of the bedrock) suggesting that all weathered material has been already eroded and the saprolite is closer to the surface.

It is interesting to notice that a redistribution of biogenic AlkExSi occurs along the slope (**Figure 3.4**). A higher slope degree, and thus higher erosion rate, provokes the loss of material through water erosion and tillage (Govers et al., 1996), transporting material down slope and resulting in an accumulation of the biogenic AlkExSi pool at the bottom of the slope. In the gently sloped sample site, biogenic AlkExSi is more stable at the higher positions of the slope while in the steep slope it accumulates at the bottom.

The biogenic AlkExSi pool in the gentle slope of the forest was ~14 kg Si m^{-2}. A high rate of phytolith production in this forest, corresponding to a high Si demand from trees and efficient internal recycling, can maintain the BSi stock of the soil system. Ferrasols in Congolese equatorial forests had a phytolith pool five times smaller than the present results (2.66 kg m^{-2} in Alexandre et al. (1997)) and in results from Clymans et al. (2011), the amorphous silica pool from temperate forests in Sweden was close to half our observations (6.7 kg m^{-2}).

The biogenic AlkExSi pool was not enriched at the lowest position of the gently sloped forest. This suggests that the physical erosion at this site is low. A study carried out in the same forest fields showed a denudation rate of 0.5 ± 0.6 mm kyr^{-1} in the gentle slope and a 5.6 ± 2.9 mm kyr^{-1} in the steep slope (Schoonejans et al., 2017). In the steeply sloped forest, higher erosion rate apparently did provoke the physical loss of biogenic AlkExSi, potentially decreasing the amount of Si recycled by the vegetation. BSi is consequently transported to the bottom of the slope before it can dissolve and be recycled

by plants, resulting in an accumulation of BSi at the bottom of the slope (AC of 37%). However, this apparent effect is not statically confirmed probably due to the strong variability of biogenic AlkExSi pools within the top and the bottom pits in the steep sloped forest. Larger biogenic AlkExSi pools are also found at the lower middle position, which suggests that the accumulation of eroded material also occurs at the lower-middle slope. Both (lower-middle and bottom) pits together accumulate the 76% of the total biogenic AlkExSi pool of the slope. These deposition zones could serve as a location for permanent BSi storage.

The average biogenic AlkExSi pool size followed the sequence: FS > FG > CG > CS. Overall, cropland gentle and steep slopes had 10% and 53% lower biogenic AlkExSi pool, respectively, compared to well-conserved forest. This loss of biogenic AlkExSi has previously been described in other studies. Vandevenne et al. (2015b) showed similar results for temperate Belgian Luvisols, where croplands showed a decrease of total biogenic AlkExSi of 35% compared to the temperate forest. Results from Clymans et al. (2011) support the same pattern, showing smaller AlkExSi pools in cultivated systems in Sweden. Our results are apparently in contrast with results from Struyf et al. (2010) who showed a large reduction in DSi export after deforestation in croplands deforested >250 years ago. Nevertheless, the absence of a larger decrease in the gently sloped cropland may indicate that deforestation occurred too recently to see such a decrease, only triggered by harvest. Opfergelt et al. (2010) found phytoliths from the previous forested system in croplands of Cameroon deforested in the early 50s. However, top and bottom positions do not differ statistically between the cropland and its forest counterpart for any of the slopes. The difference relies only on the mid-positions where erosion is higher (Doetterl et al., 2015), highlighting the importance of erosion as an added factor, as a consequence of the agricultural tillage (Govers et al., 1996).

A depletion of >50% is seen at the steep slope of the cropland compared to its forested counterpart. Although it has been shown that an increase in erosion rate occurs after the conversion from forests to croplands (Vanacker

et al., 2014) and this may affect both croplands, Montgomery and Brandon (2002) described how the erosion rate depends directly on the slope and stressed the importance of landslides. The consequence is an increase of the accumulation of biogenic AlkExSi pool at the bottom of the steep slope of the cropland (AC of 67%).

Importance of scales and methods

The present study clearly shows how deforestation may have a strong impact on the silica cycling in subtropical soils under steep slopes, and potentially also on gentler slopes in the long-term. The croplands in earlier studies, e.g. Vandevenne et al. (2015b), had usually been cultivated for more than 200 years, and BSi depletion was explained as a result of long-term cultivation. However, the croplands in the present study were deforested 50 years ago, highlighting how fast the biogenic AlkExSi pool can be depleted from the soil system when physical erosion is high.

Our results confirm the importance of using a continuous extraction to determine BSi pools in soils (Barão et al., 2014). The non-biogenic AlkExSi fractions would have been determined as BSi if conventional alkaline extractions, applying only analyses during the linear phase of the extraction, had been used (i.e. adaptations of the method from DeMaster, 1981). We acknowledge that some difficulties still remain when applying the method we have used. The dissolution in NaOH does not show a true reactivity within soils: the non-biogenic AlkExSi fractions probably have lower solubility in soils (Ronchi et al., 2015) or water (Unzué-Belmonte et al., 2016) than BSi. Using the Si/Al ratio thresholds described for temperate soils to determine the character of the fractions in a different soil introduces some concerns. Without physical extraction we cannot verify that fractions showing specific ratios (below 5) correspond to the same pedogenic compounds as those found in temperate soils. The method is also unable to distinguish, among the Si/Al > 5 fractions, between phytoliths and opal A/CT. Under a silica saturated system, silica can precipitate in amorphous structures called Opal-A, that in further transformations could be transformed into Opal-CT and

finally microquartz (Chadwick et al., 1987; Drees et al., 1989). Opal deposits were identified at more than one meter deep layers in temperate pastures (Vandevenne et al., 2015b) and the tropics (Alexandre et al., 1997). Moreover, results from (Saccone et al., 2007) showed that the amounts of easy-soluble silica were larger in deeper horizons, agreeing with the possibility of having Opal-A at deeper layers in our systems. Despite some concerns, the method used allowed us to identify a new non-biogenic AlkExSi pool which might have been affected by land use and erosion as well.

Effects of erosion and land use change on the non-biogenic AlkExSi pool along the toposequence

The averaged total pool of non-biogenic AlkExSi followed the sequence: FS > CG > FG > CS. A study in Belgian Luvisols under long-term cropland management (Vandevenne et al., 2015a) showed a larger non-biogenic AlkExSi pool in the croplands relative to a forested site. The authors explained the result by the fact that the high Si-demand from the crops increases the weathering rate of the mineral phases, transforming low-solubility compounds into high-solubility ones (with the caveat that solubility is determined in NaOH). A combination of a relatively short time period since deforestation, and the increased demand for Si by the crops compared to forest species, could thus explain the larger non-biogenic AlkExSi pool in gently sloping cropland, compared to forests.

However, the non-biogenic AlkExSi pool of the steeply sloping cropland is almost non-existent. As with the biogenic AlkExSi pool, the high Si-demand by crops together with the higher erosion rate results in a complete depletion of the non-biogenic AlkExSi pool in the steeply sloped cropland.

The steeply sloped forest showed a larger non-biogenic AlkExSi pool, mainly accumulated at top and bottom positions (**Figure 3.4**). It is clear that the continuous long-term biogenic AlkExSi deposition at bottom positions (apparent also at the lower middle position) triggers the formation of new non-biogenic AlkExSi phases that correspond with lower TRB values. Weathering degree has previously been correlated to the amount of

pedogenic silica accumulation in sedimentary soils (Kendrick and Graham, 2004). Further, clay minerals and Si absorbed onto oxides were reported by Delvaux et al. (1989) and Opfergelt et al. (2009) respectively, to be largest at most weathered sites in a study carried out in volcanic soils from Cameroon.

Implications

We show how slope and land use change have strong interacting effects on the distribution of the AlkExSi pool in a subtropical soil. In general, our study agrees well with earlier findings in temperate climates: landscape cultivation diminishes soil BSi stocks. Even though deforestation occurred only 50 years ago, the biogenic AlkExSi pool in the steeply sloped cropland was only 50% of the pool in steeply sloped forests. In contrast, on the gentle slopes, no similar depletion was observed. This highlights the importance of erosion strength for the rate of depletion. To our knowledge, almost no studies have included slope as a potential factor (Ibrahim and Lal, 2014). It could therefore also be relevant to include erosion rates in studies of BSi in temperate ecosystems.

The presence of phytoliths from the past in soils helps to reconstruct former vegetation (Kirchholtes et al., 2015; Rovner, 1971). Here, we consider the biogenic Si pool as a single biogeochemical pool that is able to supply readily available DSi for plants. Although the presence of two Si pools within the plant is well documented (Fraysse et al., 2009; Watteau and Villemin, 2001) and different pools may show different solubilities, the higher solubility of phytoliths in soils compared to non-biological solid Si phases has been confirmed by several studies (Fraysse et al., 2006b; Lindsay, 1979; Ronchi et al., 2015; Sommer et al., 2013). Moreover, Alexandre et al., (1997) described how 92% of the BSi in top soil is rapidly recycled, while only 8% seems to be permanently stored due to a lower turnover.

The silicon and carbon cycles are closely related through the production of phytoliths. A recent study showed a positive relation between soil organic carbon (SOC) and amorphous silica content along a toposequence and along the depth profile (Ibrahim and Lal, 2014). However, a comparison between their results and ours is not possible due to the different methods used to

extract the silica fractions. The assumed tight relationship between both elements together with the SOC depletion (reported at 45%) after 11-50 years of conversion from forest to cropland (Wei et al., 2014), hints at similar mechanisms behind both observations. Some studies have indicated that silica could act as a 'carbon protector' through phytolith formation: carbon is occluded within the phytoliths and remains stored until they dissolve (Song et al., 2014). Although there are different opinions regarding this topic (Santos and Alexandre, 2017) some have suggested that atmospheric carbon sequestration could be enhanced through phytolith production and subsequent burial (Li et al., 2013; Parr et al., 2010; Song et al., 2016).

Our study highlights the accumulation of biogenic AlkExSi at deposition zones in croplands. Very little is known on the potential Si sink associated with such deposition zones, as little research has actually focused on Si biogeochemistry in these zones. Deposition of BSi here could be an important sink for Si in the long-term. As shown earlier in tidal marshes (Struyf et al., 2007), rapid accumulation of BSi can prevent its complete dissolution, resulting in long-term burial and removal from the global biogeochemical Si cycle.

Chapter 4

An alkaline continuous extraction to determine BSi content of biochars, soils and soil:biochar amendment mixtures

Dácil Unzué-Belmonte

This study was an integral part of the larger project: *Phytolith content in biochar affects the biological Si cycle in soil-wheat systems*. Cooperation with: Zimin Li , Jean-Thomas Cornelis and Bruno Delvaux.

My main role was the determination of BSi in complicated soil-soil amendment mixtures. This chapter focuses on the methodological application.

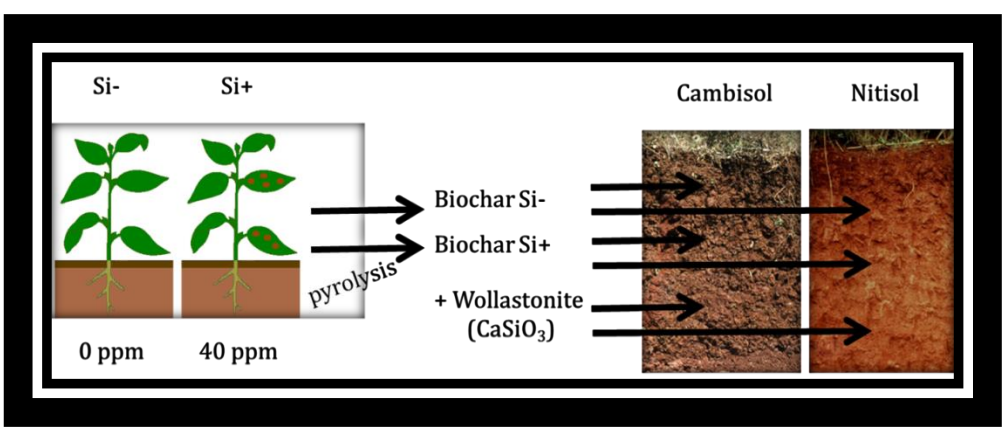

4

An alkaline continuous extraction to determine BSi content of biochars, soils and soil:biochar amendment mixtures

4.1. Introduction

The role of biota, especially plants, in terrestrial silicon (Si) cycle has drawn the attention of the scientific community in the last decades (Alexandre et al., 1997; Ma et al., 2001; Meunier et al., 1999). Although dissolved Si (aqueous $H_4SiO_4^0$, DSi) is released into the soil solution originally through mineral weathering, final DSi concentrations in soils are often governed by parallel biogeochemical processes, such as plant uptake, secondary mineral precipitation, DSi leaching and Si adsorption onto Fe and Al oxyhydroxides (Conley, 2002; Cornelis et al., 2011a; McKeague and Cline, 1963; Sommer et al., 2006). Si uptake by plants has been described as an important process affecting the biogeochemical Si cycle (Carey and Fulweiler, 2012; Hodson et al., 2005). After plant uptake, DSi is polymerized to form amorphous $SiO_2 \bullet nH_2O$ in plant cell tissues (Epstein, 1994; Piperno, 2006), often in the form of phytoliths, also referred to as biogenic silica (BSi). Phytoliths are more soluble than inorganic silicates (Fraysse et al., 2009), and can thus contribute to a large extent to DSi dissolution in soils, depending on

their abundance (Alexandre et al., 1997; Conley, 2002; Derry et al., 2005; Meunier et al., 1999). This biomineralization of Si in plants is considered an important reservoir in the global Si budget (Conley and Carey, 2015; Frings et al., 2014a; Trembath-Reichert et al., 2015), exerting an important control on soil Si biogeochemical cycling, by influencing DSi concentration in soil solution, especially in highly weathered soils (Cornelis and Delvaux, 2016; Henriet et al., 2008).

In croplands, the input of BSi to topsoils is disrupted by the harvest of the crops, when large amounts of phytoliths are exported from the system (Guntzer et al., 2012a; Keller et al., 2012). Phytolith removal results in Si depleted ecosystems in the long-term (Vandevenne et al., 2015a). As highly weathered soils are depleted in both lithogenic (LSi) and secondary pedogenic Si pools (PSi), the disruption of BSi recycling can result in low Si bioavailability (Cornelis and Delvaux, 2016). In tropical regions, a Si amendment is therefore often applied to sustain a cropping system.

Si is widely recognized to benefit plants through protecting against a range of biotic and abiotic stresses (Fauteux et al., 2005). Si application is estimated to increase wheat growth by 4.1–9.3%, and rice crops up to 17% in field experiments (Liang et al., 2015; Ma and Takahashi, 2002). The most common Si-fertilizers used are silicate slags and natural silicate minerals (Datnoff and Heckman, 2014). Yet, the solubility of these Si fertilizers and the possible release of toxic heavy metals into the soil often limit their use (Haynes et al., 2013). Wollastonite ($CaSiO_3$), a commonly used Si-fertilizer and also a liming material, is by far the most used inorganic fertilizer, due to its high solubility and absence of toxic components (Gascho, 2001). However, the finite occurrence of wollastonite, the extraction cost and its environmental consequences of its use forces the scientific community to look for alternatives to silicate minerals.

A potential alternative are biochars. Pyrolyzed biomass is already used as amendment and is known to increase biomass productivity by improving soil fertility in tropical and subtropical regions (i.e., organic carbon (OC), pH and

CEC), (Liang et al., 2006; Major et al., 2010). Whereas the impact of biochar incorporation on soil properties is the object of numerous publications (Sohi et al., 2010), the potential ability of biochars to enrich bioavailable Si in soil solution and the effect on the biological Si cycle is still poorly quantified. Although structural changes may occur to phytoliths after pyrolysis with temperature change (Xiao et al., 2014), several studies have confirmed their presence after pyrolysis (Houben et al., 2013). Moreover, phytolith solubility increases after burning (Unzué-Belmonte et al., 2016; Xiao et al., 2014). Dissolution of phytoliths in biochars could thus rapidly supply DSi into the soils (Houben et al., 2013) so that biochars could be a promising cost-effective and environmentally friendly alternative to conventional Si amendments in agro-ecosystems.

A recent study suggests that the application of biochar derived from the high Si-accumulator *Miscanthus* could increase Si mineralomass in cotton plants (Li et al., 2017). However, the increasing soil fertility parameters and plant biomass cannot be directly assigned to higher Si bioavailability, as biochar effect has not been isolated. The overall objective of the project consists of studying the ability of Si-enriched and Si-depleted biochars with strictly identical physicochemical properties (besides Si content) to supply bioavailable Si for wheat plants (Si-accumulator) in two soils with contrasting weathering degree. The objective of the present study consisted of measuring and characterizing the BSi pool in the two soils used, the amendments and the soil:amendment mixtures.

4.2. Materials and Methods

An overview of all methodological procedures and analyses carried out for the study is presented below (**Figure 4.1**). Further details can be found in (Li et al., 2018).

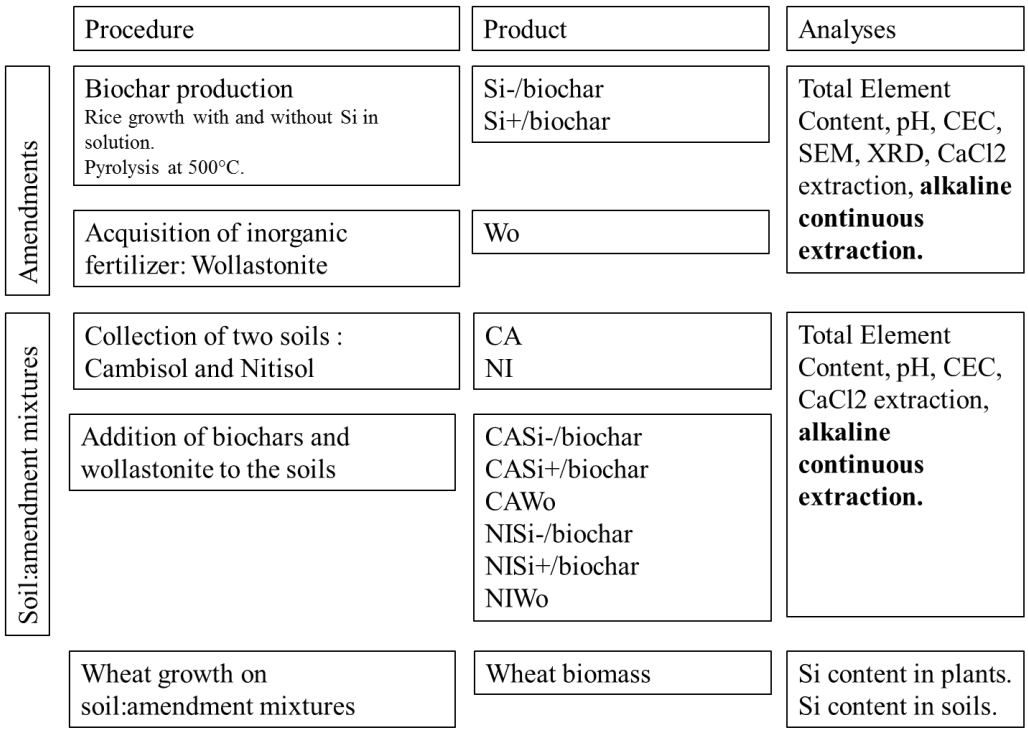

Figure 4.1. Overview of all methodological procedures and analyses carried out for the study.

Rice plants were grown from seeds in hydroponic systems to produce biochars (pyrolyzed biomass). Half of the plants grown were supplied with Si in solution while the other half weren't. Thus, one of the produced biochars contained pyrolyzed biomass with Si (Si+/biochar) while the other one contained pyrolyzed biomass without Si (Si-/biochar). An inorganic fertilizer commonly used, wollastonite, was as well used as amendment. Total element content, CEC and pH were measured for the three amendments. An X-Ray diffraction and Scanning Electron Microscopy were applied on biochar samples to confirm the presence or absence of phytoliths. A kinetic extraction in $CaCl_2$ was performed for 128 days to determine the release of bioavailable Si. A continuous alkaline extraction was performed to determine the BSi content of each of the amendments.

Two types of soils, with different weathering stage degrees, were collected for the study: a moderate weathered Cambisol (CA) and a highly weathered Nitisol (NI). Cambisols cover 10% of the land surface worldwide and

commonly occur in cool climates of high latitudes; Nitisols only cover 1.3% of the land surface worldwide and are present commonly in tropical and subtropical regions at low latitudes. Overall, highly weathered soils (Nitisols, Acrisols, Lixisols, Arenosols and Ferrasols) represent more than 25% of the total worldwide surface (IUSS Working Group WRB, 2015). Properties of both soils differed. The two soils (CA and NI) were amended with Wollastonite, Si-/biochar and Si+/biochar. The same amount of both biochars was added (1.5% of Si-/biochar and Si+/biochar), and the same amount of Si was added through the Si+/biochar and Wo amendments (0.81 mg g^{-1} of soil). Thus, the Si addition through Si-/biochar amendment results in 0.003 mg g^{-1} of soil. The mixtures were then analyzed for total element content, CEC and pH as done for the amendments. A kinetic extraction in $CaCl_2$ and the continuous alkaline extraction were as well performed on the soils and soil:amendment mixtures.

After the study of the release of bioavailable Si in the two types of soils and with the addition of the amendments, wheat plants were grown on those soils and soil:amendment mixtures. After four weeks of growth, biomass was collected and weighted. Si content in plants and the remaining Si in soil was then measured.

A budget calculation was performed afterwards taking into account the Si added through the amendments, the Si uptake by wheat plants and the remaining Si in the soil solution. An analysis of the obtained results was carried out in order to study the Si recycling by plants depending on type of soil and type of amendment added.

Here, the method and results from the continuous alkaline extraction are detailed. An overview of the whole study framework can be found in Li et al., (2018).

Alkaline Continuous Extraction

Three replicates of each sample (for the amendments, soils and the soil:amendment mixtures), resulting in 33 samples, were analyzed in a continuous flow analyzer (Skalar, Breda, the Netherlands), using a continuous

analysis technique recently refined for soils by (Barão et al., 2014). Samples were gently crushed prior to analysis. The extraction was accomplished in 180 mL of 0.5 M NaOH, at 85°C for 30 min. Dissolved Si and dissolved aluminum (Al) extracted are analyzed continuously, obtaining two dissolution curves which are fitted with first order equations: **Eq (1)** and **(2).**

$$Si_t(mg\ g^{-1}) = \left(\sum_{i=1}^{n} AlkExSi_i \times (1 - e^{-k_i \times t})\right) + b \times t \qquad \textbf{(1)}$$

$$Al_t(mg\ g^{-1}) = \left(\sum_{i=1}^{n} \frac{AlkExSi_i}{Si/Al_i} \times (1 - e^{-k_i \times t})\right) + \frac{b \times t}{Si/Al_{min}} \qquad \textbf{(2)}$$

The method distinguishes between the mineral fractions which have a linear dissolution behavior (DeMaster, 1981; Koning et al., 2002) and the fractions exhibiting a non-linear dissolving behavior. The curve model (with one, two or three non-linearly reactive fractions) exhibiting the lowest error was kept. For the mineral fraction, the model renders a linear dissolution rate (b) and the Si/Al ratio (Si/Al_{min}). Non-linearly reactive fractions are characterized by: the total amount of Si (alkaline extractable Si (AlkExSi), mg g^{-1} dry weight of initial sample mass), the Si/Al ratio (Si/Al) of that fraction and its reactivity (*k*, how fast it dissolves). The Si/Al ratio of the fraction is used to determine the origin of the non-linear fraction. Barão et al., (2014) distinguished the following fractions: ratio > 5 was considered as indicative of a biogenic fraction (Biogenic Si, BSi), as the proportion of Al in phytoliths is low (Bartoli, 1985; Piperno, 2006). A fraction with a Si/Al ratio between 1 and 5 was considered as representative of the mineral fractions (secondary clays) and Si/Al ratios <1 can indicate multiple pedogenic Si fractions (Oxides-Si), including Si adsorption. Although it is not possible to distinguish BSi from pedogenic Opal A/CT among the Si/Al>5 fraction, the absence of other sources in our soils allow us to assign the fraction characterized with a Si/Al>5 as BSi.

Few more replicates (a total of 5) were run for the NIWo samples, due to the variable results of the three first ones that were run. The Wollastonite

samples were modeled with only **Eq. (1)** due to the absence of aluminum in the mineral. Only AlkExSi and k values are given.

Data analyses

The increment of biogenic AlkExSi after the amendment addition was considered to be the result from the subtraction of the amount of AlkExSi in the non-amended soil (CA and NI) from the AlkExSi in the soil:amendment mixture (**Eq. 3**).

$$\Delta\text{Biogenic AlkExSi (Increment of biogenic AlkExSi)} = \text{AlkExSi\_soil}_i\text{:amendment} - \text{AlkExSi\_non-amended soil}_i \quad \textbf{(3)}$$

Considering the Si-/biochar as a Si-absent amendment, the biogenic AlkExSi obtained in soils amended with Si-/biochar might be the result of an experimental or modeling error. Subtracting then the amount of biogenic AlkExSi obtained in soils amended by Si-/biochar to the amount of biogenic AlkExSi in the other soil:amendment mixtures (soils amended by Si+/biochar and Wo) we estimate then the final and more accurate effect of the addition of Si+/biochar and Wo (**Eq. 4**).

$$\text{Net } \Delta\text{Biogenic AlkExSi} = \Delta\text{Biogenic AlkExSi\_soil}_i\text{:amendment} - \text{AlkExSi\_soil}_i\text{:Si-/biochar} \quad \textbf{(4)}$$

Tukey's test was carried out using Excel 2010.

4.3. Results

Figure 4.2 shows the content of alkaline extractable silica (AlkExSi, g kg^{-1}) in the biochars, wollastonite, soils and soil:amendment mixtures. **Figure 4.2a** shows a dominant biogenic silica fraction in biochars. Yet, the content of biogenic AlkExSi in the Si+/biochar (35.0 g kg^{-1}) is much larger than the biogenic AlkExSi in Si-/biochar (0.13 g kg^{-1}). AlkExSi values for the

Wollastonite are 10 times lower than the biogenic AlkExSi in the Si+/biochar (3.63 g kg^{-1}).

In the CA, there is only one consistent biogenic AlkExSi fraction, although one replicate shows a small Si/Al<1 fraction as well. The biogenic AlkExSi (Si-Al > 5) measured in the soil:amendment mixtures compared to the biogenic AlkExSi measured in the non-amended CA (3.64 g kg^{-1}) does not differ after the Si-/biochar application (3.68 g kg^{-1}); is slightly larger after the Si+/biochar application (4.49 g kg^{-1}); and slightly smaller after Wo application (3.24 g kg^{-1}). In the NI, no biogenic AlkExSi is found in the non-amended NI. Only one of the replicas again shows a small Si/Al<1 fraction. The biogenic AlkExSi measured in the soil:amendment mixtures compared to the biogenic AlkExSi measured in the non-amended NI (0 g kg^{-1}) is larger after the Si-/biochar application (0.96 g kg^{-1}), larger after Si+/biochar application (1.88 g kg^{-1}) and larger as well after Wo application (0.53 g kg^{-1}).

In **Table 4.1** the results of the biogenic AlkExSi fractions described are detailed. The total Si input and the relative and net increase are as well included.

Statistically, only the addition of Si+/biochar was significant compared to the non-amended soil in both soils. In the case of the NI, the addition of Si-/biochar is as well significantly different from the non-amended NI.

The increment of biogenic AlkExSi was positive after the addition of Si-/biochar and Si+/biochar in the CA (+0.04 and +0.81 for the Si-/biochar and the Si+/biochar, respectively), and negative after the addition of Wo (-0.40). The increment of biogenic AlkExSi was positive after the addition of all amendments in the NI (+0.96, +1.88 and +0.53 for the Si-/biochar, Si+/biochar and Wo, respectively). The net increment of biogenic AlkExSi was positive after the addition of Si+/biochar in both soils (+0.81 and +0.92 in CA and NI, respectively), and negative after the addition of Wo (-0.44 and -0.43 in CA and NI, respectively).

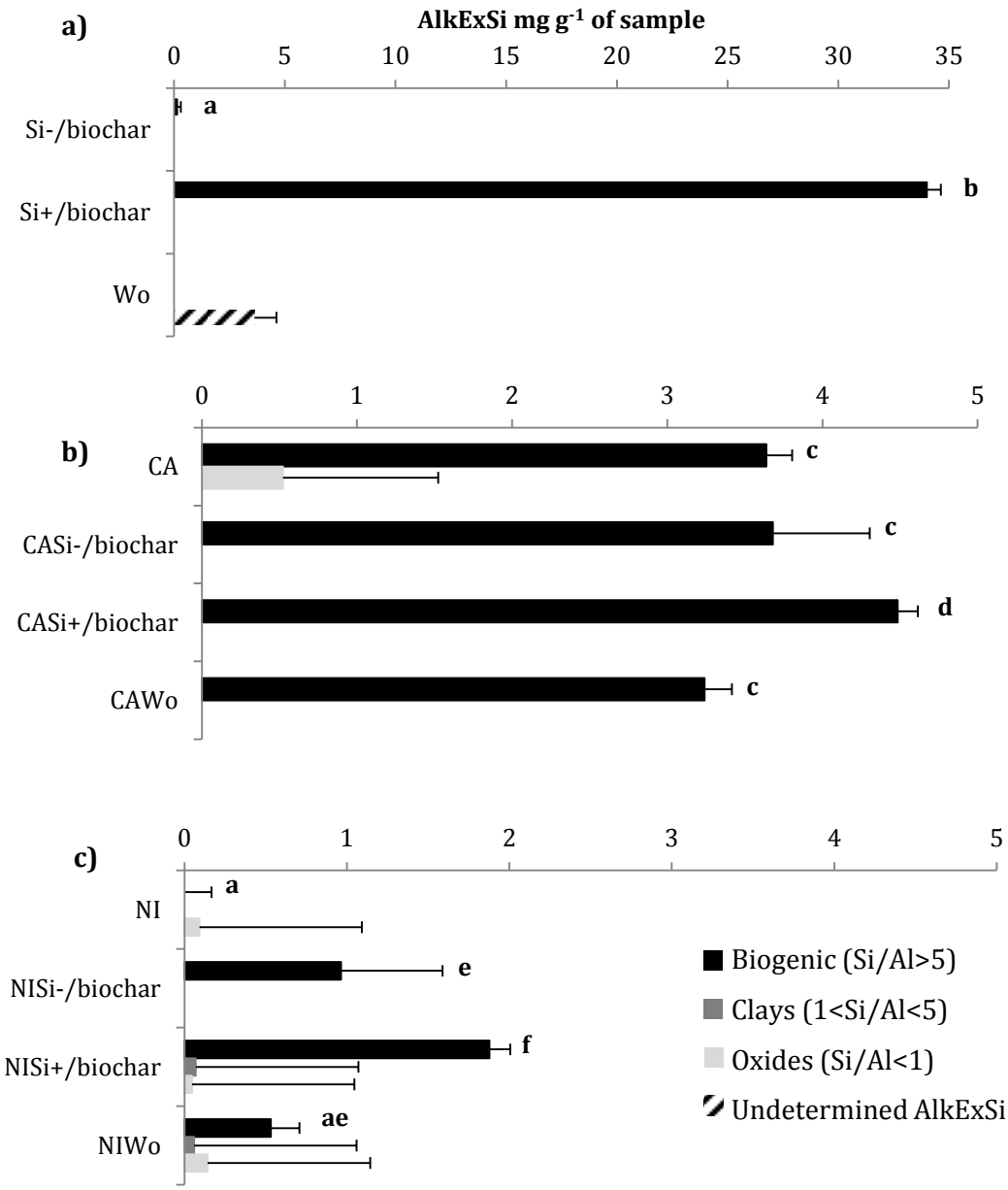

Figure 4.2. Alkaline extractable silica (AlkExSi, mg g^{-1} of sample) of the different treatments. **a**: Amendments: biochars (Si- and Si+) and wollastonite (Wo). **b**: Cambisol (CA) and Cambisol amended by Si-/biochar (CASi-/biochar), Si+/biochar (CASi+/biochar) and Wollastonite (CAWo). **c**: Nitisol (NI) and Nitisol amended by Si-/biochar (NISi-/biochar), Si+/biochar (NISi+/biochar) and wollastonite (NIWo). Note that Wo sample was modeled only with **Eq. (1)**. The character of the fraction according to a Si/Al ratio is thus not determined for the Wo sample. The average values presented with distinct letters (a, b, c, d, e and f) are significantly different at the $p<0.05$ level of confidence according to Tukey's test.

Table 4.1. Biogenic AlkExSi content in the amendments (Si-/biochar, Si+/biochar and Wo), soils (CA and NI) and soil:amendment mixtures (CASi-/biochar, CASi+/biochar, CAWo, NISi-/biochar, NISi+/biochar and NIWo). The Si input added through the addition of the amendments. The average values presented with distinct letters (a, b, c, d, e and f) are significantly different at the $p<0.05$ level of confidence according to Tukey's test.

	Total Si input	Biogenic AlkExSi	ΔBiogenic AlkExSi	Net ΔBiogenic AlkExSi
	g kg^{-1} of soil	g kg^{-1} of soil	g kg^{-1} of soil	g kg^{-1} of soil
Si-/biochar		0.13±0.02a		
Si+/biochar		34.01±0.56b		
Wo		3.63±0.04†		
CA	0.00	3.64±0.17c		
CASi-/biochar	0.003	3.68±0.62c	+0.04	
CASi+/biochar	0.81	4.49±0.13d	+0.85	+0.81
CAWo	0.81	3.24±0.18c	-0.40	-0.44
NI	0.00	0.00a		
NISi-/biochar	0.003	0.96±0.78e	+0.96	
NISi+/biochar	0.81	1.88±0.65f	+1.88	+0.92
NIWo	0.81	0.53±0.35ae	+0.53	-0.43

†Only modeled with Eq. (1) and impossible to determine the character of the AlkExSi. No statistics were done.

4.4. Discussion

Biogenic AlkExSi in soils

The alkaline continuous extraction allows us to characterize fractions showing a non-linear dissolution behavior (AlkExSi) in 0.5 M NaOH. The Si contained in the wollastonite did not show a specific non-linear dissolution behavior; yet, 1.5% of the total Si present as wollastonite was characterized as AlkExSi. In the extraction of both biochars however, it is clear that the majority of Si is contained in an AlkExSi fraction: 42-67% of the total Si is characterized as AlkExSi, more precisely as biogenic AlkExSi. The Si content of the biochars is assumed to correspond to phytoliths and/or Si embedded

within the cell walls (Fraysse et al., 2010). This secondary pool has been recently confirmed to show, as phytoliths, high reactivities in NaOH and high Si/Al ratios when samples were analyzed using the same method (Unzué-Belmonte et al., 2016). This finding confirms that phytoliths can resist to pyrolytic temperatures up to 500°C and still persist as amorphous BSi, although some structural changes can occur (Xiao et al., 2014).

Despite the high total Si content in NI (Li et al., 2017), our results confirmed that this type of soil did not contain any biogenic AlkExSi. This is perfectly in line with the fact that the NI used is a buried paleosol that was not in recent contact with vegetation. This soil thus represents a soil with complete absence of BSi, that allows to study the Si cycling after the addition of inorganic or biogenic Si in BSi depleted soils. On the contrary, the Cambisol showed the presence of a BSi pool (**Figure 4.2**, **Table 4.1**). This BSi pool (~3.64 mg g^{-1} of soil) was in the same range than that observed in Barão et al., (2014) who observed biogenic AlkExSi values of ~3.5 mg g^{-1} of soil for a cultivated slightly weathered Cambisol.

Our results also demonstrate that Si-/biochar could not significantly increase the biogenic AlkExSi pool in the Cambisol, confirming the absence of phytoliths in that biochar. However, the still apparent small increase in the amount of biogenic AlkExSi obtained in the Nitisol amended by Si-/biochar indicates even the treatment with no Si addition actually resulted in the appearance of an NaOH reactive Si fraction. The reason could be an experimental error, supported by the high deviation obtained between the three replicates, or a possible change on solubility condition of Si compounds present in the Nitisol due to the effect of the biochar on soil properties. Considering such error or effect, a net and more accurate increase is calculated for the soils amended with the same amount of Si added per kg of soil (Si+/biochar and Wo amendments) consisting on the subtraction of the increase measured after the addition of Si-/biochar to the increases obtained after the addition of Si+/biochar and Wollastonite (see Methods, **Table 4.1**).

The addition of Si+/biochar clearly increases the biogenic AlkExSi pool in both NI and CA. The addition of 0.81 mg of Si per g^{-1} of soil, corresponds exactly with the net increment resulted of biogenic AlkExSi in the CA (+0.81 mg g^{-1} of soil). In the NI, the resulting increase (0.92 mg g^{-1} of soil) slightly exceeded the concentration added by the Si+/biochar (**Table 4.1**). We can determine that the addition of 1 mg of biogenic AlkExSi from Si+/biochar per gram of soil results in an increase of 1 mg gram of biogenic AlkExSi per gram of soil. Our results confirm the accurate precision of the continuous alkaline extraction method when analyzing samples with biogenic silica content even in a challenging environment.

The application of Wo only shows a small non-linear dissolving AlkExSi pool in NI (NIWo), not significantly different from the AlkExSi pool in the non-amended NI. However, considering 1) the non-biogenic character of the Si supplied by wollastonite, 2) the absence of a biogenic AlkExSi fraction in the non-amended NI and 3) the 1.5% of the total Si content in Wo was described as AlkExSi in the continuous analysis of Wo, we can confirm that this fraction was not biogenic. The continuous extraction method can indeed not distinguish silicate minerals without Al from BSi (Unzué-Belmonte et al. 2017), for the mineral part that shows non-linear dissolution. The Si/Al>5 AlkExSi fraction corresponds to the alkaline-soluble part of the inorganic Si added from the Wo. Special care should be applied when analyzing soils with larger Wollastonite addition if applying the present method.

The negative net increase occurring after the addition of Wollastonite suggests that the inorganic mineral seems to decrease the solubility of the pre-existent BSi pool in the Cambisol. The dissolution of Wollastonite releases DSi and Ca^{2+} in solution. The addition of bivalent cations in solution was shown to decrease the solubility of phytoliths from biochars derived from rice-straw in an experiment carried out under controlled conditions (Nguyen et al., 2014). However, the real process occurring in our mixtures cannot be confirmed based on the present data.

Importance of results from the alkaline continuous extraction in the study

The XRD and SEM analyses carried out by Li et al., (2018) help to confirm the absence and presence of phytoliths in Si-/biochar and Si+/biochar respectively. However, the quantification of biogenic silica is not possible using such methods. The alkaline continuous extraction is able to determine the character of the AlkExSi (whether a fraction is biogenic or not) and quantifying the biogenic silica in one single extraction.

It is commonly accepted that phytoliths show higher solubilities in soils than other solid phases, confirmed by several studies carried out under controlled conditions (Fraysse et al., 2006b; Ronchi et al., 2015). Moreover, burned plant material has been shown to have higher solubilities than fresh plant material (Unzué-Belmonte et al., 2016). The solubility however depends on *in situ* conditions which may influence phytolith solubility: bioavailable Si concentrations in soils might not correspond to the amount of BSi.

In the complete study which our results are part from, a quantification of the amount of bioavailable Si in the non-amended soils and amended soils was performed. As such, it is only possible to relate the BSi content to the bioavailable Si content in soils using an accurate analysis as performed here, to draw conclusions regarding phytolith solubility. Furthermore, in this study, wheat plants were grown in the soils and soil:amendment mixtures and Si content in the plants were quantified afterwards. The study of the relation between Si uptake by plants, soil bioavailable Si and soil biogenic AlkExSi contributes to better understand the recycling by plants of Si from organic and inorganic origin in different weathering stage soils.

The samples analyzed in the study were specially challenging for the method. The analysis of wollastonite, a mineral with no Al content, gave us some insights about how these kind of minerals might be determined using our method. The result shows that indeed, wollastonite can be erroneously described as a biogenic fraction. However, the fraction of total Si that dissolves non-linearly seems to be extremely low, accounting for only 1.5% of

the total amount of the Si in the mineral. Even though, this conclusion should be taking into account when analyzing soil samples with non-Al minerals content.

Overview of results in *Phytolith content in biochar affect the biological Si cycle in soil-wheat systems*

SEM and XRD analyses

Results from the SEM and XRD analyses confirm the absence of phytoliths in Si-/biochar and the presence in Si+/biochar.

Kinetic extraction in $CaCl_2$

During the 128 days of extraction the release of Si in soils amended with Si-/biochar was equal to the release in the non-amended soils. However when comparing the release of Si in soils amended with Si+/biochar and Wollastonite a different pattern was found regarding the soil. While in the Nitisol the highest release of Si occurred after the application of Si+/biochar, in the Cambisol, the highest release of Si occurred after the application of Wollastonite. The explanation behind lies in the presence in the non-amended CA of BSi, confirmed and measured with the continuous alkaline extraction, and overall properties that probably prevent the added BSi from the biochar to dissolve and release bioavailable Si. As the addition of the inorganic fertilizer, wollastonite, does not increase the biogenic AlkExSi pool in any of the soils, the Si released in the NI is obviously coming from the dissolution of the mineral.

Wheat growth

The addition of Si+/biochar and Wo increased indistinctly the biomass of plants grown in the CA. Si-/biochar did not increase the biomass of plants grown in the CA. The addition of both biochars (Si-/biochar and Si+/biochar) increased the biomass of the plants grown in the NI. Wo did not increase the biomass of the plants grown in the NI.

However, the Si content per gram of biomass showed different patterns. While in soils amended by Si-/biochar the biogenic AlkExSi pool only varied in the NI, plants grown with the addition of Si-/biochar showed higher Si content (mg Si per g of biomass) than plants grown in both non-amended soil, probably due to the improvement of soil conditions through the biochar properties (addition of other nutrients, changes in pH and CEC). Plants grown in any of the soils amended by Wo clearly showed a higher concentration of Si than the plants grown on the non-amended soils. Finally, plants grown with the addition of Si+/biochar showed higher Si concentration than plants grown in the non-amended soils. This increase was higher than the experimented by plants grown with Si-/biochar but lower than the increase experimented by plants grown with Wo addition. Regarding the soil type, a higher concentration of Si in plants grown in NI resulted, than in CA.

Si budget

Considering the Si added through the amendments, the release of bioavailable Si in the soils and the Si taken up by plants (per g of biomass) it is concluded that: Si-/biochar contributes only to increase in biomass in NI, but no effect on the Si pool or recycling is observed. The beneficial condition added through the biochar properties (pH, CEC, C…) contributes to increase the Si uptake by plants. The Si+/biochar increases the bioavailable Si (largely in NI) and the Si uptake by plants (largely in NI as well). The Wo increases the bioavailable Si (largely in CA) and the Si uptake by plants in both soils. In conclusion, the soil properties determine the recycling of Si by plants. The ability of Si-enhanced biochar in the enrichment of bioavailable Si in soils and increase of Si mineralomass in crops is also proved. However, this effect will be larger in highly weathered soils than in moderately weathered soils with background BSi content.

The main conclusion of the study “Phytolith content in biochar affect the biological Si cycle in soil-wheat systems” relates to the differences of BSi content and soil properties in the CA and NI soils, and determines that the

recycling of Si by plants depends directly on the soil properties and the type of Si-fertilizer added.

Chapter 5

Biogenic alkaline extractable silica (AlkExSi) in Kenya: addendum to 'Hippos (*Hippopotamus amphibius*): the animal silica pump'.

Dácil Unzué-Belmonte

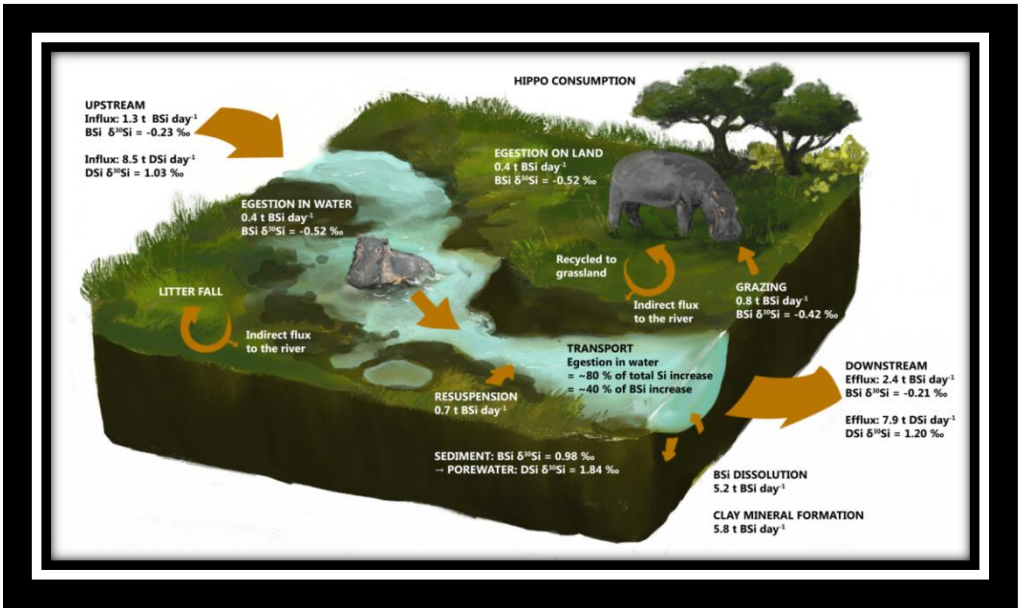

Simon De Meulenaer

5

Biogenic alkaline extractable silica (AlkExSi) in Kenya: addendum to 'Hippos (*Hippopotamus amphibius*): the animal silica pump'.

5.1. Introduction

The Schoelynck et al. (2017) paper studies the influence of large grazers (hippopotamuses) on the Si fluxes in the Mara River, Kenya. The influence of animals is known to affect elemental cycles like carbon or phosphorous (Bakker et al., 2016; Doughty et al., 2016), but little has been quantified in relation to the terrestrial Si-cycle. Large herbivores feeding on grasses affect Si translocation, as Si is not an essential element for animals and is commonly excreted through feces deposition. Vandevenne et al., (2013) showed how the solubility of phytoliths increased after large grazer's digestion. Hippos in Africa are an interesting species to study at this respect because their particular ethology. Hippos feed on savannah grasses during the night and excrete their feces, which contain large amounts of Si, into the river water during daytime. Thus, hippos could be considered as large vectors transferring from the savannah grasses directly into the river highly soluble BSi. Such hippo influence on the Si load in the Mara river, and thus potentially

on the Si input into Lake Victoria is studied through the analysis of BSi content in grasses and hippo's feces, DSi in the river- and porewater, BSi content of suspended matter and of sediments from the riparian area of the river, and the isotopic fractionation of the mentioned Si compartments. An estimation of fluxes is calculated. The complete detailed study is presented in Schoelynck et al. (2017) (see Supplementary material). The present work corresponds to the analyses to characterize and quantify the BSi pool along hippos' activity: from the savannah grasses to the sediments in the river.

5.2. Methods

Study area and sampling

The study area is located in the Maasai Mara National Reserve (MMNR) in the south-west of Kenya. The Mara River eventually flows into Lake Victoria, the most important water reservoir in East-Africa. The studied savannah soils were Vertisols with high clay content (Mati et al., 2008).

The sampling campaigns took place during the dry season (Feb. 2014). Ten positions along the Mara River were selected for sampling (**Figure 5.1**). Site 1 is located outside the MMNR; here, hippo influence is negligible. Along the river, the presence of hippos is fairly constant thus the cumulative effect can be expected to increase progressively. Site 10 is situated right before the Tanzanian border. Three additional tributary sites were also sampled: contributing to the Mara before the reserve were the Amala and Nyangores. The third one, Talek, flows into the Mara within the Reserve, between sites 8 and 9. Suspended matter and sediment cores in the riparian area were collected in the river (details, see Schoelynck et al. (2017)), with the exception of the sediment core at Talek and the suspended matter at Nyangores. Savannah cores were collected at sites 2, 5, 7, 8, 9 and 10 at a perpendicular distance of >1 km to the river. Grass and fresh dung samples were collected at sites 1, 3, 5, 6, 8 and 10, and at Amala and Nyangores at the flanks of the river.

Extended descriptions of the study area, site location and sampling protocols are detailed in the Supplementary material in Schoelynck et al. (2017).

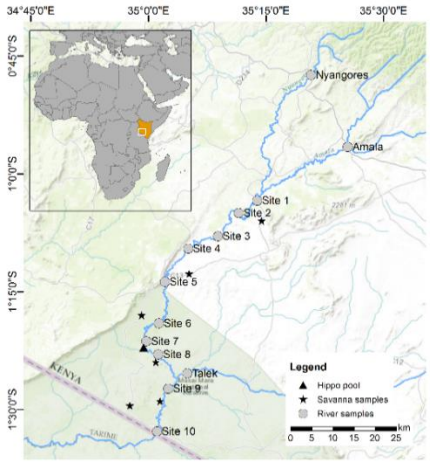

Figure 5.1. Map showing the sample points along the Mara River. From Schoelynck et al. (2017).

Methodology

The continuous alkaline extraction in NaOH was carried out on the samples mentioned according to the methodology described in Barão et al. (2014). Briefly, samples were extracted in NaOH at 85°C and through different chemical reactions dissolved Si and dissolved Al are measured continuously for half an hour. The dissolution curves are fitted into the following model (**Eq. 1**), which corrects for the mineral dissolution:

$$\mathrm{Si}_t\ (mg\ g^{-1}) = \left(\sum_{i=1}^{n} \mathrm{AlkExSi}_i \times \left(1 - \mathrm{e}^{-\mathrm{k}_i \times t}\right)\right) + \mathrm{b} \times t$$

$$\mathrm{Al}_t\ (mg\ g^{-1}) = \left(\sum_{i=1}^{n} \frac{\mathrm{AlkExSi}_i}{\mathrm{Si/Al}_i} \times \left(1 - \mathrm{e}^{-\mathrm{k}_i \times t}\right)\right) + \frac{\mathrm{b} \times t}{\mathrm{Si/Al}_{\mathrm{min}}} \quad \textbf{(1)}$$

where b is the slope of the mineral Si component, $\mathrm{Si/Al}_{\mathrm{min}}$ is the ratio between the two elements in the mineral Si component; AlkExSi is the amount of alkaline extractable silica of the non-linear dissolving fraction(s), k the reactivity or how fast that fraction dissolves in NaOH and the Si/Al is the ratio between the two elements in that corresponding fraction. According to

the Si/Al ratio of the non-linearly dissolving fractions the character of that fraction can be determined. In Barão et al. (2015), Si/Al ratios above 5 were considered to be biogenic silica, due to the proportion of the elements in phytoliths; fractions showing Si/Al ratios were considered to be clay minerals; and fractions showing Si/Al ratios below 1 were considered to be oxides, hydroxialuminosilicates (HAS) and Si absorbed onto other compounds.

In the present work we set the boundaries to determine the origin of the fraction as follows: Si/Al <1 for oxides and Si absorbed onto surface of different compounds, 1<Si/Al<4 for clay minerals and Si/Al>4 for biogenic silica (phytoliths). A fraction was considered to be 'non-linearly dissolving' when k value was higher than 0.08 min^{-1}.

5.3. Results

The results of different fractions described for the grass and hippo fresh dung, savannah soil, suspended matter and sediment samples are presented in **Table 5.1**.

Table 5.1. Results of the continuous alkaline extraction. Fractions described according to the equations used (**Eq. 1**). The AlkExSi, k value and Si/Al ratio of each non-linearly dissolving fraction described for the samples collected are presented for the grass and dung, savannah soil, suspended matter and sediments samples. Biogenic, clay minerals and oxides fractions are noted in green, purple and orange, respectively. Fractions discarded due to a low k value (k<0.1 min^{-1}) are noted in light red.

GRASS AND DUNG

Site	Type	$AlkExSi_1$	k_1	Si/Al_1	$AlkExSi_2$	k_2	Si/Al_2
1	grass	18.8	0.52	>100	4.14	2.74	>100
3	grass	13.7	0.56	44.0	8.05	0.07	9.64
5	grass	27.1	0.44	>100			
6	grass	11.8	0.47	>100	2.84	0.11	>100
8	grass	11.1	0.83	>100	6.99	0.17	34.4
10	grass	12.6	0.30	49.2	8.67	0.90	>100
1!	dung						
3	dung	41.1	0.38	>100	22.0	0.13	45.5

5	dung	14.3	0.50	14.9	22.1	0.16	>100
6	dung	31.1	0.63	92.9	24.4	0.08	65.7
8	dung	29.1	0.64	99.3	20.7	0.13	>100
10	dung	31.8	0.50	>100	15.6	0.09	28.1

SAVANNAH SOIL

Site	Depth	$AlkExSi_1$	k_1	Si/Al_1	$AlkExSi_2$	k_2	Si/Al_2
2	-5	1.88	0.78	>100	17.1	0.10	2.54
2'	-13						
5	-5	34.4	0.12	12.1	1.66	1.01	1.27
5'	-13						
7	-5	27.1	0.12	>100			
7'	-13						
8	-5	27.0	0.08	6.18	9.66	0.33	5.57
8	-13	28.0	0.13	63.6	0.66	0.05	0.07
9	-5	5.04	0.45	1.77	41.3	0.05	4.17
9	-16	7.20	0.29	1.19	75.0	0.03	3.16
10	-5	26.2	0.08	11.2			
10	-13	28.1	0.05	>100			

SUSPENDED MATTER

Site	$AlkExSi_1$	k_1	Si/Al_1	$AlkExSi_2$	k_2	Si/Al_2
Amala	24.2	0.26	>100	26.2	0.05	1.12
1	14.1	0.31	4.21	42.8	0.07	6.95
2†	32.8	0.14	42.9	1.36	1.07	4.64
3	10.4	0.42	6.31	68.7	0.05	4.47
4†	39.4	0.08	88.7	8.27	0.31	3.26
5	3.81	0.49	5.68	31.8	0.10	4.38
6	13.1	0.30	7.83	66.8	0.04	4.80
7	9.71	0.34	10.5	61.3	0.05	5.14
8	9.32	0.32	4.42	49.4	0.05	6.04
9	9.68	0.38	14.3	42.1	0.07	3.76
10	38.6	0.09	5.50	7.39	0.43	3.69
Talek	4.03	0.98	>100	31.8	0.14	4.97

SEDIMENT

Site	Depth	$AlkExSi_1$	k_1	Si/Al_1	$AlkExSi_2$	k_2	Si/Al_2
Amala	0 to -2	27.9	0.14	6.74	2.41	0.70	2.42
Amala	-2 to -6	16.2	0.22	5.25			
Amala	-6 to -10	10.7	0.27	6.80			
Nyangores	0 to -2	13.3	0.12	62.3	1.15	0.46	0.82
Nyangores	-2 to -6	0.57	0.59	1.29			
Nyangores	-6 to -10	5.60	0.17	5.09			
1	0 to -2	7.64	0.42	5.41			
1	-2 to -6	8.87	0.17	>100			
1	-6 to -10	6.12	0.26	>100			
2	0 to -2	5.11	0.14	10.6			
2	-2 to -6	5.08	0.14	14.9			
2	-6 to -10	0.96	0.25	>100	6.23	0.06	>100
3	0 to -2	11.4	0.16	5.23			
3	-2 to -6	11.0	0.20	6.34			
3	-6 to -10	14.3	0.08	42.5	2.69	0.32	4.25
4	0 to -2	4.00	0.23	9.45			
4	-2 to -6	0.92	1.12	24.1	6.55	0.11	7.47
4	-6 to -10	4.89	0.35	5.89			
5	0 to -2	3.84	0.16	8.39			
5	-2 to -6	10.9	0.21	>100	25.3	0.02	1.79
5	-6 to -10	4.57	0.28	5.47	38.3	0.02	4.05
6	0 to -2	11.8	0.32	6.95	88.4	0.03	3.22
6	-2 to -6	18.8	0.14	>100	4.98	0.35	2.48
6	-6 to -10	10.6	0.22	4.96	82.2	0.02	5.39
7	0 to -2	5.88	0.27	>100			
7	-2 to -6	11.0	0.13	>100	0.68	0.60	3.29
7	-6 to -10	5.54	0.37	8.05			
8	0 to -2	12.3	0.29	7.43			
8	-2 to -6	7.63	0.50	5.91			
8	-6 to -10	13.4	0.28	6.25			
9	0 to -2	8.81	0.28	4.23	16.5	0.08	8.05
9	-2 to -6	10.5	0.22	4.34			

9	-6 to -10	8.77	0.25	4.28	1.63	4.34	3.98
10	0 to -2	10.1	0.41	4.93	28.5	0.10	4.74
10	-2 to -6	17.5	0.30	7.59	119	0.02	4.74
10	-6 to -10	21.2	0.13	>100	2.35	0.96	375

[!]Samples were not analyzed due to the absence of hippos for the dung sample in site 1, and the impossibility to sample that depth by the device used at the moment those sites were sampled for the soil samples.
†An additional third fraction was described for these samples. The parameters were: AlkExSi (1.25), k (0.06), Si/Al (0.09) for sample of Site 2 and AlkExSi (71.9), k (0.02), Si/Al (1.67) for sample of Site 4.

All samples but two from grass and fresh dung showed similar results: two non-linearly dissolving fractions with high Si/Al ratios, both corresponding to a biogenic silica origin. Samples from the savannah soil showed a biogenic silica fraction (Si/Al>4) at all lower depths (-5 cm) except for site 9. However, there are also non-linearly dissolving fractions with Si/Al~2 in four of the samples and fractions with low k values ($k<0.08$ min^{-1}) in another four samples. Such low values correspond to an almost linear dissolution.

Samples of suspended matter showed in all cases a non-linearly dissolving fraction with Si/Al>4 which corresponds to biogenic silica, and an additional variable fraction. In five of the sites the additional fraction showed a non-linear dissolution, three of them with Si/Al>4 and two with Si/Al<4. Nine of the additional fractions showed k values<0.08 min^{-1}, which is considered to be an almost linearly dissolving fraction. There were no apparent differences between samples from the Mara River and the samples collected outside the River (Amala and Talek), although Talek had a particularly low BSi content.

Sediment samples from the riparian zone showed in all cases (except only one sample from Nyangores), as in the suspended matter, a non-linearly dissolving fraction with Si/Al>4 which corresponds to biogenic silica. Additional fractions were found in 16 of the 20 samples: only five at 0 to -2 cm depth (two reactive biogenic silica, one reactive clay fraction, one reactive oxide fraction and one non-reactive ($k<0.08$ min^{-1})), five at -2 to -6 cm depth (one reactive biogenic silica, two reactive clay fractions and two non-reactive), and six at -6 to -10 cm depth (two reactive biogenic silica, one reactive clay fraction and three non-reactive). Samples collected outside the

MMNR (Amala and Nyangores) showed similar values than samples collected in the Mara River.

Figure 5.2 shows the BSi content (non-linear dissolving fractions with Si/Al>4) in the sediments per depth analyzed (from 0 to -2 cm, from -2 to -6 cm and from -6 to -10 cm) and the BSi content in the suspended matter along the river. The average of BSi of the three depths is also included.

5.4. Discussion

In the present work, we decided to use different parameter boundaries than proposed in Barão et al. (2014, 2015) to determine the biogenic silica fraction (phytoliths) (Si/Al>4 and k>0.08 min^{-1} instead of Si/Al>5 and k>0.1 min^{-1}). Some shallow sediments samples that were hypothesized to contain mostly BSi (as all the rest of shallow sediments samples) showed only one non-linear dissolving fraction with Si/Al ratio between 4 and 5. Earlier studies confirmed that the larger part of the suspended matter (and hence also recently deposited material) consists of hippo feces (Cary et al., 2005; Subalusky et al., 2015). Additionally, the work carried out in Unzué-belmonte et al. (2017) (**Chapter 3**), showed that a strongly weathered soil from the south of Brazil, containing high amounts of secondary clay minerals and oxides, showed no Si/Al ratios between 4 and 5. The work carried out in Clymans et al., (2015) also determined the Si/Al ratio of clay minerals between 1 and 4. This suggests (in detail in **Chapter 6**) that secondary clay minerals do not show ratios as high as 5, and probably these fractions consist of old phytoliths with some structural changes due to dissolution processes and aging (Bartoli and Wilding, 1980). Some authors already suggested that old diatoms show lower ratios and reactivity than fresh diatoms (Koning et al., 2002). In soils, the progressive weathering of phytoliths and consequent possible adsorption of free Al^{3+} will theoretically decrease Si/Al ratios and *in situ* solubility of phytoliths. However, the solubility in NaOH, expressed through the k-value, does not represent the real solubility in soils and

drawing a clear assumption about how the k-value could vary is not possible (see **Chapter 6** for more insights).

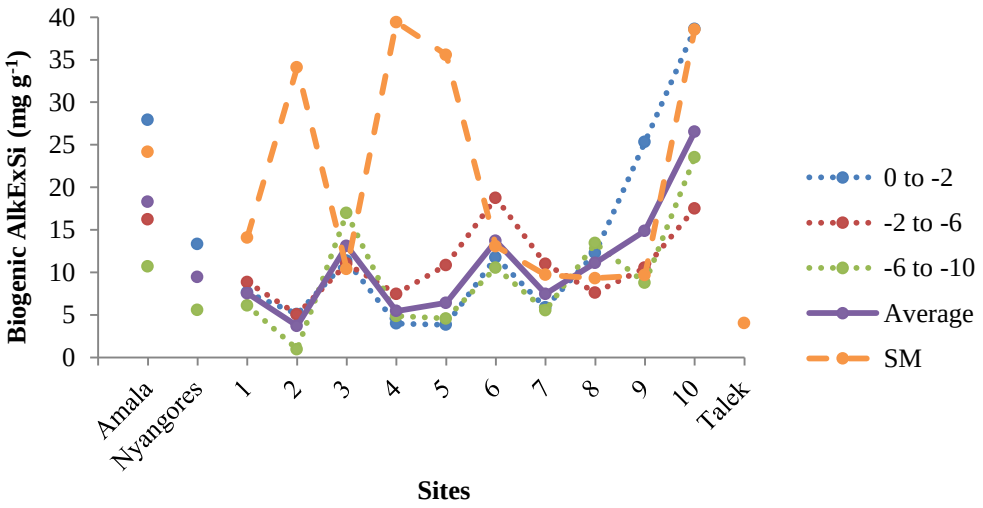

Figure 5.2. Biogenic AlkExSi of the sediments cores of the three depths analyzed (0 to -2 cm, -2 to -6 cm and -6 to -10 cm depth), the average of the three depths and the suspended matter (SM) along the river.

The boundary to determine whether a fraction is considered to be non-linearly dissolving was also slightly varied from Barão et al. (2014, 2015) from k>0.1 min^{-1} to k>0.08 min^{-1}. The reason is the presence in some of the grass and dung samples of biogenic fractions with such a low k value. Considering that grasses may contain only biogenic silica such described fractions (k>0.08 min^{-1}) should correspond to phytoliths. Thus, we decided to consider fractions with k values higher than 0.08 as non-linearly dissolving fractions and include them in the final results.

Our results clearly show that grasses from the Kenyan savannah contain two distinguishable silica pools (**Table 5.1**, 'Grass and dung'). Four of the six samples analyzed showed two biogenic fractions. The existence of a secondary biogenic pool in plants consisting of small polymers of H_4SiO_4 embedded in an organic matrix has been previously described by Fraysse et al. (2010). This secondary pool was identified in spruce and beech organic matter using the same continuous extraction method applied here (Unzué-Belmonte et al., 2016). However, Fraysse et al., (2010) suggested that the

secondary Si pool in plants might account for 10-20% of the total Si-plant content. Here, we clearly observe that the secondary biogenic Si-pool can represent between 18 and 41% of the total Si-plant content in savannah grasses. The fact that the dung collected in the savannah soils showed similar fractions (**Table 5.1**, 'Grass and dung') confirms that most of the Si passes through the digestive tract relatively unchanged. As described in Vandevenne et al. (2013), BSi is not digested by the animals' digestive system and is excreted almost in the totality through the feces.

The savannah soil contained BSi at every location and depth: it was the majority of the extracted AlkExSi (**Table 5.1**, 'Savannah soil'). However, some fractions with Si/Al ratios lower than 4 exist, which suggest the presence of secondary clay minerals and oxides, products of weathering processes. Some of these fractions showed k-values close to linearity ($k<0.08$ min^{-1}). Primary minerals as well as some secondary minerals dissolve linearly due to their crystalline structure (DeMaster, 1981), which can result in lowly reactive fractions with low k-values ($k\leq0.07$ min^{-1}). However, high reactive ($k>0.08$ min^{-1}) secondary clays were described in four of the samples. The presence of high reactive clays in extractions with alkaline solvents was already pointed out by Koning et al. (2002). Using conventional methods (like in DeMaster, 1981) these fractions would be described as BSi. The clear advantage of the continuous alkaline extraction method indeed, is the possibility to distinguish between these fractions; biogenic silica and reactive secondary clays and oxides in one single extraction (Unzué-Belmonte et al., 2017).

The suspended matter form the Mara River is composed of biogenic silica in suspension (**Table 5.1**, 'Suspended matter') which likely originates mostly from the input of hippos' feces (Cary et al., 2005). A lower averaged k value compared to the fresh dung's samples may suggest the partial dissolution of the phytoliths contained within the dung in suspension. However, the k-values rendered by our model do not show real reactivity in nature, so this remains a hypothesis. Nevertheless, the lower reactivity was confirmed also in the dissolution experiments in the Schoelynck et al. (2017) work. The additional fractions in suspended matter similar to the fractions from the

savannah soil suggest that the presence of reactive clays and non-dissolving fractions are a product of erosion processes occurring during rain events in the savannah. The low k values of these fractions may be the reason why these fractions are present along the whole river. The core sediments collected along the river were composed mainly of biogenic silica as well (**Table 5.1**, 'Sediment'). The dung is directly deposited in the river and entails 0.4-0.7 t day^{-1} (Subalusky et al., 2015) of BSi input. Thus, considering that the suspended matter carries a large amount of dung in suspension we can assume then that the majority down to 10 cm deep in the sediment corresponds to biogenic silica (phytoliths) passed through the hippo's digestive system. The punctual additional fractions present in a few samples are probably the same type of additional fractions present in the suspended matter that originate from the savannah soil. The presence of these fractions in relation to the sediment depth appears to be distributed randomly, appearing at different depths and locations. Possibly the stream flow and geomorphology of the river is determining where the products from the savannah soil carried in suspension are more prone to deposition. Moreover, the local distribution of hippos along the river, with the creation of pools with higher abundance of hippos, may influence the local deposition at areas less affected by the stirring of sediments by hippos. Another possibility is that new autogenic clays are formed within the sediment. The fact that additional non-biogenic fractions became more abundant only after site 5, suggests that the presence of dung deposits from hippos is related to this presence. Our AlkExSi results cannot solely rule out any of both possibilities. The analyses of the isotopic fractionation and fluxes calculation carried out in Schoelynck et al. (2017) however, suggest that the result is probably a combination of both processes of deposition and new clays formation taking place at the same time.

Biogenic silica content in sediments was mostly constant and no distribution patterns along the river are found (**Figure 5.2**). The biogenic silica content of the material in suspension is already high before entering the Masai Mara (Amala suspended matter, **Figure 5.2**). The high BSi content of

the sediments of the tributaries outside the Mara River (Amala and Nyangores) confirms this. However, the averaged biogenic silica of the whole sediment cores analyzed showed a slight tendency to increase towards the end of the river (sites 9 and 10), a tendency also apparent on the suspended matter. Considering that the suspended matter content or sediment load in the river increases towards the end (see Schoelynck et al. 2017), it is clear that in order to keep a constant Si concentration in the suspended matter, the addition of Si should increase at the same rate as the increase of material load in suspension. Clearly, these AlkExSi results confirm the influence of the hippos in the BSi input to the Mara River. In Schoelynck et al. (2017), combining all analyses carried out, is demonstrated that the hippo's influence accounts for 80% of the total Si increase along the Mara River.

5.5. Conclusion

Our results show that the boundary chosen to determine whether a fraction is biogenic or not as well as the k value to consider whether a fraction is reactive or not, when using the continuous alkaline extraction of Si and Al, might slightly vary depending on the characteristics of the samples analyzed.

The savannah grasses contain two different biogenic silica pools and the majority of hippos dung is made of grass material. Soil samples of the savannah consist largely of BSi and a small portion of other non-biogenic phases, products of weathering processes. The suspended matter and sediments within the river were confirmed to contain BSi from the hippos dung and a small contribution from soil material, probably a consequence of erosion. The influence of the hippos presence on the BSi accumulation along the river can clearly be inferred but cannot be quantified based on the present results. A more detailed study is published in Schoelynck et al. (2017).

Chapter 6

A mathematical refinement for the modeling of the dissolutions curves of NaOH-extracted Si and Al to determine biogenic silica in soils

Dácil Unzué-Belmonte and Nick Schenkels

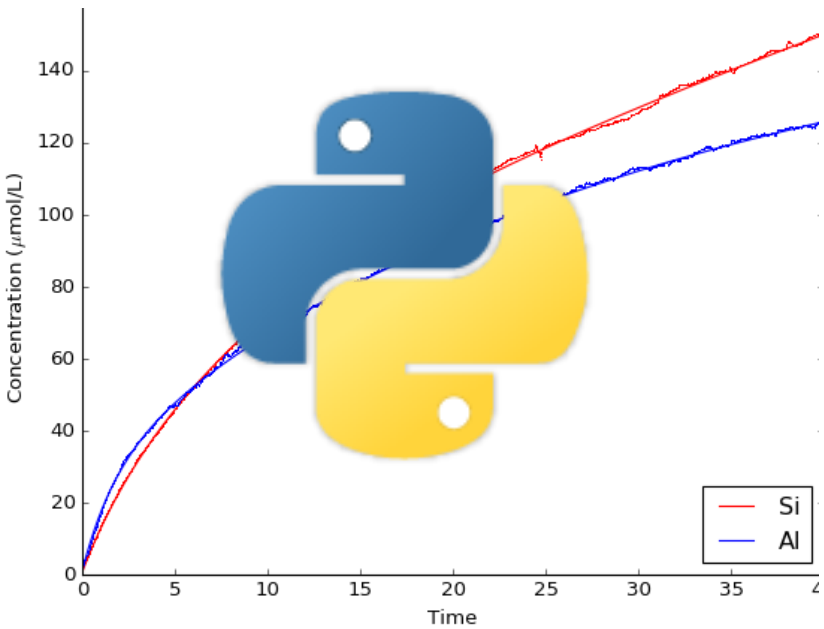

6

A mathematical refinement for the modeling of the dissolutions curves of NaOH-extracted Si and Al to determine biogenic silica in soils.

6.1. Introduction

The continuous alkaline extraction, as described and applied in earlier chapters, has been proven to extract and provide reliable results to estimate the biogenic silica pool in subtropical and temperate soils (Barão et al., 2015; Clymans et al., 2014; Vandevenne et al., 2015a). The analyses carried out in the framework of my thesis confirm that the methodology is able to extract, describe and distinguish the biogenic silica (BSi) from other silicate fractions in samples, even in challenging environments such as burned and pyrolyzed biomass (**Chapter 2** and **4**), soils with high content of oxides (**Chapter 3**) and volcanic soils and suspended matter in tropical rivers (**Chapter 5**).

The advantage of using the continuous alkaline extraction method to extract and quantify the BSi in soils and sediments is also increasingly recognized. It has a stronger affinity for biogenic phases than the original DeMaster extraction (DeMaster, 1981), and is less time-consuming than heavy-liquid phytolith extraction and separation (Parr et al., 2001). It is clear that, if an alkaline extraction is used for BSi analysis in soils with significant

other extractable fractions of Si, the advantage of using this or a similar corrective method is large (Alfredsson et al., 2015; Clymans et al., 2014).

Based on the novel experience acquired during this thesis, it became apparent that further improvements can be made however to how the model is currently solved numerically, and to improve its general applicability. The model is currently fitted to the extraction curve using a standard Solver plug-in in Excel. This Solver is essentially a 'black box' that only allows a limited number of user specified options to minimize the sum of square errors for the dissolution curve models. Furthermore, the maximum number of iterations is limited, which implies that the optimization has to be repeated multiple times in order to achieve the minimum sum of square errors. Finally, a set of initial parameters has to be provided manually. The eventual result is thus potentially influenced by the choice of these parameters.

Another aspect that is limited in the current analysis relates to the quantification of the accuracy of the estimates given. The adequacy of using one, two or three fractions is tested using a simple F-test and an extra Akaike test (Akaike, 1974). However, an extra sensitivity approach is needed in order to determine not only which model to choose, but also quantify the accuracy of the estimates that the model renders.

Once the extraction has been performed on the continuous extraction setup, and the data have been extracted from the interface unit of the Skalar-analyzer, multiple different samples that were analyzed need to be isolated; the precise starting point of each curve has to be picked manually. Although normally this is not a problem, in samples with low concentrations this can prove challenging and a mathematical solution would be a strong advantage.

Although the current method has thus proven to be robust and is able to provide an improved quantification of confounding fractions in alkaline extraction of BSi, its assumed more widespread implementation in the future would strongly benefit from adaptations to the:

- Robustness, accuracy and run time

- Inputs of the initial estimates
- Accuracy of the estimates
- Automation of the isolation of independent curves

These aspects were specifically addressed in this chapter, written in collaboration with the Maths Department of the University of Antwerp. The new script will be published online, freely available to all interested researchers.

6.2. Methodology

Overview

The specific steps we followed, the method used and the deliveries obtained are summarized in the scheme below (**Figure 6.1**), and elaborated further in this section.

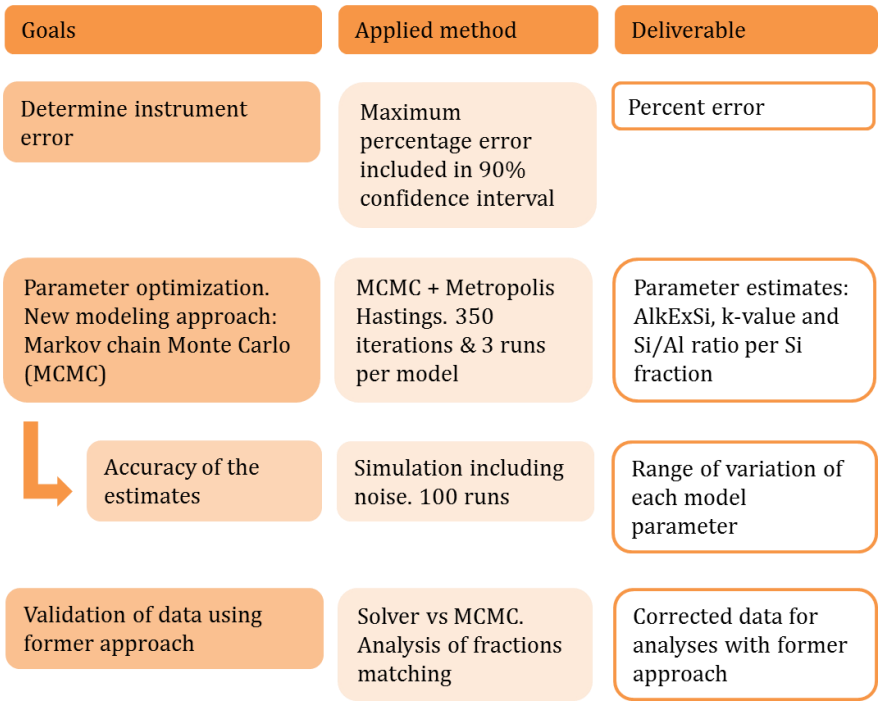

Figure 6.1. Summary of the methodology carried out: specific steps we followed, method used and deliverables.

Instrument error

A total of 4 samples from **Chapter 4** (amended soils) were analyzed with the Skalar-analyzer three times in order to calculate the instrument error. An averaged curve was rendered from the three replicated curves per element (Si and Al). Results of the four samples analyzed are shown in **Figure 6.2**.

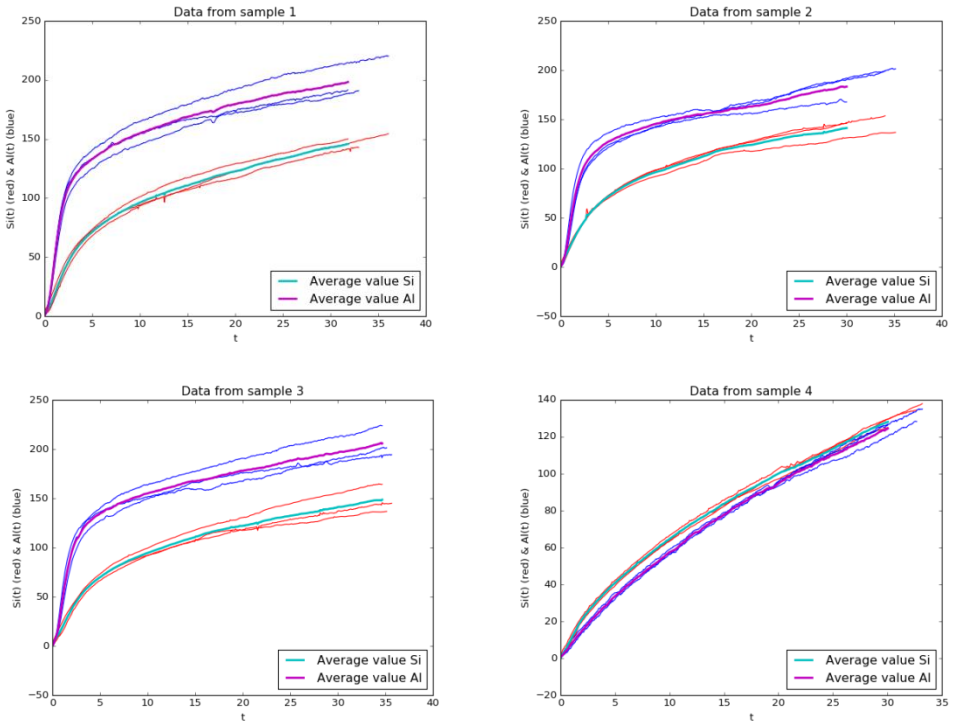

Figure 6.2. Results of the three runs and the average curve rendered for the four samples analyzed to calculate the instrument error. Si and Al dissolution curves (mg g^{-1}) for the three replicates in red and blue, respectively. Averages curves for Si and Al in magenta and cyan, respectively.

The standard deviation for each data point of each replicate curve compared to the averaged curve was calculated. In **Figure 6.3**, the variation of the standard deviation along the dissolution time for the three replicates of two of the Si-curve samples is presented.

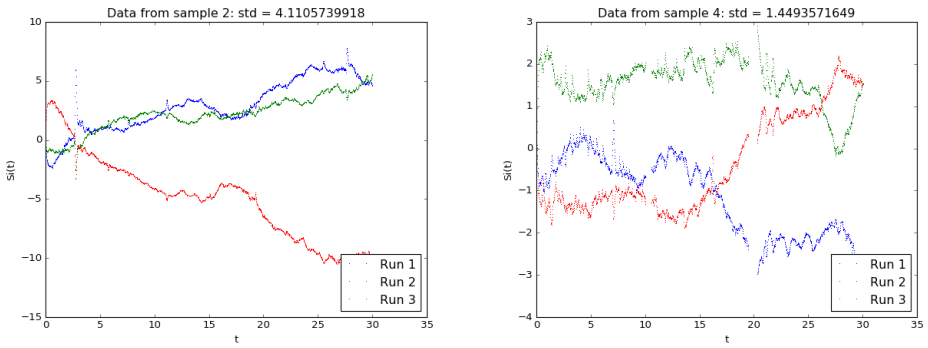

Figure 6.3. Standard deviation (error, mg g^{-1}) of each data point compared to the averaged curve at that time. Results for the three replicates runs of two of the Si-curves of the four samples analyzed.

The standard deviations were transformed into percentages in order to compare the errors of small and large values, and to study how the error was distributed. The error did not follow a normal distribution. In **Figure 6.4** a histogram with the number of cases of occurrence of each error percentage (by 0.5% intervals) for one of the samples is presented as an example.

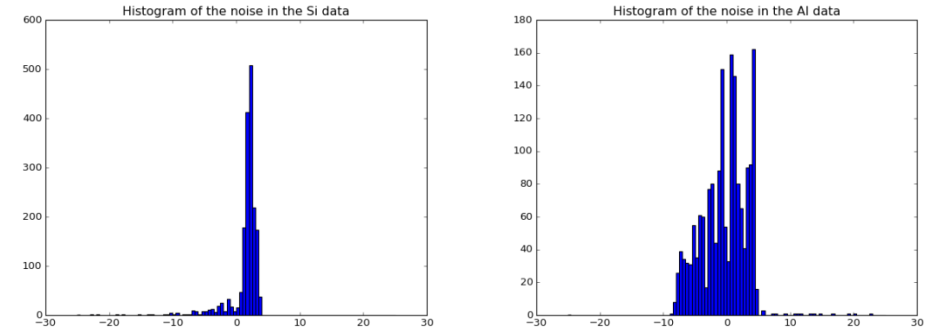

Figure 6.4. Distribution of the frequency of occurrence of each error percentage (by 0.5% intervals) for sample 2, for the Si (left) and Al (right) data.

Although not distributed normally, the large majority of percentual errors were below 10%. In order to avoid including outliers and only consider the most representative data, a confidence band including 90% of the error percentages was applied. Thus, highest and less abundant errors were dismissed. Afterwards, the maximum error percentage for each element curve that was included in the 90% of the total of error percentages was determined. In **Table 6.1** the maximum error percentage included in the 90% of the total of error percentages per curve analyzed are shown.

Table 6.1. Maximum error percentage included in the 90% of the data.

	Sample 1			Sample 2			Sample 3			Sample 4		
	R1	R2	R3	R1	R2	R3	R1	R2	R3	R1	R2	R3
Si	6	8	7	5	4	8	8	6	11	9	6	5
Al	9	7	4	8	6	11	7	7	9	8	4	8

An example of two samples is represented in **Figure 6.5**. The bounds (dashed lines) represent the 11% of error percentage. Data points inside show thus lower error percentage than 11% and data points outside the bounds show error percentages larger than 11%. The outer data points represent less than the 10% of the data per definition.

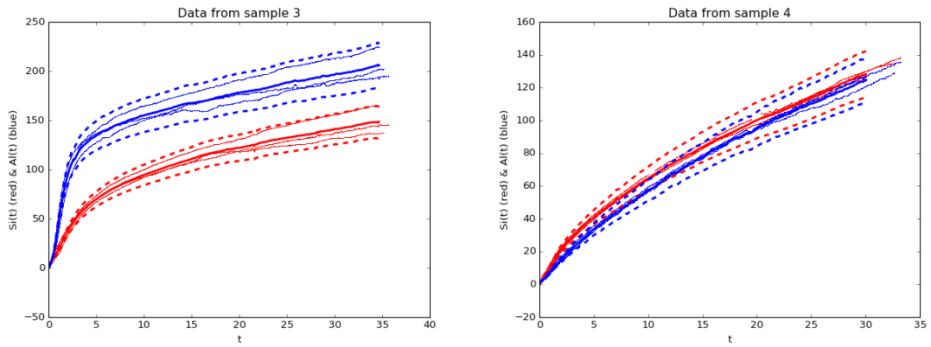

Figure 6.5. Results of the two of the samples: the three runs (replicates) with the average curve and the bounds (dashed lines) showing error percentages lower than 11%.

Conservatively, based on this approach, we assumed the maximum error encountered (11%) to be the instrument error. The percentage of data points included between the ±11% bounds are detailed in **Table 6.2**. The higher the percentage included the more conservative the percentage chosen.

Table 6.2. Percentages of data points of each curve that show an error lower than 11%.

	Sample 1			Sample 2			Sample 3			Sample 4		
	R1	R2	R3	R1	R2	R3	R1	R2	R3	R1	R2	R3
Si	93	93	97	97	99	96	96	95	98	97	95	96
Al	99	97	98	95	99	91	96	96	100	93	98	94

Parameter optimization in Python

The optimization of the Si and Al dissolution curves to determine BSi focuses on determining the parameter values in the model equations that minimize the error. In other words, we should find the parameters that describe the dissolution curves most accurately. To achieve this goal, the Excel solver was replaced with a Python implementation. The Python language is widely used and has an extensive open source library of mathematical packages. It allows better control over how the curve model optimization is performed, thus potentially providing improved insight in the obtained results.

The model equations consist of two well differentiated parts, the first order equation, representing the non-linearly dissolving sample fractions, and the linear equations to correct for the mineral and linear dissolution. Both are subsequently related through the Si/Al ratio. Different fractions are distinguished according to the Si/Al ratio obtained, assuming that both elements are released from the same fraction in a fixed ratio at the same rate.

$$Si\ (t) = \sum_{i=1}^{n} \mathrm{AlkExSi}_i \left(1 - e^{-k(t-t_0)}\right) + b\ (t - t_0)$$

$$Al\ (t) = \sum_{i=1}^{n} \frac{\mathrm{AlkExSi}_i}{\mathrm{Si/Al}_i}\left(1 - e^{-k(t-t_0)}\right) + \frac{b}{\mathrm{Si/Al}_0}\ (t - t_0)$$

The parameters to be estimated are thus:

$$k_i \text{ for } i \in \{1, \dots, n\}$$
$$\mathrm{AlkExSi}_i \text{ for } i \in \{1, \dots, n\}$$
$$\mathrm{Si/Al}_i \text{ for } i \in \{1, \dots, n\}$$

$$b$$
$$\mathrm{Si/Al_0}$$
$$t_0$$

where AlkExSi is the total amount of alkaline extractable Si (mg g^{-1}), *k* is the dissolution rate (min^{-1}), Si/Al is the molar concentration of Si divided by the molar concentration of Al, *b* is the linear dissolution rate of the mineral fraction and Si/Al_0 is the element ratio of the mineral part. A new parameter (t_0) was included as a correction for the possible displacement of the manually-selected starting point of the dissolution curve.

The model for the Si and Al concentration can be seen as the sum of a linear part and one to three exponentially decaying parts. Assuming that the exponential part decays to zero before the end of the experiment, a linear regression can be adjusted on the last ten minutes of the observational data in order to estimate all the parameters except for k and t_0.

For the model n = 1, we can subtract our linear estimate from the data, use a logarithmic transformation for the first 10 minutes of the dissolution and once again perform a linear regression analysis in order to estimate k. t_0 is simply set to zero.

For model n = 2, the optimal parameters found for model n = 1 can be used with the extra parameters set to 0 (or 1 in order to avoid division by 0). This will ensure that model 2 will always find a better or the same fit than model 1. For model n = 3 the same is done starting from the optimal parameters found for model n = 2.

The optimization itself was done using the stochastic Newton Markov chain Monte Carlo method (MCMC, Martin et al., 2012). In this method new estimates for the optimal parameters are determined by drawing a sample from a local Gaussian distribution centered at the current set of parameters. The new parameters are used based on a Metropolis Hastings criterion which will sometimes accept less accurate estimates. This method is slower than most local optimization methods, but if enough samples are drawn, a global minimum for the sum of square error can be found. Number of iterations and

runs per model (1, 2 or 3 decaying parts) can be modified. Here we run each model three times and applied 350 iterations per run.

The difference between the model output and the real data was evaluated through the minimization of the cost function:

$$J = \|Si - \overline{Si}\|_2^2 + \left\|Al - \overline{Al}\right\|_2^2$$

where $\overline{Si}$ and $\overline{Al}$ are vectors in $\mathbb{R}$ containing the observation data at every measured time $\{t_1, \ldots, t_m\}$ and Si and Al are the vectors in $\mathbb{R}$ with our model predictions.

An Akaike test was performed afterwards to select the best model fit (among the models with one, two or three non-linear dissolving fractions). The advantage compared to a simple F-test is that the Akaike test considers the number of parameters of each model in the calculation of the Akaike's index:

$$AIC = 2 \times (n\ parameters) + (n\ samples) \times \ln\left(\frac{RSS}{n\ samples}\right)$$

A correction is made in order to account for the difference between n of parameters and n of samples:

$$AICc = AIC + 2 \times \frac{(n\ parameters) \times (n\ parameters + 1)}{(n\ samples) - (n\ parameters) - 1}$$

This correction becomes important when (n parameters)$^2 \ll$ (n samples).

The model showing the smallest *AICc* is the preferred model. Instead of performing the Akaike test in an online service (https://www.graphpad.com/quickcalcs/aic1/) which requires manual input, the inclusion of the Akaike test as another step in the run script after the modeling automatize the performance.

The result of the modeling is the parameter estimates for: t_0, b, $SiAl_{lin}$, parameters for the first ($AlkExSi_1$, k_1, Si/Al_1), second ($AlkExSi_2$, k_2, Si/Al_2, if applicable) and third ($AlkExSi_3$, k_3 and Si/Al_3, if applicable) decaying fraction.

Accuracy of the estimates

In order to verify the accuracy of the estimates, we could choose to run the same sample multiple times, perform the Monte Carlo optimization and compare the results of every run to see how much the estimated parameters differ in each analysis. However, since this is time consuming and expensive, we decided to apply an alternative approach. Since even in the largest model only 12 parameters need to be estimated, an accurate estimate of the curve parameters can be made theoretically using only a selection of the data points.

A random subset of 50 measurements of the raw dissolution curve data was therefore taken in order to "simulate" new analyses of the same sample. To increase the accuracy of the simulation, a random noise (error) between -11% and +11% (instrument error) was added to the selected subset of data measurements. With this, the overall simulation includes the instrument variation.

With the optimal parameters provided by the MCMC analysis, a new local optimization is subsequently performed on the smaller data set, in order to find a new estimate for the parameters.

If this is repeated 100 times, we can subsequently estimate the average and the standard deviation of all estimated parameters. The solution of each run is kept and compared parameter by parameter to all other runs, which allows the standard deviation of every parameter to be calculated. The smaller the SD, the larger the confidence is on the estimate of that particular parameter. The simulation was performed for all 50 test samples obtaining a mean and a SD value per parameter. The SD obtained for each parameter was converted into a percentage to obtain the percent deviation and compare different range of values. We present the results of all non-linearly dissolving fractions ($k>0.1\ min^{-1}$), classified as main and secondary fractions (fractions showing the largest AlkExSi and second largest AlkExSi values, respectively), obtained for the 50 samples and highlighting particularly the results for the biogenic fractions.

Validation of earlier data

The results obtained using the two approaches for the same 50 samples mentioned above were compared. Matches and mismatches between the fractions described by the new and the former approach were analyzed. The following considerations were applied to determine the match or mismatch between fractions:

- If the character of the fraction according to the Si/Al ratio distinction as in Barão et al., (2014) is identical, the characterization of the fraction was considered to match.
- k value was considered to match if the identification as non-linear or semi-linear was identical ($k>0.1$ and $k<0.1$ respectively).
- When one or both of the above conditions was not fulfilled the results were consider to 'mismatch'.
- The AlkExSi amount in a particular fraction was considered to match if the difference in amount was <25%. The percentage from the total number of fractions showing a difference between the estimates of <10%, <25% and higher than 25% was counted.

Separate comparisons were performed according to the importance and the character of the fraction: fractions included in the results (main fraction and secondary fraction) and fractions discarded (due to AlkExSi<1% of total AlkExSi or values of $k<0.1$, following (Barão et al., 2014)), as well as comparisons for only biogenic fractions.

When a mismatch occurred, the samples characterized wrongly were checked for: 1) if the value obtained using the former approach was included within the +- standard deviation of that parameter rendered by the simulation and 2) if the mismatching value was close to the relevant boundaries. If no one of these statements occurred, it was considered that the result obtained using the former approach was wrong, since boundaries would have to be shifted to unrealistic values to obtain same fraction definition.

6.3. Results

Parameter optimization in Python

The estimates values obtained applying the new approach for the 50 samples analyzed are detailed in **Table 6.3** ('Estimates MCMC'). The values presented are the result of the MCMC modeling (350 iterations and 3 runs per model and sample) and the afterwards best model selection showing lowest error.

Accuracy of the estimates

Results of the analysis of accuracy of the estimates after the simulations are shown in **Table 6.3.** The mean and the standard deviation per parameter (AlkExSi, k and Si/Al) and the percent deviations are shown for the main and the secondary fraction. Percent deviations ranged from 0 to 10%, 10 to 25%, 25 to 50% and larger than 50% are shaded in different colors, and will be discussed later.

For the main fraction, the majority (38 out of 50) of percent deviations for the AlkExSi value were lower than 10%. For the k value the majority (34 out of 50) showed percent deviations between 10 and 25%. Finally the majority (31 out of 50) of percent deviations for the Si/Al value were lower than 10%. For the secondary fractions the percent deviations were overall higher than for the main fraction and more variable. The majority (12, 12 and 11 out of the 33 samples, for the AlkExSi, k and Si/Al value respectively) of percent deviations were higher than 50%.

For both main and secondary fractions, the parameter Si/Al showed the highest percent deviations, but the percent deviation for the k value was in more cases higher than 10% or 25%. The relation between these percentages and the characteristic of the fractions will be discussed later.

Table 6.3. Results of the parameter optimization in Python (new approach) and the accuracy of the estimates analysis. Estimates for AlkExSi (mg g^{-1}), k (min^{-1}) and Si/Al for the 50 samples (separated by main and secondary fraction) resulted from the MCMC modeling. Mean and standard deviations of all parameters after the 100 times simulations and percent deviations that the SD entails from the mean value of every parameter estimated. Biogenic fractions are shaded in green. Percent deviations lower than 10%, between 10 and 25%, between 25 to 50% and higher than 50% are shaded in white, blue, purple and orange respectively. In bold, results of biogenic fractions showing percent deviations higher than 25%. In bold light red, parameters with SD overlapping the boundary (k=0.1 or Si/Al=5) for BSi fractions.

	Estimates MCMC						Simulation Results. Mean ± SD (SD %)					
	Main fraction			Secondary fraction			Main fraction			Secondary fraction		
Sample	AlkExSi	k	Si/Al	AlkExSi	k	Si/Al	AlkExSi	k	Si/Al	AlkExSi	k	Si/Al
1 - Cropland Acrisol UM 0-10	11.17	0.10	7.70				11.17 ± 0.01 (0.06)	**0.10 ± 0.01 (11.7)**	7.70 ± 0.00 (0.03)			
2 - Cropland Acrisol UM 40-50	15.93	0.25	0.72				15.88 ± 0.53 (3.34)	0.25 ± 0.03 (10.5)	0.71 ± 0.08 (11.5)			
3 - Forested Acrisol GT 40-50	6.78	0.48	0.84	2.22	0.18	0.17	6.69 ± 0.44 (6.62)	0.54 ± 0.16 (29.2)	2.23 ± 10.3 (463)	2.44 ± 3.03 (124)	0.19 ± 0.05 (23.8)	0.17 ± 0.13 (77.6)
4 - Forested Acrisol GUM 30-40	9.28	0.41	0.64				9.11 ± 0.48 (5.31)	0.42 ± 0.04 (8.46)	0.63 ± 0.06 (8.81)			
5 - Forested Acrisol GB 40-50	16.78	0.10	1.41	3.33	0.49	0.25	16.21 ± 2.76 (17.0)	0.12 ± 0.03 (23.5)	1.31 ± 0.32 (24.7)	3.26 ± 0.76 (23.2)	0.66 ± 0.23 (34.5)	0.28 ± 0.06 (23.1)
6 - Forested Acrisol SLM 180-	16.30	0.41	0.67	3.80	0.12	0.23	15.08 ± 1.98 (13.1)	0.46 ± 0.10 (21.9)	0.70 ± 0.07 (10.3)	3.82 ± 0.20 (5.29)	0.14 ± 0.03 (23.3)	0.21 ± 0.04 (17.1)
7 - Forested Acrisol SB 0-10	17.00	0.16	9.26	0.15	0.33	0.03	17.08 ± 0.21 (1.21)	0.17 ± 0.01 (7.81)	**9.53 ± 1.96 (20.6)**	0.21 ± 0.17 (80.0)	0.33 ± 0.02 (6.82)	0.04 ± 0.03 (80.1)
8 - Forested Acrisol GB 20-30	11.08	0.11	6.42	1.20	0.57	0.27	11.08 ± 0.01 (0.10)	**0.11 ± 0.01 (10.6)**	6.42 ± 0.00 (0.08)	1.20 ± 0.01 (0.60)	0.57 ± 0.04 (6.89)	0.27 ± 0.02 (7.96)
9 - Forested Acrisol GB 75-85	10.15	0.40	0.48	1.46	2.62	455	9.85 ± 0.83 (8.44)	0.43 ± 0.07 (15.9)	0.48 ± 0.05 (10.0)	**1.66 ± 0.40 (24.1)**	**45.5 ± 229 (503)**	455 ± 0.01 (0.00)
10 - Forested Acrisol SUM 10-20	28.51	0.16	10.9				28.52 ± 0.03 (0.12)	**0.16 ± 0.03 (18.9)**	10.9 ± 0.01 (0.12)			
11 - Forested Acrisol SB 75-85	17.13	0.13	1.35	3.24	1.09	602	16.82 ± 1.24 (7.39)	0.14 ± 0.02 (14.3)	3.29 ± 10.1 (306)	**3.15 ± 0.93 (29.6)**	**28.4 ± 83.4 (294)**	602 ± 0.00 (0.00)
12 – Forested Acrisol SLM 75-85	11.52	0.62	0.45	0.00			11.25 ± 0.86 (7.67)	0.75 ± 0.12 (16.5)	0.46 ± 0.05 (10.8)			
13 - Cropland Acrisol T 10-20	9.61	0.16	314	0.00			9.69 ± 0.84 (8.70)	**0.15 ± 0.03 (19.4)**	314 ± 0.00 (0.00)			

14 - Cropland Acrisol B 40-50	10.03	0.29	41.1	0.23	0.37	0.02	10.12 ± 0.34 (3.39)	0.30 ± 0.03 (10.5)	41.1 ± 0.00 (0.01)	0.32 ± 0.32 (102)	0.39 ± 0.06 (15.5)	0.03 ± 0.03 (97.6)
15 - Cropland Acrisol B 55-65	10.31	0.24	0.62				10.07 ± 0.92 (9.16)	0.26 ± 0.05 (18.9)	0.63 ± 0.06 (9.34)			
16 – Cropland Leptosol M 10-20	2.91	0.26	2.36	0.14	0.79	0.08	2.86 ± 0.21 (7.34)	0.25 ± 0.04 (13.8)	2.35 ± 0.76 (32.2)	0.21 ± 0.25 (115)	0.96 ± 0.31 (32.5)	0.12 ± 0.13 (106)
17 - Cropland Leptosol B 30-40	4.49	0.29	972	1.34	0.61	0.20	**4.29 ± 0.75 (17.5)**	**0.31 ± 0.08 (25.9)**	972 ± 0.00 (0.00)	1.59 ± 0.68 (43.1)	0.69 ± 0.11 (15.2)	0.25 ± 0.11 (43.9)
18 – Cropland Acrisol B 0-10	1.88	0.17	0.29				1.89 ± 0.09 (4.67)	0.17 ± 0.02 (11.1)	0.30 ± 0.02 (7.83)			
19 - Cropland Leptosol M 40-50	8.55	0.61	2297				8.55 ± 0.00 (0.02)	**0.65 ± 0.08 (12.3)**	2297 ± 0.00 (0.00)			
20 - Forested Acrisol GlM 95-	13.82	0.30	1448	0.71	0.48	0.04	13.86 ± 0.44 (3.21)	**0.31 ± 0.04 (13.6)**	1448 ± 0.00 (0.00)	0.73 ± 0.41 (56.2)	0.52 ± 0.08 (14.6)	0.04 ± 0.02 (56.4)
21 - Cambisol +Wollastonite	2.87	0.39	132				2.87 ± 0.00 (0.01)	0.39 ± 0.03 (7.09)	132 ± 0.00 (0.00)			
22 - Nitisol	1.24	0.12	501	0.04	0.22	0.06	1.24 ± 0.00 (0.01)	0.12 ± 0.01 (7.20)	501 ± 0.00 (0.00)	0.04 ± 0.00 (2.94)	0.23 ± 0.05 (19.9)	0.06 ± 0.01 (21.7)
23 - Nitisol Si-/biochar	0.11	53.5	40.0	0.05	0.23	0.07	**0.12 ± 0.02 (16.7)**	53.6 ± 0.00 (0.01)	40.0 ± 0.00 (0.00)	0.05 ± 0.05 (101)	0.25 ± 0.07 (27.2)	0.06 ± 0.06 (87.7)
24 - Nitisol Si+/biochar	2.12	0.11	0.94	0.66	0.48	20.0	2.08 ± 0.38 (18.4)	0.11 ± 0.01 (13.1)	0.95 ± 0.19 (20.0)	**0.70 ± 0.25 (35.8)**	**0.49 ± 0.13 (26.2)**	20.2 ± 0.75 (3.72)
25 - Cambisol	3.00	0.33	93.6				3.00 ± 0.00 (0.04)	**0.34 ± 0.05 (14.1)**	93.6 ± 0.00 (0.00)			
26 - Si-/biochar	3.81	0.28	2279				3.81 ± 0.00 (0.03)	**0.29 ± 0.04 (12.9)**	2279 ± 0.00 (0.00)			
27 - Si+/biochar	3.21	0.21	232	1.79	0.57	0.31	3.27 ± 0.15 (4.53)	**0.20 ± 0.05 (25.5)**	232 ± 0.00 (0.00)	1.85 ± 0.20 (10.8)	0.77 ± 0.33 (43.1)	0.35 ± 0.07 (18.7)
28 - Cambisol +Wollastonite	1.64	0.43	58.4	1.09	0.55	0.17	1.65 ± 0.07 (4.54)	**0.47 ± 0.13 (28.4)**	58.4 ± 0.00 (0.00)	1.09 ± 0.08 (7.72)	0.58 ± 0.10 (16.4)	0.18 ± 0.02 (8.72)
29 - Nitisol	0.30	0.43	0.73				0.35 ± 0.10 (27.9)	0.40 ± 0.11 (28.3)	0.75 ± 0.09 (12.3)			
30 - Cambisol Si-/biochar	2.63	0.50	168	0.17	0.66	0.03	2.61 ± 0.10 (3.64)	**0.56 ± 0.10 (17.5)**	168 ± 0.00 (0.00)	0.14 ± 0.10 (67.0)	0.74 ± 0.11 (15.5)	0.02 ± 0.02 (66.2)
31 - Savannah Grass	27.62	0.80	92.6	22.16	0.14	632	27.27 ± 2.44 (8.95)	**19.7 ± 193 (981)**	**97.9 ± 57.8 (59.0)**	**22.49 ± 2.46 (10.9)**	**0.16 ± 0.21 (128)**	**648 ± 175 (27.0)**
32 - Sediment Kenya 4-6	6.62	0.11	20.9	0.93	1.11	42.2	**6.79 ± 1.08 (16.0)**	**0.10 ± 0.02 (19.5)**	**20.7 ± 2.19 (10.6)**	**1.00 ± 0.15 (15.5)**	**1.42 ± 0.99 (69.2)**	42.2 ± 0.11 (0.26)

33 - Sediment Kenya 8-10	12.45	0.35	6.08				12.47 ± 0.15 (1.18)	**0.36 ± 0.04 (12.1)**	6.26 ± 0.42 (6.72)			
34 - Sediment Kenya 4-6	8.96	0.27	4.28				**9.21 ± 0.94 (10.2)**	0.26 ± 0.02 (7.54)	**6.12 ± 11.7 (191)**			
35 - Sediment Kenya 0-2	2.39	0.37	4.91				2.38 ± 0.07 (3.13)	**0.40 ± 0.08 (19.1)**	5.02 ± 0.42 (8.35)			
36 - Sediment Kenya 8-10	14.30	0.08	13.1	2.11	0.43	4.57	14.50 ± 0.64 (4.41)	**0.08 ± 0.01 (15.4)**	13.3 ± 0.46 (3.49)	**2.20 ± 0.42 (19.3)**	**0.43 ± 0.24 (54.7)**	**4.77 ± 0.88 (18.4)**
37 - Savannah soil Kenya 0-10	16.76	0.10	2.51	1.69	0.73	8965	14.98 ± 3.06 (20.4)	0.12 ± 0.01 (12.1)	2.36 ± 0.47 (19.7)	**2.35 ± 4.64 (197)**	**303 ± 1739 (573)**	8965 ± 0.05 (0.00)
38 - Savannah soil Kenya 0-10	26.23	0.12	27.7	0.68	0.58	1.04	26.57 ± 0.81 (3.06)	**0.11 ± 0.02 (18.3)**	27.7 ± 0.07 (0.24)	0.96 ± 0.66 (68.5)	1.00 ± 1.35 (135)	1.34 ± 0.84 (62.6)
39 - Sediment Kenya 8-10	5.65	0.30	903	0.12	0.15	0.10	5.66 ± 0.13 (2.27)	**0.33 ± 0.05 (16.4)**	903 ± 0.00 (0.00)	0.12 ± 0.07 (54.8)	0.16 ± 0.04 (26.4)	0.10 ± 0.05 (53.8)
40 - Hippos dung deposit	24.15	0.17	61.3	12.24	0.73	17.7	24.74 ± 1.48 (6.00)	**0.16 ± 0.03 (19.3)**	61.2 ± 0.58 (0.94)	12.23 ± 1.20 (9.84)	**2.42 ± 8.08 (334)**	18.0 ± 1.61 (8.95)
41 - Spruce 550°C burned OM	223	0.50	28.8				220 ± 15.2 (6.89)	**0.55 ± 0.08 (14.6)**	28.2 ± 2.88 (10.2)			
42 - Peat 350°C burned OM	2.49	0.21	524	0.32	0.77	0.18	2.53 ± 0.06 (2.47)	0.20 ± 0.02 (8.85)	524 ± 0.00 (0.00)	0.35 ± 0.09 (24.9)	0.81 ± 0.25 (30.4)	0.20 ± 0.06 (28.8)
43 - Beech 550°C burned OM	27.39	0.92	20.6	21.77	0.11	4.92	27.41 ± 0.34 (1.23)	**1.01 ± 0.24 (23.7)**	20.2 ± 1.22 (6.05)	21.62 ± 2.34 (10.8)	0.11 ± 0.03 (27.9)	4.73 ± 1.28 (27.1)
44 - Peat 550°C burned OM	7.15	1.63	6248	2.10	0.58	0.16	7.02 ± 0.64 (9.07)	**2.32 ± 1.31 (56.4)**	6248 ± 0.00 (0.00)	2.31 ± 0.7 (30.4)	0.64 ± 0.10 (15.2)	0.18 ± 0.06 (32.1)
45 - Spruce 350°C burned OM	69.67	0.73	53.7	8.93	0.09	59.8	**65.44 ± 12.5 (19.0)**	**0.81 ± 0.20 (24.7)**	**55.1 ± 9.70 (17.6)**	**13.45 ± 12.51 (93.0)**	**0.12 ± 0.15 (130)**	**69.4 ± 49.8 (71.8)**
46 - Beech 350°C burned OM	22.98	0.98	2706	12.95	0.15	6.29	23.13 ± 0.49 (2.10)	**1.05 ± 0.19 (18.4)**	2706 ± 0.00 (0.00)	13.32 ± 1.04 (7.79)	**0.17 ± 0.31 (179)**	**6.35 ± 1.12 (17.7)**
47 - Spruce 550°C burned OM	165.3	0.91	66.6	15.68	0.15	23.4	**146 ± 49.1 (33.7)**	**2.19 ± 7.03 (321)**	**64.8 ± 28.4 (43.8)**	**38.12 ± 50.1 (131)**	**0.24 ± 0.25 (102)**	**53.9 ± 67.8 (126)**
48 - Beech 550°C burned OM	37.40	0.92	107	19.58	0.10	4.82	37.42 ± 0.12 (0.33)	**0.97 ± 0.17 (17.4)**	107 ± 0.00 (0.00)	19.59 ± 0.06 (0.30)	0.10 ± 0.04 (43.5)	4.80 ± 0.21 (4.30)
49 - Peat 550°C burned OM	7.25	0.52	0.48	1.74	3.91	76.4	6.97 ± 0.74 (10.6)	0.57 ± 0.06 (10.2)	0.49 ± 0.05 (10.6)	**1.79 ± 0.35 (19.8)**	**102 ± 492 (485)**	76.9 ± 3.13 (4.07)
50 - Beech 350°C burned OM	18.76	1.14	539	11.85	0.21	16.9	18.40 ± 1.18 (6.39)	**1.42 ± 0.55 (38.8)**	539 ± 0.02 (0.00)	12.38 ± 1.01 (8.16)	**0.20 ± 0.06 (29.9)**	**16.9 ± 5.01 (29.7)**

Validation of data analyzed using former approach

A total of 98% of the analyzed samples showed a better result (lower cost value) using the new refinement than the previous approach (data not shown). Comparisons between results from the two approaches are shown in **Table 6.4**. Results are divided in results of the main fraction and result of the secondary fraction. The main fraction was considered to be the largest fraction (AlkExSi) from the non-linearly dissolving fractions ($k>0.1$ min^{-1}). The discarded fractions correspond to fractions not included in results due to a low k ($k<0.1$ min^{-1}) or a low AlkExSi amount (<1% of the total AlkExSi). The number of new extra fractions described by the new approach and fractions absent using the new approach and the overall totals of included in results and discarded fractions are included in **Table 6.4** as well.

Table 6.4. Comparison between results obtained using Solver (GRG Nonlinear) in Excel and MCMC in Python. Percentages of the fractions from the 50 samples analyzed matching (% cor) the character of the fraction (Si/Al ratio) or the k value (k>0.1 or k<0.1). Percentage of the fractions differing less than 10%, 25% and more than 25% in AlkExSi amount. Results for all fractions and biogenic fractions.

	All fractions						Biogenic fractions					
		Si/Al	k	AlkExSi				Si/Al	k	AlkExSi		
	N	% cor	% cor	<10 %	<25 %	>25 %	N	% cor	% cor	<10 %	<25 %	>25 %
Included fractions	79	87	98	43	63	37	45	91	100	58	78	22
Main fraction	50	86	100	52	72	28	35	91	100	57	77	23
Secondary fraction	28	89	93	29	50	50	10	90	100	60	80	20
Third fraction	1	100	100	0	0	100						
Discarded	48	90	92	21	33	67	9	78	89	11	44	56
New fractions	12						4					
Absent	3											
Total	127	88	95	35	52	48	54	89	98	50	72	28

For the main fraction 86% of the samples (from the 50 samples analyzed) had the same character ($Si/Al<1$, $1<Si/Al<5$ and $Si/Al>5$) according to both models, and all (100%) were in the same k-boundary. A total of 72% of all main fractions had a deviation of less than 25% for the total AlkExSi. For the secondary fraction, 89% of the fractions described (28) had the same

character and 93% were in the same k-boundary. A total of 50% of all samples had a deviation of less than 25% for the total AlkExSi. From the fractions discarded, a 90% and 92% of the fractions had the same character and were in the same k-boundary respectively, but only 33% had a deviation of less than 25% for the total AlkExSi. A new 12 fractions were described using the new approach, and 3 fractions were absent in the results using the new approach.

The results of only the biogenic fractions were overall better than the results taking into account all fractions described. So that, for the main biogenic fractions, a 91% of the samples (from the total of 35 fractions) had the same character, and all of them (100%) were in the same k-boundary. A total of 77% of all main biogenic fractions had a deviation of less than 25% for the total AlkExSi. For the secondary biogenic fractions, 90% of the fractions described (10) had the same character and 100% were in the same k-boundary. A total of 80% of the secondary biogenic fractions had a deviation of less than 25% for the total AlkExSi.

Results of fractions showing an incorrect SiAl or k, or with a variation >25% for the AlkExSi (only biogenic fractions shown) are detailed in **Table 6.5**. A total of 12 fractions were described wrongly regarding the Si/Al or k value (7 and 5 main and secondary fractions respectively). From that total, three biogenic fractions were described as clays using the new approach, and four fractions previously described as clays or oxides were now characterized as biogenic. Considering the SD's obtained and the proximity of values to the boundaries chosen, three of those biogenic fractions could 'accord' for both approaches.

Table 6.5. Detailed values of mismatching fractions. Parameters estimated using Solver (former approach) and MCMC (new approach). Fractions are separated by fractions included in results (main and secondary fractions) and discarded fractions. Mismatching fractions ('Mism.') are classified by the inclusion of the parameter value obtained using the former approach within the error determined by the SD obtained in the simulation or the proximity of the value to the boundaries set: 'Yes' when one of the circumstances applies or 'No' when any of those applied. In green, fractions described as biogenic (Si/Al>5) and in red SD values that overlap the boundary Si/Al=5 or k=0.1 for biogenic fractions. Note that for fractions showing a >25% of difference in AlkExSi only biogenic fractions are included.

	Solver			Simulation (Mean + SD)			
Sample	AlkExSi	k	Si/Al	AlkExSi	k	Si/Al	Mism.
Included fractions							
Main fraction							
Incorrect SiAl							
3 – Forested Acrisol GT 40-50	8.71	0.35	1.02	6.69 ± 0.44	0.54 ± 0.16	2.23 ± 10.33	Yes
8 – Forested Acrisol GB 20-30	11.13	0.11	4.34	11.08 ± 0.01	0.11 ± 0.01	6.42 ± 0.00	Yes
11 – Forested Acrisol SB 75-85	18.33	0.14	5.11	16.82 ± 1.24	0.14 ± 0.02	3.29 ± 10.05	Yes
14 – Cropland Acrisol B 40-50	7.87	0.26	0.59	10.12 ± 0.34	0.30 ± 0.03	41.13 ± 0.00	No
15 – Cropland Acrisol B 55-65	25.94	0.13	4.27	10.07 ± 0.92	0.26 ± 0.05	0.63 ± 0.06	No
19 – Cropland Leptosol M 40-50	12.02	0.38	0.57	8.55 ± 0.00	0.65 ± 0.08	2297 ± 0.00	No
24 – Nitisol Si+/biochar	2.17	0.16	25.58	2.08 ± 0.38	0.11 ± 0.01	0.95 ± 0.19	No
AlkExSi >25%							
13 – Cropland Acrisol T 10-20	19.15	0.11	12.08	9.69 ± 0.84	0.15 ± 0.03	314 ± 0.00	
17 – Cropland Leptosol B 30-40	6.09	0.29	41.51	4.29 ± 0.75	0.31 ± 0.08	972 ± 0.00	
19 – Cropland Leptosol M 40-50	12.02	0.38	0.57	8.55 ± 0.00	0.65 ± 0.08	2297 ± 0.00	
22 - Nitisol	1.97	0.09	15.91	1.24 ± 0.00	0.12 ± 0.01	501 ± 0.00	
27 – Si+/biochar	4.64	0.29	29.94	3.27 ± 0.15	0.20 ± 0.05	232 ± 0.00	
28 – Cambisol + Wollastonite	3.04	0.36	28.24	1.65 ± 0.07	0.47 ± 0.13	58.36 ± 0.00	
35 – Sediment Kenya 0-2	4.00	0.23	9.45	2.38 ± 0.07	0.40 ± 0.08	5.02 ± 0.42	
47 – Spruce 550°C burned OM	456.1	0.60	36.60	146 ± 49.1	2.19 ± 7.03	64.8 ± 28.4	
Secondary fraction							
Incorrect SiAl							
24 - Nitisol Si+/biochar	0.21	0.84	1.02	0.70 ± 0.25	0.49 ± 0.13	20.16 ± 0.75	No
38 – Savannah soil Kenya 0-10	0.00	0.44	0.00	0.96 ± 0.66	1.00 ± 1.35	1.34 ± 0.84	Yes
43 – Beech 550°C	21.88	0.10	5.22	21.62 ± 2.34	0.11 ± 0.03	4.73 ± 1.28	Yes

burned OM							
Incorrect k							
14 – Cropland Acrisol B 40-50	0.12	0.04	0.00	0.32 ± 0.32	0.39 ± 0.06	0.03 ± 0.03	No
27 – Cambisol Si+/biochar	2.07	0.02	0.65	1.85 ± 0.20	0.77 ± 0.33	0.35 ± 0.07	No
AlkExSi >25%							
24 - Nitisol Si+/biochar	0.21	0.84	1.02	0.70 ± 0.25	0.49 ± 0.13	20.16 ± 0.75	
36 – Sediment Kenya 6-10	2.69	0.32	4.25	2.20 ± 0.42	0.43 ± 0.24	4.77 ± 0.88	
Discarded fraction							
Low k value							
Incorrect SiAl							
3 - Forested Acrisol GT 40-50	35.46	0.05	3.42	31.00 ± 3.08	0.06 ± 0.01	5.76 ± 2.47	Yes
6 – Forested Acrisol SLM 180-190	32.85	0.04	1.95	22.65 ± 0.32	0.07 ± 0.02	207.2 ± 0.00	No
14 – Cropland Acrisol B 40-50	32.90	0.07	18.40	48.16 ± 0.09	0.04 ± 0.00	0.84 ± 0.06	No
28 - Cambisol + Wollastonite	6.22	0.04	40.47	6.27 ± 0.11	0.05 ± 0.01	3.71 ± 4.34	Yes
30 - Cambisol Si-/biochar	7.38	0.03	1.06	4.61 ± 0.00	0.04 ± 0.00	0.75 ± 0.06	Yes
Incorrect k							
5 – Forested Acrisol GB 40-50	26.14	0.05	1.66	16.21 ± 2.76	0.12 ± 0.03	1.31 ± 0.32	Yes
27 - Cambisol Si+/biochar	0.00	0.45	0.00	0.18 ± 0.21	0.10 ± 0.09	0.06 ± 0.05	Yes
45 - Spruce 350°C burned OM	0.00	0.39	17.75	13.45 ± 12.5	0.12 ± 0.15	69.4 ± 49.8	Yes
Low AlkExSi							
Incorrect k							
24 - Nitisol Si+/biochar	0.01	0.09	0.00	0.02 ± 0.14	4.77 ± 1.68	0.13 ± 0.57	Yes

The script

The script file with the code to run the analysis can be found in: https://github.com/nschenkels/AlkExSi/tree/v1.0.0. The DOI of the script can be found in: 10.5281/zenodo.1184427. The script is presented in **Supplementary Material Chapter 6**.

6.4. Discussion

The MCMC automated parameter optimization in Python is able to obtain better results than the Solver function in Excel. The modeling of the curves consists in finding the best set of parameters values that adjust better to the experimental dissolution curves. To do so, the model varies the estimate values, applies the equations to obtain the expected Si and Al concentration at any given time and calculates the error of that particular fitting. The error or cost value consists in the sum of the differences between each measured data point and the corresponding modeled data point. The lower the cost the better the adjustment is. Standard approaches will search for a better adjustment decreasing the cost in each try.

The Metropolis Hastings criterion added in the MCMC approach allows to try a set of estimates less accurate (higher error) than the previous try, in the search for a further possible better set of estimates. Every model can feature several local minimums, and one global minimum. In **Figure 6.6**, a visualization of the performances of a model without and with the Metropolis-Hastings criterion is detailed. In conclusion, including the Metropolis-Hastings criterion increases the possibility to find the global minimum.

Besides the acquisition of a better solution, the provision of an error per parameter calculated in the simulation adds sensitivity to the estimates. Finally, the new conservative 11% instrument error added to the simulation is included in the analysis.

The settings (number of iterations and runs carried out for the MCMC modeling, number of data points selected and number of runs for the simulation) can be adjusted. Moreover, extra analysis can be easily added. The adjustability of all settings provides the flexibility for researchers to adapt to the trade-off between the acquisition of more robust and precise results and the time constraints related to the available time for analyzing the data.

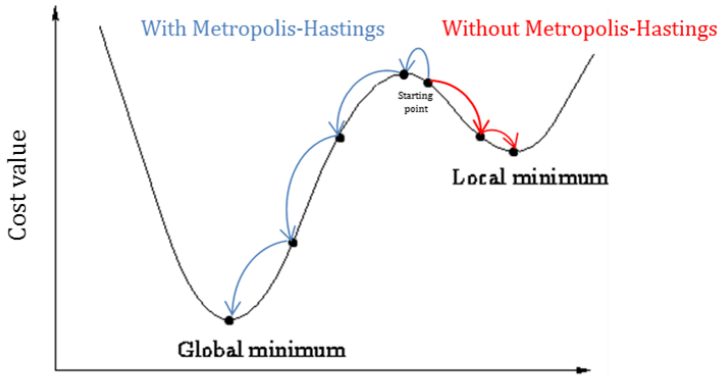

Figure 6.6. Visualization of a hypothetical modeling including and not including the Metropolis-Hastings criterion. The Metropolis-Hastings criterion allows selecting a set of parameters resulting in a higher cost value in the search of possible lower local minimum and eventually the global minimum.

Our approach also speeds up the analysis compared to the earlier Solver solution. Although we did not automatize the extraction of the data (isolation of each data curve from the day-run and the consequent transformations), the average time of the whole run was less than ~15 min using an Intel® Core™ i7-4600U CPU @2.10GHz and 16GB Ram memory, far faster than the ~30 min using Solver. However the time needed may vary depending on the hardware properties. In case multiple samples have to be analyzed, the running time could be a constraint. The bottle neck in this regard resides in the MCMC analysis.

The method to quantify BSi in soils and sediments evolved from an estimation based on three-data points from DeMaster, (1981) to a mineral interference corrected method but with a blind acceptance of estimates in Barão et al. (2014). The new refinement includes the mineral correction and adds errors on the estimates resulting in a huge progress in the quantification of BSi in soils and sediments.

Instrument error

To our knowledge, this is the first time an instrument error is determined for the continuous extraction of Si and Al based on an evaluation of potential

error contributed by all analysis points of the dissolution curves. The estimate of a conservative error of 11% should in the future be verified using a larger variety of samples, and could potentially be adapted if only a specific sample type is analyzed (e.g. only marsh sediments, only soil horizon O and A samples). Considering that previous methodologies used to determine BSi (Barão et al., 2014; DeMaster, 1981; Koning et al., 2002) did not include a targeted sensitivity analysis or confidence interval for the parameters, the present refinement is a clear progress in the determination of BSi in soils.

We demonstrate that there is variability in the measurements that accounts up to 11% of the value, with possibly even higher deviations in specific outliers. In the hypothetical case that the same variation is applied to the DeMaster (1981) extraction, where the quantification of BSi is based on three data points that are assumed to represent the linear stage of the extraction, the over- or underestimation of BSi is potentially much larger, as the intercept used to calculate the BSi amount would vary drastically. In the example presented in **Figure 6.7**, a realistic error was applied to hypothetical traditional three point extraction data. A huge difference in the quantification of BSi is clearly obtained when calculating the intercept based on only three data points, taking into account potential instrument and sample variability error.

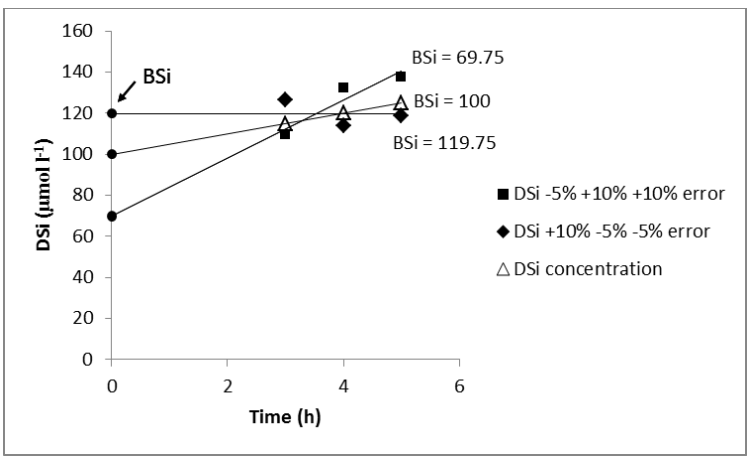

Figure 6.7. Representation of DeMaster method applying different errors to the data points. The hypothetical real DSi concentration data (triangle) and two data sets with errors (square and diamond). For each including-error-data set, the errors applied are detailed in the legend. The estimated BSi concentration (the intercept) hypothetically obtained from each data set are detailed by each trend line.

Data

The validation of the data presented in this thesis, modeled with the former approach, was in most cases consistent to the results obtained applying the new refined approach, that we developed based on the experiences obtained in this thesis. The 'character' (Si-Al ratio) of the largest fraction, was described identically in 86% of the cases. The mismatches in Si/Al determination for the secondary fraction were even slightly lower than for the main fraction (fractions described correctly: 89%). Moreover, the fractions discarded because of a low k or low AlkExSi values were all identical.

Based on our results it is clear that the accuracy in describing the BSi fractions is higher than the accuracy for the totality of fractions. The character of the largest BSi fraction was described correctly in 91% of the cases. The mismatches in Si/Al determination for the secondary BSi fractions were slightly lower than for the main fraction (fractions described correctly: 90%). Moreover, all fractions included in results matched in relation to the k-value (**Table 6.4**). As our methodological objective is to distinguish the BSi from other fractions that also dissolve non-linearly in 0.5 NaOH, here we focus on results regarding mismatching fractions described as BSi.

Fractions with large errors in BSi quantitative determination

Our results suggest that the quantification of BSi using the former and current curve analysis procedures can vary quite strongly: a total of ten fractions identified as BSi (out of 45) showed a difference in AlkExSi >25%. In these cases the MCMC approach renders smaller amounts of AlkExSi than the Solver approach, associated with higher k values. The ample variety in the samples that were in this case (including cropland soils, biochars, sediments and burned organic matter, and with AlkExSi ranges between 1.24 and 146 mg g^{-1}, k values between 0.12 and 2.19 min^{-1} and Si/Al ratios between 4.77 and >100) makes it impossible to assign a higher uncertainty of AlkExSi estimation to a specific type of sample.

It is clear from our results that the amount of AlkExSi of BSi main fractions is consistently described using the MCMC approach, with generally low deviations (<34%). Results for the BSi secondary fractions showed high deviations only for three fractions, two of which corresponded to a secondary BSi fraction.

Determination of the k-value

Only two k-values were misidentified using the former approach. Interestingly none of them corresponded to a BSi fraction. We can thus confirm that based on our results, the BSi fractions were accurately described in relation to the k value.

The boundary set is important at this regard. We divide fractions as reactive ($k>0.1$ min^{-1}) and non-reactive ($k<0.1$ min^{-1}) in 0.5 M NaOH, with k<0.1-fractions visually (near-) linear. However, the k value estimated only shows how fast the fraction is dissolving in 0.5 M NaOH: it does not represent solubility in soils, and thus should not be assigned an ecological meaning. In soils, the solubility of phytoliths depends on several factors: the plant species, as the characteristics of phytoliths are specific for every species; age of the phytoliths, which may affect the phytolith structure potentially decreasing their solubility (Fraysse et al., 2006; White et al., 2012; Koning et al., 2002); the phytolith's Al-content which is known to decrease phytolith's solubility; and soil conditions like water content, high pH, presence of humic acids and other compound that may react with phytoliths increasing their solubility. A base assumption of the method is that all BSi dissolves non-linearly, and phytoliths (and other plant BSi) should thus show k values higher than 0.1 min^{-1} in the extraction in 0.5 M NaOH (Barão et al., 2015). Here, we obtained k values for biogenic fractions between 0.10 and 54 min^{-1}. Koning et al. (2002) showed biogenic silica in sediments showing k values down to 0.06 min^{-1}. Similarly, we detailed in **Chapter 5** the possibility of having old phytoliths in Kenyan soils with $k=0.08$ min^{-1}. The reason was the presence of only one fraction with a lower k value (0.08 min^{-1}) in some of the samples

where a large amount of phytoliths should be present (as confirmed through microscopic analyses).

Using the former approach, the best solution rendered by the model was assumed to be correct with no concerns. Originally, the new method delivers also a standard deviation for the k value, which provides valuable information to decide whether a fraction is 'reactive' and will be included as a result or not. Some of the samples analyzed in the simulation showed ranges of variation for the k parameter that overlap the boundary k=0.1. Such fractions correspond to samples of soils (from depths between 20 and 85 cm deep), Kenyan riparian sediments and grass, and burned organic matter. Interestingly, the majority of them correspond to a secondary biogenic fraction from plant material (**Table 6.4**). These secondary BSi fractions were described in previous chapters (**Chapters 2** and **5**) as a secondary biogenic Si pool in plants consisting of Si polymers of H_4SiO_4 embedded within the plant cell walls. The dissolution of the secondary BSi pool was described as having a strong in situ solubility (faster than phytolith's) (Fraysse et al., 2010). The majority of fractions showing k-values >1min^{-1} shows as well high SD values that overlap the boundary. The methodological approach seems to be less accurate when a BSi fraction is extremely reactive in 0.5 M NaOH. According to our results, there is an apparent difficulty to assign a consistent k-value to this secondary plant BSi pool, possibly related to dissolution patterns. However, the presence of large BSi fractions (main fractions) in burned OM samples showing such high k-values confirms that phytoliths are possibly described with k-values >1 m^{-1} in the extraction in 0.5 M NaOH.

Determination of the Si/Al ratio

The determination of the Si/Al is arguably the most important parameter, as biogenic-non-biogenic characterization of any fraction is based on this estimate. We obtained a total of 4 biogenic fractions (out of 45) misidentified as non-biogenic and another 3 fractions misidentified as BSi by the former approach (**Table 6.5**). The majority of the fractions corresponded to soil samples from Acrisols from **Chapter 3**. The complexity of these soils samples

results in an apparent difficulty to assign a consistent Si/Al ratio to the fractions. The presence of secondary clay minerals, high content of Si adsorbed onto oxides or the occurrence of more than three non-linearly dissolving fractions are possibly the reason of the uncertainty in the modeling of these samples.

In theory, secondary silicate minerals with no Al may show, after modeling, similar characteristics as a BSi fraction (high k value, Si/Al>5). However, when analyzing Olivine ($(Mg, Fe)_2SiO_4$) with the present method, a reactive 'biogenic' AlkExSi fraction that accounted only for 2% of the total amount of olivine-Si added, was described (unpublished data/personal information). Wollastonite (**Chapter 4**) also showed a first order dissolving behavior corresponding only to 1.5% from the total amount of Si added. Assuming the linear dissolution of primary minerals and the experience from previous chapters, we can argue that the mistakes associated to rapidly dissolving minerals are small.

It is clear that the SD values are extremely relevant for the determination of the character of the fractions: three of the misidentified fractions showed a SD that overlaps the boundary to distinguish clay minerals from BSi (Si/Al=5). Thus, a clear determination of the character of those fractions should be done with care.

We here applied the boundaries determined by Barão et al. (2014). These authors assumed that phytoliths could show Si/Al ratios down to 5 in a study on temperate soils. However, it has also been shown how some sediment samples, that contain mostly phytoliths, showed a single fraction with Si/Al ratios between 4 and 5 (**Chapter 5**). Some authors already discussed the existence of fresh and old phytoliths that show changes in structures (Fraysse et al., 2006a; White et al., 2012). Such changes may affect the elemental proportion of Si and Al, possibly decreasing the Si/Al ratio. Moreover, it is known that Al can be adsorbed onto the surface of phytoliths during soil processes, possibly decreasing Si/Al ratios as well. Koning et al. (2002)

described how old diatoms showed lower Si/Al ratios than fresh diatoms using the same extraction.

In the simulation results, the majority of the cases showing a percent deviation higher than 50% for the Si/Al value corresponded to biogenic fractions with ratios higher than >50, and fractions with extremely low ratios (<0.17) (**Table 6.3**), that corresponded to several type of samples: sediments, soils and burned organic matter. This implies that a differentiation between biogenic fractions, based on Si/Al ratios obtained, is challenging. Vandevenne et al. (2015) assigned a specific range of k values and Si/Al ratio's to distinguish BSi from Opal-CT in AlkExSi fractions in a study in temperate pastured soils. Opal CT is an accumulation of amorphous Si due to an oversaturation of DSi in soils, that normally occurs at soil depths deeper than 1 m with strong leaching of elements (Chadwick et al., 1987; Drees et al., 1989). Deposits of Opal CT were identified at more than 1m deep layers in temperate pastures (Vandevenne et al., 2015a) and the tropics (Alexandre et al., 1997). The presence however of Opal CT was confirmed in the mentioned study by additional analyses. Unfortunately, the method itself cannot distinguish between biogenic Si and Opal CT. It is recommended when BSi fractions are described more than 1 m deep, especially if the soil profile pattern is so different from the BSi patterns observed above, to use other methods for instance, microscopy, to confirm the origin of such fraction.

The (im)-possibility to quantify non-biogenic fractions in the extraction

It is generally assumed that a linear dissolution in an alkaline extraction corresponds to the dissolution of primary minerals (DeMaster, 1981). The solubility of clay minerals is known to decrease with the increase of pH (Amram and Ganor, 2005; Cama et al., 2002; Hiemstra et al., 2007). The 0.5 M NaOH extraction takes place in a pH 13 solution (Barão et al., 2015), which strongly reduces the dissolution of clays. However, the dissolution rates of secondary clays and oxides in 0.5 M NaOH can show a non-linear behavior and the range of dissolution rates can be ample. Barão et al. (2014) showed some results for temperate soils in order to describe the non-biogenic

AlkExSi fractions. Clay minerals on average showed k values between 0.14 and 0.79 min^{-1} (Barão et al., 2015), and oxides normally above 0.7 min^{-1} (Barão et al., 2014). Here we obtained a range between 0.10 and 0.58 min^{-1} for clay minerals and a range between 0.11 and 0.79 min^{-1} for oxides.

In Koning et al. (2002), clay minerals such as kaolinite or illite showed ratios close to their elemental Si to Al proportion (~1 and ~2 respectively). However, other minerals like montmorillonite ($(Na,Ca)_{0.33}(Al,Mg)_2(Si_4O_{10})(OH)_2 \cdot nH_2O$) did not show an elemental ratio in the analysis (~3) in the mentioned study but lower (~2). Barão et al. (2015), also found Si/Al ratios for clay minerals between 1 and 4. Moreover, the Si/Al ratios of the fractions determined as clay minerals that were analyzed for **Chapter 3**, although clays were not physically separated, corresponds to the results of the mineralogy. Si/Al ratios from 1-4 matched the presence of kaolinite, hallyosite, sanidine etc. (see Supplementary data of **Chapter 3**).

Even though a clear Si/Al ratio for non-biogenic fractions can thus be obtained in the continuous alkaline extraction, the quantitative interpretation of fractions considered as oxides and reactive clay minerals is impossible: the extraction is not designed to extract the totality of such fractions. The analysis is not able to characterize the non-linearly dissolving oxide's fractions further than the mere identification of a fraction present with low Si/Al ratio with a high solubility in 0.5 M NaOH. The high deviations of Si/Al values for some oxides fractions indicate the high uncertainty in the estimation of a precise Si/Al ratio for oxides. Whether these oxides are Fe-oxides, Si adsorbed onto other oxides or hydroxy-aluminum silicates should be studied using other methods such as physical separation, mineralogy or XRD analyses.

Final recommendations

The description of fractions using the former approach revealed that the sensitivity analyses and standard deviations for the different characterizing parameters (k and Si/Al), are an essential new asset for the characterization of the fractions. The identification of such 'challenging fractions' allows for

the first time to have an objective indication of potential "BSi-like" fractions in the dissolution.

The following considerations should be taken into account when identifying BSi under these challenging conditions:

- A thorough consideration of the set of boundaries applied for k and Si/Al parameters, considering the type of sample and additional analyses. When several estimate values are close to the boundary a re-set of boundaries could be considered, based on microscopy, physical separation or XRD analyses.
- Especially when the SD overlaps the Si/Al boundaries set, extra characterization should be considered using other methods like mineralogy or microscopy in order to confirm the presence of phytoliths and/or highly soluble clay minerals.
- Large SD values: A clear uncertainty exists about the modeling of these fractions, possibly due to a difficulty to model the curve (dissolution anomalies, noise, outliers). In this case, the re-run of the sample is recommended. Another possible suggestion to improve/decrease the SD is to run again the analysis in the search of a global minimum previously not found, and/or just the simulation in case the errors taken randomly during the simulation were particularly high.

6.5. Conclusion

Nowadays, several authors are still using the traditional DeMaster (1981) methodological extraction (Krause et al., 2017; Ribeiro et al., 2017), or the correction from Ragueneau et al. (2000) (Wang et al., 2015; Zhu et al., 2016) to determine BSi in soil or sediments. The work presented here shows that the continuous alkaline extraction of Si and Al and consequent modeling of the dissolution curves is however strongly recommended, since it allows defining potential challenges associated confounding fractions with strong

accuracy. We showed that the phytolith pool is accurately determined showing more accuracy than the non-biogenic fractions in a broad type of samples: highly weathered tropical soils, burned organic matter, riparian sediments and moderate and highly weathered soils mixed with organic and inorganic fertilizers. An apparent uncertainty only exists in the modeling of the BSi embedded within the plant cell walls.

Moreover, the adapted modeling approach was able to find a more accurate solution than the modeling carried out in the former software. All the parameters used in the test can easily be adjusted (the number of runs, the number of iterations, etc.) and other test or analyses can be easily added. The new selection of the starting parameters provides a complete independence of human biased results and contributes to save time in the modeling. The addition of the calculation of a standard deviation or range of variability for each parameter estimated allows us to detect the presence of complex fractions and give a more precise characterization of the BSi pool.

Chapter 7

Conclusions

7

Conclusions

7.1. Synthesis of results

This work aimed to identify multiple effects of global change on the terrestrial Si cycle, specifically on the biogenic silica pool that is present in soils, and transported through rivers. The environments studied were all considered to be challenging for the accurate determination of the biogenic silica pool, and hence a novel continuous alkaline extraction of Si and Al in 0.5 M NaOH throughout the thesis was applied. Generally, the present work helped to better understand the dynamics of the terrestrial BSi pool and to update the analysis protocol, that allows a fully automated quantification and characterization of the BSi pool based on Si and Al concentrations. In detail, these are the overarching novel outcomes of my thesis:

- Fire increases the solubility of BSi. In **Chapter 2**, two different BSi pools in organic matter were identified using the continuous alkaline extraction. The burned organic matter was more soluble than the non-burned material. However, BSi solubility did not increase when low BSi-content-organic matter was burned. The fate of released DSi and depends on the *in situ* conditions.

- Land use change and associated erosion strongly affects the distribution of BSi in subtropical ecosystems. In **Chapter 3**, the results showed that erosion processes increase the deposition of BSi at bottom-slopes, where a strong potential for long-term BSi storage arises; cultivation decreased the BSi pool in slope soils; and the synergic effect of both together results in a larger decrease and storage of BSi at bottom positions.

- The type of Si-source and soil weathering stage controls the Si-recycling by plants. In **Chapter 4** results showed that in highly weathered soils the addition of Si through biochars increase to a higher degree the growth and Si content in plants than the addition of Si through an inorganic fertilizer but in the moderately weathered soil the inorganic fertilizer was able to provide better results. The analysis of BSi in the applied soil mixtures was particularly challenging: we showed that application of a continuous BSi extraction is absolutely necessary to obtain trustworthy results.

- The study carried out in **Chapter 5** was a strong test-case for the method. Is it possible to follow the transport of BSi from savannah grasslands, through the intestines of hippos, to a river system, even in conditions with strong volcanic interference (and hence strong inorganic Si solubility)? We were able to show that the BSi of the savannah plants corresponded to the BSi observed in the suspended matter and the sediments in the river as a consequence of hippo BSi transfer through the feeding on grasses and egestion into the river. As the BSi content from the suspended matter remained constant along the river but the loads of material in suspension increased, it could be concluded that the BSi in the river increases at the same rate as the input material (hippo depositions).

- The experience acquired during my PhD culminated in the development of a refined methodology to model the Si and Al curves in the continuous BSi extraction (**Chapter 6**). A more precise approach was developed including a new simulation that provides a confidence interval for each estimated parameter. With the new refinement proposed we reached a clear progress in the determination of BSi in soils, evolving from a three-data-points based estimation and a 'blind' acceptance of estimates, to an addition of an interval of variance for every parameter estimated.

7.2. Global change effects on the Si cycle

Global change is indisputably affecting the global Si cycle. Effects on the ocean Si sub-cycle were already studied. For instance, the increase of the ocean temperature increases the dissolution of Si-minerals releasing DSi, and also diatom growth; sediment translocation and dam construction decrease Si transfer from the rivers to the oceans decreasing ocean DSi content. A minimum amount of Si in the ocean is needed to maintain the ocean food chain. The opposite could lead to undesirable consequences ranging from punctual algae blooms and eutrophication processes to the complete disruption of the ocean food chain.

In the terrestrial system scarce knowledge about the possible consequences of global change on the large BSi pools in ecosystem soils is available. Climate change (temperature rise and changes in precipitation patterns) affects the weathering of Si (Amram and Ganor, 2005; Cama et al., 2002; Hiemstra et al., 2007). However, effects on the BSi pool remained under the radar before this thesis. It is now clear that the potential effect of increasing fire events should be considered.

Next to climate change, land cultivation is one of the main drivers in the contribution to the global change. The need of providing food to an exponentially increasing population led to an exponential increase on the

conversion from forest to cropland, together with the increase of the use of fertilizers, which add exogenous elements to the ecosystem altering its functioning. This thesis showed potentially large consequences for the distribution of BSi pools, with the creation of long-term sinks for BSi in downslope positions

Animal extinction's rates are dramatically increasing due to human activities (for instance: land use change, pollution, and hunting). The consequences affect biodiversity, ecosystem functioning and element cycles. This thesis was the first to highlight that grazer extinction can also lead to strong shifts in BSi distribution at the landscape scale.

A more detailed look at small scales

Fire affects the structure of phytoliths, thus increasing its solubility and its bioavailability, which can be beneficial for plants. Si uptake is known to decrease plant stress and increase resistance to toxicity (Mn and Al toxicity, (Che et al., 2016; Ma et al., 2001)). Consequently, the increase of solubility could benefit plant growth and especially performance. The extent of that benefit however, will depend on plant species and other soil properties. Some species, for instance rice, show production increases with higher soil Si content (Liang et al., 2015; Ma and Takahashi, 2002). However, plant uptake is not the only potential loss from soil. In the case a rain event occurs after a fire, a large amount of Si could be eventually exported and lost from the soil system. This could thus cause a large landscape translocation of BSi, to DSi transported in the aquatic system. Similar soil BSi loss occurs after the harvesting of the crops, in the form of long-term plant BSi export through harvest (Vandevenne et al., 2015a). We now showed that the reduction of BSi in the soil can rapidly be increased with coupled slope-cultivation effects. This subsequently plays a role in the detriment of plants and crops performance.

Fertilizers play a crucial role at this respect. The re-supply of Si to soils by fertilizers compensates the loss due to the harvest of the crops. The type of fertilizer and the quantities supplied are extremely important for the

effective management. In the case the Si added equals the Si amount taken up by the crops the system will remain in a steady-state for next growing season. However, in the case the Si supply excesses the Si amount taken up by the crops, an extra accumulation of Si will result. The fate of this Si surplus will depend on soil conditions.

BSi at large scales

The erosion process changes the distribution of BSi consequently storing BSi at bottom-slopes. The accumulation of BSi and possible subsequent dissolution can result in precipitation of Opal CT and re-crystallization processes, already explained by Drees et al., (1989). Moreover, the immobilization of stored BSi results in a net Si loss from the source system. Carbon I has also been reported to be accumulated at the bottom of the slopes due to the physical transport to lower areas. Processes altering the distribution of BSi and C in large amounts i.e. damn's construction and urban development, are extremely relevant for the global Si cycle. It has been shown in this thesis that the activity of large herbivores, like hippos, control to a large extent as well the Si cycle in specific ecosystems like the African savannah. They transfer huge amounts of Si into the riverine system. In other words, they are a key factor to the Si input into large African lakes where some of the highest food provision to the continent occurs. Massive species extinction, specifically large herbivores that contribute to the mobilization (Vandevenne et al., 2013) and transport of Si (Subalusky et al., 2015), are affecting the global Si cycle and should be taken into account in future research.

An overview of the effects studied and their consequences at small and large scales can be seen in **Figure 7.1**.

7.3. Towards a management of the terrestrial Si cycle

In the early Earth, Si was only present in silicate rocks in the Earth's crust (and in the nucleus) (Ohtani et al., 2016). Climatic conditions transformed,

fragmented and weathered silicate rocks. There are some authors that suggest that silicate minerals played a role in the origin of the first protocells, precursors of life (Maurel and Leclerc, 2016). With the onset of plants in terrestrial ecosystems, and the development of soils, a whole new Si equilibrium emerged. A large pool of plant BSi and pedogenic was built up in soils: a new sub-pool thus emerged of reactive terrestrial Si. This could be seen as the first massive terrestrial translocation of Si from a relatively unreactive mineral pool, to a relatively easily soluble Si pool on the short term. A similar to the current Si cycle thus developed: Si was taken up by plants and reached the ocean where diatoms growth maintained the ocean food web. Humans evolved and eventually induced a fast ongoing change at all ecosystem levels, the so-called 'global change'.

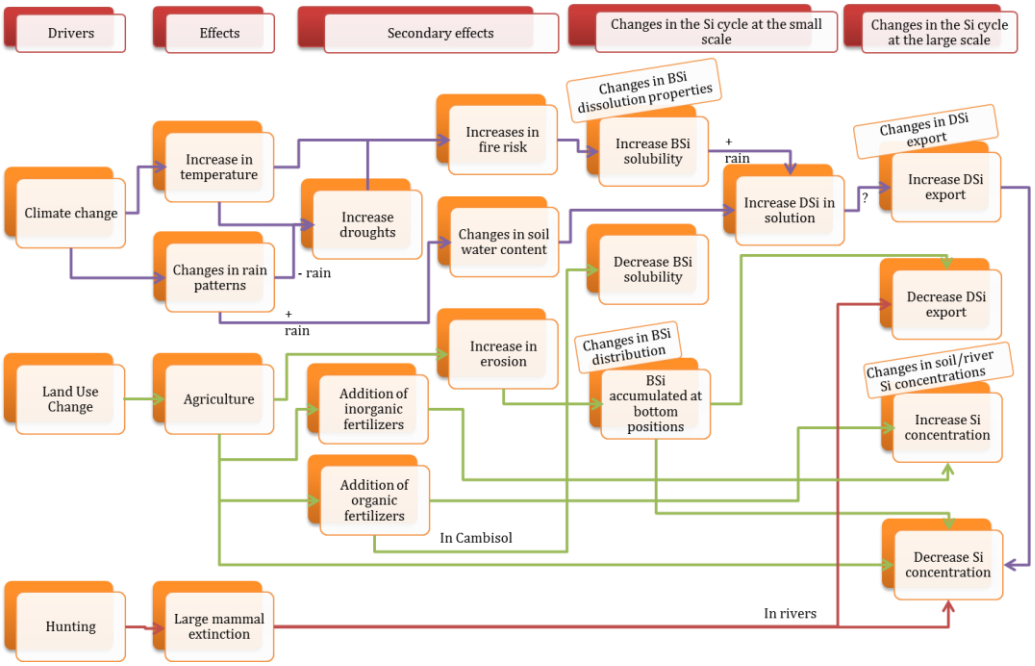

Figure 7.1. Overview of effects at small and large scales of the effects studied.

My thesis shows clearly that human induced-change in climate, land use and biodiversity directly impact on this biological sub-pool. In this context, it is interesting to note that, although we can consider the global Si cycle to be a factual cycle where Si eventually recycles completely, this process can only occur on a geological timescale. In an ecosystem management context, the Si

cycle can thus be considered unidirectional: Si fluxes from land to the ocean, with the rate determined by weathering rates, but equally also by the storage of BSi at the landscape scale and DSi export.

In a management context, there will always be a source of BSi and a sink for the translocated BSi: a negative consequence (reduced Si availability of Si due to BSi loss) for the terrestrial system could actually represent a desirable condition for the ocean's compartment (improved Si-N-P ratios). If the objective is eventually to be able to manage the Si cycle, how do we solve the compromise between the terrestrial and the ocean sub-system?

The most important issue to answer this is the lack of knowledge about many aspects of the cycle. There is a vast unknown about the whole functioning and specifically about local soil processes involving Si, for instance the contribution of oxides to the bioavailable Si-pool, isotopic preferences of different Si-compounds, the role of microbiota in the Si-filter and the effect of organic acids on the solubility of compounds containing Si. My thesis shows that a central point in a potential management of the Si cycle lies in the understanding of where BSi is buried along the land-ocean continuum. A need to investigate and determine the Si fluxes from the terrestrial system towards the river is crucial in order to move forward a better understanding. Only few studies had been carried out at this regard (Frings et al., 2016; Ronchi et al., 2013). Moreover, the contribution to the soil DSi supply from non-biogenic phases appears now as being more relevant that was previously thought (Barão et al., 2018). Finally, there is a large compartment of the Si cycle that has been clearly ignored up to now in relation to Si fluxes: the waste human system. (Vandevenne and Struyf, 2018) roughly estimated that only 7% of the amount of Si that enters the human loop and the waste management system returns to the natural system. Targeted studies should be performed at these respects in order to move forward a complete understand of the Si cycle.

Despite the need of gathering more knowledge about the terrestrial Si cycle, it is possible to draw some advices for good practices based on the results of this thesis:

It was clearly shown how the conversion from forest to cropland together with erosion can deplete the BSi pool in the short-term in Acrisols from the south of Brazil (**Chapter 3**). Thus, the cultivation of such highly weathered soils under steep slopes is not recommended. If no-action is taken these ecosystems will become a complete Si-depleted systems in the long-term (Vandevenne et al., 2015b). The supply of nutrients by fertilizers could compensate such loss. However, the weathering stage of the soil should be considered when selecting the fertilizers to apply, as well as the type of crop intended to grow. When growing high Si-accumulator crops (i.e. rice), in highly weathered soils, organic fertilizers, for instance biochars, can be applied in case the objective is to increase the Si plant content and crop growth. On the other hand, if the same Si-accumulator crop is grown in moderate weathered soils; inorganic fertilizers are preferred in this case to increase Si plant content.

Despite the negative consequence of erosion leading to large BSi accumulations at bottom-slopes, this new finding should be considered in conservation purposes: First, it shows the importance of field geomorphology regarding the Si cycle. Field geomorphology should be considered to avoid deposition zones for instance in Si-accumulator croplands and estuaries. And second, the soil translocation from deposition to active zones could return the BSi back into the turnover between plants and soil.

Finally, the re-introduction of grazers is another possibility to compensate the scarcity of soil-Si in croplands or highly weathered soils. However in order to determine the correct procedure, a whole understanding and description of BSi in the system is needed. To do so a method able to distinguish and characterize BSi in soil is extremely important.

7.4. Methodological considerations

Although some studies apply already the continuous alkaline extraction to determine BSi in soils, it is not the preferred method in many cases. Many researchers are applying modified DeMaster (1981) type-extractions (Krause et al., 2017; Ribeiro et al., 2017; Wang et al., 2015; Zhu et al., 2016). From the work carried out here and also in former studies (Barão et al., 2015; Vandevenne et al., 2015b), it is clear that the dissolution of other secondary phases like clay minerals or oxides during the alkaline extraction (Na_2CO_3, NaOH) strongly interfere in the estimation of BSi in most terrestrial environments. Some clay minerals or oxides show alkaline solubilities similar to BSi. Applying the continuous alkaline extraction and subsequent modeling with the equations from Barão et al., (2014), the BSi can be distinguished from other non-linearly dissolving fractions.

In **Chapter 6**, we went further and include a refinement of the latter methodology which allows us to get a more accurate estimation of parameters. A simulation was included in order to calculate a confidence interval for each parameter that is estimated. We have now developed a method that can be readily used through the constructed script, and points researchers to challenges potentially associated with the extraction: Si/Al ratios near the boundary to distinguish between biogenic and non-biogenic fractions, or k-values that could actually almost be considered linear. This can be a good indicator to apply additional methods for BSi analysis.

There are still limitations to the method developed. It is known that the distinction between BSi and Opal CT cannot be made using the continuous alkaline extraction (**Chapter 3**). In addition, it is still unknown if some clay mineral with no Al could show similar signals than BSi (**Chapter 4**). Groups like quartz's, the pyroxene group ($MgSiO_3$) or the amphibole group ($Mg_7Si_8O_{22}(OH)_2$) would be described as the linear part of the equations used to model the dissolution curves, or lacking that, as a non-linearly dissolving fraction with a low k-value. Still, other minerals like the humite group or the serpentine group, as well as several minerals (datolite, titanite, hemimorphite

(calamine), ilvaite, benitoite, bazzite, talc, sepiolite, milarite) might show as well a non-linearly dissolving behavior when analyzed with the continuous alkaline extraction. Moreover, some Si absorbed onto Fe-oxides like ferrihydrite or hematite should be considered in this regard. Finally, some minerals with theoretical Si/Al ratios higher than 4 (sugilite (Al_2 Si_{12}), mordenite (Al_2Si_{10})) may possibly be described as BSi. Further experiments are needed in order to confirm the dissolution behavior of these minerals in 0.5 M NaOH and how the model may describe them.

7.5. Future research

On the methodological aspect

Future research regarding the methodology should focus on:

The possibility to distinguish the currently undistinguishable fractions applying the alkaline continuous extraction: Opal CT and biogenic silica. Can specific parameters characteristics distinguish the two fractions? Another possibility is applying a previous gravimetric separation (Parr et al., 2001; Piperno, 2006) to separate the biogenic silica from the Opal CT.

The characterization of non-biogenic phases: We cannot characterize fractions showing Si/Al ratios <1 besides a fraction highly reactive in NaOH with a low Si content. One option consists on measuring other elements as well during the extraction, for instance iron (Fe). Having the three dissolution curves (Si, Al and Fe), the equations could be adapted in order to determine Si/Fe ratios that could help to understand and characterize the oxide fraction described with the help of additional analyses i.e. mineralogy or XRD. However a quantification of oxides will still not be possible as the dissolution of oxides in NaOH is probably only partial. The additional measurement of other elements could only contribute to perform a better distinction of fractions. The continuous alkaline extraction method is not to be used to quantify other soil phases than BSi.

On human impacts on the biological Si cycle

If we want to determine which of the studied drivers is most important for future research, we should consider future trends. Although some authors recently showed some discrepancy (Doerr and Santín, 2016), it is commonly accepted that climate change contributes to an increase in occurrence of natural wildfires through the increase in temperature and drought periods (Joyce et al., 2014; Kovats et al., 2014). With global warming, a progressive increase in fire risk is highly probable (Kovats et al., 2014). However, fire is not a risk that affects the whole globe, besides the secondary effect related to CO_2 emissions (Joyce et al., 2014). Therefore, studies linking fire and the Si cycle are mostly important at local scales.

Only 10% of the megafauna present during Pleistocene survived up to now and human impact is known to have contributed the most to the extinction (Sandom et al., 2014). Around 60% of large herbivores' species are considered endangered or threatened nowadays, with vast ecological implications expected in the near future (Ripple et al., 2015). Hunting for meat is the activity mostly affecting the large herbivores' decline (Ripple et al., 2015), which in turn is related to the increase in food demand. Since largest extinction occurred already in the past, studies relating impacts of large grazer to Si cycling are mainly relevant to natural reserves where they are still abundant.

Deforestation rates have been recently estimated in several countries, showing the highest increases in tropical countries in South America and Southern Asia, increasing by 15% in the last decade compare to the period 2000-2006 (Austin et al., 2017). Agriculture is estimated to drive 80% of the total deforestation (Kissinger et al., 2012). Considering the lack of conservationist policies in low-developed countries and the high demand for food supply parallel to the population increase, expectations for the future are not optimistic. Deforestation was also shown recently to increase local temperature (Joyce et al., 2014), which might increase fire risk in turn. On a global scale, deforestation could therefore be considered the most important human driver for the global Si cycle.

Studies about solubility *in situ* could provide important information about interrelations between soil compounds like oxides, secondary clays and BSi in croplands. Such studies need to take into account the vegetation as well, as the recycling by plants is a fundamental actor in the soil Si cycle: little or nothing is known about the effect of plants on the soil water DSi concentrations, although the latter drive dissolution rates of Si in the soil. Moreover, the contribution of microfauna on the Si cycle at small scales has been as well neglected. Although a little influence is expected, direct and indirect effects of the microbial activity on Si mobilization and distribution is still unknown.

Studies measuring isotopic composition could help at this regard. However, it has been recently shown that secondary or tertiary clay minerals in subsoils can be enriched in light isotopes (Cornelis et al., 2014b), which make the distinction between BSi and secondary clay minerals isotopically undistinguishable. To avoid so, studies applying isotope spiking of Si and subsequent analysis could be an option to approach this. A combination of methods is needed in order to accurately describe soil fractions playing a role on the Si filter at small scales and their interactions. A whole understanding of processes involved at small scales could be extrapolated to explain processes and distribution of BSi at larger scales. In order to approach the study of the Si cycle at large scales additional global effects on the Si cycle should be considered.

The human loop and waste treatment of Si residues should be an objective to include in future studies. First, a precise of Si quantification entering the human system through the harvesting of the crops and how the BSi is transformed afterwards during food production is needed. Besides, a huge technologic industry extracting and using inorganic Si from silicate rocks exists. Humans extract Si silicate rocks to produce chips, photovoltaic plates and other electronic assets. However the treatments and processes performed in waste treatment plants and the possible recycling of such organic or inorganic Si from the food or industrial system are not clear. Special effort should be applied to investigate the properties of the Si

returning the natural system from the waste treatment plants to further study a possible sustainable Si return to the global cycle.

Ecosystem services (ES) are defined as the services that nature provides to humans. ES are classified regarding the type of service they provide: recreation, food and water supply, protection, regulation, etc. Nowadays, the study of ES is crucial in order to communicate to the population and policy makers about the value of a particular ecosystem. Unfortunately, there is no ES's described regarding the Si cycle. The conservation of a healthy Si system able to provide protection for plants against herbivores is possibly the line to follow regarding this research. For instance, one of the direct benefits of the application of Si to rice crops, which results in growth increase, could be perfectly consider as an ecosystem service in relation to food provision.

7.6. Final words

In this thesis we have shown that the effects due to climate change on an apparently ignored elemental cycle like silicon are real and could experiment some crucial affection in the future. We only covered a little research on a particular element which not much was known about. Thus, effects on systems or processes we are not aware of are possible and could as well have some future implications for ecosystems functioning and biodiversity in the future. A strong continuous effort studying possible consequences of climate change on ecosystems is needed to convince and prove to the society, policy makers and ecosystem' managers that we do need to act now if we want to stop or mitigate the global change.

References

Adrees, M., Ali, S., Rizwan, M., Zia-ur-rehman, M., Ibrahim, M., Abbas, F., Farid, M., Farooq, M. and Kashif, M.: Ecotoxicology and environmental safety mechanisms of silicon-mediated alleviation of heavy metal toxicity in plants: A review, Ecotoxicol. Environ. Saf., 119, 186–197, doi:10.1016/j.ecoenv.2015.05.011, 2015.

Alexandre, A., Meunier, J.-D., Colin, F. and Koud, J.-M.: Plant impact on the biogeochemical cycle of silicon and related weathering processes, Geochim. Cosmochim. Acta, 61(3), 677–682, doi:10.1016/S0016-7037(97)00001-X, 1997.

Alfredsson, H., Hugelius, G., Clymans, W., Stadmark, J., Kuhry, P. and Conley, D. J.: Amorphous silica pools in permafrost soils of the Central Canadian Arctic and the potential impact of climate change, Biogeochemistry, 124(1–3), 441–459, doi:10.1007/s10533-015-0108-1, 2015.

Alleman, L. Y., Cardinal, D., Cocquyt, C., Plisnier, P.-D., Descy, J.-P., Kimirei, I., Sinyinza, D. and André, L.: Silicon isotopic fractionation in Lake Tanganyika and its main tributaries, J. Great Lakes Res., 31(4), 509–519, doi:10.1016/S0380-1330(05)70280-X, 2005.

Almendros, G., Gonzfilez-Vila, F. J., Martin, F., Fründ, R. and Lfidemann, H.-D.: Solid state NMR studies of fire-induced changes in the structure of humic substances, Sci. Total Environ., 117/118, 63–74, doi:10.1016/0048-9697(92)90073-2, 1992.

Ameijeiras-Mariño, Y.: Changes in soil chemical weathering intensity after forest conversion to cropland: importance of slope geomorphology. In: The response of soil chemical weathering to physical erosion: integrating the impact of forest conversion (PhD thesis), Université Catholique de Louvain (UCL), Belgium., 2017.

Amram, K. and Ganor, J.: The combined effect of pH and temperature on smectite dissolution rate, Geochim. Cosmochim. Acta, 69(10), 2535–2546, doi:10.1016/j.gca.2004.10.001, 2005.

Aoki, Y., Hoshino, M. and Matsubara, T.: Silica and testate amoebae in a soil under pine–oak forest, Geoderma, 142(1–2), 29–35, doi:10.1016/j.geoderma.2007.07.009, 2007.

Armbrust, E. V.: The life of diatoms in the world's oceans, Nature, 459(7244), 185–192, doi:10.1038/nature08057, 2009.

Austin, K. G., González-Roglich, M., Schaffer-Smith, D., Schwantes, A. M. and Swenson, J. J.: Trends in size of tropical deforestation events signal increasing dominance of industrial-scale drivers, Environ. Res. Lett., 12(54009), doi:10.1088/1748-9326/aa6a88, 2017.

Bakker, E. S., Pages, J. F., Arthur, R. and Alcoverro, T.: Assessing the role of large herbivores in the structuring and functioning of freshwater and marine angiosperm ecosystems, Ecography (Cop.)., 39(2), 162–179, doi:10.1111/ecog.01651, 2016.

Barão, L., Clymans, W., Vandevenne, F., Meire, P., Conley, D. J. and Struyf, E.: Pedogenic and biogenic alkaline-extracted silicon distributions along a temperate land-use gradient, Eur. J. Soil Sci., 65(5), 693–705, doi:10.1111/ejss.12161, 2014.

Barão, L., Teixeira, R., Vandevenne, F., Ronchi, B., Unzué-Belmonte, D. and Struyf, E.: Silicon mobilization in soils: the broader impact of land use., , In prep, 2018.

Barão, L., Vandevenne, F., Clymans, W., Frings, P., Ragueneau, O., Meire, P., Conley, D. J. and Struyf, E.: Alkaline-extractable silicon from land to ocean: A challenge for biogenic silicon determination, Limnol. Oceanogr. Methods, 13(7), 329–344, doi:10.1002/lom3.10028, 2015.

Bartoli, F.: Crystallochemistry and surface properties of biogenic opal, J. Soil Sci., 36(3), 335–350, doi:10.1111/j.1365-2389.1985.tb00340.x, 1985.

Bartoli, F. and Wilding, L. P.: Dissolution of biogenic opal as a function of its physical and chemical properties, Soil Sci. Soc. Am. J., 44(4), 873, doi:10.2136/sssaj1980.03615995004400040043x, 1980.

Bauer, S. and Hoye, B. J.: Migratory animals couple biodiversity and ecosystem functioning worldwide, Science (80-.)., 344(6179), 124255, doi:10.1126/science.1242552, 2014.

Bélanger, R. R., Bowen, P. A., Ehret, D. L. and Menzies, J. G.: Soluble Silicon: Its role in crop and disease management of greenhouse crops, Plant Dis., 79(4), 329–336, 1995.

Bennett, P. C., Siegel, D. I., Hill, B. M. and Glaser, P. H.: Fate of silicate minerals in a peat bog, Geology, doi:10.1130/0091-7613, 1991.

Berg, B. and McClaugherty, C.: Plant litter, Springer-Verlag Berlin Heidelberg., 2008.

Berger, G., Patricia, M. and Is, I. T.: Dissolution rate of quartz in lead and sodium electrolyte solutions between 25 and 300°C: Effect of the

nature of surface complexes and reaction affinity., Geochim. Cosmochim. Acta, 58(2), 541–551, doi:10.1016/0016-7037(94)90487-1, 1994.

Bienfang, P. K., Harrison, P. J. and Quarmby, L. M.: Sinking rate response to depletion of nitrate, phosphate and silicate in four marine diatoms, Mar. Biol., 67(3), 295–302, doi:10.1007/BF00397670, 1982.

Blecker, S. W., Mcculley, R. L., Chadwick, O. A. and Kelly, E. F.: Biologic cycling of silica across a grassland bioclimosequence, Global Biogeochem. Cycles, 20(May), 1–11, doi:10.1029/2006GB002690, 2006.

Blinnikov, M. S.: Phytoliths in plants and soils of the interior Pacific Northwest, USA., Rev. Palaeobot. Palynol., 135, 71–98, doi:10.1016/j.revpalbo.2005.02.006, 2005.

Bodí, M. B., Martin, D. A., Balfour, V. N., Santín, C., Doerr, S. H., Pereira, P., Cerdà, A. and Mataix-solera, J.: Wildland fire ash : Production , composition and eco-hydro-geomorphic effects, Earth-Science Rev., 130, 103–127, doi:10.1016/j.earscirev.2013.12.007, 2014.

Bodí, M. B., Mataix-Solera, J., Doerr, S. H. and Cerdà, A.: The wettability of ash from burned vegetation and its relationship to Mediterranean plant species type, burn severity and total organic carbon content, Geoderma, 160(3–4), 599–607, doi:10.1016/j.geoderma.2010.11.009, 2011.

Bootsma, H. A., Hecky, R. E., Johnson, T. C., Kling, H. J. and Mwita, J.: Inputs, outputs, and internal cycling of silica in a large, tropical lake, J. Great Lakes Res., 29, 121–138, doi:10.1016/S0380-1330(03)70543-7, 2003.

Bowman, D. M. J. S., Balch, J., Artaxo, P., Bond, W. J., Cochrane, M. a, D'Antonio, C. M., Defries, R., Johnston, F. H., Keeley, J. E., Krawchuk, M. a, Kull, C. a, Mack, M., Moritz, M. a, Pyne, S., Roos, C. I., Scott, A. C., Sodhi, N. S., Swetnam, T. W. and Whittaker, R.: The human dimension of fire regimes on Earth., J. Biogeogr., 38(12), 2223–2236, doi:10.1111/j.1365-2699.2011.02595.x, 2011.

Von Braun, J.: The world food situation: new driving forces and required actions. Food Policy Reports 18. International Food Policy Research Institute, Washington D.C., 2007.

Bray, R. H. and Kurtz, L. T.: Determination of total, organic, and available forms of phosphorus in soils., Soil Sci., 59(1), 39–46 [online] Available from: http://journals.lww.com/soilsci/Fulltext/1945/01000/DETERMINATION_OF_TOTAL,_ORGANIC,_AND_AVAILABLE.6.aspx, 1945.

Cama, J., Metz, V. and Ganor, J.: The effect of pH and temperature on kaolinite dissolution rate under acidic conditions, Geochim. Cosmochim. Acta, 66(22), 3913–3926, doi:10.1016/S0016-7037(02)00966-3, 2002.

Van Cappellen, P.: Biomineralization and global biogeochemical cycles, Rev. Mineral. Geochemistry, 54(1), 357–381, doi:10.2113/0540357, 2003.

Van Cappellen, P. and Qiu, L. Q.: Biogenic silica dissolution in sediments of the Southern Ocean .1. Solubility., Deep Sea Res. Part II Top. Stud. Oceanogr., 44(5), 1109–1128, doi:10.1016/S0967-0645(96)00113-0, 1997.

Cardinal, D., Alleman, L. Y., de Jong, J., Ziegler, K. and Andre, L.: Isotopic composition of silicon measured by multicollector plasma source mass spectrometry in dry plasma mode., J. Anal. At. Spectrom., 18(3), 213–218, doi:10.1039/B210109B, 2003.

Carey, J. C. and Fulweiler, R. W.: Human activities directly alter watershed dissolved silica fluxes, Biogeochemistry, 111(1–3), 125–138, doi:10.1007/s10533-011-9671-2, 2011.

Carey, J. C. and Fulweiler, R. W.: The terrestrial silica pump, PLoS One, 7(12), e52932, doi:10.1371/journal.pone.0052932, 2012.

Cary, L., Alexandre, A., Meunier, J. D., Boeglin, J. L. and Braun, J. J.: Contribution of phytoliths to the suspended load of biogenic silica in the Nyong basin rivers (Cameroon), Biogeochemistry, 74, 101–114, doi:10.1007/s10533-004-2945-1, 2005.

Chadwick, O. A., Hendricks, D. M. and Nettleton, W. D.: Silica in Duric Soils: II. Mineralogy 1, Soil Sci. Soc. Am. J., 51, 982–985, doi:10.2136/sssaj1987.03615995005100040029x, 1987.

Chao, T. T. and Sanzolone, R. F.: Decomposition techniques, J. Geochemical Explor., 44(1–3), 65–106, 1992.

Che, J., Yamaji, N., Shao, J. F., Ma, J. F. and Shen, R. F.: Silicon decreases both uptake and root-to-shoot translocation of manganese in rice, J. Exp. Bot., 67(5), 1535–1544, doi:10.1093/jxb/erv545, 2016.

Chou, L. and Wollast, R.: Steady-state kinetics and dissolution mechanisms of albite, Am. J. Sci., 285, 963–993, doi:10.2475/ajs.285.10.963, 1985.

Clarke, J.: The occurrence and significance of biogenic opal in the regolith, Earth Sci. Rev., 60, 175–194, doi:10.1016/S0012-8252(02)00092-2, 2003.

Clymans, W., Barão, L., Van der Putten, N.,

Wastegård, S., Gísladóttir, G., Björck, S., Moine, B., Struyf, E. and Conley, D. J.: The contribution of tephra constituents during biogenic silica determination: implications for soil and palaeoecological studies, Biogeosciences, 12, 3789–3804, doi:10.5194/bg-12-3789-2015, 2015a.

Clymans, W., Lehtinen, T., Gísladóttir, G., Lair, G. J., Barão, L., Ragnarsdóttir, K. V., Struyf, E. and Conley, D. J.: Si Precipitation During Weathering in Different Icelandic Andosols, Procedia Earth Planet. Sci., 10, 260–265, doi:10.1016/j.proeps.2014.08.040, 2014.

Clymans, W., Struyf, E., Govers, G., Vandevenne, F. and Conley, D. J.: Anthropogenic impact on amorphous silica pools in temperate soils, Biogeosciences, 8(8), 2281–2293, doi:10.5194/bg-8-2281-2011, 2011.

Clymans, W., Struyf, E., Van den Putte, A., Langhans, C., Wang, Z. and Govers, G.: Amorphous silica mobilization by inter-rill erosion: Insights from rainfall experiments, Earth Surf. Process. Landforms, 40(9), 1171–1181, doi:10.1002/esp.3707, 2015b.

Cockerton, H. E., Street-perrott, F. A., Barker, P. A., Leng, M. J., Sloane, H. J., Ficken, K. J. and Victoria, L.: Orbital forcing of glacial / interglacial variations in chemical weathering and silicon cycling within the upper White Nile basin , East Africa : Stable-isotope and biomarker evidence from Lakes Victoria and Edward, Quat. Sci. Rev., 130, 57–71, doi:10.1016/j.quascirev.2015.07.028, 2015.

Conley, D. J.: Terrestrial ecosystems and the global biogeochemical silica cycle, Global Biogeochem. Cycles, 16(4), 1–8, doi:10.1029/2002GB001894, 2002.

Conley, D. J. and Carey, J. C.: Biogeochemistry: Silica cycling over geologic time, Nat. Geosci., 8(6), 431–432, doi:10.1038/ngeo2454, 2015.

Conley, D. J., Likens, G. E., Buso, D. C., Saccone, L., Bailey, S. W. and Johnson, C. E.: Deforestation causes increased dissolved silicate losses in the Hubbard Brook Experimental Forest, Glob. Chang. Biol., 14, 2548–2554, doi:10.1111/j.1365-2486.2008.01667.x, 2008.

Cornelis, J.-T., Delvaux, B., Georg, R. B., Lucas, Y., Ranger, J. and Opfergelt, S.: Tracing the origin of dissolved silicon transferred from various soil-plant systems towards rivers: a review, Biogeosciences, 8(1), 89–112, doi:10.5194/bg-8-89-2011, 2011a.

Cornelis, J.-T., Dumon, M., Tolossa, A. R., Delvaux, B., Deckers, J. and Van Ranst, E.: The effect of pedological conditions on the sources and sinks of silicon in the Vertic Planosols in south-western Ethiopia, Catena, 112, 131–138, doi:10.1016/j.catena.2013.02.014, 2014a.

Cornelis, J.-T., Ranger, J., Iserentant, A. and Delvaux, B.: Tree species impact the terrestrial cycle of silicon through various uptakes, Biogeochemistry, 97(2–3), 231–245, doi:10.1007/s10533-009-9369-x, 2010a.

Cornelis, J.-T., Titeux, H., Ranger, J. and Delvaux, B.: Identification and distribution of the readily soluble silicon pool in a temperate forest soil below three distinct tree species, Plant Soil, 342(1–2), 369–378, doi:10.1007/s11104-010-0702-x, 2011b.

Cornelis, J. and Delvaux, B.: Soil processes drive the biological silicon feedback loop, Funct. Ecol., 1, 1298–1310, doi:10.1111/1365-2435.12704, 2016.

Cornelis, J. T., Delvaux, B. and Titeux, H.: Contrasting silicon uptakes by coniferous trees: A hydroponic experiment on young seedlings, Plant Soil, 336(1), 99–106, doi:10.1007/s11104-010-0451-x, 2010b.

Cornelis, J. T., Weis, D., Lavkulich, L., Vermeire, M. L., Delvaux, B. and Barling, J.: Silicon isotopes record dissolution and re-precipitation of pedogenic clay minerals in a podzolic soil chronosequence, Geoderma, 235–236, 19–29, doi:10.1016/j.geoderma.2014.06.023, 2014b.

Currie, H. A. and Perry, C. C.: Silica in Plants: Biological, Biochemical and Chemical Studies, Ann. Bot., (100), 1383–1389, doi:10.1093/aob/mcm247, 2007.

Datnoff, L. E. and Heckman, J. R.: Silicon fertilizers for plant disease protection, in Proceedings of the 16th World Fertilizer Congress of CIECRio, pp. 36–38, De Janeiro-RJ, Brazil,., 2014.

Delvaux, B., Herbillon, A. J. and Vielvoye, L.: Characterization of a weathering sequence of soils derived from volcanic ash in Cameroon. Taxonomic, mineralogical and agronomic implications, Geoderma, 45, 375–388, doi:10.1016/0016-7061(89)90017-7, 1989.

Demarest, M. S., Brzezinski, M. A. and Beucher, C. P.: Fractionation of silicon isotopes during biogenic silica dissolution, Geochim. Cosmochim. Acta, 73(19), 5572–5583, doi:10.1016/j.gca.2009.06.019, 2009.

DeMaster, D. J.: The supply and accumulation of silica in the marine environment, Geochim. Cosmochim. Acta, 45(10), 1715–1732, doi:10.1016/0016-7037(81)90006-5, 1981.

Derry, L. A., Kurtz, A. C., Ziegler, K. and Chadwick, O. A.: Biological control of terrestrial silica cycling and export fluxes to watersheds., Nature, 433(7027), 728–31, doi:10.1038/nature03299, 2005.

Descy, J.-P., Darchambeau, F., Lambert, T., Stoyneva-Gaertner, M. P., Bouillon, S. and Borges, A. V.: Phytoplankton dynamics in the Congo River, Freshw. Biol., 62(1), 87–101, doi:10.1111/fwb.12851, 2017.

Ding, T. P., Tian, S. H., Sun, L., Wu, L. H., Zhou, J. X. and Chen, Z. Y.: Silicon isotope fractionation between rice plants and nutrient solution and its significance to the study of the silicon cycle, Geochim. Cosmochim. Acta, 72(23), 5600–5615, doi:10.1016/j.gca.2008.09.006, 2008a.

Ding, T. P., Zhou, J. X., Wan, D. F., Chen, Z. Y., Wang, C. Y. and Zhang, F.: Silicon isotope fractionation in bamboo and its significance to the biogeochemical cycle of silicon, Geochim. Cosmochim. Acta, 72(5), 1381–1395, doi:10.1016/j.gca.2008.01.008, 2008b.

Dobson, A., Borner, M. and Sinclair, T.: Road will ruin Serengeti, Nature, 467(7313), 272–273, doi:doi:10.1038/467272a, 2010.

Doerr, S. H. and Santín, C.: Global trends in wildfire and its impacts: perceptions versus realities in a changing world, Philos. Trans. R. Soc. B., 371, 20150345, doi:10.1098/rstb.2015.0345, 2016.

Doetterl, S., Cornelis, J.-T., Six, J., Bodé, S., Opfergelt, S., Boeckx, P. and Van Oost, K.: Soil redistribution and weathering controlling the fate of geochemical and physical carbon stabilization mechanisms in soils of an eroding landscape, Biogeosciences, 12(5), 1357–1371, doi:10.5194/bg-12-1357-2015, 2015.

Doughty, C. E., Roman, J., Faurby, S., Wolf, A., Haque, A., Bakker, E. S., Malhi, Y., Dunning, Jr.g, J. B. and Svenningd, J.-C.: Global nutrient transport in a world of giants, PNAS, 113(4), 868–873, doi:10.1073/pnas.1502549112, 2016.

Doughty, C. E., Wolf, A. and Malhi, Y.: The legacy of the Pleistocene megafauna extinctions on nutrient availability in Amazonia, Nat. Geosci., 6(9), 761–764, doi:10.1038/ngeo1895, 2013.

Dove, P. M. and Icenhower, J.: Kinetic and thermodynamic controls on silica reactivity: An analog for waste disposal media., Sch. Earth Atmos. Sci., 2, 237–255, 1997.

Drees, L. R., Wilding, L. P., Smeck, N. E. and Senkayi, A. L.: Silica in soils: quartz and disorders polymorphs, in Minerals in soil environments, pp. 914–974, Soil Science Society of America, Madison., 1989.

Drever, J. I.: The effect of land plants on weathering rates of silicate minerals, Geochim. Cosmochim. Acta, 58(10), 2325–2332, doi:10.1016/0016-7037(94)90013-2, 1994.

Dunn, P. H. and DeBano, L. F.: Fire's effect on biological and chemical properties of chaparral soils, in The Proceedings of Symposium on Environmental Conservation: Fire and Fuel Management in Mediterranean Ecosystems., edited by H. A. Mooney and C. E. Conrad, pp. 75–84, USDA Forest Service WO-3, Palo Alto, CA.Washington D.C., USA., 1977.

Dutton, C., Anisfeld, S. C. and Ernstberger, H.: A novel sediment fingerprinting method using filtration: application to the Mara River, East Africa, J. Soils Sediments, 13(10), 1708–1723, doi:10.1007/s11368-013-0725-z, 2013.

Eleuterius, L. N. and Lanning, F. C.: Silica in relation to leaf decomposition of Juncus roemerianus, J. Coast. Res., 3((4)), 531–534 [online] Available from: http://journals.fcla.edu/jcr/article/view/77642, 1987.

Engle, D. L., Sickman, J. O., Moore, C. M., Esperanza, A. M., Melack, J. M. and Keeley, J. E.: Biogeochemical legacy of prescribed fire in a giant sequoia–mixed conifer forest: A 16-year record of watershed balances, J. Geophys. Res., 113(G1), G01014, doi:10.1029/2006JG000391, 2008.

Engstrom, E., Rodushkin, I., Baxter, D. C. and Ohlander, B.: Chromatographic purification for the determination of dissolved silicon isotopic compositions in natural waters by high-resolution multicollector inductively coupled plasma mass spectrometry, Anal. Chem., 78(1), 250–257, doi:10.1021/ac051246v, 2006.

Eppley, R. W.: Temperature and phytoplankton growth in the sea, Fish. Bull., 70(4), 1063–1085, 1972.

Epstein, E.: The anomaly of silicon in plant biology, Proc. Natl. Acad. Sci., 91(January), 11–17, doi:11607449, 1994.

European Soils Bureau Network, E. C.: Soil Atlas of Europe, Office for Official Publications of the European Communities, L-2995 Luxembourg., 2005.

Fauteux, F., Rémus-Borel, W., Menzies, J. G. and Bélanger, R. R.: Silicon and plant disease resistance against pathogenic fungi, FEMS Microbiol. Lett., 249(October), 1–6, doi:10.1016/j.femsle.2005.06.034, 2005.

Field, C. R.: A study of the feeding habits of the hippopotamus (Hippopotamus amphibius Linn.) in the Queen Elizabeth National Park, Uganda, with some management implications., Zool. Africana, 5(1), 71–86, doi:10.1080/00445096.1970.11447382, 1970.

Fraysse, F., Cantais, F., Pokrovsky, O. S., Schott, J. and Meunier, J. D.: Aqueous reactivity of

phytoliths and plant litter: Physico-chemical constraints on terrestrial biogeochemical cycle of silicon, J. Geochemical Explor., 88(1–3), 202–205, doi:10.1016/j.gexplo.2005.08.039, 2006a.

Fraysse, F., Pokrovsky, O. S. and Meunier, J.-D.: Experimental study of terrestrial plant litter interaction with aqueous solutions, Geochim. Cosmochim. Acta, 74(1), 70–84, doi:10.1016/j.gca.2009.09.002, 2010.

Fraysse, F., Pokrovsky, O. S., Schott, J. and Meunier, J.: Surface properties, solubility and dissolution kinetics of bamboo phytoliths, , 70, 1939–1951, doi:10.1016/j.gca.2005.12.025, 2006b.

Fraysse, F., Pokrovsky, O. S., Schott, J. and Meunier, J.: Surface chemistry and reactivity of plant phytoliths in aqueous solutions, Chem. Geol., 258(3–4), 197–206, doi:10.1016/j.chemgeo.2008.10.003, 2009.

Frings, P. J., Clymans, W., Fontorbe, G., Rocha, C. L. D. La and Conley, D. J.: The continental Si cycle and its impact on the ocean Si isotope budget, Chem. Geol., 425, 12–36, doi:10.1016/j.chemgeo.2016.01.020, 2016.

Frings, P. J., Clymans, W., Jeppesen, E., Lauridsen, T. L., Struyf, E. and Conley, D. J.: Lack of steady-state in the global biogeochemical Si cycle: Emerging evidence from lake Si sequestration, Biogeochemistry, 117(2–3), 255–277, doi:10.1007/s10533-013-9944-z, 2014a.

Frings, P. J., De La Rocha, C., Struyf, E., Van Pelt, D., Schoelynck, J., Murray-Hudson, M., Gondwe, M. J., Wolski, P., Mosimane, K., Gray, W., Schaller, J. and Conley, D. J.: Tracing silicon cycling in the Okavango Delta, a sub-tropical flood-pulse wetland using silicon isotopes, Geochim. Cosmochim. Acta, 142, 132–148, doi:10.1016/j.gca.2014.07.007, 2014b.

Gascho, G. J.: Silicon sources for agriculture, in Silicon in Agriculture, vol. Volume 8, edited by L. E. Datnoff, G. H. Snyder, and B. T. Korndörfer, pp. 197–207, Elsevier., 2001.

Georg, R. B., Reynolds, B. C., Frank, M. and Halliday, A. N.: New sample preparation techniques for the determination of Si isotopic compositions using MC-ICPMS, Chem. Geol., 235(1–2), 95–104, doi:10.1016/j.chemgeo.2006.06.006, 2006.

Georgiadis, A., Sauer, D., Breuer, J., Herrmann, L., Rennert, T. and Stahr, K.: Optimising the extraction of amorphous silica by NaOH from soils of temperate-humid climate, Soil Res., 53(4), 392–400, doi:10.1071/SR14171, 2015.

Georgiadis, A., Sauer, D., Herrmann, L., Breuer, J., Zarei, M. and Stahr, K.: Testing a new method for sequential silicon extraction on soils of a temperate – humid climate, Soil Res., 52, 645–657, doi:10.1071/SR14016, 2014.

Giovannini, G., Lucchesi, S. and Giachetti, M.: Effect of heating on some phsical and chemical parameters related to soil aggregation and erodibility, Soil Sci., 146(4), 255–262 [online] Available from: http://journals.lww.com/soilsci/Abstract/1988/10000/EFFECT_OF_HEATING_ON_SOME_PHYSICAL_AND_CHEMICAL.6.aspx, 1988.

Gómez-Rey, M. X., Couto-Vázquez, A., García-Marco, S., Vega, J. A. and González-Prieto, S. J.: Reduction of nutrient losses with eroded sediments by post-fire soil stabilisation techniques, Int. J. Wildl. Fire, 22, 696–706, doi:10.1071/WF12079, 2013.

Govers, G., Quine, T. A., Desmet, P. J. J. and Walling, D. E.: The relative contribution of soil tillage and overland flow erosion to soil redistribution on agricultural land, Earth Surf. Process. Landforms, 21, 929–946, doi:10.1002/(SICI)1096-9837(199610)21:10<929::AID-ESP631>3.0.CO;2-C, 1996.

Grasse, P., Brzezinski, M. A., Cardinal, D., de Souza, G. F., Andersson, P., Closset, I., Cao, Z., Dai, M., Ehlert, C., Estrade, N., François, R., Frank, M., Jiang, G., Jones, J. L., Kooijman, E., Liu, Q., Lu, D., Pahnke, K., Ponzevera, E., Schmitt, M., Sun, X., Sutton, J. N., Thil, F., Weis, W., Wetzel, F., Zhang, A., Zhang, J. and Zhang, Z.: GEOTRACES inter-calibration of the stable silicon isotope composition of dissolved silicic acid in seawater, J. Anal. At. Spectrom., 32(3), 562–578, doi:10.1039/C6JA00302H, 2017.

Gregorich, E. G., Greer, K. J., Anderson, D. W. and Liang, B. C.: Carbon distribution and losses: erosion and deposition effects, Soil Tillage Res., 47, 291–302, doi:10.1016/S0167-1987(98)00117-2, 1998.

Grünwald, T. and Bernhofer, C.: A decade of carbon, water and energy flux measurements of an old spruce forest at the Anchor Station Tharandt, Tellus, Ser. B Chem. Phys. Meteorol., 59(3), 387–396, doi:10.1111/j.1600-0889.2007.00259.x, 2007.

Guntzer, F., Keller, C. and Meunier, J.: Benefits of plant silicon for crops: a review, Agron. Sustain. Dev, 32, 201–213, doi:10.1007/s13593-011-0039-8, 2012a.

Guntzer, F., Keller, C., Poulton, P. R., McGrath, S. P. and Meunier, J. D.: Long-term removal of wheat straw decreases soil amorphous silica at Broadbalk, Rothamsted, Plant Soil, 352(1–2), 173–184, doi:10.1007/s11104-011-0987-4, 2012b.

Guo, J. and Chen, B.: Insights on the molecular

mechanism for the recalcitrance of biochars: Interactive effects of Carbon and Silicon components, Environ. Sci. Technol., 48, 9103–9112, doi:10.1021/es405647e, 2014.

Haglund, N. and Expert group: Guideline for classification of ash from solid biofuels and peat utilised for recycling and fertilizing in forestry and agriculture. Nordic Innovation Centre. Project number: 06180. [online] Available from: http://p29596.typo3server.info/fileadmin/Files/Documents/06_Publications/GUIDELINE_FOR_CLASSIFICATION_OF_ASH.pdf, 2008.

Hall, T. B., Rosillo-Calle, F., Williams, R. H. and Woods, J.: Biomass for energy: supply prospects, in Renewable Energy: Sources for Fuels and Electricity., edited by R. H. Hall, T.B., Kelly, H., Reddy, A.K.N., Williams, pp. 593–651, Island Press, Washington D.C., 1993.

Hartmann, J., Jansen, N., Dürr, H. H., Kempe, S. and Köhler, P.: Global CO2 -consumption by chemical weathering: What is the contribution of highly active weathering regions?, Glob. Planet. Change, 69(4), 185–194, doi:10.1016/j.gloplacha.2009.07.007, 2009.

Haynes, R. J., Belyaeva, O. N. and Kingston, G.: Evaluation of industrial wastes as sources of fertilizer silicon using chemical extractions and plant uptake, J. Plant Nutr. Soil Sci., 176, 238–248, doi:10.1002/jpln.201200372, 2013.

Henriet, C., De Jaeger, N., Dorel, M., Opfergelt, S. and Delvaux, B.: The reserve of weatherable primary silicates impacts the accumulation of biogenic silicon in volcanic ash soils, Biogeochemistry, (90), 209–223, doi:10.1007/s10533-008-9245-0, 2008.

Herbillon, A. J.: Chemical estimation of weatherable minerals present in the diagnostic horizons of low activity clay soils., in Proceedings of the 8th International Soil Classification Work- shop: Classification, Characterization and Utilization of Oxisols, Part 1, edited by EMBRAPA, pp. 39–48, Rio de Janeiro., 1986.

Hiemstra, T., Barnett, M. O. and Riemsdijk, W. H. Van: Interaction of silicic acid with goethite, J. Colloid Interface Sci., 310, 8–17, doi:10.1016/j.jcis.2007.01.065, 2007.

Hilli, S., Stark, S. and Derome, J.: Litter decomposition rates in relation to litter stocks in boreal coniferous forests along climatic and soil fertility gradients, Appl. Soil Ecol., 46(2), 200–208, doi:10.1016/j.apsoil.2010.08.012, 2010.

Hodson, M. J., White, P. J., Mead, a. and Broadley, M. R.: Phylogenetic variation in the silicon composition of plants, Ann. Bot., 96(6), 1027–1046, doi:10.1093/aob/mci255, 2005.

Houben, D., Sonnet, P. and Cornelis, J.-T.: Biochar from Miscanthus: a potential silicon fertilizer, Plant Soil, (C), doi:10.1007/s11104-013-1885-8, 2013.

Hughes, H. J., Sondag, F., Cocquyt, C., Laraque, A., Pandi, A., André, L. and Cardinal, D.: Effect of seasonal biogenic silica variations on dissolved silicon fluxes and isotopic signatures in the Congo River, Limnol. Oceanogr., 56(2), 551–561, doi:10.4319/lo.2011.56.2.0551, 2011.

Humborg, C., Ittekkot, V., Cociasu, A. and Bodungen, B. v.: Effect of Danube River dam on Black Sea biogeochemistry and ecosystem structure, Nature, 386(6623), 385–388, doi:10.1038/386385a0, 1997.

Ibrahim, M. A. and Lal, R.: Catena Soil carbon and silicon pools across an un-drained toposequence in central Ohio, Catena, 120, 57–63, doi:10.1016/j.catena.2014.04.006, 2014.

Iler, R. K.: The Colloid Chemistry of Silica and Silicates., Soil Sci., 80(1) [online] Available from: http://journals.lww.com/soilsci/Fulltext/1955/07000/The_Colloid_Chemistry_of_Silica_and_Silicates_.14.aspx, 1955.

IPCC: Summary for Policymakers, in Climate Change 2014: Mitigation of Climate Change. Contribution of Work- ing Group III to the Fifth Assessment Report of the Intergovernmental Panel on Climate Change, edited by T. Z. and J. C. M. [Edenhofer, O., R. Pichs-Madruga, Y. Sokona, E. Farahani, S. Kadner, K. Seyboth, A. Adler, I. Baum, S. Brunner, P. Eickemeier, B. Kriemann, J. Savolainen, S. Schlömer, C. von Stechow, Cambridge University Press, Cambridge, United Kingdom and New York, NY, USA., 2014.

Ittekkot, V., Humborg, C. and Schäfer, P.: Hydrological alterations and marine biogeochemistry: A silicate issue?, Bioscience, 50(9), 776–782, doi:10.1641/0006-3568(2000)050[0776:HAAMBA]2.0.CO;2, 2000.

IUSS Working Group WRB: World Reference Base for Soil Resources 2014, update 2015. International soil classification system for naming soils and creating legends for soil maps., edited by World Soil Resources Reports No.106, FAO, Rome., 2015.

Jeandel, C. and Oelkers, E. H.: The influence of terrigenous particulate material dissolution on ocean chemistry and global element cycles, Chem. Geol., 395, 50–66, doi:10.1016/j.chemgeo.2014.12.001, 2015.

Johnson, T. C., Chan, Y., Beuning, K., Kelts, K., Ngobi, G. and Verschuren, D.: Biogenic silica profiles in Holocene cores from Lake Victoria: Implications for lake level history and initiation of the Victoria Nile., in Environmental Change and Response in East African Lakes, edited by J. T. Lehman, pp. 75–88, Springer, Dordrecht., 1998.

Jones, L. H. P. and Handreck, K. A.: Effects of Iron and Aluminium Oxides on Silica in Solution in Soils, Nature, 198(4883), 852–853 [online] Available from: http://dx.doi.org/10.1038/198852a0, 1963.

Jones, L. H. P. and Handreck, K. A.: Silica in soils, plants, and animals, vol. Volume 19, edited by A. G. N. B. T.-A. in Agronomy, pp. 107–149, Academic Press., 1967.

Jones, R. L. and Beavers, A. H.: Aspects of catenary and depth distribution of opal phytoliths in Illinois soils, Soil Sci. Soc. Am. J., 28, 413–416, doi:10.2136/sssaj1964.03615995002800030033x, 1964.

Joyce, L. A., Running, S. W., Breshears, D. D., Dale, V. H., Malmsheimer, R. W., Sampson, R. N., Sohngen, B. and Woodall, C. W.: Chapter 7: Forests, in Climate Change Impacts in the United States: The Third National Climate Assessment, edited by J. M. Melillo, T. Richmond, and G. W. Yohe, pp. 175–194, U.S. Global Change Research Program., 2014.

Kamatani, A., Ejiri, N. and Treguer, P.: The dissolution kinetics of diatom ooze from the Antarctic area, Deep. Res. Part a-Oceanographic Res. Pap., 35(7), 1195–1203, doi:10.1016/0198-0149(88)90010-6, 1988.

Kanga, E. M., Ogutu, J. O., Olff, H. and Santema, P.: Population trend and distribution of the Vulnerable common hippopotamus Hippopotamus amphibius in the Mara Region of Kenya., Oryx, 45(1), 20–27, doi:10.1017/S0030605310000931, 2011.

Keeley, J. E.: Fire intensity, fire severity and burn severity: a brief review and suggested usage, Int. J. Wildl. Fire, 18(1), 116–126, doi:10.1071/WF07049, 2009.

Keeping, M. G.: Uptake of Silicon by sugarcane from applied sources may not reflect plant-available soil Silicon and total silicon content of sources, Front. Plant Sci., 8(May), 1–14, doi:10.3389/fpls.2017.00760, 2017.

Keller, C., Guntzer, F., Barboni, D., Labreuche, J. and Meunier, J. D.: Impact of agriculture on the Si biogeochemical cycle: Input from phytolith studies, Comptes Rendus - Geosci., 344(11–12), 739–746, doi:10.1016/j.crte.2012.10.004, 2012.

Kelly, E. F., Chadwick, O. A. and Hilinski, T. E.: The effect of plants on mineral weathering, Biogeochemistry, (42), 21–53, doi:10.1007/978-94-017-2691-7_2, 1998.

Kendrick, K. J. and Graham, R. C.: Pedogenic silica accumulation in chronosequence soils, southern California, Soil Sci. Soc. Am. J., 68(4), 1295–1303 [online] Available from: http://pubs.er.usgs.gov/publication/70026998, 2004.

Kilham, P.: Hypothesis concerning silica and freshwater planktonic diatoms, Limnol. Oceanogr., 16(1), 10–18, doi:10.4319/lo.1971.16.1.0010, 1971.

Kirchholtes, R. P. J., van Mourik, J. M. and Johnson, B. R.: Phytoliths as indicators of plant community change: A case study of the reconstruction of the historical extent of the oak savanna in the Willamette Valley Oregon, USA, Catena, 132, 89–96, doi:10.1016/j.catena.2014.11.004, 2015.

Kissinger, G., Herold, M. and De Sy, V.: Drivers of deforestation and forest degradation: A synthesis report for REDD+ Policymakers, Vancouver Canada. [online] Available from: https://www.gov.uk/government/uploads/system/uploads/attachment_data/file/65505/6316-drivers-deforestation-report.pdf, 2012.

Knicker, H.: How does fire affect the nature and stability of soil organic nitrogen and carbon? A review, Biogeochemistry, 85(1), 91–118, doi:10.1007/s10533-007-9104-4, 2007.

Kodama, H. and Ross, G. J.: Tiron dissolution method used to remove and characterize inorganic components in soils, Soil Sci. Soc. Am. J., 55(August), 1180–1187, doi:10.2136/sssaj1991.03615995005500040047x, 1991.

Kokfelt, U., Struyf, E. and Randsalu, L.: Diatoms in peat - Dominant producers in a changing environment?, Soil Biol. Biochem., 41(8), 1764–1766, doi:10.1016/j.soilbio.2009.05.012, 2009.

Koning, E., Epping, E. and Van Raaphorst, W.: Determining biogenic silica in marine samples by tracking silicate and aluminium concentrations in alkaline leaching solutions, Aquat. Geochemistry, 8(1), 37–67, doi:10.1023/A:1020318610178, 2002.

Kottek, M., Grieser, J., Beck, C., Rudolf, B. and Rubel, F.: World Map of the Köppen-Geiger climate classification updated, Meteorol. Zeitschrift, 15(3), 259–263, doi:10.1127/0941-2948/2006/0130, 2006.

Kovats, R. S., Jacob, D., Martin, E., Rounsevell, M. and Soussana, E.: Europe. In: Climate Change 2014: Impacts, Adaptation, and Vulnerability. Part B: Regional Aspects. Contribution of

Working Group II to the Fifth Assessment Report of the Intergovernmental Panel on Climate Change., 2014.

Krause, W., Darrow, E. S., Pickering, R. A., Carmichael, R. H., Larson, A. M. and Basaldua, J. L.: Reactive silica fractions in coastal lagoon sediments from the northern Gulf of Mexico, Cont. Shelf Res., 151(July), 8–14, doi:10.1016/j.csr.2017.09.014, 2017.

De La Rocha, C. L., Brzezinski, M. A. and DeNiro, M. J.: Purification, recovery, and laser-driven fluorination of silicon from dissolved and particulate silica for the measurement of natural stable isotope abundances, Anal. Chem., 68(21), 3746–3750, doi:10.1021/ac960326j, 1996.

Legesse, D., Vallet-Coulomb, C. and Gasse, F.: Hydrological response of a catchment to climate and land use changes in Tropical Africa: case study South Central Ethiopia, J. Hydrol., 275, 67–85, doi:10.1016/S0022-1694(03)00019-2, 2003.

Lewison, R., Oliver, W. and Subgroup), (IUCN SSC Hippo Specialist: Hippopotamus amphibius. The IUCN Red List of Threatened Species 2008: e.T10103A3163790., 2008.

Li, Z., Delvaux, B., Yans, J., Dufour, N., Houben, D. and Cornelis, J.-T.: Phytolith-rich biochar increases cotton biomass and silicon-mineralomass in a highly weathered soil, Biogeochemistry, Submitted, 2017.

Li, Z., Song, Z., Parr, J. F. and Wang, H.: Occluded C in rice phytoliths: implications to biogeochemical carbon sequestration, Plant Soil, 370, 615–623, doi:10.1007/s11104-013-1661-9, 2013.

Li, Z., Unzué-Belmonte, D., Cornelis, J.-T., Ronsse, F. and Delvaux, B.: Phytolith content in biochar affect the biological Si cycle in soil-wheat system, , In prep, 2018.

Liang, Y., Hua, H., Zhu, Y., Zhang, J., Cheng, C. and Römheld, V.: Importance of plant species and external silicon concentration to active silicon uptake and transport, New Phytol., 172, 63–72, doi:10.1111/j.1469-8137.2006.01797.x, 2006.

Liang, Y., Nikolic, M., Bélanger, R., Gong, H. and Song, A.: Silicon in Agriculture, Springer Netherlands., 2015.

Lindsay, W. L.: Chemical equilibria in soils, Wiley, New York. [online] Available from: http://soils.ifas.ufl.edu/lqma/SEED/CWR6252/Handout/Chemical equilibira.pdf, 1979.

Loucaides, S., Cappellen, P. Van and Behrends, T.: Dissolution of biogenic silica from land to ocean : Role of salinity and pH, Limnol. Oceanogr., 53(4), 1614–1621, doi:10.1029/2002GB001894, 2008.

Lucas, Y.: The role of plants in controlling rates and products of weathering: Importance of biological pumping, Annu. Rev. Earth Planet. Sci. Lett., 29, 135–63, doi:10.1146/annurev.earth.29.1.135, 2001.

Lucas, Y., Luizao, F. J., Chauvel, A., Rouiller, J. and Nahon, D.: The RelationBetweenBiologicalActivityof the RainForestand MineralCompositionof Soils, Science (80-.)., 260(April), 521–523, doi:10.1126/science.260.5107.521, 1993.

Ma, F. M. and Takahashi, A.: Soil, fertilizer and plant silicon in Japan, Elsevier Science B.V., Amsterdam, The Netherlands., 2002.

Ma, J. F., Miyake, Y. and Takahashi, E.: Silicon as a beneficial element for crop plants, in Silicon in Agriculture, vol. 8, edited by L. E. Datnoff, G. H. Snyder, and G. H. Korndörfer, pp. 17–39, Elsevier., 2001.

Ma, J. F., Tamai, K., Yamaji, N., Mitani, N., Konishi, S., Katsuhara, M., Ishiguro, M., Murata, Y. and Yano, M.: A silicon transporter in rice, Nature, 440(7084), 688–691, doi:10.1038/nature04590, 2006.

Mackay, A. W., Swann, G. E. A., Brewer, T. S., Leng, M. J., Morley, D. W., Piotrowska, N., Rioual, P. and White, D.: A reassessment of late glacial - Holocene diatom oxygen isotope record from Lake Baikal using a geochemical mass-balance approach, J. Quat. Sci., 26(6), 627–634, doi:10.1002/jqs.1484, 2011.

Major, J., Rondon, M., Molina, D., Riha, S. J. and Lehmann, J.: Maize yield and nutrition during 4 years after biochar application to a Colombian savanna oxisol, Plant Soil, 333(August), 117–128, doi:10.1007/s11104-010-0327-0, 2010.

Marschner, H.: Mineral nutrition of higher plants., Academic Press, Elsevier, London., 1995.

Martin-Jezequel, V., Hildebrand, M. and Brzezinski, M. A.: Silicon metabolism in diatoms: Implications for growth, J. Phycol., 36(5), 821–840, doi:10.1046/j.1529-8817.2000.00019.x, 2000.

Martin, J., Wilcox, L., Burstedde, C. and Ghattas, O.: A Stochastic Newton MCMC Method for Large-Scale Statistical Inverse Problems with Application to Seismic Inversion, SIAM J. Sci. Comput., 34(3), A1460–A1487, doi:10.1137/110845598, 2012.

Masese, F. O. and McClain, M. E.: Trophic resources and emergent food web attributes in rivers of the Lake Victoria Basin: a review with reference to anthropogenic influences,

Ecohydrology, 5(6), 685–707, doi:10.1002/eco.1285, 2012.

Mati, B. M., Mutie, S., Gadain, H., Home, P. and Mtalo, F.: Impacts of land-use / cover changes on the hydrology of the transboundary Mara River , Kenya / Tanzania, , 169–177, doi:10.1111/j.1440-1770.2008.00367.x, 2008.

Maurel, M.-C. and Leclerc, F.: From foundation stones to life: Concepts and results, Elements, 12(6), 407–412, doi:10.2113/gselements.12.6.407, 2016.

McCauley, D. J., Pinsky, M. L., Palumbi, S. R., Estes, J. A., Joyce, F. H. and Warner, R. R.: Marine defaunation: Animal loss in the global ocean, Science (80-.)., 347(6219), 1255641, doi:10.1126/science.1255641, 2015.

McClain, M. E., Subalusky, A. L., Anderson, E. P., Behailu Dessu, S., Melesse, A. M., Ndomba, P. M., Mtamba, J. O. D., Tamatamah, R. A. and Mligo, C.: Comparing flow regime, channel hydraulics, and biological communities to infer flow-ecology relationships in the Mara River of Kenya and Tanzania, Hydrol. Sci. J., 59(3–4), 801–819, doi:10.1080/02626667.2013.853121, 2014.

McFadden, L. D. and Hendricks, D. M.: Changes in the content and composition of pedogenic iron oxyhydroxides in a chronosequence of soils in southern California, Quat. Res., 23, 189–204, doi:10.1016/0033-5894(85)90028-6, 1985.

McKeague, J. A. and Cline, M. G.: Silica in soil solutions: II. The adsorption of monosilicic acid by soil and other substances, Can. J. Soil Sci., 43, 83–96, doi:10.4141/cjss63-011, 1963.

McMichael, A. J., Woodruff, R. E. and Hales, S.: Climate change and human health: present and future risks, Lancet, 367, 859–69, doi:10.1016/S0140-6736(06)68079-3, 2005.

Melzer, S. E., Knapp, A. K., Kirkman, K. P., Smith, M. D., Blair, J. M. and Kelly, E. F.: Fire and grazing impacts on silica production and storage in grass dominated ecosystems, Biogeochemistry, 97(2–3), 263–278, doi:10.1007/s10533-009-9371-3, 2009.

Meunier, J. D., Colin, F. and Alarcon, C.: Biogenic silica storage in soils, Geology, 27(9), 835–838, doi:10.1130/0091-7613, 1999.

Meunier, J. D., Kirman, S., Strasberg, D., Nicolini, E., Delcher, E. and Keller, C.: The output and bio-cycling of Si in a tropical rain forest developed on young basalt flows (La Reunion Island), Geoderma, 159(3–4), 431–439, doi:10.1016/j.geoderma.2010.09.010, 2010.

Meyer, J. and Keeping, M.: Past , present and future research of the role of silicon for sugarcane in southern Africa, in Silicon in Agriculture, edited by and G. H. K. L. E. Datnoff, G. H. Snyder, pp. 257–275, Elsevier, Amsterdam, The Netherlands., 2001.

Minella, J. P. G., Walling, D. E. and Merten, G. H.: Establishing a sediment budget for a small agricultural catchment in southern Brazil , to support the development of effective sediment management strategies, J. Hydrol., 519, 2189–2201, doi:10.1016/j.jhydrol.2014.10.013, 2014.

Mitani, N. and Ma, J. F.: Uptake system of silicon in different plant species, J. Exp. Bot., 56(414), 1255–1261, doi:10.1093/jxb/eri121, 2005.

Montagnes, D. J. S. and Franklin, D. J.: Effect of temperature on diatom volume, growth rate, and carbon and nitrogen content: Reconsidering some paradigms, Limnol. Oceanogr., 46(8), 2008–2018, doi:10.4319/lo.2001.46.8.2008, 2001.

Montgomery, D. R. and Brandon, M. T.: Topographic controls on erosion rates in tectonically active mountain ranges, Earth Planet. Sci. Lett., 201, 481–489, doi:10.1016/S0012-821X(02)00725-2, 2002.

Navas, A., Gaspar, L., Quijano, L., López-vicente, M. and Machín, J.: Catena patterns of soil organic carbon and nitrogen in relation to soil movement under different land uses in mountain fields (South Central Pyrenees), Catena, 94, 43–52, doi:10.1016/j.catena.2011.05.012, 2012.

Neal, C., Neal, M., Reynolds, B., Maberly, S. C., May, L., Ferrier, R. C., Smith, J. and Parker, J. E.: Silicon concentrations in UK surface waters, J. Hydrol., 304, 75–93, doi:10.1016/j.jhydrol.2004.07.023, 2005.

Nelson, D. M., Treguer, P., Brzezinski, M. A., Leynaert, A. and Quéguiner, B.: Production and dissolution of biogenic silica in the ocean. Revised global estimates, comparison with regional data and relationship to biogenic sedimentation, Global Biogeochem. Cycles, 9, 359–372, doi:10.1029/95GB01070, 1995.

Nguyen, M. N., Dultz, S. and Guggenberger, G.: Effects of pretreatment and solution chemistry on solubility of rice-straw phytoliths, J. Plant Nutr. Soil Sci., 0, 1–11, doi:10.1002/jpln.201300056, 2013.

Nguyen, M. N., Dultz, S. and Guggenberger, G.: Effects of pretreatment and solution chemistry on solubility of rice-straw phytoliths, J. Plant Nutr. Soil Sci., 177(3), 349–359, doi:10.1002/jpln.201300056, 2014.

Oelze, M., von Blanckenburg, F., Bouchez, J., Hoellen, D. and Dietzel, M.: The effect of Al on Si isotope fractionation investigated by silica precipitation experiments., Chem. Geol., 397,

94–105, doi:10.1016/j.chemgeo.2015.01.002, 2015.

Oelze, M., von Blanckenburg, F., Hoellen, D., Dietzel, M. and Bouchez, J.: Si stable isotope fractionation during adsorption and the competition between kinetic and equilibrium isotope fractionation: Implications for weathering systems, Chem. Geol., 380, 161–171, doi:10.1016/j.chemgeo.2014.04.027, 2014.

Ohtani, E., Sakamaki, T., Fukui, H., Tanaka, R., Shibazaki, Y., Kamada, S., Sakairi, T., Takahashi, S., Tsutsui, S. and Baron, A. Q. R.: Sound velocity of iron-light element compounds and the chemical structure of the inner core, in AGU Fall Meeting; 2016. Dec 12-16. San Francisco. [online] Available from: https://agu.confex.com/agu/fm16/meetingapp.cgi/Paper/153611, 2016.

Opfergelt, S., de Bournonville, G., Cardinal, D., André, L., Delstanche, S. and Delvaux, B.: Impact of soil weathering degree on silicon isotopic fractionation during adsorption onto iron oxides in basaltic ash soils, Cameroon, Geochim. Cosmochim. Acta, 73(24), 7226–7240, doi:10.1016/j.gca.2009.09.003, 2009.

Opfergelt, S., Cardinal, D., André, L., Delvigne, C., Bremond, L. and Delvaux, B.: Variations of δ30Si and Ge/Si with weathering and biogenic input in tropical basaltic ash soils under monoculture, Geochim. Cosmochim. Acta, 74(1), 225–240, doi:10.1016/j.gca.2009.09.025, 2010.

Opfergelt, S., Cardinal, D., Henriet, C., Draye, X., André, L. and Delvaux, B.: Silicon isotopic fractionation by banana (Musa spp.) grown in a continuous nutrient flow device., Plant Soil, 285, 333–345, doi:10.1007/s11104-006-9019-1, 2006.

Opfergelt, S. and Delmelle, P.: Silicon isotopes and continental weathering processes: Assessing controls on Si transfer to the ocean, Comptes Rendus Geosci., 344(11–12), 723–738, doi:10.1016/j.crte.2012.09.006, 2012.

Opfergelt, S., Georg, R. B., Delvaux, B., Cabidoche, Y.-M., Burton, K. W. and Halliday, A. N.: Silicon isotopes and the tracing of desilication in volcanic soil weathering sequences, Guadeloupe, Chem. Geol., 326–327, 113–122, doi:10.1016/j.chemgeo.2012.07.032, 2012.

Parr, J. F., Lentfer, C. J. and Boyd, W. E.: A comparative analysis of wet and dry ashing techniques for the extraction of phytoliths from plant material, J. Archaeol. Sci., 28(8), 875–886, doi:10.1006/jasc.2000.0623, 2001.

Parr, J., Sullivan, L., Chen, B., Ye, G. and Zheng, W.: Carbon bio-sequestration within the phytoliths of economic bamboo species, Glob. Chang. Biol., (16), 2661–2667, doi:10.1111/j.1365-2486.2009.02118.x, 2010.

Patrick, R.: Ecology of freshwater diatom-diatom communities, in The biology of diatoms. Botanical Monography. vol. 13, edited by D. Wener, pp. 284–332, Blackwell, London., 1977.

Pereira, P., Úbeda, X. and Martin, D. a.: Fire severity effects on ash chemical composition and water-extractable elements, Geoderma, 191, 105–114, doi:10.1016/j.geoderma.2012.02.005, 2012.

Pereira, P., Ubeda, X., Martin, D., Mataix-Solera, J. and Guerrero, C.: Effects of a low severity prescribed fire on water-soluble elements in ash from a cork oak (Quercus suber) forest located in the northeast of the Iberian Peninsula., Environ. Res., 111(2), 237–47, doi:10.1016/j.envres.2010.09.002, 2011.

Piperno, D. R.: Phytoliths: A comprehensive guide for archaeologists and paleoecologists, Altamira Press, San Diego., 2006.

Qian, L. and Chen, B.: Dual role of biochars as adsorbents for aluminum: The effects of oxygen-containing organic components and the scattering of silicate particles, Environ. Sci. Technol., 47, 8759–8768, doi:10.1021/es401756h, 2013.

Quinton, J. N., Govers, G., Van Oost, K. and Bardgett, R. D.: The impact of agricultural soil erosion on biogeochemical cycling, Nat. Geosci, 3(5), 311–314, doi:10.1038/ngeo838, 2010.

Quirk, J., Leake, J. R., Banwart, S. a., Taylor, L. L. and Beerling, D. J.: Weathering by tree-root-associating fungi diminishes under simulated cenozoic atmospheric CO2 decline, Biogeosciences, 11(2), 321–331, doi:10.5194/bg-11-321-2014, 2014.

Ragueneau, O., Schultes, S., Bidle, K., Claquin, P. and Moriceau, B.: Si and C interactions in the world ocean: Importance of ecological processes and implications for the role of diatoms in the biological pump, Global Biogeochem. Cycles, 20, GB4S02, doi:10.1029/2006GB002688., 2006.

Ragueneau, O., Treguer, P., Leynaert, A., Anderson, R. F., Brzezinski, M. A., Demaster, D. J., Dugdale, R. C., Dymond, J., Fischer, G., Franc, R., Heinze, C., Nelson, D. M. and Queguiner, B.: A review of the Si cycle in the modern ocean: recent progress and missing gaps in the application of biogenic opal as a paleoproductivity proxy, Glob. Planet. Change, 26, 317–365, 2000.

Reynolds, B. C., Aggarwal, J., André, L., Baxter, D., Beucher, C., Brzezinski, M. A., Engström, E.,

Georg, R. B., Land, M., Leng, M. J., Opfergelt, S., Rodushkin, I., Sloane, H. J., van den Boorn, S. H. J. M., Vroonm, P. Z. and Cardinal, D.: An inter-laboratory comparison of Si isotope reference materials, J. Anal. At. Spectrom., 22(5), 561–568, doi:10.1039/B616755A, 2007.

Ribeiro, S., Sejr, M. K., Limoges, A., Heikkilä, M., Andersen, T. J., Tallberg, P., Weckström, K., Husum, K., Forwick, M., Dalsgaard, T., Massé, G., Seidenkrantz, M. and Rysgaard, S.: Sea ice and primary production proxies in surface sediments from a High Arctic Greenland fjord : Spatial distribution and implications for palaeoenvironmental studies, Ambio, 46, 106–118, doi:10.1007/s13280-016-0894-2, 2017.

Rickert, D., Schluter, M. and Wallmann, K.: Dissolution kinetics of biogenic silica from the water column to the sediments, Geochim. Cosmochim. Acta, 66(3), 439–455, doi:10.1016/S0016-7037(01)00757-8, 2002.

Rimstidt, J. D. and Barnes, H. L.: The kinetics of silica-water reactions, Geochim. Cosmochim. Acta, 44, 1683–1699, doi:1101168350200, 1980.

Ripple, W. J., Newsome, T. M., Wolf, C., Dirzo, R., Everatt, K. T., Galetti, M., Hayward, M. W., Kerley, G. I. H., Levi, T., Lindsey, P. A., Macdonald, D. W., Malhi, Y., Painter, L. E. and Sandom, C. J.: Collapse of the world ' s largest herbivores, Sci. Adv., (May), 1:e1400103, doi:10.1126/sciadv.1400103, 2015.

Robert, M. and Tessier, D.: Méthode de préparation des argiles des sols pour des études minéralogiques, Ann. Agron., 25, 859–882, 1974.

Ronchi, B., Barão, L., Clymans, W., Vandevenne, F., Batelaan, O., Govers, G., Struyf, E. and Dassargues, A.: Factors controlling Si export from soils: A soil column approach, Catena, 133, 85–96, doi:10.1016/j.catena.2015.05.007, 2015.

Ronchi, B., Clymans, W., Barão, A. L. P., Vandevenne, F., Struyf, E., Batelaan, O., Dassargues, A. and Govers, G.: Transport of Dissolved Si from Soil to River: A Conceptual Mechanistic Model, Silicon, 5(1), 115–133, doi:10.1007/s12633-012-9138-7, 2013.

Round, F. E., Crawford, R. M. and Mann, D. G.: The diatoms: biology and morphology of the genera, Cambridge University Press, UK., 1990.

Rovner, I.: Potential of opal phytoliths for use in paleoecological reconstruction, Quat. Res., 1(3), 343–359, doi:10.1016/0033-5894(71)90070-6, 1971.

Rundel, P. W.: Impact of fire on nutrient cycles in Mediterranean-type ecosystems with reference to chaparral., in Mediterranean-Type Ecosystems: The Role of Nutrients., edited by J. U. M. Kruger, F.J., Mitchell, D.T., Jarvis, pp. 192–2207, Ecological Studies Volume 43., 1983.

Saccone, L., Conley, D. J., Koning, E., Sauer, D., Sommer, M., Kaczorek, D., Blecker, S. W. and Kelly, E. F.: Assessing the extraction and quantification of amorphous silica in soils of forest and grassland ecosystems, Eur. J. Soil Sci., 58(6), 1446–1459, doi:10.1111/j.1365-2389.2007.00949.x, 2007.

Saccone, L., Conley, D. J. and Sauer, D.: Methodologies for amorphous silica analysis, J. Geochemical Explor., 88(1–3), 235–238, doi:10.1016/j.gexplo.2005.08.045, 2006.

Sandom, C., Faurby, S., Sandel, B. and Svenning, J.: Global late Quaternary megafauna extinctions linked to humans , not climate change, Proc. R. Soc. B, 281:20133254, doi:10.1098/rspb.2013.3254, 2014.

Santos, G. M. and Alexandre, A.: Earth-Science Reviews The phytolith carbon sequestration concept : Fact or fiction? A comment on "Occurrence , turnover and carbon sequestration potential of phytoliths in terrestrial ecosystems by Song et al . doi : 10 . 1016 /j.earscirev.2016.04.007," Earth Sci. Rev., 164, 251–255, doi:10.1016/j.earscirev.2016.11.005, 2017.

Sauer, D., Saccone, L., Conley, D. J., Herrmann, L. and Sommer, M.: Review of methodologies for extracting plant-available and amorphous Si from soils and aquatic sediments, Biogeochemistry, 80(1), 89–108, doi:10.1007/s10533-005-5879-3, 2006.

Savant, N. K., Datnoff, L. E., Snyder, G. H., Savant, N. K., Datnoff, L. E. and Snyder, G. H.: A possible cause of declining rice yields depletion of plant-available silicon in soils: A possible cause of declining rice yields, Commun. Soil Sci. Plant Anal., 28(January), 1245–1252, doi:10.1080/00103629709369870, 1997.

Schaetzl, R. J. and Anderson, S.: Soils Genesis and Geomorphology, Cambridge University Press, New York., 2005.

Schaller, J. and Struyf, E.: Silicon controls microbial decay and nutrient release of grass litter during aquatic decomposition, Hydrobiologia, 709(1), 201–212, doi:10.1007/s10750-013-1449-1, 2013.

Schaller, J., Tischer, A., Struyf, E., Bremer, M., Unzué-Belmonte, D. and Potthast, K.: Fire enhances phosphorus availability in top soils depends on binding properties, Ecology, doi:10.1890/14-1311.1, 2015.

Schmidt, M. W. I., Torn, M. S., Abiven, S., Dittmar, T.,

Guggenberger, G., Janssens, I. A., Kleber, M., Kögel-Knabner, I., Lehmann, J., Manning, D. a. C., Nannipieri, P., Rasse, D. P., Weiner, S. and Trumbore, S. E.: Persistence of soil organic matter as an ecosystem property, Nature, 478(7367), 49–56, doi:10.1038/nature10386, 2011.

Schmitz, O. J., Raymond, P. A., Estes, J. A., Kurz, W. A., Holtgrieve, G. W., Ritchie, M. E., Schindler, D. E., Spivak, A. C., Wilson, R. W., Bradford, M. A., Christensen, V., Deegan, L., Smetacek, V., Vanni, M. J. and Wilmers, C. C.: Animating the carbon cycle, Ecosystems, 17(2), 344–359, doi:10.1007/s10021-013-9715-7, 2014.

Schoelynck, J., Müller, F., Vandevenne, F., Bal, K., Barão, L., Smis, A., Opdekamp, W., Meire, P. and Struyf, E.: Silicon-vegetation interaction in multiple ecosystems: a review, edited by M. W. Palmer, J. Veg. Sci., n/a-n/a, doi:10.1111/jvs.12055, 2013.

Schoelynck, J., Subalusky, A. L., Struyf, E., Dutton, C. L., Unzué-Belmonte, D., Van de Vijver, B., Post, D. M., Rosi, E. J., Meire, P. and Frings, P.: Hippos (Hippopotamus amphibius): the animal silica pump, PNAS, Submitted, 2017.

Schoonejans, J., Vanacker, V., Opfergelt, S. and Christl, M.: Long-term soil erosion derived from in-situ 10 Be and inventories of meteoric Be in deeply weathered soils in southern Brazil, Chem. Geol., 466(June), 380–388, doi:10.1016/j.chemgeo.2017.06.025, 2017.

Smis, A., Van Damme, S., Struyf, E., Clymans, W., Van Wesemael, B., Frot, E., Vandevenne, F., Van Hoestenberghe, T., Govers, G. and Meire, P.: A trade-off between dissolved and amorphous silica transport during peak flow events (Scheldt river basin, Belgium): Impacts of precipitation intensity on terrestrial Si dynamics in strongly cultivated catchments, Biogeochemistry, 106(3), 475–487, doi:10.1007/s10533-010-9527-1, 2011.

Sohi, S. P., Krull, E. and Bol, R.: A review of biochar and its use and function in soil, Elsevier Inc., 2010.

Sommer, M., Jochheim, H., Höhn, a., Breuer, J., Zagorski, Z., Busse, J., Barkusky, D., Meier, K., Puppe, D., Wanner, M. and Kaczorek, D.: Si cycling in a forest biogeosystem – the importance of transient state biogenic Si pools, Biogeosciences, 10(7), 4991–5007, doi:10.5194/bg-10-4991-2013, 2013.

Sommer, M., Kaczorek, D., Kuzyakov, Y. and Breuer, J.: Silicon pools and fluxes in soils and landscapes—a review, J. Plant Nutr. Soil Sci., 169(3), 310–329, doi:10.1002/jpln.200521981, 2006.

Song, Z., McGrouther, K. and Wang, H.: Occurrence, turnover and carbon sequestration potential of phytoliths in terrestrial ecosystems, Earth-Science Rev., 158, 19–30, doi:10.1016/j.earscirev.2016.04.007, 2016.

Song, Z., Müller, K. and Wang, H.: Biogeochemical silicon cycle and carbon sequestration in agricultural ecosystems, Earth-Science Rev., 139, 268–278, doi:10.1016/j.earscirev.2014.09.009, 2014.

Song, Z., Wang, H., Strong, P. J., Li, Z. and Jiang, P.: Plant impact on the coupled terrestrial biogeochemical cycles of silicon and carbon: Implications for biogeochemical carbon sequestration, Earth-Science Rev., 115(4), 319–331, doi:10.1016/j.earscirev.2012.09.006, 2012.

Stager, C., Hecky, R. E., Grzesik, D., Cumming, B. F. and Kling, H.: Diatom evidence for the timing and causes of eutrophication in Lake Victoria, East Africa, Hydrobiologia, 636(1), 463–478, doi:10.1007/s10750-009-9974-7, 2009.

Steenari, B., Schelander, S. and Lindqvist, O.: Chemical and leaching characteristics of ash from combustion of coal, peat and wood in a 12 MW CFB – a comparative study, Fuel, 78, 249–258, doi:10.1016/S0016-2361(98)00137-9, 1999.

Steffen, W., Sanderson, A., Tyson, P. D., Jager, J., Matson, P. A., Moore III, B., Oldfield, F., Richardson, K., Schellnhuber, H.-J., Turner II, B. L. and Wasson, R. J.: Global Change and the Earth System, Springer., 2004.

Struyf, E. and Conley, D. J.: Silica: an essential nutrient in wetland biogeochemistry, Front. Ecol. Environ., 7(2), 88–94, doi:10.1890/070126, 2009.

Struyf, E. and Conley, D. J.: Emerging understanding of the ecosystem silica filter, Biogeochemistry, 107(1–3), 9–18, doi:10.1007/s10533-011-9590-2, 2012.

Struyf, E., Mosimane, K., Van Pelt, D., Murray-Hudson, M., Meire, P., Frings, P. J., Wolski, P., Schaller, J., Gondwe, M. J., Schoelynck, J. and Conley, D. J.: The role of vegetation in the Okavango Delta silica sink, Wetlands, 35(1), 171–181, doi:10.1007/s13157-014-0607-1, 2015.

Struyf, E., Mrth, C. M., Humborg, C. and Conley, D. J.: An enormous amorphous silica stock in boreal wetlands, J. Geophys. Res. Biogeosciences, 115(4), 1–8, doi:10.1029/2010JG001324, 2010a.

Struyf, E., Smis, A., Van Damme, S., Garnier, J., Govers, G., Van Wesemael, B., Conley, D. J., Batelaan, O., Frot, E., Clymans, W., Vandevenne, F., Lancelot, C., Goos, P. and

Meire, P.: Historical land use change has lowered terrestrial silica mobilization., Nat. Commun., (8), 1:129, doi:10.1038/ncomms1128, 2010b.

Struyf, E., Smis, A., Van Damme, S., Meire, P. and Conley, D. J.: The Global Biogeochemical Silicon Cycle, Silicon, 1(4), 207–213, doi:10.1007/s12633-010-9035-x, 2010c.

Struyf, E., Temmerman, S. and Meire, P.: Dynamics of biogenic Si in freshwater tidal marshes: Si regeneration and retention in marsh sediments (Scheldt estuary), Biogeochemistry, 82, 41–53, doi:10.1007/s10533-006-9051-5, 2007.

Subalusky, A. L., Dutton, C. L., Rosi-Marshall, E. J. and Post, D. M.: The hippopotamus conveyor belt: vectors of carbon and nutrients from terrestrial grasslands to aquatic systems in sub-Saharan Africa, Freshw. Biol., 60, 512–525, doi:10.1111/fwb.12474, 2015.

Takahashi, E., Ma, J. F. and Miyake, Y.: The possibility of silicon as an essential element for higher plants, Comments Agric. Food Chem., 2(2), 99–102, 1990.

Tierney, J. E., Mayes, M. T., Meyer, N., Johnson, C., Swarzenski, P. W., Andrew, S., Cohen, A. S. and Russell, J. M.: Late-twentieth-century warming in Lake Tanganyika unprecedented since AD 500, Nat. Geosci., 3, 422–425, doi:10.1038/ngeo865, 2010.

Tréguer, P. J. and De La Rocha, C. L.: The world ocean silica cycle, Ann. Rev. Mar. Sci., 5, 477–501, doi:10.1146/annurev-marine-121211-172346, 2013.

Tréguer, P., Nelson, D. M., Van Bennekom, A. J., DeMaster, D. J., Leynaert, A. and Quéguiner, B.: The Silica balance in the World Ocean: A reestimate, Science (80-.)., 268(5209), 375–379, doi:10.1126/science.268.5209.375, 1995.

Trembath-Reichert, E., Wilson, J. P., McGlynn, S. E. and Fischer, W. W.: Four hundred million years of silica biomineralization in land plants, Proc. Natl. Acad. Sci., 201500289, doi:10.1073/pnas.1500289112, 2015.

Uehara, G. and Gillman, G.: The Mineralogy, Chemistry, and Physics of Tropical Soils With Variable Charge Clays, West View Press, Boulder, CO, USA., 1981.

Unzué-Belmonte, D., Ameijeiras-Mariño, Y., Opfergelt, S., Cornelis, J., Barão, L., Minella, J., Meire, P. and Struyf, E.: Land use change affects biogenic silica pool distribution in a subtropical soil toposequence, Solid Earth, 8, 737–750, doi:10.5194/se-8-737-2017, 2017.

Unzué-Belmonte, D., Struyf, E., Clymans, W., Tischer, A., Potthast, K., Bremer, M., Meire, P. and Schaller, J.: Fire enhances solubility of biogenic silica, Sci. Total Environ., 572, 1289–1296, doi:10.1016/j.scitotenv.2015.12.085, 2016.

Vanacker, V., Bellin, N., Molina, A. and Kubik, P. W.: Erosion regulation as a function of human disturbances to vegetation cover : a conceptual model, Landsc. Ecol, 29, 293–309, doi:10.1007/s10980-013-9956-z, 2014.

Vandevenne, F. I., Barão, A. L., Schoelynck, J., Smis, A., Ryken, N., Van Damme, S., Meire, P. and Struyf, E.: Grazers: biocatalysts of terrestrial silica cycling., Proc. R. Soc. B, 280:20132083, doi:10.1098/rspb.2013.2083, 2013.

Vandevenne, F. I., Barão, L., Ronchi, B., Govers, G., Meire, P., Kelly, E. F. and Struyf, E.: Silicon pools in human impacted soils of temperate zones, Global Biogeochem. Cycles, 29(9), 1439–1450, doi:10.1002/2014GB005049, 2015a.

Vandevenne, F. I., Delvaux, C., Hughes, H. J., André, L., Ronchi, B., Clymans, W., Barão, L., Cornelis, J.-T., Govers, G., Meire, P. and Struyf, E.: Landscape cultivation alters δ30Si signature in terrestrial ecosystems, Sci. Rep., 5, 7732, doi:10.1038/srep07732, 2015b.

Vandevenne, F. and Struyf, E.: The silicon footprint of urban ecosystems, Elementa, In prep, 2018.

Vandevenne, F., Struyf, E., Clymans, W. and Meire, P.: Agricultural silica harvest: have humans created a new loop in the global silica cycle?, Front. Ecol. Environ., 10(5), 243–248, doi:10.1890/110046, 2012.

Verschuren, D., Edgington, D. N., Kling, H. J. and Johnson, T. C.: Silica depletion in Lake Victoria: Sedimentary signals at offshore stations., J. Great Lakes Res., 24(1), 118–130, doi:10.1016/S0380-1330(98)70804-4, 1998.

Verschuren, D., Johnson, T. C., Kling, H. J., Edgington, D. N., Leavitt, P. R., Brown, E. T., Talbot, M. R. and Hecky, R. E.: History and timing of human impact on Lake Victoria, Proc. Biol. Sci., 269(1488), 289–294, doi:10.1098/rspb.2001.1850, 2002.

Wang, C., Zhu, H., Wang, P., Hou, J., Ao, Y. and Fan, X.: Early diagenetic alterations of biogenic and reactive silica in the surface sediment of the Yangtze Estuary, Cont. Shelf Res., 99, 1–11, doi:10.1016/j.csr.2015.03.003, 2015.

Watteau, F. and Villemin, G.: Ultrastructural study of the biogeochemical cycle of silicon in the soil and litter of a temperate forest, Eur. J. Soil Sci., 52(September 1999), 385–396, doi:10.1046/j.1365-2389.2001.00391.x, 2001.

Wedepohl, K. H.: The composition of the continental crust, Geochim. Cosmochim. Acta,

59(7), 1217–1232, doi:10.1016/0016-7037(95)00038-2, 1995.

Weeks, M. E.: The discovery of the elements. XII. Other elements isolated with the aid of potassium and sodium: Beryllium, boron, silicon, and aluminum, J. Chem. Educ., 9(8), 1386, doi:10.1021/ed009p1386, 1932.

Wei, X., Shao, M., Gale, W. and Li, L.: Global pattern of soil carbon losses due to the conversion of forests to agricultural land, Sci. Rep., 1, 6–11, doi:10.1038/srep04062, 2014.

Van der Werf, A.: A new method of concentrating and cleaning diatoms and other organisms, Proc. Int. Assoc. Theor. Appl. Limnol., 12, 276–277, doi:10.1080/03680770.1950.11895297, 1955.

White, A. F., Vivit, D. V., Schulz, M. S., Bullen, T. D., Evett, R. R. and Aagarwal, J.: Biogenic and pedogenic controls on Si distributions and cycling in grasslands of the Santa Cruz soil chronosequence, California, Geochim. Cosmochim. Acta, 94, 72–94, doi:10.1016/j.gca.2012.06.009, 2012.

Wollast, R. and Mackenzie, F. T.: The global cycle of Silica, in Silicon geochemistry and biochemistry, edited by S. R. Aston, pp. 39–76, Academic Press, London., 1984.

Xiao, X., Chen, B. and Zhu, L.: Transformation, morphology, and dissolution of silicon and carbon in rice straw-derived biochars under different pyrolytic temperatures., Environ. Sci. Technol., 48(6), 3411–9, doi:10.1021/es405676h, 2014.

Yool, A. and Tyrrell, T.: Role of diatoms in regulating the ocean's silicon cycle, Global Biogeochem. Cycles, 17(4), n/a-n/a, doi:10.1029/2002GB002018, 2003.

Zhao, Z. and Pearsall, D. M.: Experiments for improving phytolith extraction from soils, J. Archaeol. Scien, 25, 587–598, doi:10.1006/jasc.1997.0262, 1998.

Zhu, H., Wang, C., Wang, P., Hou, J., Qian, J. and Ao, Y.: Speciation of potentially mobile Si in Yangtze Estuary surface sediments: estimates using a modified sequential extraction technique, Environ. Sci. Pollut. Res., 23, 18928–18941, doi:10.1007/s11356-016-6944-2, 2016.

Ziegler, K., Chadwick, O. a., Brzezinski, M. a. and Kelly, E. F.: Natural variations of δ30Si ratios during progressive basalt weathering, Hawaiian Islands, Geochim. Cosmochim. Acta, 69(19), 4597–4610, doi:10.1016/j.gca.2005.05.008, 2005a.

Ziegler, K., Chadwick, O. A., White, A. F. and Brzezinski, M. A.: δ30Si systematics in a granitic saprolite, Puerto Rico., Geology, 33(10), 817–820, doi:10.1130/G21707.1, 2005b.

Zisadza, P., Gandiwa, E., Westhuizen, H., van der Westhuizen, E. and Bodzo, V.: Abundance, distribution and population trends of Hippopotamus in Gonarezhou National Park, Zimbabwe, South African J. Wildl. Res., 40(2), 149–157, doi:10.3957/056.040.0206, 2010.

Supplementary material

Chapter 3

Table S3.1. Results from the continuous extraction. From left to right: Pit codes (**Figure 3.2**) and depth, AlkExSi fractions obtained ordered by Si/Al ratio (Si/Al > 5 and Si/Al < 5). The amount of AlkExSi (AlkExSi, mg g^{-1} of sample), the reactivity (k, min^{-1}) and the Si/Al ratio (Si/Al) are shown for biogenic and non-biogenic fractions (see Eq. (1)). Missing values indicate the absence of additional fractions according to the curve model.

Code	Depth	AlkExSi1	k1	Si/Al 1	AlkExSi2	k2	Si/Al2
FGTR3	0 - 10	27.78	0.11	88.09			
	10 - 20	28.45	0.14	54.54			
	20 - 30	12.95	0.22	19.05			
	30 - 40	18.59	0.19	7.96			
	40 - 50				9.09	0.35	1.30
	55 - 65	31.34	0.14	26.28			
	75 - 85	20.75	0.21	28.55	0.25	0.31	0.01
FGUMR1	75 -85	32.11	0.17	92.99			
FGUMR2	0 - 10	18.32	0.11	139.96			
	10 - 20				17.77	0.15	2.32
	20 - 30				11.38	0.22	1.36
	30 - 40				10.78	0.35	0.67
	40 - 50				12.20	0.36	0.62
	55 - 65				17.54	0.30	0.67
	75 - 85				22.72	0.26	0.88
	95 - 105	14.69	0.11	15.49	12.17	0.31	0.41
	130 - 140	20.65	0.24	8.49	1.03	0.30	0.05
	180 - 190				9.47	0.41	0.67
FGLMR2	0 - 10	15.00	0.10	12.38	1.09	0.16	0.11
	10 - 20	6.81	0.27	108.60			
	20 - 30				9.24	0.17	0.99
					0.80	0.57	0.22
	30 - 40				7.05	0.30	0.59
	40 - 50	11.53	0.25	12.15			
	55 - 65	13.78	0.23	381.88			
	75 - 85				33.89	0.07	1.24
					13.93	0.32	0.57
	95 - 105	17.09	0.22	140.85			
	130 - 140				13.49	0.29	0.68
FGLMR3	00 -10	14.51	0.22	1528.41			
	20 -30				8.10	0.25	2.40
	55 - 65	20.72	0.11	10.03	9.06	0.35	0.45
	95 - 105				12.88	0.29	0.61

FGBR1	0 - 10	17.26	0.09	39.92			
	10 - 20	11.78	0.15	100.60			
	20 - 30	4.67	0.38	43.06	0.16	0.52	0.02
	30 - 40	9.25	0.26	281.92			
	40 - 50				8.66	0.39	0.55
	55 - 65				12.83	0.25	0.48
	75 - 85				13.14	0.36	0.60
	95 - 105	10.36	0.25	18.21			
FGBR2	155				3.46	0.54	0.54
FGBR3	00 - 20				14.88	0.16	2.06
	20 - 30				11.13	0.11	4.34
					1.30	0.64	0.31
	55 - 65	8.57	0.23	11.79	0.45	0.34	0.04
	75 - 85	19.69	0.18	20.49	0.29	0.35	0.02
	130 - 140				14.59	0.18	0.94
FSTR2	0 - 10				35.75	0.16	1.03
	10 - 20	47.62	0.12	46.31			
	20 - 30				45.40	0.13	4.33
	30 - 40				43.14	0.13	2.53
	40 - 50				26.06	0.18	3.76
					11.45	0.12	0.40
	55 - 65				44.25	0.13	1.07
	75 - 85	25.29	0.21	20.11			
	95 - 105				56.02	0.15	2.96
FSUMR1	00 - 10	18.08	0.13	6.93			
	20 - 30				24.61	0.15	2.43
FSUMR2	0 - 10	30.06	0.13	43.93			
	10 - 20	30.07	0.14	120.87			
	20 - 30				10.65	0.27	1.49
	30 - 40				17.40	0.13	1.96
					6.25	0.47	0.38
FSLMR2	0 - 10	16.37	0.13	536.57			
	10 - 20				4.32	0.32	1.08
	20 - 30				9.21	0.19	1.15
	30 - 40				4.76	0.43	0.58
	40 - 50				6.47	0.58	0.58
	55 - 65				10.92	0.40	0.46
					9.01	0.12	0.46
	75 - 85				11.71	0.50	0.45
	95 - 105	6.88	0.10	28.34	16.63	0.40	0.48
	130 - 140	35.13	0.18	14.03			
	180 - 190				20.98	0.30	0.64
FSLMR3	00 - 10	18.58	0.16	89.46			

	20 - 30	11.65	0.25	53.74			
	55 - 65				15.62	0.26	3.57
	75 - 85				16.92	0.36	0.66
	95 - 105	29.07	0.23	52.20			
	180 - 190				17.86	0.44	0.74
FSBR2	0 - 10	19.57	0.15	23.97			
	10 - 20	13.43	0.13	76.64			
	20 - 30	14.35	0.14	35.86			
	30 - 40	5.46	0.30	96.05			
	40 - 50	7.26	0.12	20.19	4.71	0.46	0.44
	55 - 65	17.83	0.09	57.64	6.22	0.54	0.42
	75 - 85	3.38	0.68	265.09			
		18.33	0.14	5.11			
	95 - 105	14.84	0.18	16.90	8.64	0.10	0.31
					2.58	0.60	0.20
	130 - 140	3.05	0.79	388.21	12.61	0.23	0.52
	180 - 190				13.04	0.31	0.75
CGTR1	0 - 10				0.29	1.16	0.15
	10 - 20	19.15	0.11	12.08			
	20 - 30				28.23	0.11	1.38
					2.12	0.54	0.68
	30 - 40	27.74	0.14	8.93			
	40 - 50	45.69	0.10	6.37	2.30	0.24	0.13
	55 - 65	41.00	0.15	5.36	0.37	0.25	0.02
	75 - 85				2.66	0.38	0.32
	95 - 105				22.35	0.23	0.78
	130 - 140	20.33	0.19	5.75	0.35	0.23	0.01
CGTR2	0 - 10						
	20 - 30				22.52	0.11	2.98
	55 - 65	65.56	0.09	14.87			
	95 - 105				25.63	0.17	0.97
	130 - 140	24.50	0.08	7.56	12.05	0.33	0.50
	180 - 190				21.59	0.24	0.72
CGMR1	0 - 10	11.86	0.08	5.04			
	20 - 30	19.40	0.12	15.14			
	40 - 50				18.04	0.20	0.71
	75 - 85				36.62	0.12	1.03
	95 - 105				34.00	0.11	2.35
					3.77	0.60	0.40
CGMR3	0 - 10	0.61	237.60	5.10			
	10 - 20	0.84	0.24	106.43			
	20 - 30				0.45	1.57	0.15
	30 - 40				3.17	0.35	0.36

	40 - 50				36.04	0.10	0.98
	55 - 65				10.38	0.27	0.56
CGBR2	0 - 10						
	20 - 30				23.03	0.12	1.50
	40 - 50				29.48	0.16	1.03
	95 - 105				72.96	0.11	1.51
CGBR3	0 - 10						
	10 - 20				15.51	0.10	1.35
					2.24	0.70	0.83
	20 - 30				5.60	0.27	0.52
	30 - 40				9.65	0.26	0.85
	40 - 50				7.87	0.26	0.59
	55 - 65				25.94	0.13	4.27
					0.46	0.17	0.02
	75 - 85	21.03	0.16	64.19			
	95 - 105				24.13	0.22	0.86
CSTR1	0 - 10	5.40	0.16	21.78	0.38	0.89	0.15
	10 - 20				2.06	0.45	0.65
CSTR3	0 - 10	9.15	0.09	186.97			
	10 - 20	10.17	0.08	128.40			
	20 - 30						
	30 - 40				1.42	0.41	0.37
	40 - 50	5.50	0.37	5.94			
	55 - 65				12.71	0.42	0.55
	75 - 85	10.76	0.41	9.60			
	95 - 105	9.87	0.17	239.81	3.95	0.77	0.97
CSMR1	0 - 10				3.51	0.26	4.66
					0.57	0.69	0.24
	10 - 20				3.25	0.25	2.46
	20 - 30	3.58	0.20	12.35			
CSMR2	0 - 10				2.15	0.35	0.86
	40 - 50				12.02	0.38	0.57
CSBR3	0 - 10	9.32	0.13	29.94	2.69	0.53	0.34
	10 - 20	5.63	0.27	12.79			
	20 - 30	8.19	0.22	42.84	0.94	0.65	0.12
	30 - 40	6.09	0.29	41.51			
	40 - 50	14.29	0.10	13.41	1.93	0.72	0.42
	55 - 65	16.91	0.32	13.16			
	75 - 85	17.89	0.34	30.91	0.42	0.39	0.02
	95 - 105	14.18	0.36	17.11			

Table S3.2. Bulk density (g cm^{-3}) and TRB values ($cmol_c$ kg^{-1}) of depths from selected pits. [!]Missing bulk densities. The value assigned is the bulk density average of that slope.

CODE	BD	TRB	CODE	BD	TRB	CODE	BD	TRB
FGT_0010	1.16	55	FST_2030	0.90	28	CGT_7585	1.36	30
FGT_1020	1.00	46	FST_3040	1.02	28	CGT_95105	1.42	28
FGT_2030	0.96	42	FST_4050	0.90	28	CGT_130140	1.44	27
FGT_3040	1.25	42	FST_5565	0.93	28	CGM_0010	1.44	50
FGT_4050	1.15	39	FST_7585	0.99	30	CGM_1020	1.48	29
FGT_5565	0.92	45	FST_95105	1.01	29	CGM_2030	1.39	28
FGT_7585	0.92	55	FSUM_0010	1.16[!]	88	CGM_3040	1.43	36
FGUM_0010	0.89	53	FSUM_1020	1.16[!]	92	CGM_4050	1.39	40
FGUM_1020	1.06	44	FSUM_2030	1.16[!]	88	CGM_5565	1.35	38
FGUM_2030	1.21	44	FSUM_3040	1.16[!]	93	CGBR3_0010	1.23	59
FGUM_3040	1.25	45	FSLM_0010	1.05	59	CGB_1020	1.25	42
FGUM_4050	1.22	47	FSLM_1020	1.14	55	CGB_2030	1.25	33
FGUM_5565	1.03	47	FSLM_2030	1.27	55	CGB_3040	1.28[!]	38
FGUM_7585	1.20	44	FSLM_3040	1.28	54	CGB_4050	1.28[!]	42
FGUM_95105	1.37	42	FSLM_4050	1.23	56	CGB_5565	1.28[!]	44
FGUM_130140	1.38	44	FSLM_5565	1.16	57	CGB_7585	1.28[!]	36
FGUM_180190	1.45	68	FSLM_7585	1.33	57	CGB_95105	1.28[!]	34
FGLM_0010	0.72	61	FSLM_95105	1.37	57	CST_0010	1.27	151
FGLM_1020	1.07	44	FSLM_130140	1.46	49	CST_1020	1.24	122
FGLM_2030	1.19	44	FSLM_180190	1.38	51	CST_2030	1.27	112
FGLM_3040	1.32	44	FSB_0010	1.04	44	CST_3040	1.22	84
FGLM_4050	1.07	45	FSB_1020	1.12	41	CST_4050	1.09	87
FGLM_5565	1.19	50	FSB_2030	1.10	40	CST_5565	1.03	90
FGLM_7585	1.25	52	FSB_3040	1.36	39	CST_7585	1.22	88
FGLM_95105	1.39	52	FSB_4050	1.34	43	CST_95105	1.19	100
FGLM_130140	1.53	53	FSB_5565	1.33	50	CSM_0010	1.33	133
FGB_0010	0.92	42	FSB_7585	1.37	51	CSM_1020	1.20[!]	132
FGB_1020	1.18	39	FSB_95105	1.38	53	CSM_2030	1.20[!]	130
FGB_2030	1.25	37	FSB_130140	1.45	46	CSB_0010	1.06	88
FGB_3040	1.30	40	FSB_180190	1.54	48	CSB_1020	1.32	84
FGB_4050	1.38	42	CGT_0010	1.48	43	CSB_2030	1.32	80
FGB_5565	1.18	44	CGT_1020	1.43	34	CSB_3040	1.31	76
FGB_7585	1.31	45	CGT_2030	1.49	25	CSB_4050	1.21	73
FGB_95105	1.29	45	CGT_3040	1.32	25	CSB_5565	1.06	76
FST_0010	0.72	37	CGT_4050	1.33	31	CSB_7585	1.18	76
FST_1020	0.86	30	CGT_5565	1.24	32	CSB_95105	1.26	76

Table S3.3. Total element content averages and standard deviation in brackets (g kg^{-1}) for the different positions along the slopes.

			Al	Fe	Si	Ti	Ba	Ca	K	Mg	Mn	Na	P	Sr	Zr
Forest (F)	Gentle (G)	Top (T) FGT	73 (16)	47 (3)	314 (21)	6.3 (0.6)	0.2 (1.0E-02)	0.9 (0.6)	5 (0.4)	3.0 (0.5)	0.5 (0.1)	1.2 (0.2)	0.4 (3.6E-02)	1.7E-02 (5.1E-03)	0.4 (2.6E-02)
		Upper Middle (UM) FGUM	80 (19)	58 (6)	301 (23)	7.1 (0.4)	0.2 (6.2E-02)	0.7 (0.5)	6 (1.3)	2.6 (0.5)	0.7 (0.2)	1.6 (0.6)	0.5 (8.8E-02)	2.0E-02 (5.5E-03)	0.4 (3.1E-02)
		Lower Middle (LM) FGLM	69 (22)	47 (7)	322 (29)	6.5 (0.7)	0.3 (2.6E-02)	0.7 (1.0)	7 (0.5)	2.5 (0.8)	0.8 (0.2)	1.7 (0.3)	0.5 (5.5E-02)	2.3E-02 (7.0E-03)	0.5 (4.9E-02)
		Bottom (B) FGB	72 (18)	49 (5)	318 (22)	6.7 (0.4)	0.2 (1.8E-02)	0.9 (0.3)	4 (0.1)	2.8 (0.5)	0.8 (0.3)	0.8 (0.1)	0.5 (5.2E-02)	2.1E-02 (2.6E-03)	0.5 (4.5E-02)
	Steep (S)	Top (T) FST	93 (12)	51 (3)	286 (10)	6.6 (0.3)	0.2 (8.2E-02)	0.4 (0.1)	3 (0.2)	2.3 (0.1)	0.3 (0.1)	0.4 (0.4)	0.5 (8.8E-02)	1.1E-02 (1.2E-03)	0.4 (2.8E-02)
		Upper Middle (UM) FSUM	60 (5)	47 (2)	302 (11)	6.3 (0.2)	0.3 (1.1E-02)	2.0 (0.7)	16 (1.3)	2.2 (0.1)	1.5 (0.2)	5.1 (0.5)	0.6 (9.4E-02)	3.8E-02 (4.6E-03)	0.4 (2.8E-02)
		Lower Middle (LM) FSLM	76 (23)	56 (4)	306 (28)	7.5 (0.9)	0.3 (1.9E-02)	1.0 (0.6)	8 (0.8)	2.4 (0.7)	0.8 (0.3)	2.2 (0.6)	0.4 (1.0E-01)	2.3E-02 (4.7E-03)	0.5 (4.1E-02)
		Bottom (B) FSB	66 (22)	56 (10)	321 (31)	8.2 (0.7)	0.2 (1.8E-02)	1.0 (0.2)	6 (0.5)	2.4 (0.7)	0.9 (0.3)	1.5 (0.3)	0.4 (6.0E-02)	2.3E-02 (2.6E-03)	0.5 (4.2E-02)
Cropland (C)	Gentle (G)	Top (T) CGT	90 (23)	64 (3)	287 (25)	8.5 (0.4)	0.1 (4.4E-02)	0.7 (0.5)	2 (0.6)	2.3 (0.3)	0.7 (0.2)	0.5 (0.2)	0.5 (2.1E-01)	1.9E-02 (5.2E-03)	0.5 (1.3E-02)
		Upper Middle (UM) CGM	82 (27)	65 (5)	295 (33)	8.2 (0.3)	0.1 (3.3E-02)	1.3 (0.8)	2 (0.2)	2.7 (0.6)	1.1 (0.5)	0.4 (0.2)	0.5 (1.2E-01)	1.7E-02 (2.7E-03)	0.5 (1.5E-02)
		Bottom (B) CGB	94 (23)	63 (6)	278 (26)	8.8 (0.5)	0.2 (6.9E-02)	1.3 (0.8)	2 (0.4)	3.2 (0.5)	1.1 (0.8)	0.4 (0.2)	0.5 (2.4E-01)	1.7E-02 (6.2E-03)	0.6 (4.3E-02)
	Steep (S)	Top (T) CST	70 (17)	49 (3)	316 (19)	6.2 (0.8)	0.4 (6.9E-02)	2.3 (1.4)	18 (3.6)	3.8 (1.1)	0.8 (0.3)	3.6 (0.8)	0.4 (2.3E-01)	3.2E-02 (7.7E-03)	0.4 (3.5E-02)
		Upper Middle (UM) CSM	65 (2)	44 (1)	321 (2)	5.5 (0.1)	0.5 (1.7E-02)	2.6 (0.1)	26 (1.2)	3.2 (0.3)	0.8 (0.1)	5.9 (0.3)	0.5 (7.9E-02)	4.6E-02 (1.3E-03)	0.4 (1.0E-02)
		Bottom (B) CSB	69 (21)	54 (1)	315 (22)	7.3 (1.2)	0.3 (3.7E-02)	1.2 (0.4)	14 (2.2)	3.0 (0.9)	1.0 (0.4)	2.8 (0.6)	0.6 (3.3E-01)	2.1E-02 (3.8E-03)	0.5 (3.3E-02)

Table S3.4. Granulometry (Average % (SD) of total texture) and mineralogy content (% of total minerals) for the different positions along the slope. For the mineralogy analysis only samples at 20-30 and 55-65 depths were analyzed. [!]Sample CGB_5565 was not analyzed due to the scarce of sample remaining. In the case of FG slope, instead of the bottom position, upper middle position was selected in order to avoid repeatability with the bottom of FS. Matrix consists on a mixture of sanidine, goethite, hematite, gibbsite, smectite, vermiculite and illite. *Values below 5% might not be reliable due to the limitations of the quantifying method.

			Granulometry			Mineralogy*				
			% sand	% silt	% clay	% quartz	% cristobalite	% halloysite	% kaolinite	% matrix
Forest (F)	Gentle (G)	Top (T) - FGT	14 (5)	70 (3)	15 (4)	55	0 - 3	18 - 25	14 - 16	4 - 10
		Upper Middle (UM) - FGUM	15 (8)	67 (5)	18 (4)	51 - 66	0 – 5	12 - 17	11 - 27	5 - 6
		Lower Middle (LM) - FGLM	14 (4)	69 (3)	17 (2)					
		Bottom (B) - FGB	9 (2)	73 (4)	18 (4)					
	Steep (S)	Top (T) - FST	13 (4)	70 (3)	16 (1)	54 - 66	1 – 3	15 - 26	13	4 – 5
		Upper Middle (UM) - FSUM	22 (1)	68 (1)	10 (1)					
		Lower Middle (LM) - FSLM	15 (2)	67 (3)	18 (2)					
		Bottom (B) - FSB	9 (5)	73 (4)	18 (2)	63 - 79	0	7 - 16	0 - 15	6 - 14
Cropland (C)	Gentle (G)	Top (T) - CGT	18 (4)	64 (6)	18 (6)	38 - 60	5 – 6	19 - 20	8 - 19	9 - 17
		Upper Middle (UM) - CGM	16 (5)	60 (3)	25 (4)					
		Bottom (B) - CGB	18 (8)	57 (4)	25 (5)	58[!]	8[!]	10[!]	11[!]	13[!]
	Steep (S)	Top (T) - CST	21 (6)	61 (6)	17 (2)	45 - 61	2	4 – 8	14 - 19	19 - 27
		Upper Middle (UM) - CSM	43 (7)	45 (5)	13 (2)					
		Bottom (B) - CSB	19 (3)	62 (2)	19 (2)	52 - 61	1	4 – 5	7 - 18	24 - 27

Table S3.5. Biogenic and non-biogenic AlkExSi pools (kg Si m^{-2}). [!]pools interpolated

Position	Depth	Biogenic	Non-biogenic
FGT	0 - 10	3.23	0.00
	10 - 20	2.84	0.00
	20 - 30	1.24	0.00
	30 - 40	2.33	0.00
	40 - 50	0.00	1.05
	50 - 55[!]	0.81	0.24
	55 - 65	2.88	0.00
	65 - 75[!]	2.39	0.01
	75 - 85	1.90	0.02
FGUM	0 - 10	1.63	0.00
	10 - 20	0.00	1.89
	20 - 30	0.00	1.37
	30 - 40	0.00	1.35
	40 - 50	0.00	1.48
	50 - 55[!]	0.00	0.84
	55 - 65	0.00	1.81
	65 - 75[!]	0.00	0.00
	75 - 85	0.00	2.72
	85 - 95[!]	0.94	2.24
	95 - 105	2.01	1.67
	105 - 115[!]	2.25	1.23
	115 - 125[!]	2.49	0.80
	125 - 130[!]	1.34	0.24
	130 - 140	2.86	0.14
	140 - 150[!]	2.31	0.38
	150 - 160[!]	1.75	0.62
	160 - 170[!]	1.17	0.87
	170 - 180[!]	0.59	1.12
	180 - 190	0.00	1.37
FGLM	0 - 10	1.08	0.01
	10 - 20	0.73	0.00
	20 - 30	0.00	1.19
	30 - 40	0.00	0.93
	40 - 50	1.23	0.00
	50 - 55[!]	0.71	0.00
	55 - 65	1.64	0.00
FSLM	130 - 140	5.14	0.00
	140 - 150[!]	4.07	0.61
	150 - 160[!]	3.02	1.20
	160 - 170[!]	1.99	1.78
	170 - 180[!]	0.98	2.35
	180 - 190	0.00	2.90
FSB	0 - 10	2.04	0.00
	10 - 20	1.51	0.00
	20 - 30	1.57	0.00
	30 - 40	0.74	0.00
	40 - 50	0.97	0.63
	50 - 55[!]	0.84	0.36
	55 - 65	2.38	0.83
	65 - 75[!]	2.67	0.42
	75 - 85	2.98	0.00
	85 - 95[!]	2.51	0.77
	95 - 105	2.05	1.55
	105 - 115[!]	1.61	1.63
	115 - 125[!]	1.15	1.71
	125 - 130[!]	0.40	0.88
	130 - 140	0.44	1.83
	140 - 150[!]	0.36	1.86
	150 - 160[!]	0.27	1.90
	160 - 170[!]	0.18	1.94
	170 - 180[!]	0.09	1.97
	180 - 190	0.00	2.01
CGT	0 - 10	0.00	0.04
	10 - 20	2.74	0.02
	20 - 30	0.00	4.53
	30 - 40	3.66	0.00
	40 - 50	6.06	0.31
	50 - 55[!]	2.78	0.09
	55 - 65	5.09	0.05
	65 - 75[!]	2.67	0.20
	75 - 85	0.00	0.36
	85 - 95[!]	0.00	1.74

	65 - 75!	0.84	0.85
	75 - 85	0.00	1.74
	85 - 95!	1.13	0.92
	95 - 105	2.38	0.00
	105 - 115!	1.75	0.55
	115 - 125!	1.08	1.13
	125 - 130!	0.27	0.79
	130 - 140	0.00	2.06
FGB	0 - 10	1.60	0.00
	10 - 20	1.39	0.00
	20 - 30	0.58	0.02
	30 - 40	1.20	0.00
	40 - 50	0.00	1.20
	50 - 55!	0.00	0.69
	55 - 65	0.00	1.52
	65 - 75!	0.00	1.62
	75 - 85	0.00	1.73
	85 - 95!	0.67	0.86
	95 - 105	1.34	0.00
FST	0 - 10	0.00	2.57
	10 - 20	4.08	0.00
	20 - 30	0.00	4.10
	30 - 40	0.00	4.42
	40 - 50	0.00	3.36
	50 - 55!	0.00	1.87
	55 - 65	0.00	4.12
	65 - 75!	1.21	2.13
	75 - 85	2.50	0.00
	85 - 95!	1.27	2.80
	95 - 105	0.00	5.67
FSUM	0 - 10	3.49	0.00
	10 - 20	3.49	0.00
	20 - 30	0.00	1.24
	30 - 40	0.00	2.74
FSLM	0 - 10	1.72	0.00
	10 - 20	0.00	0.49
	20 - 30	0.00	1.17
	30 - 40	0.00	0.61
	95 - 105	0.00	3.18
	105 - 115!	0.83	2.29
	115 - 125!	1.66	1.40
	125 - 130!	2.29	0.73
	130 - 140	2.92	0.05
CGUM	0 - 10	0.09	0.00
	10 - 20	0.12	0.00
	20 - 30	0.00	0.06
	30 - 40	0.00	0.45
	40 - 50	0.00	4.99
	50 - 55!	0.00	1.59
	55 - 65	0.00	1.41
CGB	0 - 10	0.00	0.00
	10 - 20	0.00	2.22
	20 - 30	0.00	0.70
	30 - 40	0.00	1.24
	40 - 50	0.00	1.01
	50 - 55!	0.00	1.10
	55 - 65	0.00	3.38
	65 - 75!	1.35	1.70
	75 - 85	2.69	0.02
	85 - 95!	1.35	1.56
	95 - 105	0.00	3.09
CST	0 - 10	1.16	0.00
	10 - 20	1.26	0.00
	20 - 30	0.00	0.00
	30 - 40	0.00	0.17
	40 - 50	0.60	0.00
	50 - 55!	0.15	0.34
	55 - 65	0.00	1.31
	65 - 75!	0.61	0.72
	75 - 85	1.31	0.00
	85 - 95!	1.24	0.24
	95 - 105	1.18	0.47
CSM	0 - 10	0.00	0.54
	10 - 20	0.00	0.39
	20 - 30	0.43	0.00
CSB	0 - 10	0.99	0.28

	40 - 50	0.00	0.80	10 - 20	0.74	0.00
	50 - 55!	0.00	0.79	20 - 30	1.08	0.12
	55 - 65	0.00	2.31	30 - 40	0.80	0.00
	65 - 75!	0.00	1.97	40 - 50	1.72	0.23
	75 - 85	0.00	1.56	50 - 55!	0.89	0.05
	85 - 95!	0.47	1.92	55 - 65	1.80	0.00
	95 - 105	0.94	2.28	65 - 75!	1.95	0.02
	105 - 115!	2.09	1.66	75 - 85	2.11	0.05
	115 - 125!	3.28	1.01	85 - 95!	1.95	0.03
	125 - 130!	2.10	0.26	95 - 105	1.79	0.00

Chapter 5

Hippos (*Hippopotamus amphibius*): the animal silica pump

Schoelynck, J., Subalusky, A. L., Struyf, E., Dutton, C. L., Unzué-Belmonte, D., Van de Vijver, B., Post, D. M., Rosi, E. J., Meire, P. and Frings, P., 2017. *In prep*.

1. Introduction to the silica cycle

Animals play an important role in the distribution of resources across landscapes, because of their capacity to ingest large quantities of food in a different location to that in which they egest, excrete, or die (Bauer and Hoye, 2014; Doughty et al., 2016). This resource translocation has important effects on carbon and nutrient cycling, ecosystem productivity and food web structure in both the source and recipient ecosystems (Bakker et al., 2016; Schmitz et al., 2014). Lateral phosphorous transport in the Amazon basin dropped by 98 % following late-Pleistocene megafauna extinctions (Doughty et al., 2013). Studies of animals predominantly focused on the biogeochemical cycles of major nutrients, but animals also move other elements that are essential to biological processes, such as Si. Although our understanding of the biogeochemical Si cycle, and the strong biotic control on global Si fluxes, has evolved dramatically over the past decades, we have yet to integrate the potential role of large fauna into this cycle.

The scientific understanding of the Si cycle has progressed from conceptualizing it as almost purely driven by geological processes, to a much more nuanced understanding that includes biological transformation and cycling. Mineral weathering is the ultimate source of all dissolved Si (DSi) in rivers and the oceans, but biota in terrestrial ecosystems typically control an important portion of continental Si fluxes (Struyf and Conley, 2012). Studies in various ecosystems demonstrate that vegetation increases the retention time of Si as it moves from the land towards the rivers and ultimately the ocean (see Schoelynck et al., (2013) for a review). Plants take up weathered Si from the soil and accumulate it in amorphous biogenic silica (BSi). When plants die and decompose, a large BSi stock is built up in ecosystem soils, and

its persistence, transformation into secondary Si-pools, and stability exerts a strong control on continental Si export (Struyf and Conley, 2012).

Quantifying Si export from land to water is crucial for understanding lake and coastal biogeochemistry (Carey and Fulweiler, 2012). Diatoms (Bacillariophyta) – that utilize biologically available silica from the water to form their frustrules – are predominant contributors to global carbon fixation, carrying out about 20 % of photosynthesis on Earth (Armbrust, 2009). Si limitation can put a strong constraint on their production (Martin-Jezequel et al., 2000). Multiple studies highlight how the East African Lakes depend on riverine Si input to maintain their high productivity, as diatoms dominate the base of the food web (e.g. Lake Victoria (Cockerton et al., 2015; Johnson et al., 1998), Lake Albert (Cockerton et al., 2015), Lake Malawi (Bootsma et al., 2003), Lake Tanganyika (Kilham, 1971). If riverine Si delivery to the lakes is reduced, this could induce algal community shifts with knock-on effects on the food web structure and human wellbeing in that region (Verschuren et al., 2002).

2. Maasai Mara hippo study

The common hippopotamus (*Hippopotamus amphibius* L. 1758, hereafter 'hippo') attracts attention when considering Si mobility in the East African Lakes area, due to its unique feeding patterns. Hippos are semi-aquatic and have a diel activity pattern: hippos feed in savannah grasslands at night, and typically rest communally in wallowed out river meanders during the day. Hippos contribute large amounts of C, N and P to aquatic systems through these grazing and movement patterns, by egesting 2.1 - 4.0 kg (dry mass) per day (Subalusky et al., 2015). The accompanying, yet unknown, transfer of Si (both in the form of fecal BSi, and DSi dissolved out of the faeces in suspension) could therefore bypass the cycling of Si in soils, where re-uptake of DSi by plants or precipitation of DSi as authigenic (alumino-)silicate phases greatly slows Si export (Struyf and Conley, 2012). This process is analogous to the loss of BSi from soils via crop harvest, inducing soil Si depletion (Vandevenne et al., 2012, 2015a). In contrast however to the large amounts

of harvested BSi from crops that are potentially lost to biological cycling on longer time scales and stored in the anthroposphere (Vandevenne et al., 2012), the BSi consumed by hippos is largely transported directly to the river and becomes readily available for downstream primary producers: a land-to-river Si pump driven by animals.

Hippo population density in the Maasai Mara National Reserve (MMNR) reaches 36 hippos per km river (Kenyan side), which is the largest population density of hippos on the African continent and represents 3 % of the global population (Kanga et al., 2011). We quantified dissolved and biogenic Si (solid phases) in river water, pore water, grass, hippo faeces, suspended matter, river sediment and savannah soil along a transect on the Mara River and its main tributaries in the dry season of 2014 (see map in **Figure 5.1** in supplementary online material (SOM)). BSi was analysed using a novel method that allows to separate BSi from other alkaline extractable Si phases, which is essential in a volcanically imprinted environment such as the MMNR (Clymans et al., (2015); see SOM for specific methodical details). The Si isotopic composition of a subset of BSi samples was determined by MC-ICP-MS after Si extraction and purification. Values are expressed in per mil as δ^{30}Si and an isotope mass-balance model was created (see SOM for specific methodical details). BSi particles were visually inspected via light microscopy to identify their origin. Finally, dissolution rates of various solid phases were determined in a series of batch dissolution experiments.

3. Fluxes and mass-balance of Si

At the time of sampling, daily fluxes of DSi and BSi through the Mara River were up to 2.4 t of BSi and 7.9 t DSi (**Figure 5.1**). Along the sampling gradient, BSi flux gradually increased. *In situ* diatom production can be excluded as a cause, as very few diatom frustules or chrysophyte stomatocysts (1 - 2 % of total BSi particle count) were found in suspended matter or in the sediment (**Figure 5.2** and **S5.6**), contrary to observations made in other African rivers (e.g. Congo River (Descy et al., 2017; Hughes et al., 2011)). BSi in the Mara River suspended matter and sediment samples

consisted almost entirely of phytoliths or phytolith remains, confirming its terrestrial origin (Cary et al., 2005). MMNR grass has high BSi concentrations (average 1.8 % of plant dry weight, **Table S5.1**), and BSi concentrations are further elevated in hippo faeces (average 4.1 % of faeces dry weight, **Table S5.1**). Increasing concentration in temperate domestic grazer faeces was related to the digestion of organic matter in the digestive tract, consequently increasing BSi concentrations (Vandevenne et al., 2013). The flux of grass BSi through the hippos towards the river is large: the daily loading directly into the river by excretion and egestion of the hippo population equals 8.6 - 16.4 t DM of faeces, which renders a flux of 0.4 - 0.7 t day^{-1} of BSi into the river (Subalusky et al., 2015).

This estimated direct BSi influx to the river through hippos (based on the estimate of 0.4 - 0.7 t hippo BSi egestions day^{-1}) accounts only for 40 - 70 % of the increase in BSi flux from the most upstream sample site to the most downstream site (**Figure S5.1**). The remaining 30 - 60 % is likely attributed to resuspension of bed material (Dutton et al., 2013), alternative inputs (e.g. dust) and indirect inputs (e.g. hippo faeces on the banks close to the river). This corroborates the high-resolution monitoring of a hippo pool over a 24-hour period: over a 250 m stretch with up to 80 hippos present, river BSi concentrations doubled relative to upstream values (**Figure S5.3**). This was solely attributed to fresh egestion by the animals, and stirring up of bed and bank material. A detailed balance (see below) shows that the direct BSi influx through hippos accounts for more than 80 % of the increase in total Si flux (BSi + DSi) from up- to downstream.

While DSi concentrations were identical above and below the hippo pool (**Figure S5.3**), the total DSi flux decreased by ca. 7 % towards the end of the sampling gradient (**Figure S5.1; Table S5.1**). This suggests there is a slight net retention of DSi within the Mara River. $\delta^{30}Si$ values of river DSi fluctuate, with a net increase of ca. 0.17 ‰ over the entire study reach (**Figure S5.4**). This behavior is not compatible with the small DSi removal required by the mass-balance: fractionations associated with e.g. biogenic uptake or authigenic clay formation resulting in a 7 % load reduction, are too small to

have such an impact. Additionally, there is a positive correlation between the flux of Si and $\delta^{30}Si$ of the DSi at individual sampling points, counter to that observed in other large river studies (Frings et al., 2016). This implies competing processes with counteracting isotopic impacts.

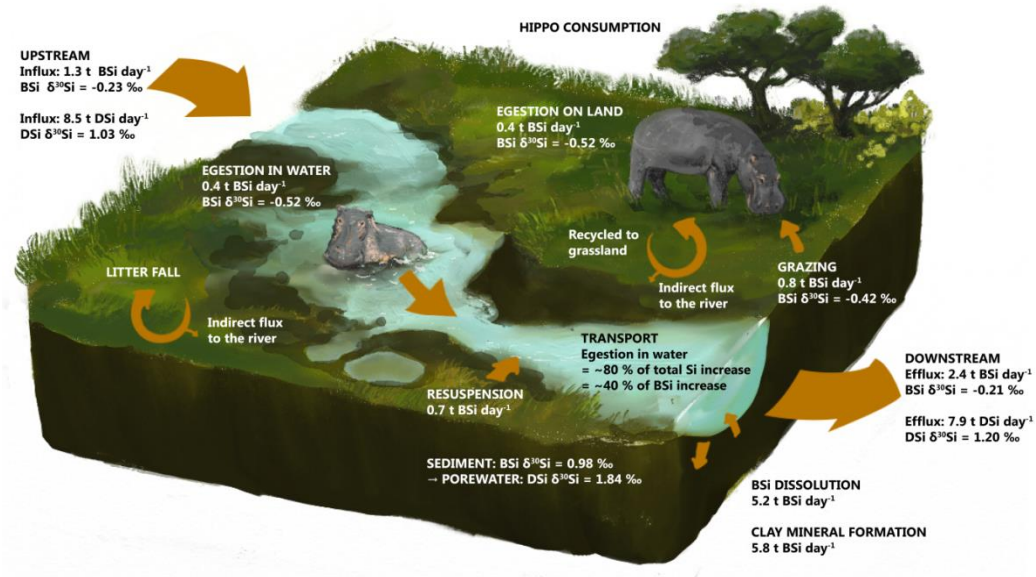

Figure S5.1. Conservative Si mass balance of the Mara River. Upstream influx and downstream efflux is calculated by multiplying DSi and BSi concentrations at site 1 and 10 (**Table S5.1**) with a 10-day averaged discharge at both locations, respectively. The lateral influx by hippo egestion is calculated by multiplying the average BSi concentration in faeces (**Table S5.1**) with the amount of faeces deposited (8.6 t DM day^{-1} (Subalusky et al., 2015)). Average BSi concentration in grass (**Table S5.1**) is multiplied with the amount of grass eaten (42.0 t DM day^{-1} (Subalusky et al., 2015)) to calculate the uptake of BSi by grazing. The difference between uptake and egestion in the water is the egestion on land. The difference between BSi flux upstream and downstream is the BSi that is added to the water in the MMNR. Hippos directly contribute at least ~40 % to this BSi, ~60 % comes indirectly from resuspension of old hippo faeces in the sediment. BSi dissolution and clay mineral formation are calculated using a Si isotope mass-balance model (see SOM). Total Si transport (DSi + BSi) increases with 0.5 kg Si from upstream to downstream, which is attributed over 80 % to daily hippo egestion in water.

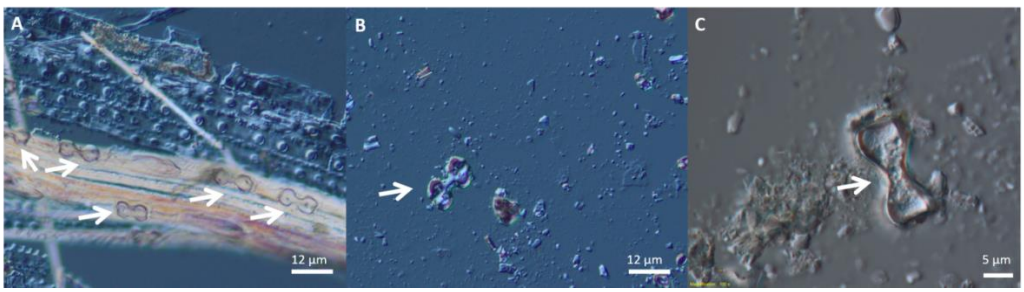

Figure S5.2. Dumbbell-shaped phytoliths (indicated with white arrow). These phytoliths were found in grass (A), hippo faeces (B) and suspended matter and sediment (C). Phytoliths account for 98 – 99 % of total biogenic silica particle counts in suspended matter and sediment samples (see also **Figure S5.6** for more different pictures).

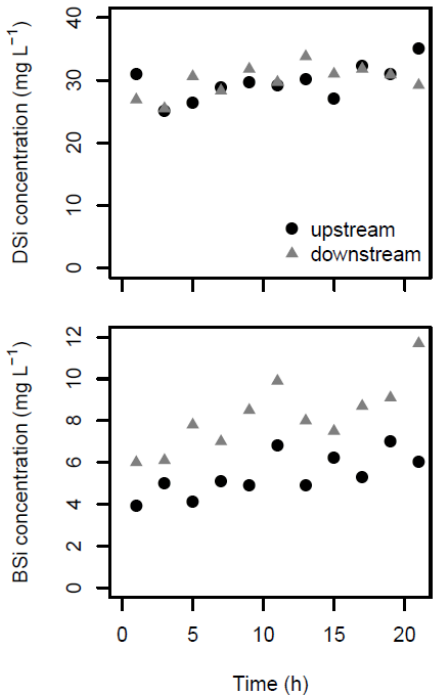

Figure S5.3. Change in DSi (A) and BSi (B) concentrations after river water has passed through a hippo pool. Duration = 24 hours, length of reach = 250 m, up to 80 hippos were present.

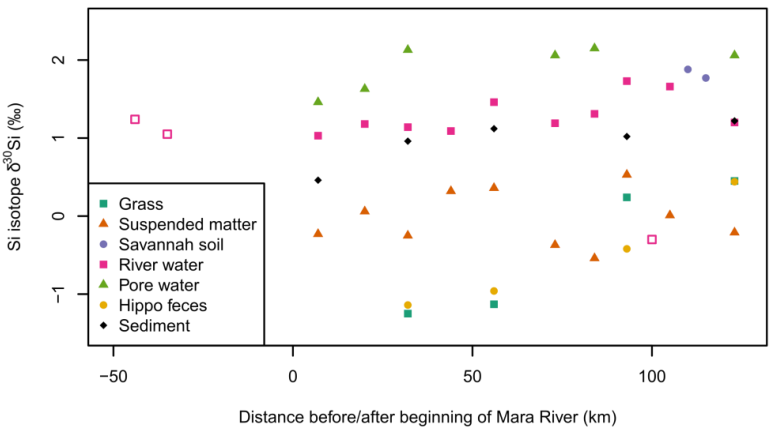

Figure S5.4. δ^{30}Si values (in ‰ relative to NBS28) of different ecosystem compartments. Closed symbols are from in and around the Mara River, open symbols are from the main tributaries. Each compartment of the terrestrial-aquatic Si-supply chain had a relatively narrow range of δ^{30}Si values. Mean values (±1σ) in grass (-0.42 ± 0.89 ‰), hippo faeces (-0.52 ± 0.71 ‰) and suspended matter (-

0.04 ± 0.35 ‰) are in close agreement with each other, although suspended matter is somewhat higher. δ^{30}Si values in sediment (0.93 ± 0.43 ‰), river water DSi (1.30 ± 0.24 ‰), savannah soil (1.83 ± 0.08) and pore water DSi (1.84 ± 0.33 ‰) are higher, with savannah soil and pore water clearly distinct from river water and sediment.

To quantify Si processing in more detail in the MMNR, a simple mass-balance of the system was used, constrained by the isotopic signatures (see details in SOM). Together with a Monte Carlo approach to propagate the uncertainties, this analysis suggests that two processes acting in unison can explain the observations: one removes Si from solution, while the second adds Si at approximately the same rate. Schematically, we refer to these processes as 'clay mineral formation' and 'BSi dissolution', respectively (**Figure S5.1**), though we recognize a suite of other processes could be contributing. The mass balance predicts that cumulatively, over the course of the entire study reach, ca. 5.2 t Si day^{-1} is solubilised from phytoliths in the channel or riparian zone, whereas 5.8 t Si day^{-1} is precipitated into secondary clays. This 0.6 t of Si difference is lost from the system as clay minerals; entrainment of secondary clays into the river suspended load probably does not alter their stability against dissolution. This magnitude is similar to the amount of presumed resuspension (see above). The balance in internal processes explains (i) why direct hippo inputs account for more than 80 % of the increase in total Si flux from up- to downstream, and also provides a novel and internally consistent explanation for (ii) the high δ^{30}Si, high [Si] in porewaters and (iii) the positive co-variation between DSi flux and δ^{30}Si of the DSi.

This Si cycling balance requires the assumption of an 'infinitely' large sediment BSi stock from which (i) BSi may resuspend and (ii) phytoliths may dissolve and precipitate into clays. Notwithstanding the sediment layer can be quite thick (pers. obs.), a more likely explanation is that sedimentation and resuspension dynamics are spatially and seasonally (and even day-to-day) strongly variable, and depend on fluctuations in flow velocity in the river. During periods of slow flow and low turbulence hippos oversaturate the river with faeces, and the sediment BSi stock is replenished. During periods of fast flow and high turbulence, BSi is resuspended. To our knowledge, there is no

other study yet showing a similar impact of phytoliths on internal Si cycling in rivers, which highlights the uniqueness of the hippo as a land-to-river Si pump.

4. Isotope fractionation

The Si cycle in the MMNR is particularly dynamic and the observed riverine Si fluxes are at or near a dynamic equilibrium. Individual Si isotope values, dissolution kinetics and continuous Si analyses of the various types of samples justify the assumptions made in the proposed mass balance.

Biological Si uptake, secondary abiotic Si precipitation and DSi release through weathering all discriminate against the heavier Si isotopes. The increase in $\delta^{30}Si$ of residual DSi therefore reflects processes that remove Si from solution. Grass had the lowest $\delta^{30}Si$ in the MMNR: plants discriminate against ^{30}Si during Si uptake (Opfergelt et al., 2006). The amount of Si retained in an animal after ingestion of plants is negligible (Jones and Handreck, 1967), and this is reflected in the identical $\delta^{30}Si$ of grass and faeces. Grass $\delta^{30}Si$ values showed considerable variability along the river transect, which could be related to variable plant rooting depth (i.e. DSi source), plant age and grazing intensity (affecting the age of sampled material). However, the exact mechanism at work here goes beyond the scope of this study, but this pattern warrants further future investigation.

Given the significant contribution of hippo faeces to the total BSi flux in the river, one could expect that $\delta^{30}Si$ of suspended matter simply reflects $\delta^{30}Si$ of faeces and grass. However, while it falls within the variability observed for grass and faeces samples, it tends to show lower variability, assumed to result from weighted mixture of different sources. The continuous Si analysis confirmed that almost all of the alkaline reactive Si in suspended matter was of biological origin (**Table S5.1**). A small alkaline-extractable fraction of non-biological origin (found at sites 3, 4 and 10) likely originates from erosion of the savannah soil, where similar fractions are found (**Table S5.1**).

Partial dissolution of faeces with an associated isotope fractionation that leaves the residual BSi enriched in ^{30}Si may also be an important process. It is

clear from the dissolution kinetics that the rate of Si dissolving from faeces in water decreases with the age of the faeces (**Figure S5.5**). A kinetic fractionation should favor the transfer of lighter isotopes to solution, leaving the residual faeces with a relatively higher δ^{30}Si value (Demarest et al., 2009). This corroborates the δ^{30}Si value of faeces of different ages: fresh faeces (-0.52 ‰) has a lighter signature than old faeces (0.20‰), though the assumption of a shared initial value is hard to verify.

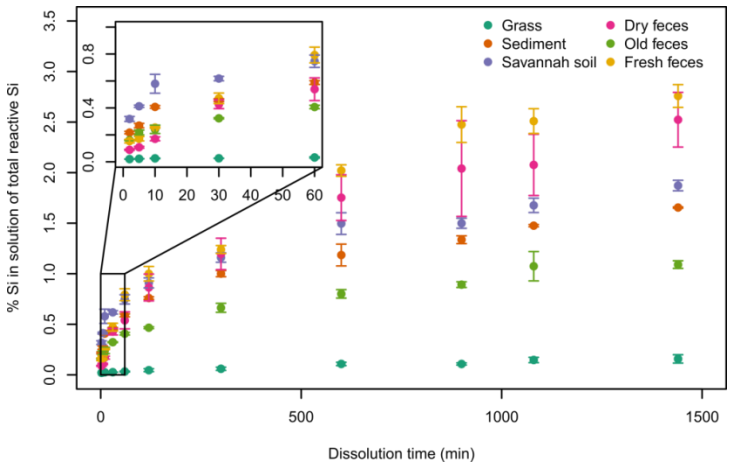

Figure S5.5. Dissolution of reactive Si in samples of different river compartments after exposure to rain water during 24 h (1440 min). Results are expressed as % of the total reactive Si in the samples (BSi in grass and faeces, and AlkExSi determined with the continuous analysis method (Barão et al., 2014)), and are plotted as mean values (symbols) with standard deviations (error bars; n = 5). Series are fresh faeces (order of hours old), dried faeces (order of days old), old faeces (order of weeks old), grass, sediment, savannah soil. Blank rain water samples were also incubated and sampled per time step and remained unaltered (not shown in this plot). The first 60 min of the dissolution experiment are visualised in detail in a smaller inset graph.

Sediment BSi δ^{30}Si values are considerably higher than the suspended matter it derives from. This sediment is likely a mixture of relatively slow dissolving old faeces with lower δ^{30}Si values (but higher than fresh faeces values which make up the majority in suspended matter), and relatively quickly dissolving savannah soil particles (**Figure S5.5**) with higher δ^{30}Si. This mixture of material with different dissolution kinetics and consequently different δ^{30}Si values can explain the generally high δ^{30}Si values in the sediment.

The formation of secondary mineral phases in the sediment in turn can explain the high pore water δ^{30}Si. In general, secondary phase formation is

characterised by a fractionation that leaves the heavier isotopes in the residual solution (Oelze et al., 2014). Other processes might also contribute to the high pore water δ^{30}Si values. Dissolution of savannah soil particles in the sediment (with similarly high δ^{30}Si values as in pore water; **Figure S5.4**) may push pore water values even higher.

5. How would the Mara ecosystem look like without hippos?

We conclude that hippos play a key role in silica cycling as a terrestrial-aquatic pump, contributing more than 80 % to the increased total Si flux along the Mara River. Unintended downstream repercussions to Lake Victoria and other Rift Valley lake ecology are possible if hippos are removed from the savannah ecosystem. A substantial part of the silica is transported downstream into Tanzania and potentially further into Lake Victoria. Most rivers draining into Lake Victoria however, have been cleared of hippo populations, which are currently confined to the mouths of major rivers and littoral areas around the lake (Masese and McClain, 2012). Throughout Africa, hippo populations have decreased by 7 – 20 % from 1996 – 2004 and are expected to decrease by a further 30 % over the next 3 generations (Lewison et al., 2008) following global defaunation trends (McCauley et al., 2015).

If all hippos in the Mara river disappeared and the direct input of BSi ceased, we could expect a 10 % reduction in total Si transport compared to the current situation. This is a rough but conservative estimate based on the mass balance of **Figure S5.1**, assuming similar magnitudes of DSi precipitation. This reduction can be enough to further limit diatom growth in Lake Victoria where increased N:Si and P:Si ratios have caused a phytoplankton transition to year-round dominance by cyanobacteria since in the late 1980s (Verschuren et al., 1998), and the diversity of planktonic diatom communities has declined dramatically (Stager et al., 2009). Similar transitions have been documented for other Rift Valley Lakes too where mostly climate change and changing N and P concentrations due to intensified human activity in the watershed are pointed as main cause (e.g. Lake Tanganyika (Tierney et al., 2010)). Yet a decreased Si flux to the lakes

can also be part of the problem. It cannot be excluded that the decimation of the hippo population over the past decades has contributed to this decreased Si flux to the lakes. This might be especially true for regions where the lithology of the catchment delivers a lower basal Si concentration in the water than it is the case for the volcanic lithology of the Mara river basin (e.g. 3 times lower in the Congo river (Hughes et al., 2011)).

River turbidity could also decrease in the absence of hippos, creating an opportunity for diatom growth in the river, which has the capacity to decrease the DSi flux even further. To complicate matters, BSi dynamics in the savannah ecosystem could substantially change, as the grassland would transform from a system where BSi is continuously removed through grazing, to a system with the potential for strong internal recycling of BSi and higher within-soil retention of Si (potentially reducing Si fluxes even more). Similar conclusions have previously been made in the Okavango Delta, a subtropical flood-pulse wetland in northern Botswana (Frings et al., 2014b; Struyf et al., 2015).

To our knowledge, there is no other study yet showing a similar impact of grazers on the flux of Si from land to the rivers and ultimately to the receiving big lakes (*in casu* Lake Victoria). A decimation of the hippo population can cause a reduced Si flux to these lakes which depend greatly on fresh Si influx from rivers to maintain their high productivity and a diatom dominated phytoplankton community which is essential for the lakes' ecosystem.

Supplementary material to "Hippos (*Hippopotamus amphibius*): the animal silica pump".

Field site description

The Mara River (Kenya-Tanzania) has a long-year average discharge of 12.5 m^3s^{-1} at the Kenya-Tanzania border, and contributes about 5 % of the volume of water flowing into Lake Victoria (Masese and McClain, 2012). The Lake Victoria basin is of environmental and biodiversity conservation

interest, particularly the Maasai Mara-Serengeti ecosystem (Dobson et al., 2010). While hippo populations have declined strongly across the African continent due to hunting and terrestrial and aquatic habitat degradation (Zisadza et al., 2010), local densities can still be high. Hippo densities in the Mara River (Kenyan side) reach 36 hippos per km river (Kenyan side), which is the largest single population on the African continent and represents 3 % of the total population (Kanga et al., 2011).

This study was undertaken in the Maasai Mara National Reserve (MMNR) in SW-Kenya. Local soils are Versitols, high in clay content and dark in colour (Mati et al., 2008). This region has generally bimodal rainy seasons, with short rains from Oct.-Dec. and long rains from March-May (McClain et al., 2014). Ten main field sites were selected on the Mara River based on their accessibility and equal distribution along the river (see map in **Figure 5.1**). The most upstream site 1 lies just outside MMNR, and has almost no hippo activity. Once in the privately managed wildlife conservancies (boundary between sites 1 and 2), hippo densities rise abruptly (Kanga et al., 2011). Site 10 is the most downstream site, just before the Tanzanian border. Three additional sites were selected on the main tributaries of the river Mara. Sites on the Amala and Nyangores lie upstream in urban areas (no wild animals) while the site on the Talek lies between sites 8 and 9 in the MMNR and is inhabited by hippos. All sites were sampled during the dry season (Feb. 2014), when a 10-day average discharge was 5.3 m^3s^{-1} upstream (site 1) and 5.4 m^3s^{-1} downstream (site 10).

Sampling protocols

River discharge was measured upstream (site 1) and downstream (site 10) using depth transducers at rated cross sections. At site 1, stage height was measured every 15 minutes using a RuggedTroll 100 pressure transducer that was corrected for atmospheric pressure changes (In-Situ Inc., Fort Collins, CO, USA). At site 10, stage height was measured every 15 minutes with a pressure transducer connected to a Eureka Manta2 sonde (Eureka Water Probes, Austin, TX, USA). Rating curves were developed at both sites

by measuring discharge using the area-velocity method on multiple occasions in 2011 and 2014 using either a handheld staff gauge or weighted measuring tape for depth and velocimeter for velocity, or a HydroSurveyor (SonTek, San Diego, CA, USA). Stage height was converted to discharge using a rating curve developed for each site. Discharge measurements were averaged over a 10-day period prior to our sampling campaign.

River water was sampled at all 10 river sites and at all 3 tributary sites. Water quality parameters including temperature (°C), pH, EC (µS cm^{-1}), O_2 (% and mg L^{-1}) and salinity (PSU), were monitored with a Eureka Manta2 sonde (Eureka Water Probes, Austin, TX, USA). Total suspended sediments (TSS in mg L^{-1}) was measured by filtering water samples through pre-weighed filter papers. A plastic syringe was used and samples were filtered through 0.45 µm nitrocellulose Chromafil syringe filters (A-45/25) into sample bottles and stored cool (4°C) until analysis for DSi concentration (mg L^{-1}) and DSi $\delta^{30}Si$ values.

Suspended matter was sampled at all 10 river sites and at all 3 tributary sites. Water samples of known volume (50 mL) were filtered over nitrocellulose filters with pore size 0.45 µm (Porafil Membranfilter, Macherey-Nagel, Düren, Germany). Filters were dried for 72 h at 70 °C and analysed for BSi concentration in the river (in mg L^{-1} water). To analyze the quality of the BSi (in mg g^{-1} suspended matter) and $\delta^{30}Si$ values, extra samples (~20 L) were taken at the same locations. Particles could settle for 48 h after which overlaying water was removed and the remaining slurry was dried at 70 °C for 72 h. Too few material could be sampled from the Nyangores site to do a BSi (mg g^{-1}) analysis.

Pore water was sampled at river sites 1, 2, 3, 5, 6, 7 and 10 (not on sites 4, 8 and 9 and not at tributary sites). Three standard rhizons (Rhizosphere Research Products, Wageningen, The Netherlands) were inserted 10 cm deep into the sediment (no overlaying water present), and vacuum force was implemented using a standard plastic syringe of 50 mL. The water accumulated over a period of 15 min was then pooled into 1 sample for each

site, filtered through 0.45 µm nitrocellulose Chromafil syringe filters (A-45/25) into sample bottles and stored cool (4°C) until analysis for DSi concentration (mg L^{-1}) and DSi $\delta^{30}Si$ values (no analysis for site 5).

Sediment was sampled at all 10 river sites. Cores (20 cm long and 28 mm in diameter) were sampled per site using a hammer auger with a removable plastic lining (Eijkelkamp 04.15.SA Foil sampler, Giesbeek, The Netherlands). Immediately after sampling, each core was sub-sectioned into 6 slices, with intervals at each 2 cm in the top 10 cm of the core, and the 6^{th} slice containing the rest of the core. All slices were packed in vacuum plastic bags and stored cool (4 °C) on return to the laboratory. Samples were dried for 72 h at 70 °C and homogenised by manual grinding before analysis. BSi concentration (mg g^{-1}) was determined in slices 1 (0 to -2 cm), 3 (-4 to -6 cm) and 5 (-8 to -10cm). BSi $\delta^{30}Si$ values were determined on all slices.

Grass and hippo faeces were sampled at all 10 river sites, and at tributaries Amala and Nyangores (not at Talek). Monospecific stands of the dominating *Cynodon dactylon* (L.) Pers. grass species was selected on the hippo grazing lawns flanking the different sites. These lawns are areas relatively close to the river that are frequently grazed by hippos (Field, 1970). One sample per site was cut in a quadrant of 60 × 60 cm. Hippo faeces (if present) was sampled as close as possible to the grass plot. An ad hoc grab sample was taken from faeces that visibly appeared to be fresh (still moist, uncontaminated with dust). Grass and faeces samples were dried for 72 h at 70 °C and mechanically ground before analysis for BSi concentration (mg g^{-1}) and BSi $\delta^{30}Si$ values.

One hippo pool was selected on the Mara River between sites 7 and 8 (see map in **Figure 5.1**). The hippo pool is a local aggregation of hippos that remain in their territory. Automatic water samplers (3700C Compact Portable Sampler, Teledyne Isco, Lincoln, NE, USA) were placed upstream and downstream of this hippo pool and programmed to collect 1 sample per hour for a 24-hour period (18-2-2014 11.00am till 19-2-2014 11.00am). Samples stayed cool in the samplers during this period and weather and river hydraulic conditions remained stable. The distance between both samplers

was 250 m measured along the river and a maximum of 80 hippos was counted. Subsamples of all 48 water samples were filtered through 0.45 µm nitrocellulose Chromafil syringe filters (A-45/25) into sample bottles and stored cool (4°C) until analysis for DSi concentration (mg L^{-1}). Subsamples of 50 mL were filtered over nitrocellulose filters with pore size 0.45 µm (Porafil Membranfilter, Macherey-Nagel, Düren, Germany). Filters were dried for 72 h at 70 °C and analysed for BSi concentration (mg L^{-1}).

Finally, in the savannah grassland three random plots were sampled in February 2014 and supplemented by three extra plots in August 2016 (see map in **Figure 5.1**). These plots were roughly located near sites 2, 5, 6, 8, 9 and 10, but were not under direct influence of the river (distance >1 km perpendicular to the river). Soil cores of the Versitol that dominates the MMNR savannah were sampled in a similar way as the sediment cores. Immediately after sampling, each core was sub-sectioned into 2 slices of 5 and 10 cm (2014 samples) or into 1 slice of the top 5 cm (2016 samples), packed in vacuum plastic bags and stored cool (4 °C) on return to the laboratory. Samples were dried for 72 h at 70 °C and homogenised by manual grinding before analysis. BSi concentration (mg g^{-1}) was determined on all slices. BSi $\delta^{30}Si$ values were determined for the top slices of samples near sites 9 and 10.

Chemical analyses protocols

All water samples (river water, pore water and from the hippo pool) were analysed for DSi concentration on an Inductive Coupled Plasma Atomic Emission Spectrophotometer (ICP-AES, Thermo Scientific, ICAP 6000 Series).

Grass, faeces and suspended matter sampled on filters were analysed for BSi concentration in a classical manner. A sample of 25 mg dry matter (for grass and faeces) or the entire filter (for suspended matter) was incubated in 25 mL 0.5 M NaOH at 80 °C for 5 h (DeMaster, 1981). The extracted and dissolved silica was analysed colourimetrically on a segmented flow analyser (SAN++, Skalar, Breda, The Netherlands). The extraction in 0.1 M NaOH at 80° has been well established and tested; it is capable of fully dissolving the BSi

from plant phytoliths at the solid-solution ratios and extraction time we applied (Saccone et al., 2007).

Sediment, soil and suspended matter sampled by settlement are usually a mixture of BSi and mineral Si and a classic analysis as for grass and faeces will not distinguish between different reactive fractions. Therefore the samples were extracted using a novel alkaline continuous extraction in NaOH, according to the method from (Koning et al., 2002), and adapted for soils by Barão et al., (2014). Si and Al concentrations are measured continuously and the two dissolution curves are fitted together in a first order equation (**Eq. 1** and **2**).

$$Si_t = \left(\sum_{i=1}^{n} AlkExSi_i \times \left(1 - e^{-k_i \times t}\right)\right) + b \times t \qquad \textbf{(1)}$$

$$Al_t = \left(\sum_{i=1}^{n} \frac{AlkExSi_i}{Si/Al_i} \times \left(1 - e^{-k_i \times t}\right)\right) + \frac{b \times t}{Si/Al_{min}} \qquad \textbf{(2)}$$

The method distinguishes between fractions dissolving linearly (poor reactive silica) and different fractions exhibiting a non-linear behavior (highly reactive silica). Linear fractions are characterised by parameters b (slope of the linear dissolution) and Si/Al (ratio of Si and Al in that fraction); non-linear fractions are characterised by the amount of AlkExSi (Alkaline extractable silica, in mg g^{-1} of sample), k (reactivity of the fraction in NaOH, mg g^{-1} min^{-1}) and Si/Al (ratio of Si and Al in that fraction). The method also allows distinguishing between different reactive silica fractions (with k-values > 0.1) according to their origin based on the Si/Al ratio determined by the model: true biogenic silica (Si/Al ratio ≥ 4), silica belonging to clay minerals (Si/Al ratio between 1 and 4), and silica absorbed by oxides (Si/Al ratio ≤ 1). More details about the continuous alkaline extraction of silica and aluminium method can be found in Barão et al., (2014). We present the data of the true biogenic silica (noted as AlkExSi_BSi in **Table S5.2**), and the sum of the other reactive fractions (noted as AlkExSi_non_BSi in **Table S5.2**). Non-reactive fractions are not shown.

Batch dissolution experiment protocol

To mimic *in situ* reactivity of Si after digestion, Si dissolution from six different samples was monitored over different time intervals in rain water (methodology after Vandevenne et al., (2013)). The samples were: (i) fresh hippo faeces (order of hours old, still wet when sampled), (ii) dried hippo faeces (desiccated and visual confirmation of its presence days before sampling), (iii) old hippo faeces (dried out and visual conformation of its presence weeks before sampling), (iv) grass (freshly cut in pieces of 1 cm), (v) sediment (dried and homogenised), and (vi) Versitol from the savannah grassland (dried and homogenised). All samples came from or near site 10. Fresh material (3 g) was put in 200 mL plastic boxes and spread out evenly over the bottom surface (ca 40 cm^2). In total, 341 boxes were prepared: five replicates per different sample per time interval and one blank per time interval. At the start of each experiment, all boxes were filled with 30 mL air-captured rain water (pH: 7.18, EC: 23.5 µS cm^{-1} and DSi: 0.17 mg L^{-1}). Dissolution experiments were carried out for 24 h in a dark incubator at 20°C, subsamples were taken at 11 time intervals (2, 5, 10 and 30 min, and 1, 2, 5, 10, 15, 18, 24 h). At each time interval, 10 mL of solution was sampled from a box and filtered through 0.45 µm nitrocellulose Chromafil syringe filters (A-45/25) and analysed for DSi using ICP-AES. The sampled box was not further used. Results are plotted relative to the respective reactive Si concentration (i.e. BSi for grass and faeces, AlkExSi for sediment and soil). A subsample of the 'old faeces' was also analysed for its isotopic $\delta^{30}Si$ value and compared to the average value of fresh faeces sampled before.

Diatom and phytolith fixation protocol

The presence/absence of BSi particles (diatom frustules, chrysophyte stomatocysts and phytoliths) was determined in suspended matter samples and uppermost 2 cm sediment samples of sites 1, 5 and 10. Additionally faeces and grass samples were prepared to check their phytolith contents. Samples were prepared for light microscopy (LM) following the method described in Van der Werf, (1955). Small parts of the sample were cleaned by adding 37 % H_2O_2 and heating to 80 °C for about 1 h.

The reaction was completed by addition of $KMnO_4$. Following digestion and centrifugation (three times 10 minutes at 3700 g), cleaned material was diluted with distilled water to avoid excessive concentrations of diatoms and phytoliths on the slides. Cleaned diatom material was mounted in Naphrax®. The slides were analysed using an Olympus BX53 microscope, equipped with Differential Interference Contrast (Nomarski) and the Olympus UC30 Imaging System. The variation in BSi particles was visualised (**Figure S5.6**) and were counted on random transects at 400x magnification and the relative abundance of each group (diatoms, chrysophytes and phytoliths) was determined.

Si isotope analysis protocol

A selection (n = 71) of the samples was analysed for $\delta^{30}Si$: river water samples of all 10 sites and the three tributary sites, pore water samples of sites 1, 2, 3, 6, 7 and 10, suspended matter samples of all 10 sites, grass and faeces samples of sites 3, 5, 8 and 10, sediment of sites 1, 3, 5, 8 and 10 (all slices per core were analysed and averaged per site), and finally all uppermost slices of 2 Versitol samples from the savannah grassland. Sample preparation followed a standard two-step purification procedure (Frings et al., 2014b) in which the Si was first leached or concentrated from the sample, then chromatographically purified before introduction to the mass-spectrometer. In brief, water samples were precipitated as an insoluble triethylamine silico-molybdate ('TEA-Moly') compound, collected after 24 hours by vacuum filtration with 0.2 µm polycarbonate filters and finally converted to a near-pure SiO_2 polymorph by volatilisation of the Mo for 12 hours in a Pt crucible at 1000 °C (De La Rocha et al., 1996). The SiO_2 was then dissolved in concentrated HF in large excess (1:100) to avoid formation of the volatile SiF_4. The Si was then separated from any residual cationic and anionic matrix by the anion-exchange column chromatography protocol of Engstrom, E. et al., (2006) in which Si is eluted in 0.15 M HNO_3 and 5.5 mM HF. Si concentrations in the elutant after the chromatographic separation were assessed on a 0.5 mL aliquot by molybdate-blue colourimetry on a SmartChem200 automated chemical analyser. Column yields for standard samples of known purity were always greater than 95 %. The TEA-Moly

precipitation step has previously been demonstrated to be quantitative (De La Rocha et al., 1996) and only physical loss of Si (i.e. with no attendant isotopic fractionation) is possible during the filtration and combustion steps. Grass and faeces samples were first combusted at 550 °C to remove organic matter, and the BSi content was then extracted in a 1M NaOH solution in PP tubes at 85 °C for 3 hours at a solution/solid ratio of ~150 g g^{-1}. These conditions were chosen to mimic those used for the conventional determination of BSi concentrations (above) and to ensure 100 % recovery of grass/faeces BSi. This NaOH solution was then neutralised with the addition of 0.2 M HCl and treated as the water samples above. The procedure was slightly altered for the sediment samples, to avoid the simultaneous leaching of Si from inorganic soil aluminosilicates. Here, BSi was physically isolated from the sediment by a combination of organic matter mineralisation by 15-30 % H_2O_2, sieving, and heavy liquid separation (sodium polytungstate at 2.3 g cm^{-3}). The BSi was then dissolved in a weaker base (1 % Na_2CO_3) to minimize any contamination from clay minerals that can be hard to physically disaggregate from the BSi (Mackay et al., 2011). One group of samples was processed with a cation exchange column protocol after Georg et al., (2006); laboratory intercomparison efforts have demonstrated that $\delta^{30}Si$ measurements can be reliably compared between preparation methods, MC-ICPMS instrumentation, and analytical protocols (Grasse et al., 2017; Reynolds et al., 2007).

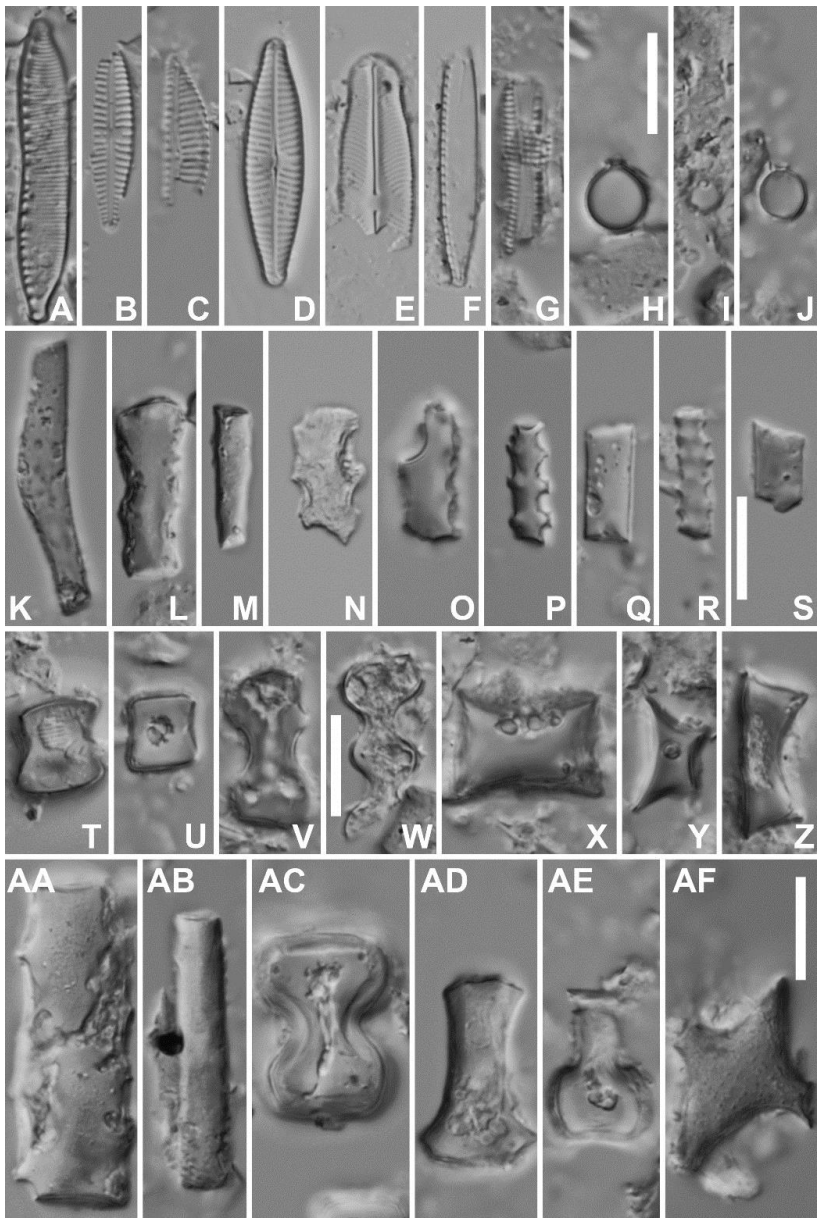

Figure S5.6. Biogenic silica particles observed in suspended matter and sediment samples. Figures A-G represent (partly broken) diatom valves. Figures H-I are stomatocysts from Chrysophyta. Figures K-AF represent phytoliths. Figures V, W, AC and AE are typical grass phytoliths. Diatoms and Chrysophyta account only for 1 – 2 % of total biogenic silica particle count. Scale bar represents 10 µm.

Si isotope data were gathered across multiple analytical sessions (detailed in **Table S5.2**) with a MC-ICPMS Neptune at the Pole Spectrometrie Ocean (Ifremer, Brest), and with a Nu Plasma MC-ICPMS at the Vegacenter, Swedish Museum of Natural History. Samples were introduced to the Neptune in 'dry-plasma' mode using an Apex desolvating nebuliser, and to the Nu Plasma II in

'wet-plasma' mode. With both instruments, measurements was made at medium resolution (m/Δm >2500) on the interference-free lower-mass side of the ^{30}Si beam. Sensitivity on the Neptune and Nu Plasma was typically ca. 12 V ppm^{-1} and 1 V ppm^{-1}, respectively. In both cases, instrumental mass-bias was corrected by standard-sample bracketing with the internationally accepted reference for Si isotope ratios NBS28 (NIST RM8546). All isotope values are reported in delta notation relative to NBS28 (**Eq. 3**):

$$\delta^{30}Si = \left(\frac{R_{sample}}{R_{NBS28}} - 1\right) * 1000 \qquad \textbf{(3)}$$

where R_{sample} and R_{NBS28} is the $^{30}Si/^{28}Si$ ratio in the sample and standard, respectively. In the Neptune sessions samples were doped to 1 ppm Mg, and ^{25}Mg and ^{26}Mg were monitored dynamically in both sample and standards to provide an additional instrumental mass-bias correction, assuming an exponential fractionation law (Cardinal et al., 2003). Representative external reproducibility at the 2σ level, based on long-term, multi-session analyses of standard solutions is 0.12‰ at Stockholm and 0.14‰ at Brest. Commonly used secondary standards (Big-Batch, Diatomite, BHVO-2) were run in all measurement sessions to ensure accuracy; results (tabulated in **Table S5.2**) agree well with published data (Reynolds et al., 2007). All results fall on the expected mass-fractionation line, confirming the successful removal of polyatomic interferences during measurement.

Si isotope mass-balance model

Assuming that the sources and sinks of DSi within MMNR can be lumped into two terms:

$$F_z = F_0 + F_{diss} - F_{precip} \qquad \textbf{(4)}$$

where F_z is the flux of DSi (mol s^{-1}) in the Mara River at point z (m), and is a function of the input flux (F_0), the removal of Si into secondary solid phases (F_{precip}) and the addition of Si from the dissolution of BSi (F_{diss}). Assuming that the dissolution and precipitation fluxes occur at consistent rates between river sampling points:

$$F_z = F_0 + k_1 z - k_2 z \qquad \textbf{(5a)}$$

$$k_2 = \frac{F_0 - F_z}{z} - k_1 \qquad \textbf{(5b)}$$

where k_1 and k_2 (mol m^{-1} day^{-1}) are equivalent to rate constants for the dissolution and precipitation reactions. Note that although we schematically separate the fluxes and assume all addition is opal dissolution and all removal is clay formation, the relevant processes could be the reverse of these reactions (plant growth; silicate mineral dissolution). The only important criterion is that these processes are isotopically distinct. Note also that these two competing processes are required because there exists no known Si source with a suitably high δ^{30}Si in the MMNR to explain the general downstream δ^{30}Si increase. Assuming the loss of Si occurs evenly throughout MMNR, then:

$$\frac{dF}{dz} = k_1 - k_2 \qquad \textbf{(6)}$$

In our dry season data in MMNR, this is equivalent to approximately -0.005 kg m^{-1} day^{-1} over the whole reach, and varies from -0.097 to 0.077 kg m^{-1} day^{-1} between individual sample points. An infinite number of combinations of k_1 and k_2 can produce this value, so we turn to the isotope data to help constrain the model. Introducing δ^{30}Si values into **Eq. (5a)**, we obtain an isotope mass-balance expression:

$$\delta_z F_z = \delta_0 F_0 + k_1 z \delta_{BSi} - k_2 z(\delta_z + \varepsilon_{clay}) \qquad \textbf{(7)}$$

where δ_z, δ_0 and δ_{BSi} are the δ^{30}Si values of the Mara River DSi at distance z, at the inflow (z = 0) and of the suspended matter, respectively, and ε_{clay} is the fractionation (in per mil) associated with clay mineral neoformation. Substituting **Eq. (5b)** into **Eq. (6)** and solving for k_1, we obtain an expression that can be evaluated at successive points *i* downstream:

$$k_{1,i} = \frac{F_{i-1}(\delta_{i-1} - \delta_i - \varepsilon) + F_i \varepsilon}{\Delta z(\delta_i - \delta_{BSi} + \varepsilon)} \qquad \textbf{(8)}$$

For each of our dry season MMNR dissolved Si δ^{30}Si datapoints, we calculate first the values of k_1 and then k_2 required to close the mass-balance at different values of ε_{clay}. Any calculated negative dissolution rates are

restored to zero, and negative clay precipitation rates are rejected, providing a suite of internally consistent results. We use a Monte Carlo approach to propagate uncertainties on these constants, assuming conservative uncertainties of ±10 % and 0.20 ‰ on the fluxes and the $\delta^{30}Si$ values, respectively. The $\delta^{30}Si$ of the dissolving phytoliths is chosen randomly for each sample from between -1.25 ‰ to 1.25 ‰, based on the range in all grass, faeces and sediment BSi $\delta^{30}Si$ determinations (n = 23; **Table S5.2**). For each iteration, ε_{clay} is randomly prescribed between +1.0 and -4.0 ‰, capturing the range of fractionations determined for precipitation of various amorphous silica and secondary aluminosilicate phases (Frings et al., 2016; Oelze et al., 2014, 2015; Opfergelt et al., 2012; Ziegler et al., 2005b). The model is iterated until 10,000 internally consistent scenarios are reached; this typically requires ca. >300000 runs. Conceptually, this implies there is a large part of the available parameter space that is physically implausible.

Detailed results of the mass-balance calculations are shown in **Figure S5.7**. Median ε_{clay} of the retained solutions for individual sample points varied between -2.80 and -1.46 ‰ (**Figures X-E**, mean = -2.11 ‰), in excellent agreement with recent compilations of laboratory and field estimates (Frings et al., 2016; Opfergelt and Delmelle, 2012). The mass-balance predicts that the mean fractionation associated with Si removal from solution is variable, with the lowest values (greatest fractionation) being found in the middle reach of the MMNR: Note also that this removal flux could be at least partially attributable to plant or other siliceous organism uptake; isotopically, their impact is indistinguishable from clay formation given they have near identical fractionations (Alleman et al., 2005; Ding et al., 2008a, 2008b; Frings et al., 2016; Opfergelt et al., 2006; Ziegler et al., 2005a). The cause of the variable fractionation is unclear, but could be related to changes in reaction rates as observed in laboratory experiments (e.g. Oelze et al., (2014), or to plant species-specific fractionations).

Median phytolith dissolution rates and clay formation rates (**Figures X-C, D**) average 0.050 and 0.052 kg m^{-1} day^{-1}, respectively. This slight imbalance over the entire study reach is enough to account for the overall net decrease

in dissolved Si flux downstream in the MMNR. The best estimate for net cumulative phytolith dissolution, based on the median phytolith dissolution rates at each successive point downstream, is 5170 kg Si day^{-1} over the entire reach.

As a check on the feasibility of this value, we estimate the required dissolution rates for biogenic silica in the MMNR. Assuming suspended load BSi concentrations of roughly 4 mg L^{-1} (**Table S5.2**), and a typical river cross-sectional area of 60 m^2 (pers. obs.), then there is approximately 0.240 g of suspended BSi per metre of river, or 29,520 kg over the entire 123 km reach. This implies a specific dissolution rate of 0.17 day^{-1}, which is an upper bound since it neglects riparian or hyporheic processes. Our dissolution experiments using MMNR sediment and faeces samples and rain water (above, and **Figure S5.5**, main text) imply specific dissolution rates of up to > 1 day^{-1} at high degrees of undersaturation for the fresh faeces sample (**Figure S5.8**). If a typical phytolith specific surface area is 5 – 150 m^2 g, these values agree well with the dissolution rate constants (in mol m^{-2} day^{-1}) derived by Fraysse et al., (2006) in a series of batch dissolution experiments. Taking a phytolith solubility of ca. 60 mg L^{-1} (**Figure S5.8A**) at *in-situ* temperatures of ca. 25 ºC and assuming phytolith dissolution is a first-order reaction, implies that the true dissolution rate in the less-undersaturated Mara river waters should be reduced by about a third, i.e. around 0.6 day^{-1}. In fact, the dissolution kinetics of the samples in the rainwater batch experiments are distinctly non-linear with respect to the degree of undersatuation, a commonly observed but poorly understood phenomenon (Van Cappellen and Qiu, 1997; Kamatani et al., 1988; Rickert et al., 2002). Even taking this non-linearity into account, specific dissolution rates for fresh faeces at Mara River levels of undersaturation are ca. 0.2 day^{-1} (**Figure S5.8B**), in good agreement with that suggested by the mass-balance. The point of this exercise is not to calculate a precise value for k_0, but rather to demonstrate the feasibility of sufficient phytolith dissolution on relatively short space- and time-scales, given sufficient material.

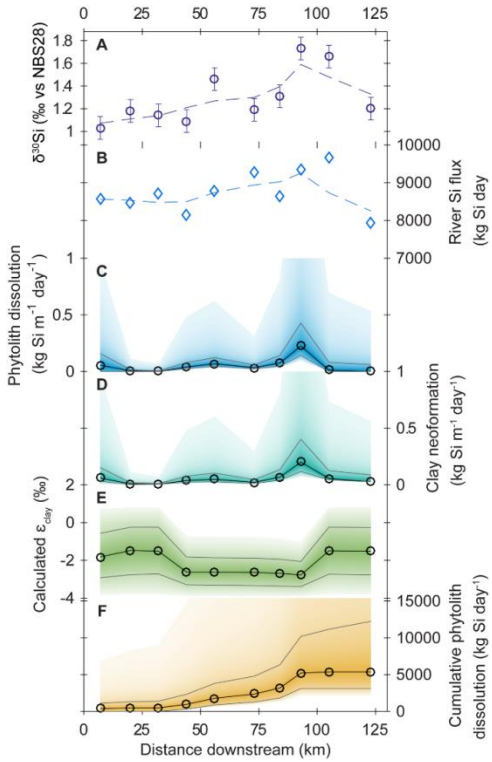

Figure S5.7. Results from the mass-balance calculations. A and B: Data used as input to the model, dissolved Si δ^{30}Si and river Si flux, respectively. Open symbols represent the original data and dashed lines a 5-point lowess smoother. C-E: Results from the calculations, showing the phytolith dissolution rate (C), clay formation rate (D), calculated fractionation associated with clay formation (E) and cumulative downstream total phytolith dissolution rates (E). In all cases, the shaded areas represent the 5-95th percentiles, with the median values being highlighted in solid black lines with open circles and the 25th and 75th percentiles as the grey bounding lines.

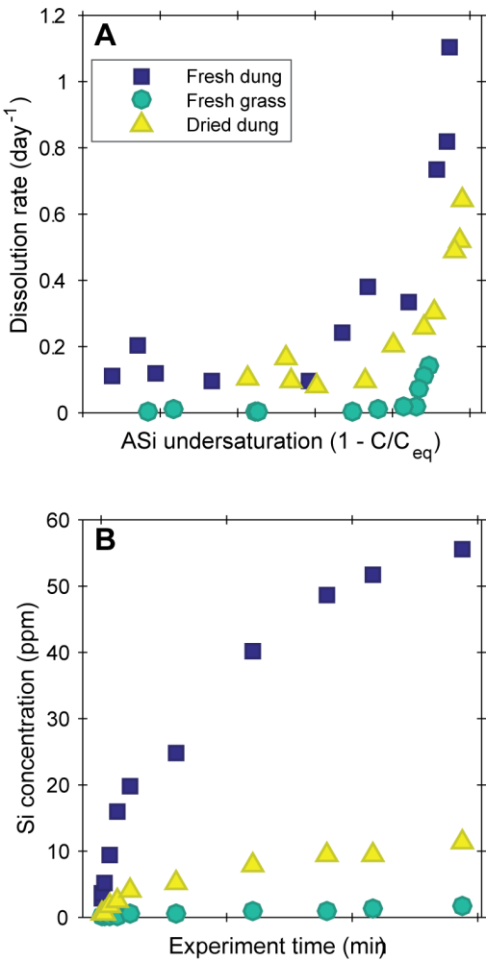

Figure S5.8. Results from rain water batch dissolution experiment. Upper pane: Increase in dissolved Si concentration in the rainwater batch dissolution solution for the 'fresh faeces' sample (see also **Figure S5.3** in the main text). Lower pane: Calculated specific dissolution rates (day^{-1}), derived from the increase in concentration in the solution between successive measurement points, normalised to the amount of available reactive Si at the beginning of the experiment. Degree of undersaturation is calculated as (1-C/Ceq), where C is the concentration at a given time and Ceq is the solubility of the reactive Si, taken to be ca. 60 mg L^{-1} (upper pane).

Table S5.1. Abiotic data and results of chemical Si analyses. Different methods are used: 'A' (Manta2 sonde, Eureka Water Probes, Austin, TX, USA), 'B' (Inductive Coupled Plasma Atomic Emission Spectrophotometer, Thermo Scientific, ICAP 6000 Series), 'C' (filtering fixed volume over pre-weighed 0.45 µm Porafil Membranfilters), 'D' (alkaline extraction method (DeMaster, 1981)), 'E' (continuous alkaline extraction method (Barão et al., 2014) separated in 2 reactive fractions: BSi (Si:Al≥4) and non-BSi (Si:Al<4)).

Sample	Method	Unit		Tributaries			Mara river									
				Amala	Nyangores	Talek	Site 1	Site 2	Site 3	Site 4	Site 5	Site 6	Site 7	Site 8	Site 9	Site 10
		Distance (km)	Depth (cm)	-44	-35	100	7	20	32	44	56	73	84	93	105	123
River water	A	Temp (°C)	Surface				23.0	22.9	24.3	24.8	20.1	19.0	19.0	18.9	18.2	21.1
	A	pH (-)	Surface				7.69	6.42	6.52							7.43
	A	EC (µS cm^{-1})	Surface				587	590	584	613		703	727	656	698	654
	A	O_2 (mg L^{-1})	Surface				6.54	5.30	5.82	2.69	7.47	7.65	7.63	7.60	7.72	2.87
	A	O_2 (%)	Surface				93.6	73.7	83.3	38.8	98.8	101	100	99.8	99.9	38.4
	A	Salinity (PSU)	Surface				0.28	0.28	0.28	0.29		0.34	0.35	0.32	0.34	0.31
	A	Chla (µg L^{-1})	Surface				4.65	12.5		16.1		18.6	20.8	24.0	24.4	12.4
	B	DSi (mg L^{-1})	Surface	20.5	15.0	26.2	18.7	18.4	18.9	17.7	19.0	20.0	18.6	20.1	20.8	17.0
Suspended matter	C	TSS (mg L^{-1})	Surface	89	8		134	115	122	217	242	311	183	294	144	264
	D	BSi (mg L^{-1})	Surface	1.6	0.6	4.1	2.9	3.1	3.7	4.7	4.8	7.0	4.9	6.0	5.1	5.2
	E	AlkExSi_BSi (mg g^{-1})	Surface	24.2		35.8	14.1	34.1	10.4	39.4	35.6	13.8	9.7	9.3	9.7	7.4
	E	AlkExSi_non-BSi (mg g^{-1})	Surface	0.01		0	0.01	0	0	8.3	0	0	0	0.03	0	0.02
Pore water	B	DSi (mg L^{-1})	Surface				19.5	23.6	31.2		27.3	38.2	27.7			30.4
Grass	D	BSi (mg g^{-1})	Surface	18.4	17.5		19.5	18.0	17.1	13.7	23.1	13.9	13.5	17.1	24.4	17.3
Feces	D	BSi (mg g^{-1})	Surface						47.3	46.4	32.7	48.4	33.0	45.4	34.6	39.9
Sediment	E	AlkExSi_BSi	0 to -2				7.6	5.1	11.4	4.0	3.8	11.8	5.9	12.3	25.4	38.6

		(mg g^{-1})														
	E	**AlkExSi_BSi (mg g^{-1})**	-2 to -6				8.9	5.1	11.0	7.5	10.9	18.8	11.0	7.6	10.5	17.5
	E	**AlkExSi_BSi (mg g^{-1})**	-6 to -10				6.1	1.0	17.0	4.9	4.6	10.6	5.5	13.4	8.8	23.6
	E	**AlkExSi_non-BSi (mg g^{-1})**	0 to -2				0	<0.1	0	0	<0.1	0	0	0	0	0
	E	**AlkExSi_non-BSi (mg g^{-1})**	-2 to -6				0	<0.1	0	0	<0.1	5.0	0.7	0	0	<0.1
	E	**AlkExSi_non-BSi (mg g^{-1})**	-6 to -10				0	<0.1	0	0	0	0	0	0	0	<0.1
Savannah soil	**E**	**AlkExSi_BSi(mg g^{-1})**	0 to -5					1.9			34.4		27.1	9.7	0	0
	E	**AlkExSi_BSi(mg g^{-1})**	-5 to -15											28.0	0	0
	E	**AlkExSi_non-BSi (mg g^{-1})**	0 to -5					17.1			1.7		0	<0.1	5.0	0.5
	E	**AlkExSi_non-BSi (mg g^{-1})**	-5 to -15											<0.1	7.2	<0.1

Table S5.2. Summary of silicon isotope analyses presented in this paper. Data from analytical sessions 1 and 3 acquired with a MC-ICPMS Neptune at the Pole Spectrometrie Ocean (Ifremer, Brest), with samples at ca. 2 ppm Si in a 0.15 M HNO_3 and 5.5 mM HF matrix. Data from analytical sessions 2 and 4 acquired with a Nu Plasma MC-ICP-MS at the Vegacenter, Swedish Museum of Natural History, with samples at 1 - 3 ppm Si in a 0.3 M HNO_3 matrix. All data presented relative to international reference material NBS28 (RM 8546). All uncertainties represent 2 standard deviations of the mean of individual measurements (n = 3 standard-sample brackets), i.e. the internal precision Typical long-term reproducibility (external precision) for both instruments, based on multi-session analysis of in-house reference materials, is ca. 0.14‰ for $\delta^{30}Si$. Accepted $\delta^{30}Si \pm 1\sigma$ values for secondary reference materials are -0.30 ± 0.09‰, +1.26 ± 0.10‰ and -10.48 ± 0.27‰ for BHVO-2, Diatomite and Big Batch, respectively.

Type	Site/code	Depth	$\delta^{30}Si$	±[a]	$\delta^{29}Si$	±[a]	Session
		cm	‰ vs NBS28	2σ	‰ vs NBS28	2σ	#
Pore water DSi	1		1.46	0.14	0.69	0.08	1
	2		1.63	0.14	0.85	0.12	2
	3		2.13	0.08	1.11	0.01	2
	6		2.06	0.11	1.05	0.03	2
	7		2.15	0.10	1.07	0.10	2
	10		2.06	0.28	1.02	0.06	1
Mara river water DSi	1		1.03	0.02	0.48	0.10	1
	2		1.18	0.22	0.64	0.08	1
	3		1.14	0.18	0.56	0.04	1
	4		1.09	0.02	0.56	0.02	1
	5		1.46	0.14	0.68	0.04	1
	6		1.19	0.06	0.58	0.06	1
	7		1.31	0.06	0.67	0.12	1
	8		1.73	0.09	0.84	0.03	1
	9		1.66	0.02	0.87	0.02	3
	10		1.20	0.02	0.64	0.02	1
Tributary water DSi	Amala		1.05	0.20	0.48	0.06	1
	Nyangores		1.24	0.16	0.57	0.12	1
	Talek		-0.30	0.04	-0.19	0.02	1
Hippo faeces BSi	3		-1.14	0.10	-0.60	0.04	2
	5		-0.96	0.06	-0.55	0.05	2
	8		-0.42	0.08	-0.22	0.09	2
	10		0.44	0.04	0.22	0.02	2
Extra hippo faeces BSi	Old faeces		0.20	0.04	0.05	0.06	3
Grass BSi	3		-1.25	0.14	-0.61	0.06	1
	5		-1.13	0.14	-0.58	0.02	3

	8		0.24	0.09	0.15	0.05	2
	10		0.45	0.06	0.23	0.03	2
River suspended matter BSi	1		-0.23	0.11	-0.10	0.03	4
	2		0.06	0.15	0.00	0.05	4
	3		-0.25	0.22	-0.15	0.11	4
	4		0.32	0.06	0.19	0.10	4
	5		0.36	0.18	0.17	0.15	4
	6		-0.37	0.13	-0.25	0.05	4
	7		-0.54	0.24	-0.33	0.08	4
	8		0.53	0.15	0.26	0.11	4
	9		0.01	0.13	0.02	0.15	4
	10		-0.21	0.09	0.00	0.09	4
Sediment BSi	1	0 to -2	0.81	0.06	0.42	0.04	3
		-2 to -4	-0.50	0.14	-0.24	<0.01	3
		-4 to -6	0.37	<0.01	0.18	<0.01	3
		-6 to -8	0.62	0.12	0.31	0.02	3
		-8 to -10	0.49	0.02	0.24	0.06	3
		-10 to -20	0.00	0.08	0.03	0.02	3
	3	0 to -2	1.01	0.06	0.49	0.02	3
		-2 to -4	0.70	0.06	0.34	0.08	3
		-4 to -6	1.14	0.10	0.58	0.04	3
		-6 to -8	1.13	0.04	0.59	<0.01	3
		-8 to -10	0.94	0.02	0.50	0.04	3
		-10 to -17	0.86	0.04	0.45	0.02	3
	5	0 to -2	1.24	0.02	0.63	0.04	3
		-2 to -4	1.31	0.16	0.70	<0.01	3
		-4 to -6	1.20	0.02	0.62	0.08	3
		-6 to -8	1.09	0.10	0.60	<0.01	3
		-8 to -10	1.21	0.02	0.63	0.04	3
		-10 to -16	0.67	0.04	0.33	0.02	3
	8	0 to -2	1.12	0.12	0.59	0.08	3
		-2 to -4	1.10	0.12	0.56	0.08	3
		-4 to -6	1.41	0.02	0.72	0.12	3
		-6 to -8	0.73	0.08	0.34	0.02	3
		-8 to -10	1.00	0.08	0.51	0.04	3
		-10 to -15	0.77	0.06	0.40	0.02	3

	10	0 to -2	1.12	0.04	0.59	<0.01	3
		-2 to -4	1.36	0.22	0.69	0.08	3
		-4 to -6	0.96	0.12	0.51	0.14	3
		-6 to -8	1.07	0.10	0.58	0.02	3
		-8 to -10	1.59	0.08	0.83	0.02	3
		-10 to -16	1.25	0.04	0.66	0.02	3
Savannah soil	Near site 9	0 to -5	1.88	0.04	0.95	0.10	3
	Near site 10	0 to -5	1.77	0.14	0.91	0.12	3
Secondary reference materials, session 2	BHVO2		-0.25	0.01	-0.13	0.07	2
			-0.37	0.11	-0.17	0.05	2
			-0.29	0.04	-0.20	0.06	2
			-0.31	0.05	-0.18	0.06	2
		Mean:	*-0.30*		*-0.17*		
	Diatomite		1.21	0.10	0.58	0.03	2
			1.20	0.05	0.54	0.02	2
		Mean:	*1.20*		*0.56*		
	Big Batch		-10.41	0.12	-5.31	0.08	2
			-10.36	0.04	-5.33	0.02	2
		Mean:	*-10.38*		*-5.32*		
Secondary reference materials, session 3	Diatomite		1.23	0.02	0.63	0.05	3
			1.25	0.04	0.68	0.01	3
			1.13	0.07	0.56	0.03	3
		Mean:	*1.20*		*0.62*		
	Big Batch		-10.28	0.10	-5.25	<0.01	3
			-10.68	0.18	-5.48	0.13	3
			-10.09	0.07	-5.18	0.03	3
		Mean:	*-10.35*		*-5.30*		
Secondary reference materials, session 4	Diatomite		1.28	0.30	0.67	0.20	4
			1.11	0.08	0.63	0.08	4
			1.19	0.09	0.61	0.01	4
		Mean:	*1.19*		*0.64*		
	Big Batch		-10.55	0.21	-5.35	0.07	4
			-10.27	0.20	-5.38	0.04	4
		Mean:	*-10.41*		*-5.37*		

[a]Internal precision; external precision should be taken into account for true data reproducibility.

Chapter 6

Script developed in Python:

Silicium-Aluminum soil concentration

This is a notebook file that discusses the Si-Al soil concentration model. Functions are defined in a seperate file: *SiAlProblem_Functions.ipynb*.

In [1]:
```
%run ./SiAlProblem_Functions.ipynb
```

Model

We have measurements of of the silicium (Si) and aluminum (Al) concentration in a soil sample at different time steps. We now wish to model both concentrations as a function of time using the following expansion:

$$\mathrm{Si}(t) = \sum_{i=1}^{n} \mathrm{AlkExSi}_i(1 - \mathrm{e}^{-k_i(t-t_0)}) + b(t - t_0)$$

$$\mathrm{Al}(t) = \sum_{i=1}^{n} \frac{\mathrm{AlkExSi}_i}{\mathrm{Si/Al}_i}(1 - \mathrm{e}^{-k_i(t-t_0)}) + \frac{b}{\mathrm{Si/Al}_0}(t - t_0)$$

Both formulas consist of a linear term plus a number of exponentially decaying parts. The number of the exponentially decaying parts can be chosen in the model. The number of parameters in the model equals $3n + 3$, namely:

$$k_i \text{ for } i \in \{1, \dots, n\}$$
$$\mathrm{AlkExSi}_i \text{ for } i \in \{1, \dots, n\}$$
$$\mathrm{Si/Al}_i \text{ for } i \in \{1, \dots, n\}$$
$$b$$
$$\mathrm{Si/Al}_0$$
$$t_0$$

Cost function

Let $\overline{\mathrm{Si}}$ and $\overline{\mathrm{Al}}$ be the vectors in $\mathbb{R}^m$ containing the observation data at the measurement times $\{t_1, \dots, t_m\}$ and Si and Al the vectors in $\mathbb{R}^m$ with our model predictions (for a certain choice of parameters). The goal now is to minimize the cost function

$$J = \left\|\mathrm{Si} - \overline{\mathrm{Si}}\right\|_2^2 + \left\|\mathrm{Al} - \overline{\mathrm{Al}}\right\|_2^2$$

with respect to all the parameters.

Read the data

We assume the data is given in a .csv file with three columns: time, Si measurements and Al meaurements.

The first row may contain names for the columns, but for consitency, these are replaced with the names 'time', 'SiBar' and 'AlBar'. If no columns names are present, the option 'header = None' should be used in stead of 'header = 0'.

We assume that decimals are denoted with a '.' and that the delimiter between the columns is a ';'. This can be changed by changing the 'delimiter = ';'' argument.

Select the data file:

Either give a relative path or a full path to the data file.

In [2]:
```
#Pathway to data file with Time, Si concentration and Al concentration. Comma delimited.
filename = 'E:/documents/Method/01Data Sets/50/mydata.csv'
```

In [3]:
```
# Read data with pandas: (possibly change the delimiter and header input)
data = pd.read_csv(filename, delimiter = ';', header = 0, names = ['time', 'SiBar', 'AlBar'])
data = data.dropna(how = 'any')

# Cast data to ndarray for later calculations with numpy:
data_np = data.as_matrix()
time = data_np[:, 0]
SiBar = data_np[:, 1]
AlBar = data_np[:, 2]

#
nmeas = time.size
nsamples = 2*time.size

# Show a figure of the measured data:
plt.figure()
lineSiBar = plt.plot(time, SiBar, 'r,', label = '$\overline{Si}$')
lineAlBar = plt.plot(time, AlBar, 'b,', label = '$\overline{Al}$')
plt.title('Measurement data')
plt.xlabel('Time')
plt.ylabel('Concentration ($\mu$mol/L)')
plt.legend(loc = 4)
plt.show()
```

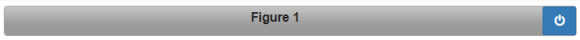

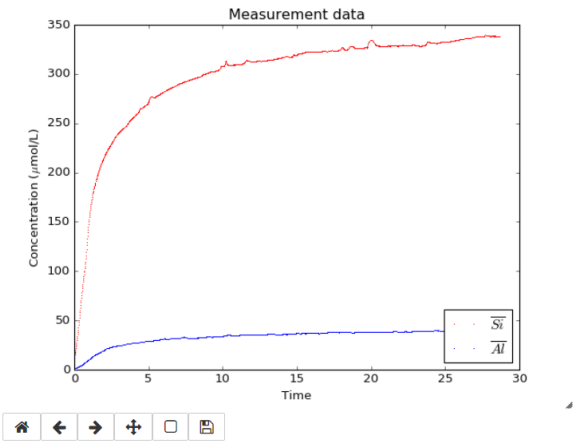

Functions

The functions needed for the optimization routine and the statistical analysis of the data are defined in the file "SiAlProblem_Functions.ipyng". We wil assume that the $3n + 3$ parameters are given as a ndarray of shape (3n + 3,) in the following order:

$$[k_1, \dots, k_n, \mathrm{AlkExSi}_1, \dots, \mathrm{AlkExSi}_n, \mathrm{Si/Al}_1, \dots, \mathrm{Si/Al}_n, b, \mathrm{Si/Al}_0, t_0]$$

Initial estimate

Because for example any permuation of the parameter tupples (α_i, β_i, k_i) is an equivalent reformulation of the optimization problem, it is to be expected that the cost function J will have multiple local minima and maxima. We therefore need a good initial guess of the optimal set of parameters.

Consider for now the case $n = 1$, where

$$\mathrm{Si}(t) = \mathrm{AlkExSi}(1 - \mathrm{e}^{-kt}) + bt.$$

The linear part of this formula is given by

$$\mathrm{AlkExSi} + bt$$

which can be estimated by a simple linear regression model on the second part of the data (where t is big). The exponential decaying part can then by approximated by looking at

$$\mathrm{e}^{-kt} = (\mathrm{AlkExSi} + bt) - \mathrm{Si}(t).$$

and thus by performing an exponential regression on the data $(t_i, \mathrm{AlkExSi} + bt - \overline{Si}(t_i))$. By doing the same for the Al concentration we can also get estimates for $\mathrm{Si/Al}$ and $\mathrm{Si/Al}_0$.

When $1 < n$ we base our initial estimate on the parameters found for the model $n - 1$.

When $1 < n$ we propose to take all the parameters equal to their $n = 1$ counterpart, except for $\mathrm{AlkExSi}$, which we replace with $\mathrm{AlkExSi}/n$. This way the inital estimate is independent of n.

In [4]:
```
# Select the linear part of the data:
M = len(time[max(time) - 10 < time])    # Take the last 10 minutes of measurents.

N = SiBar[M:].size

# Linear regression on SiBar data:
slopeSi = (np.sum(time[M:]*SiBar[M:]) - np.sum(time[M:])*np.sum(SiBar[M:])/N)/(np.sum(time[M:]**2) - np.sum(time[M:])**2/N)
intSi = np.sum(SiBar[M:])/N - slopeSi*np.sum(time[M:])/N
SiLin = intSi + slopeSi*time

# Linear regression on AlBar data:
slopeAl = (np.sum(time[M:]*AlBar[M:]) - np.sum(time[M:])*np.sum(AlBar[M:])/N)/(np.sum(time[M:]**2) - np.sum(time[M:])**2/N)
intAl = np.sum(AlBar[M:])/N - slopeAl*np.sum(time[M:])/N
AlLin = intAl + slopeAl*time

# Select the exponential part of the data:
M = len(time[time < 10])                # Take the first 10 minutes of measurements.
N = SiBar[M:].size

# Exponential decay on SiBar data:
index1 = np.where(SiLin - SiBar > 0)      # We can't take the log of negative values. However, due to the noise this might occur.
index2 = np.where(index1[0] < M)
index3 = index1[0][index2[0]]
k0Si = -np.sum((np.log((SiLin - SiBar)[index3]) - np.log(intSi))*time[index3])/np.sum(time[index3]**2)

# Exponential decay on AlBar data:
index1 = np.where(AlLin - AlBar > 0)      # We can't take the log of negative values. However, due to the noise this might occur.
index2 = np.where(index1[0] < M)
index3 = index1[0][index2[0]]
k0Al = -np.sum((np.log((AlLin - AlBar)[index3]) - np.log(intAl))*time[index3])/np.sum(time[index3]**2)

# According to the model, k0Si should be equal to k0Al:
k0Exp = (k0Si + k0Al)/2

print 'Intercept and slope SiBar data: ', intSi, '    ', slopeSi, '    ', k0Si
print 'Intercept and slope AlBar data: ', intAl, '    ', slopeAl, '    ', k0Al
print 'Decay rate used for initial guess:                                ', k0Exp
```

```
# De decay rates geven soms nan terug. Moet nog opgelost worden.
```

```
Intercept and slope SiBar data:  294.553898837      1.549928492      0.419504867411
Intercept and slope AlBar data:  30.6347292471      0.336982172837      0.374457987963
Decay rate used for initial guess:                                      0.396981427687
```

In [5]:
```
paras0 = np.array([k0Exp, intSi, intSi/intAl, slopeSi, slopeSi/slopeAl, 0])
print 'Inital parameters: ', paras0

timeFull = np.linspace(np.min(time), np.max(time), time.size)
Si0, Al0 = Model(paras0, timeFull)
```

```
plt.figure()
lineSiBar = plt.plot(time, SiBar, 'r,')
lineSi0 = plt.plot(time, Si0, 'r--', label = '$Si$')
lineAlBar = plt.plot(time, AlBar, 'b,')
lineAl0 = plt.plot(time, Al0, 'b--', label = '$Al$')
plt.title('Measurement data & inital guess')
plt.xlabel('Time')
plt.ylabel('Concentration ($\mu$mol/L)')
plt.legend(loc = 4)
plt.show()
```

```
Inital parameters:  [   0.39698143  294.55389884    9.6150319     1.54992849    4.59943765
    0.        ]
```

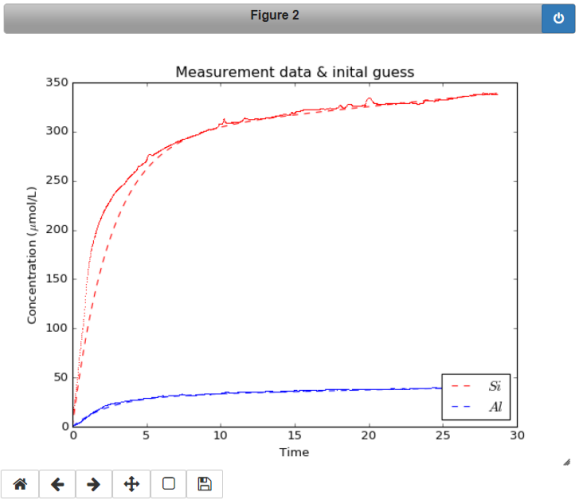

Calculate the three models

We now calcuate an optimal set of parameters for $n = 1, 2$ and 3 and compare the results.

n = 1:

In [6]:
```
%%time

#
n = 1
paras0 = np.concatenate((k0Exp*np.ones(n), intSi/n*np.ones(n), intSi/intAl*np.ones(n), [slopeSi], [slopeSi/slopeAl], [0]))

# Optimization:
runs = 3                    #Number of runs
for i in range(runs):
    results = StochasticNewtonMCMC(paras0, SiBar, AlBar, time, samples = 350)    #Number of iterations
    results['x'] = Sort_By_k(results['x'])
    print results['x'], results['fun'], results['flag_hess'], results['flag_naninf']
    if i == 0:
        results1 = results
    elif results['fun'] < results1['fun']:
        results1 = results
Si1, Al1 = Model(results1['x'], time)
Si1Full, Al1Full = Model(results1['x'], timeFull)

# Make a plot of the model:
plt.figure()
plt.plot(time, SiBar, 'r,')
plt.plot(timeFull, Si1Full, 'r', label = 'Si')
plt.plot(time, AlBar, 'b')
plt.plot(timeFull, Al1Full, 'b', label = 'Al')
plt.title('Measurements & model (n = 1)')
plt.xlabel('Time')
plt.ylabel('Concentration ($\mu$mol/L)')
plt.legend(loc = 4)
```

```
#
k1 = results1['x'][0:n]
AlkExSi1 = results1['x'][n:2*n]
SiAl1 = results1['x'][2*n:3*n]
b1 = results1['x'][3*n]
SiAl01 = results1['x'][3*n + 1]
t01 = results1['x'][3*n + 2]
```

```
print '\nThe following parameters were found:'
print '\tk:      \t', k1
print '\tAlkExSi:\t', AlkExSi1
print '\tSi/Al:  \t', SiAl1
print '\tb:      \t', b1
print '\tSi/Al0: \t', SiAl01
print '\tt0:     \t', t01
print ''
print 'Cost: ', results1['fun']
print ''
print results1['flag_hess'], '    ', results1['flag_naninf']
```

```
350
```

```
350
```

```
350
```

```
[  5.94970293e-01   2.82598070e+02   1.02028715e+01   2.09541407e+00
   4.41017950e+00  -9.36150022e-02] 59064.6037272 0 0
[  5.94970107e-01   2.82598087e+02   1.02028739e+01   2.09541308e+00
   4.41017456e+00  -9.36152387e-02] 59064.6037272 0 0
[  5.94970445e-01   2.82598049e+02   1.02028725e+01   2.09541521e+00
   4.41017940e+00  -9.36148283e-02] 59064.6037272 0 0
```

Figure 3

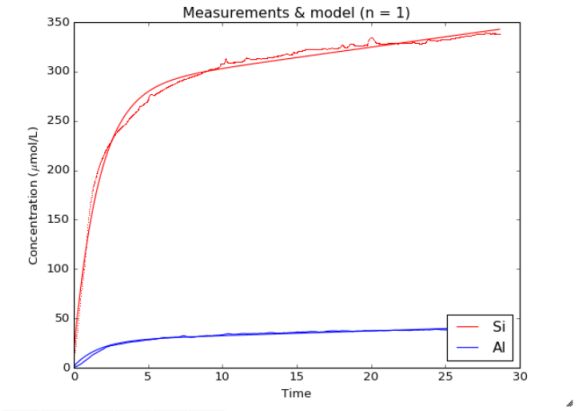

x=21.2492 y=318.327

```
The following parameters were found:
        k:              [ 0.59497029]
        AlkExSi:        [ 282.59806954]
        Si/Al:          [ 10.20287151]
        b:              2.09541407242
        Si/Al0:         4.41017949899
        t0:             -0.0936150022288

Cost:  59064.6037272

0      0
Wall time: 42.3 s
```

n = 2:

In [7]:
```
%%time

#
n = 2
paras0 = np.array([0., k1[0], 0., AlkExSi1[0], 1., SiAl1[0], b1, SiAl01, t01])
```

```
# Optimization:
runs = 3   #Number of runs
for i in range(runs):
    results = StochasticNewtonMCMC(paras0, SiBar, AlBar, time, samples = 350)  #Number of iterations
    results['x'] = Sort_By_k(results['x'])
    print results['x'], results['fun'], results['flag_hess'], results['flag_naninf']
    if i == 0:
        results2 = results
    elif results['fun'] < results2['fun']:
        results2 = results
Si2, Al2 = Model(results2['x'], time)
Si2Full, Al2Full = Model(results2['x'], timeFull)

# Make a plot of the model:
plt.figure()
plt.plot(time, SiBar, 'r,')
plt.plot(timeFull, Si2Full, 'r', label = 'Si')
plt.plot(time, AlBar, 'b')
plt.plot(timeFull, Al2Full, 'b', label = 'Al')
plt.title('Measurements & model (n = 2)')
plt.xlabel('Time')
plt.ylabel('Concentration ($\mu$mol/L)')
plt.legend(loc = 4)
```

```
#
k2 = results2['x'][0:n]
AlkExSi2 = results2['x'][n:2*n]
SiAl2 = results2['x'][2*n:3*n]
b2 = results2['x'][3*n]
SiAl02 = results2['x'][3*n + 1]
t02 = results2['x'][3*n + 2]

print '\nThe following parameters were found:'
print '\tk:      \t', k2
print '\tAlkExSi:\t', AlkExSi2
print '\tSi/Al:  \t', SiAl2
print '\tb:      \t', b2
print '\tSi/Al0: \t', SiAl02
print '\tt0:     \t', t02
print ''
print 'Cost: ', results2['fun']
print ''
print results2['flag_hess'], '    ', results2['flag_naninf']
```

350

350

350

```
[  2.11986285e-01   1.14697521e+00   1.20816279e+02   1.88775033e+02
   5.58538422e+00   1.50713845e+01   9.59007620e-01   4.97348775e+00
   4.90064378e-02] 14643.833399 1 0
[  2.53398953e-01   1.23251186e+00   1.30178074e+02   1.73157789e+02
   3.48832103e+00   3.24885035e+02   1.20250945e+00   4.05771602e+02
   4.80106751e-02] 18764.820185 1 0
[  2.11931004e-01   1.14676059e+00   1.20789571e+02   1.88806289e+02
   5.58224634e+00   1.50763427e+01   9.58876661e-01   4.97898341e+00
   4.89962047e-02] 14643.8318345 1 0
```

Figure 4

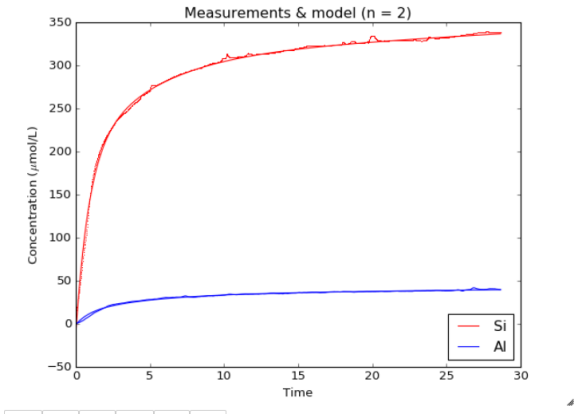

```
The following parameters were found:
        k:              [ 0.211931    1.14676059]
        AlkExSi:        [ 120.78957134  188.80628938]
        Si/Al:          [  5.58224634  15.07634266]
        b:              0.958876660753
        Si/Al0:         4.97898341013
        t0:             0.0489962047338

Cost:  14643.8318345

1     0
Wall time: 1min 51s
```

n = 3:

In [8]:

```
%%time

#
n = 3    #Number of runs
paras0 = np.array([0., k2[0], k2[1], 0., AlkExSi2[0], AlkExSi2[1], 1., SiAl2[0], SiAl2[1], b2, SiAl02, t02])

# Optimization:
runs = 3
for i in range(runs):
    results = StochasticNewtonMCMC(paras0, SiBar, AlBar, time, samples = 350)    #Number of iterations
    results['x'] = Sort_By_k(results['x'])
    print results['x'], results['fun'], results['flag_hess'], results['flag_naninf']
    if i == 0:
        results3 = results
    elif results['fun'] < results3['fun']:
        results3 = results
Si3, Al3 = Model(results3['x'], time)
Si3Full, Al3Full = Model(results3['x'], timeFull)
```

```
# Make a plot of the model:
plt.figure()
plt.plot(time, SiBar, 'r,')
plt.plot(timeFull, Si3Full, 'r', label = 'Si')
plt.plot(time, AlBar, 'b,')
plt.plot(timeFull, Al3Full, 'b', label = 'Al')
plt.title('Measurements & model n = 3')
plt.xlabel('Time')
plt.ylabel('Concentration ($\mu$mol/L)')
plt.legend(loc = 4)

#
k3 = results3['x'][0:n]
AlkExSi3 = results3['x'][n:2*n]
SiAl3 = results3['x'][2*n:3*n]
b3 = results3['x'][3*n]
SiAl03 = results3['x'][3*n + 1]
t03 = results3['x'][3*n + 2]

print '\nThe following parameters were found:'
print '\tk:       \t', k3
print '\tAlkExSi:\t', AlkExSi3
print '\tSi/Al:  \t', SiAl3
print '\tb:       \t', b3
print '\tSi/Al0: \t', SiAl03
print '\tt0:      \t', t03
print ''
print 'Cost: ', results3['fun']
print ''
print results3['flag_hess'], '    ', results3['flag_naninf']
```

```
350
```

```
350
```

```
350
```

```
[  2.05491831e-01   4.21186586e-01   1.13823686e+00   1.19617179e+02
   5.30294109e-01   1.90641835e+02   4.47467577e+01   2.10487852e-02
   6.32231670e+01   9.14132496e-01   2.77828766e+00   4.85428701e-02] 14082.4250388 1 0
[  2.06498469e-01   4.63530321e-01   1.13973759e+00   1.19969212e+02
   1.91795473e-01   1.90503494e+02   2.45170658e+01   7.73444687e-03
   1.31817597e+02   9.18185050e-01   2.88547202e+00   4.82671065e-02] 14058.0120539 1 0
[  2.00686481e-01   4.14315784e-01   1.13649961e+00   1.19247796e+02
   1.61178229e+00   1.91146869e+02   4.57626898e+02   5.74295960e-02
   8.84856435e+01   8.66404465e-01   2.50865857e+00   4.84780175e-02] 14096.9601228 1 0
```

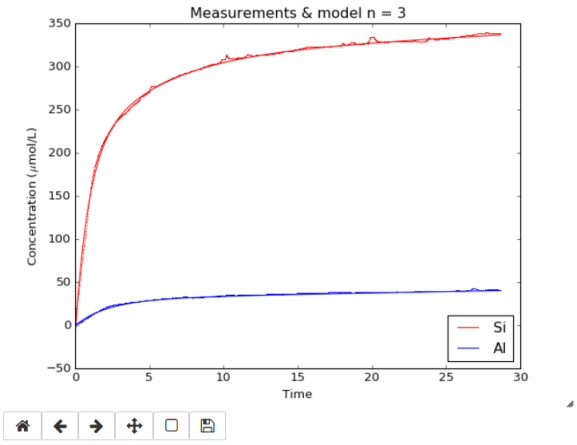


```
The following parameters were found:
        k:              [ 0.20649847  0.46353032  1.13973759]
        AlkExSi:        [ 119.96921166    0.19179547  190.50349368]
        Si/Al:          [  2.45170658e+01   7.73444687e-03   1.31817597e+02]
        b:              0.918185049921
        Si/Al0:         2.88547202468
        t0:             0.0482671065453

Cost:  14057.3802132

1      0
Wall time: 3min 29s
```

Model Selection

We will perform an Akaike test in order to determine which model, i.e. $n = 1, 2$ or 3, best fits the data.

All parameters:

In [9]:
```
print 'Model 1: Cost =', results1['fun']
print '\t[k1, AlkExSi1, SiAl1]:\t\t[', k1[0], ',', AlkExSi1[0], ',', SiAl1[0], ']'
print '\t[b, SiAl0, t0]:\t\t\t[', b1, ',', SiAl01, ',', t01, ']'

print ''

print 'Model 2: Cost =', results2['fun']
print '\t[k1, AlkExSi1, SiAl1]:\t\t[', k2[0], ', ', AlkExSi2[0], ', ', SiAl2[0], ']'
print '\t[k1, AlkExSi1, SiAl1]:\t\t[', k2[1], ', ', AlkExSi2[1], ', ', SiAl2[1], ']'
print '\t[b, SiAl0, t0]:\t\t\t[', b2, ',', SiAl02, ',', t02, ']'

print ''

print 'Model 3: Cost =', results3['fun']
print '\t[k1, AlkExSi1, SiAl1]:\t\t[', k3[0], ', ', AlkExSi3[0], ', ', SiAl3[0], ']'
print '\t[k1, AlkExSi1, SiAl1]:\t\t[', k3[1], ', ', AlkExSi3[1], ', ', SiAl3[1], ']'
print '\t[k1, AlkExSi1, SiAl1]:\t\t[', k3[2], ', ', AlkExSi3[2], ', ', SiAl3[2], ']'
print '\t[b, SiAl0, t0]:\t\t\t[', b3, ',', SiAl03, ',', t03, ']'
```

```
Model 1: Cost = 59064.6037272
        [k1, AlkExSi1, SiAl1]:          [ 0.594970208512 , 282.598080526 , 10.2028736468 ]
        [b, SiAl0, t0]:                 [ 2.09541351506 , 4.41017599362 , -0.0936150643333 ]

Model 2: Cost = 14643.8314222
        [k1, AlkExSi1, SiAl1]:          [ 0.21193060159 ,  120.79490417 ,  5.58421179363 ]
        [k1, AlkExSi1, SiAl1]:          [ 1.14679039617 ,  188.802752122 ,  15.0711124582 ]
        [b, SiAl0, t0]:                 [ 0.958799438726 , 4.97518101527 , 0.0489946168991 ]

Model 3: Cost = 14057.3802132
        [k1, AlkExSi1, SiAl1]:          [ 0.207785244411 ,  120.579154314 ,  20.9589995963 ]
        [k1, AlkExSi1, SiAl1]:          [ 0.472811081442 ,  0.118612093314 ,  0.00499236795524 ]
        [k1, AlkExSi1, SiAl1]:          [ 1.14550346804 ,  189.795365148 ,  113.360716405 ]
        [b, SiAl0, t0]:                 [ 0.924098455491 , 2.91278140396 , 0.0491470316519 ]
```

Akaike test

For a least squares problem, the Akaike information is defined as

$$AIC = 2 \times (\#parameters) + (\#samples) \times \ln\left(\frac{RSS}{\#samples}\right)$$

A correction can be made in order to account for the difference between $\#parameters$ and $\#samples$:

$$AICc = AIC + 2 \times \frac{(\#parameters) \times (\#parameters + 1)}{(\#sampels) - (\#parameters) - 1}$$

This correction becomes important when $(\#parameters)^2 \ll (\#samples)$.

The model with the smallest AICc is the prefered model.

In [10]:
```
RSS = np.array([results1['fun'], results2['fun'], results3['fun']])    # The cost function is precisely the RSS.
AIC = np.zeros(3)
AICc = np.zeros(3)
for i in range(3):
    k = 3*(i + 1) + 1                                                  # The variance has to be counted as a parameter as wel.
    AIC[i] = 2*k + nsamples*np.log(RSS[i]/nsamples)
    AICc[i] = AIC[i] + 2.0*k*(k + 1)/(nsamples- k - 1)                 # Corrected AIC information.

for i in range(3):
    if AICc[i] == AICc.min():
        modelAICc = i + 1
        print 'AICc values: ', AICc, ' ==>  Use model', i + 1
        break

print 'SELECTED MODEL: n =', n

if n == 1:
    results = results1
elif n == 2:
    results = results2
else:
    results = results3

Si, Al = Model(results['x'], time)
SiFull, AlFull = Model(results['x'], timeFull)
k = results['x'][0:n]
AlkExSi = results['x'][n:2*n]
SiAl = results['x'][2*n:3*n]
b = results['x'][3*n]
SiAl0 = results['x'][3*n + 1]
t0 = results['x'][3*n + 2]

print '\nThe following parameters were found:'
print '\tk:      \t', k
print '\tAlkExSi:\t', AlkExSi
print '\tSi/Al:  \t', SiAl
print '\tb:      \t', b
print '\tSi/Al0: \t', SiAl0
print '\tt0:     \t', t0
```

```
AICc values:  [ 9788.48325535  4997.03686043  4862.62444958]  ==>  Use model 3
SELECTED MODEL: n = 3

The following parameters were found:
        k:              [ 0.20649847  0.46353032  1.13973759]
        AlkExSi:        [ 119.96921166    0.19179547  190.50349368]
        Si/Al:          [  2.45170658e+01   7.73444687e-03   1.31817597e+02]
        b:              0.918185049921
        Si/Al0:         2.88547202468
        t0:             0.0482671065453
```

Analysis part II:

By selecting a random subset of the data points (indicated by the variable $datasize$), we can create a new set of observations for the same soil sample. If we do the optimization for this subset of the data, we will get a new (and slightly different) set of optimal parameters.

If we do this multiple times (indicated by the variable $runs$), we can calculate the average and standerd deviation over all the parameter sets that were found. These values will allow us to calculate a confidence interval for the parameters.

Confidence interval

Once again we can compute confidence intervals. This time, they do not represent the quality of the fit, but rather the range in which the parameters are likely to fall.

Remark 1: We once again use the Bonferroni correction.

Remark 2: The check indicates wether or not the parameters estimated by the Monte Carlo method fall within the confidence interval.

In [23]:
```
#
datasize = 50    # Number of points we randomly select from all the available data in order to simulate "new" data.
runs = 100       # Number of times we will simulate "new".

# Allocate output:
X = np.zeros((runs, 3*n + 3))
FUN = np.zeros(runs)
timeRUNS = np.zeros((runs, datasize))
SiRUNS = np.zeros((runs, datasize))
AlRUNS = np.zeros((runs, datasize))
```

```
# Constraints for the optimization routine:
bnds = []
for i in range(0, 2*n):
    bnds.append((0., None))
for i in range(2*n, 3*n):
    bnds.append((1e-16, None))
bnds.append((0, None))
bnds.append((1e-16, None))
bnds.append((None, None))
bnds = tuple(bnds)

#
for run in log_progress(range(runs), every = 1):
    # Select part of the data:
    #index1 = np.random.randint(0, int(0.5*nmeas), datasize)
    #index2 = np.random.randint(int(0.5*nmeas), nmeas, datasize)
    #index = np.concatenate([[0, 1], index1, index2, [nmeas - 2, nmeas - 1]])
    index = np.random.randint(0, nmeas, datasize)

    # Select the measurement times:
    timeRUN = data_np[index, 0]

    # Select the Si and Al data:
    SiBarRUN = data_np[index, 1]
    AlBarRUN = data_np[index, 2]

    # Take a random percentage shift:
    gammaSi = np.random.uniform(-0.11, 0.11)           #The noise selected
    gammaAl = np.random.uniform(-0.11, 0.11)           #The noise selected

    # Add the percentage shift to the data:
    SiBarRUN = (1 + gammaSi)*SiBarRUN                  # Here the noise is added to Si.
    AlBarRUN = (1 + gammaAl)*AlBarRUN                  # Here the noise is added to Al.

    # Perform the optimization: (local should work fine since we use a good initial estimate and since the dataset is smaller)
    resultsRUN = minimize(Cost, results['x'], args = (SiBarRUN, AlBarRUN, timeRUN), bounds = bnds)

    # Store results:
    X[run, :] = resultsRUN['x']
    FUN[run] = resultsRUN['fun']
    timeRUNS[run, :] = timeRUN
    SiRUNS[run, :] = SiBarRUN
    AlRUNS[run, :] = AlBarRUN
```

100

In [24]:

```
# Sort the data:
results['x'] = Sort_By_k(results['x'])                 #Sort results according to AlkExSi, k or SiAl
for run in range(runs):
    X[run, :] = Sort_By_k(X[run, :])                   #Sort results according to AlkExSi, k or SiAl

#
muX = np.mean(X, 0)
sigmaX =  np.std(X, 0, ddof = 3*n + 3)

#
alpha = 0.05/(3*n + 3)                                   # Bonferroni correction.
q = t.ppf(1 - alpha/2, runs - (3*n + 3))
lb = muX - q*sigmaX
ub = muX + q*sigmaX
check = (lb <= results['x']) * (results['x'] <= ub)

# Make dataframe:
if n == 1:
    indices = ['k1', 'AlkExSi1', 'SiAl1', 'b', 'SiAl0', 't0']
elif n == 2:
    indices = ['k1', 'k2', 'AlkExSi1', 'AlkExSi2', 'SiAl1', 'SiAl2', 'b', 'SiAl0', 't0']
else:
    indices = ['k1', 'k2', 'k3', 'AlkExSi1', 'AlkExSi2', 'AlkExSi3', 'SiAl1', 'SiAl2', 'SiAl3', 'b', 'SiAl0', 't0']
d = {'Lowerbound':lb, 'Mean':muX, 'Upperbound':ub, 'Width':np.abs(ub - lb), 'std':sigmaX, 'Monte Carlo value':results['x'],
     'Monte Carlo between the bounds':check}
cols = ['Lowerbound', 'Mean', 'Upperbound', 'Width', 'std', 'Monte Carlo value', 'Monte Carlo between the bounds']
df2 = pd.DataFrame(d, columns = cols, index = indices)

df2
```

Out[24]:

	Lowerbound	Mean	Upperbound	Width	std	Monte Carlo value	Monte Carlo between the bounds
k1	0.006457	0.194384	0.382311	0.375854	0.063876	0.206498	True
k2	-0.175780	0.492414	1.160607	1.336387	0.227116	0.463530	True
k3	-0.515634	1.361317	3.238268	3.753902	0.637968	1.139738	True
AlkExSi1	46.601901	122.368090	198.134279	151.532378	25.752615	119.969212	True
AlkExSi2	-97.473271	9.346229	116.165729	213.638999	36.307507	0.191795	True
AlkExSi3	107.216748	184.805021	262.393294	155.176546	26.371934	190.503494	True
SiAl1	-26.737628	24.579199	75.896026	102.633654	17.442378	24.517066	True
SiAl2	-75.431345	5.421551	86.274447	161.705791	27.481566	0.007734	True
SiAl3	41.295135	124.895265	208.495394	167.200259	28.415339	131.817597	True
b	-0.803634	0.805281	2.414195	3.217830	0.546863	0.918185	True
SiAl0	-26.035021	4.282422	34.599865	60.634886	10.304774	2.885472	True
t0	-1.024335	0.072260	1.168855	2.193190	0.372728	0.048267	True

Percentage bands:

To each subset of the data we added a random percentage shift. We can plot the percentage bands around the "optimal" curve found with the Monte Carlo analysis and see if the subsets that we used fall within the maximum percentage bands.

In [20]:
```
# The maximum size of the percentage bands:
# (can be different for Si and Al, should be the same value used to add noise to the random subsets)
gammaSi = 0.11    #Noise chosen
gammaAl = 0.11    #Noise chosen

# We will plot every 10th subset of the data that was taken:
index = 10

# Plot for Si:
plt.figure()
plt.plot(timeFull, (1 + gammaSi)*SiFull, 'r--', linewidth = 2)
plt.plot(timeFull, SiFull, 'r', label = 'Si', linewidth = 2)
plt.plot(timeFull, (1 - gammaSi)*SiFull, 'r--', linewidth = 2)
plt.plot(time, SiBar, 'r,')
for i in range(0, runs, index):
    plt.plot(timeRUNS[i, :], SiRUNS[i, :], 'd', label = 'Run ' + str(i + 1))

# Add legend: (if it's too big, you can comment it out)
plt.legend(loc = 4, bbox_to_anchor = (1.15, -0.1), ncol = 4)

# Plot for Al:
plt.figure()
plt.plot(timeFull, (1 + gammaAl)*AlFull, 'r--', linewidth = 2)
plt.plot(timeFull, AlFull, 'r', label = 'Al', linewidth = 2)
plt.plot(timeFull, (1 - gammaAl)*AlFull, 'r--', linewidth = 2)
plt.plot(time, AlBar, 'r,')
for i in range(0, runs, index):
    plt.plot(timeRUNS[i, :], AlRUNS[i, :], 'd', label = 'Run ' + str(i + 1))

# Add legend: (if it's too big, you can comment it out)
plt.legend(loc = 4, bbox_to_anchor = (1.15, -0.1), ncol = 4)
```

Figure 6

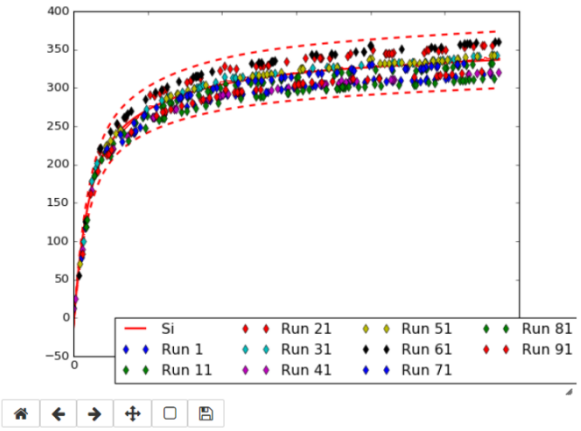

Figure 7

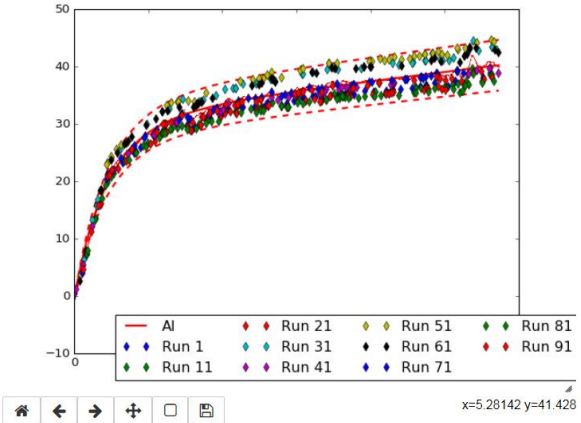

x=5.28142 y=41.428

Out[20]: <matplotlib.legend.Legend at 0x10d29048>